Synchrony affects Taylor's law in theory and data

Daniel C. Reuman[a,b,c,1], Lei Zhao[a,b], Lawrence W. Sheppard[a,b], Philip C. Reid[d,e,f], and Joel E. Cohen[c,g,h,i,1]

[a]Department of Ecology and Evolutionary Biology, University of Kansas, Lawrence, KS 66045; [b]Kansas Biological Survey, University of Kansas, Lawrence, KS 66047; [c]Laboratory of Populations, Rockefeller University, New York, NY 10065; [d]The Laboratory, Sir Alister Hardy Foundation for Ocean Science, Plymouth PL1 2PB, United Kingdom; [e]Marine Institute, Plymouth University, Plymouth PL4 8AA, United Kingdom; [f]The Laboratory, Marine Biological Association of the United Kingdom, Plymouth PL1 2PB, United Kingdom; [g]The Earth Institute, Columbia University, New York, NY 10027; [h]Department of Statistics, Columbia University, New York, NY 10027; and [i]Department of Statistics, University of Chicago, Chicago, IL 60637

Contributed by Joel E. Cohen, May 4, 2017 (sent for review March 6, 2017; reviewed by Michael J. Plank and Xiao Xiao)

Taylor's law (TL) is a widely observed empirical pattern that relates the variances to the means of groups of nonnegative measurements via an approximate power law: variance$_g \approx a \times$ mean$_g^b$, where *g* indexes the group of measurements. When each group of measurements is distributed in space, the exponent *b* of this power law is conjectured to reflect aggregation in the spatial distribution. TL has had practical application in many areas since its initial demonstrations for the population density of spatially distributed species in population ecology. Another widely observed aspect of populations is spatial synchrony, which is the tendency for time series of population densities measured in different locations to be correlated through time. Recent studies showed that patterns of population synchrony are changing, possibly as a consequence of climate change. We use mathematical, numerical, and empirical approaches to show that synchrony affects the validity and parameters of TL. Greater synchrony typically decreases the exponent *b* of TL. Synchrony influenced TL in essentially all of our analytic, numerical, randomization-based, and empirical examples. Given the near ubiquity of synchrony in nature, it seems likely that synchrony influences the exponent of TL widely in ecologically and economically important systems.

fluctuation scaling | mean variance scaling | Moran effect | correlation | aphid

Taylor's law (TL) is a widely observed empirical pattern that relates the variances to the means of groups of measurements of population densities or other nonnegative quantities via a power law: variance$_g \approx a \times$ mean$_g^b$, where g indexes the groups of measurements, $a > 0$, b is usually positive, and a and b are both independent of g. Equivalently, $\log(\text{variance}_g) \approx b \times \log(\text{mean}_g) + \log(a)$. The parameter b has the same numerical value regardless of whether it appears as the exponent of the power law or the slope of the linear relation between $\log(\text{variance}_g)$ and $\log(\text{mean}_g)$. Thus, b may be referred to as the exponent or the slope of TL.

TL has been verified in data on the population sizes and population densities of hundreds of taxa, including aphids (1), crops (2), fish (3, 4), birds (5), and humans (6). TL has also been discovered in many other nonnegative measurements (7), including recently, tornados per outbreak (8) and stocks (9). In physics, TL is sometimes called "fluctuation scaling." TL has been generalized (10) and applied or proposed for application to fisheries management (3, 4), estimation of species persistence times (11), and agriculture (2, 12, 13). Potential mechanisms of TL have been explored extensively (9, 14, 15). Because of its ubiquity, it has been suggested that TL could be another "universal law," like the central limit theorem (16).

There are multiple versions of TL. "Temporal TL" and "spatial TL," on which we focus, use time series, $Y_i(t)$, of population densities measured in locations $i = 1, \ldots, n$ at times $t = 1, \ldots, T$. For temporal TL, the groups, g, consist of all measurements made in a location, i (means and variances are computed over time). For spatial TL, groups are measurements at a single time, t (means and variances are over space).

Synchrony (metapopulation synchrony, spatial synchrony) is another ubiquitous and fundamental ecological phenomenon. It is the tendency for time series of population densities of the same species measured in geographically separated locations to be correlated through time. It has been observed in organisms as diverse as protists (17), insects (18), mammals (19, 20), and birds (21; ref. 22 has many other examples). It relates to large-scale pest or disease outbreaks and shortages of resources (23, 24) and has implications for conservation because populations are at greater risk of simultaneous extinction if they are simultaneously rare (24).

Although some empirical and theoretical connections have been made between synchrony and TL (7, 14, 20, 25), the connections are far from completely understood and do not encompass all versions of TL. Synchrony, like TL, may reflect aggregation, because the spatial extent of correlations among population time series indicates the geographic size of outbreaks (26). Engen, et al. (25) connected TL with synchrony theoretically but did not use spatial or temporal TL. Temporal TL has been related to a kind of synchrony that occurs on spatial scales smaller than that of sampling (7, 14).

The "Moran effect" refers to synchrony caused by synchronous environmental drivers. Changes in Moran effects as a consequence of climate change may alter synchrony. Long-term increases in the synchrony of caribou populations in Greenland were associated with increases in the synchrony of environmental drivers in the area, apparently through modified Moran effects (19). The latter were, in turn, linked to global warming. Similar associations held for North American bird species (21). Large-scale climatic changes in the North Atlantic Oscillation caused changes in winter temperature synchrony, which in turn caused changes in the synchrony of pest aphid species in the United Kingdom (27). Changes in the synchrony of plankton (26) and tree rings (28) have been associated with climate change. If synchrony influences TL,

Significance

Two widely confirmed patterns in ecology are Taylor's law (TL), which states that the variance of population density is approximately a power of mean population density, and population synchrony, the tendency of species' population sizes in different areas to be correlated through time. TL has been applied in many areas, including fisheries management, conservation, agriculture, finance, physics, and meteorology. Synchrony of populations increases the likelihood of large-scale pest or disease outbreaks and shortages of resources. We show that changed synchrony modifies and can invalidate TL. Widespread recent changes in synchrony, possibly resulting from climate change, may broadly affect TL and its applications.

Author contributions: D.C.R. and J.E.C. designed research; D.C.R., L.Z., L.W.S., and J.E.C. performed research; D.C.R., L.Z., L.W.S., P.C.R., and J.E.C. contributed new reagents/analytic tools; D.C.R., L.Z., and L.W.S. analyzed data; and D.C.R., L.Z., and J.E.C. wrote the paper.

Reviewers: M.J.P., University of Canterbury; and X.X., University of Maine.

The authors declare no conflict of interest.

See Commentary on page 6658.

[1]To whom correspondence may be addressed. Email: reuman@ku.edu or cohen@rockefeller.edu.

This article contains supporting information online at www.pnas.org/lookup/suppl/doi:10.1073/pnas.1703593114/-/DCSupplemental.

then changes in synchrony may change TL in ecologically and economically important systems.

We analyze connections between synchrony and spatial TL to answer the following questions. Do the presence and strength of synchrony in population time series influence whether TL holds and if so, how? Do the presence and strength of synchrony influence the slope b of TL and if so, how? Because of the fundamental importance of both TL and synchrony to population ecology, illuminating connections between these phenomena is of intrinsic interest, but we are also motivated by the applied importance of TL and concern that climate change may modify synchrony.

Results

Analytic Results. Suppose the population size or density in location i at time t is modeled by the nonnegative random variable $Y_i(t)$ for $i = 1, \ldots, n$. Assume that the multivariate stochastic process $Y(t) = (Y_1(t), \ldots, Y_n(t))$ is stationary and ergodic (29); these assumptions are standard (*SI Appendix*, *S1*). We use the standard spatial sample mean and sample variance: $m(t) = (1/n)\sum_{i=1}^{n} Y_i(t)$ and $v(t) = \sum_{i=1}^{n} Y_i(t)^2/(n-1) - nm(t)^2/(n-1)$. The traditional plot to test spatial TL is the $\log(v(t))$ vs. $\log(m(t))$ scatterplot for a finite realization of these processes. TL hypothesizes that this plot will be approximately linear. The linear regression slope is $b_t = cov_t(\ln(m(t)), \ln(v(t)))/var_t(\ln(m(t)))$ (30). The subscripts t indicate that the variance var_t and the covariance cov_t are computed across time for the finite realization, whereas each value of $m(t)$ and $v(t)$ is computed across space at time t. A standard (22) measure of average synchrony, $\Omega_t = (1/n^2)\sum_{i,j=1}^{n} cor_t(Y_i(t), Y_j(t))$, averages the temporal correlations of every pair of population dynamic time series. This summation includes the terms with $i = j$, which equal 1, and hence Ω_t is $1/n$ when the correlations with $i \neq j$ are 0; Ω_t is zero when the spatial average time series is constant, and Ω_t cannot be negative (*SI Appendix*, *S1*). We are interested in how Ω_t may affect whether the relationship between the log mean and the log variance is linear and the value of the slope b_t when linearity holds. For long time series, it suffices (*SI Appendix*, *S1*) to consider the population quantities $b = cov(\ln(m), \ln(v))/var(\ln(m))$ and $\Omega = (1/n^2)\sum_{i,j=1}^{n} cor(Y_i, Y_j)$, assuming that all of the expectations, variances, and covariances in these expressions and others exist (details are in *SI Appendix*). Thus, we work with the time-independent distribution $Y = (Y_1, \ldots, Y_n)$. Autocorrelation in time series will not influence the relationships that we study if time series are long enough for empirical and true marginal distributions to be similar (*SI Appendix*, *S1*).

Applying the delta method (31), $\ln(m) \approx \ln(E(m)) + (m - E(m))/E(m)$, $\ln(v) \approx \ln(E(v)) + (v - E(v))/E(v)$, and $var(\ln(m)) \approx var(m)/E(m)^2$; therefore (*SI Appendix*, *S1*)

$$b \approx \frac{(n-1)E(m)}{n} \frac{cov(m, v)}{(A - var(m))var(m)}, \qquad [1]$$

where the first factor in this expression and the quantity $A = (1/n)\sum_{i=1}^{n} \mathrm{E}(Y_i^2) - \mathrm{E}(m)^2$ depend solely on the marginal distributions, Y_i, and do not depend on the correlations, $cor(Y_i, Y_j)$. However, $var(m)$ equals $(1/n^2)\sum_{i,j=1}^{n} cov(Y_i, Y_j)$, which relates to synchrony, Ω, and is similar in form. Eq. **1**, therefore, provides the intuition behind our subsequent analyses: if synchrony [Ω or $var(m)$] changes and the marginals, Y_i, remain fixed, then one expects the slope b to change. The following theorem supports this intuition.

Theorem. *Suppose Y_i are identically distributed (but not necessarily independent) with $E(Y_i) = M > 0$ and finite $var(Y_i) = V > 0$. Assume that $\mu_{ij} = E((Y_i - M)(Y_j - M))$, $\mu_{ijk} = E((Y_i - M)(Y_j - M)(Y_k - M))$, and $\mu_{ijkl} = E((Y_i - M)(Y_j - M)(Y_k - M)(Y_l - M))$ are finite for all i, j, k, and l, and define $\rho_{ij} = cor(Y_i, Y_j) = \mu_{ij}/V$ and $\rho_{ijk} = \mu_{ijk}/\mu_{iii}$. Then*

$$b \approx \left(\frac{M\mu_{iii}}{V^2}\right)\left(\frac{\sum_{i,j=1}^{n} \rho_{ijj} - \frac{1}{n}\sum_{i,j,k=1}^{n} \rho_{ijk}}{n^2(1-\Omega)\Omega}\right). \qquad [2]$$

The approximation is better whenever the coefficients of variation of the sample mean $\sqrt{var(m)}/E(m) = \sqrt{V\Omega}/M$ and sample variance $\sqrt{var(v)}/E(v)$ are smaller, and is asymptotically perfect as these quantities approach zero.

Additional details, alternative mathematically equivalent expressions for b, and a proof of the theorem are in *SI Appendix*, *S2*.

This theorem extends a theorem by Cohen and Xu (15), which assumes that the Y_i are independent and identically distributed (iid). In that case, the second factor on the right of Eq. **2** is 1, and $b \approx (M\mu_{iii}/V^2)$, which equals the skewness $\mu_{iii}/V^{3/2}$ of Y_i divided by its coefficient of variation $V^{1/2}/M$. Independence of the Y_i is not necessary here: the same formula holds if $\rho_{ij} = 0$ for $i \neq j$ and $\rho_{ijk} = 0$ whenever i, j, and k are not all equal. Cohen and Xu (15) concluded that, in the iid case, skewness of Y_i is necessary and sufficient for TL to have slope $b \neq 0$. Our theorem extends this result to the case of identically distributed Y_i that may be nonindependent.

The denominator $n^2(1-\Omega)\Omega$ in Eq. **2** is a $\cap$-shaped function of Ω (i.e., it increases, has a maximum, and then decreases again as Ω increases). Therefore, Eq. **2** may seem to suggest that b is a $\cup$-shaped function of synchrony (it decreases, has a minimum, and then increases again). However, the numerator of the second factor of Eq. **2** may, a priori, also be a $\cap$-shaped function of synchrony; therefore, a $\cup$-shaped dependence of b on synchrony is not mathematically certain, and neither are any of the components of such a dependence (the initial decrease, the internal minimum, and the subsequent increase of b as Ω increases). Dependence of the numerator of Eq. **2** on Ω also means that $\lim_{\Omega \to 0} b$ and $\lim_{\Omega \to 1} b$ can be finite, although $\lim_{\Omega \to 0}(1-\Omega)\Omega$ and $\lim_{\Omega \to 1}(1-\Omega)\Omega$ are 0.

Numerical Results. To illustrate the identically distributed case, we performed numerical simulations based on multivariate normal random variables $X = (X_1, \ldots, X_n)$ with mean $(0, \ldots, 0)$ and covariance matrix with diagonal entries 1 and off-diagonal entries equal to a parameter, $\rho \geq 0$. We let $Y_i = \varphi(X_i)$, where the transformations $\varphi(.)$ were chosen, in different simulations, to make the Y_i a variety of Poisson, negative binomial, gamma, exponential, χ^2, normal, and log-normal distributions. Increases in ρ produced increases in Ω. Exponential and χ^2 distributions are special cases of gamma distributions. We produced separate results for these distributions because they are widely used. Results are in *SI Appendix*, *S3*; Fig. 1 shows typical results for Poisson and gamma examples.

Results generally agreed with the above intuitions and analyses. The linearity hypothesis of TL was usually, but not always, an adequate approximation in that linearity and homoscedasticity could not be rejected statistically (*SI Appendix*, *S6* has details on how this was tested). In agreement with our theorem and Cohen and Xu (15), when a shifted normal distribution (which has skewness 0) was used for Y_i, $b \approx 0$ for all values of Ω. For skewed distributions, the slope b was generally smaller for larger values of Ω, confirming the prediction that b depends on synchrony. Although b decreased steeply as Ω increased from zero for all skewed distributions, b most commonly continued to decrease monotonically as Ω increased further, even for large values of Ω, except for a few cases using gamma distributions, for which modest increases were observed (*SI Appendix*, Figs. S14–S20): the b vs. synchrony relationship was only occasionally $\cup$-shaped, and then only mildly so. The right side of Eq. **2** was computed analytically (i.e., with formulas) for gamma, exponential, χ^2, normal, and log-normal examples, and the formulas were compared with numerical results. For some distributions and parameters, the approximation was very accurate, and it was always at least qualitatively accurate (in the sense that it showed similar

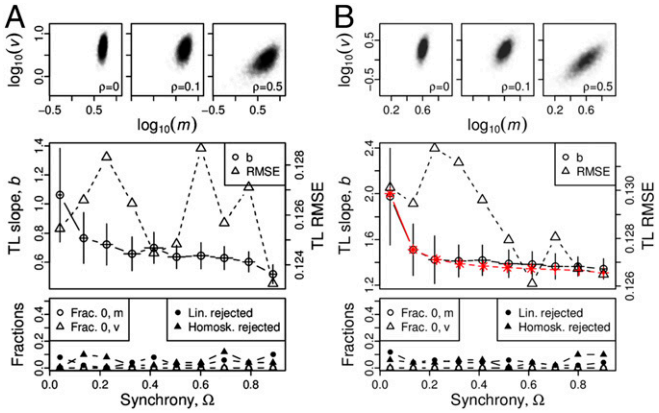

Fig. 1. Effects of spatial synchrony on spatial TL for a model with populations identically distributed in different sampling locations and iid through time at each location. Examples use (*A*) Poisson ($\lambda = 5$) and (*B*) gamma (shape $\alpha = 8$, rate $\beta = 2$) distributions (*SI Appendix, S3* shows the parameterization of the gamma distribution). (*Top*) m is spatial sample mean and v is spatial sample variance. Confirming TL visually, approximately linear $\log_{10}(v)$ vs. $\log_{10}(m)$ relationships held with selected values of ρ. Slopes were shallower for greater synchrony. (*Middle*) TL had a shallower slope for greater synchrony. Black lines show the average (across 50 simulations) TL slope plotted against average synchrony (error bars are standard deviations) and average (over 50 simulations) of the root mean squared errors (RSME) of $\log_{10}(v)$ values from $\log_{10}(v)$ vs. $\log_{10}(m)$ linear regressions (labeled TL RMSE in the axis label). (*B*) Red lines are analytic approximations (Eq. **2** and Theorem 5 in *SI Appendix, S2.3*), computable with readily available software for continuous distributions (*SI Appendix, S3*), with + and × symbols indicating points for which approximations were deemed adequate via two different methods, respectively; both symbols are plotted when both methods indicate an adequate approximation. Each simulation consisted of 25 populations sampled 100 times each. (*Bottom*) Fractions of m and v values, which were 0 and therefore ignored, and fractions of 50 simulations, for which statistical tests rejected linearity or homoskedasticity of the $\log_{10}(v)$ vs. $\log_{10}(m)$ relationship with 95% confidence. Frac, fraction; Homosk, homoskedasticity; Lin, linearity. *SI Appendix*, Figs. S1–S32 show other parameters and distributions, which often showed similar patterns. Additional details are in *SI Appendix, S3* and *S6*.

declines of b with increasing synchrony), except for the log-normal distribution, for which it was very inaccurate for some parameters because of insufficient sampling as previously observed (15). As expected from the theorem, Eq. **2** was a better approximation for smaller Ω.

We also constructed nonidentically distributed examples by applying transformations to multivariate normal random variables. Our theorem, which assumed identically distributed Y_i, did not apply here. The random variable X was the same as above, and $Y_i = \varphi_i(X_i)$, where the $\varphi_i(.)$ differed for different i. The $\varphi_i(.)$ values were chosen so that all of the Y_i were from the same family (Poisson, negative binomial, gamma, exponential, χ^2, normal, or log normal), although with different parameters. For gamma, normal, exponential, and log-normal examples, the $\varphi_i(.)$ were chosen so that Y_i was distributed in the same way as (but was not equal to) f_iY_1, where $0 < f_1 < \ldots < f_n$. This procedure was not possible for negative binomial, Poisson, or χ^2 distributions because these families are not closed under multiplication by positive real numbers. Distributions used for these families and the results are described in *SI Appendix, S4*.

Results reinforced most of the generalities that emerged from the above analytical results and simulations, although a ∪-shaped dependence of b on Ω was more common and stronger in these examples (*SI Appendix, S4*). Exceptions to general tendencies did occur. For gamma, exponential, normal, and log-normal examples, TL was usually a good approximation. Although linearity was often statistically rejected, departures from linearity were modest: log(v) vs. log(m) plots stayed very close to the regression line. The slope b always showed an initial steep decrease as Ω increased from zero for all gamma, exponential, normal, and log-normal examples. As $\Omega \to 1$, these examples approached the case for which Y_i equals f_iY_1 almost surely in addition to having the same distribution as f_iY_1. In that limit, $m = \text{mean}_i(Y_i) = \text{mean}_i(f_iY_1) = Y_1\text{mean}_i(f_i)$, whereas $v = var_i(Y_i) = var_i(f_iY_1) = Y_1^2 var_i(f_i)$. Therefore, TL should hold exactly with slope two. This argument holds even for symmetric distributions like the normal. Our numerical simulations confirmed that, as Ω increased toward one, root mean squared errors from log(v) vs. log(m) regressions went to zero, and b went to two, sometimes from above and sometimes from below. An approach from below was paired with ∪-shaped dependence of b on Ω, which was common and often pronounced in these examples. The earlier result (15) that skewness is required for TL to have slope $b \neq 0$ if Y_i are identically distributed does not hold when Y_i are not identically distributed: simulations with Y_i normally distributed had $b \neq 0$ (*SI Appendix*, Figs. S45–S50). For Poisson and χ^2 examples, TL was usually a reasonable approximation, and b declined steeply as Ω increased from zero and continued to decrease for larger Ω. Negative binomial examples often strongly violated TL, especially for large values of Ω (e.g., *SI Appendix*, Figs. S63 and S64). Nonetheless, the slope b tended to decrease with increasing Ω whenever linearity held approximately.

Another way to create families of random variables Y with fixed marginal distributions but varying synchrony is based on sums of independent random variables representing local and regional influences on populations (32). It is well-known that, for independent Poisson random variables X and X_i, the sum $X + X_i$ is Poisson distributed. Similar facts are also true for the negative binomial, gamma, and normal families. Therefore, Y was generated by setting $Y_i = X + X_i$ for independent X and X_i for $i = 1, \ldots, n$. The variable X can be interpreted as the influence of a large-spatial-scale environmental or other factor that affects all populations; the X_i are local effects. Different relative variances of X and the X_i led to different amounts of correlation (synchrony) among the Y_i. By this approach, we constructed Y, such that the Y_i were identically distributed according to a desired Poisson, negative binomial, gamma, exponential, χ^2, or normal distribution, with a desired level of synchrony among the Y_i. Details of this construction and the results are in *SI Appendix, S5*.

Results were the same in some respects as the results above and differed in others. Larger values of synchrony always decreased the slope b (except for normal Y_i, for which b was always zero as expected from the theorem because Y_i are again identically distributed). The slope b went to zero as Ω approached one. The approximation Eq. **2** applied reasonably accurately. In all cases, the right side of Eq. **2** reduced to simple, monotonically decreasing functions of Ω. However, contrary to prior simulations, log(v) vs. log(m) plots often strongly violated the linear hypothesis of TL. Values of synchrony Ω larger than zero smeared points rightward in log(v) vs. log(m) space, destroying the linear relation expected from TL. This smearing decreased b but also changed its meaning from representing the slope of a linear pattern to representing the slope of a linear approximation to a nonlinear pattern. The decrease in b did not reflect maintenance of a linear pattern with a changed slope as in prior examples (Fig. 1 and *SI Appendix, S3* and *S4*). *SI Appendix, S5* gives an explanation for this effect.

Empirical Results. We examined the influence of synchrony on empirical data using 82 spatiotemporal population datasets. The datasets included annual time series of population density for 20 species of aphid sampled for 35 y in 11 locations across the United Kingdom, annual density time series for 22 plankton groups sampled in 26 regions in the seas around the United Kingdom for 56 y, and chlorophyll-*a* density time series measured at several locations at each of 10 depths in four distance categories from the coast of southern California over 28 y. We henceforth refer to distance categories from shore in the chlorophyll-*a* data as groups 1–4, where group 1 refers to the closest

category to shore and larger group numbers correspond to farther categories from shore. *Methods* has additional descriptions of the data and their processing.

The spatial TL was reasonably well-supported by all 82 datasets. *SI Appendix*, Figs. S91–S96 plots log(v) vs. log(m) and gives statistical tests of TL. Conformity to TL was not perfect, but quite good overall, except for the chlorophyll-*a* data in group 3 (*SI Appendix*, Fig. S95). Linearity or homoskedasticity of the log(v) vs. log(m) relationship was rejected at the 1% level for 7 of 82 datasets (1 aphid species, 1 depth from group 1, and 5 depths from group 3).

We examined correlations across species, taxonomic groups, or depths (for the aphid, plankton, and chlorophyll-*a* datasets, respectively) between measurements of b and Ω. Factors other than synchrony may have influenced these results and are accounted for below after examining the raw correlations here. Fig. 2 *A*, *D*, *G*, *J*, *M*, and *P* shows that b and Ω were significantly negatively correlated across aphid species and across depths in the chlorophyll-*a* data, groups 1 and 2, and nonsignificantly negatively correlated across plankton groups in the plankton data. Higher synchrony Ω was associated with lower slope b in these data, despite possible confounding influences.

However, significant positive correlations occurred in the chlorophyll-*a* data, groups 3 and 4 (Fig. 2 *M* and *P*). These positive associations seem to conflict with simulation results, which generally support a negative association between b and Ω, unless confounding factors overwhelmed a negative influence of synchrony on b in these data. For instance, changes across depths in b may be influenced for the chlorophyll-*a* data, groups 3 and 4, by changes across depths in Ω and possible changes in time series marginal distributions. Simulations carried out above held time series marginal distributions constant when synchrony was varied.

To control for changes in time series marginal distributions that may have occurred in concert with changes in synchrony, we decomposed slopes $b = b_{marg} + b_{sync}$ into contributions due to synchrony, b_{sync}, and due to time series marginals, b_{marg}. We computed the marginal contribution, b_{marg}, by independently randomizing time series and then recomputing the log(v) vs. log(m) slope (*Methods*) to eliminate synchrony and ensure that it cannot contribute to b_{marg}. Then, we defined b_{sync} as $b - b_{marg}$. Fig. 2 *C*, *F*, *I*, *L*, *O*, and *R* shows that b_{sync} was negatively associated with Ω in all cases (albeit not always significantly), even for chlorophyll-*a* data, groups 3 and 4 (Fig. 2 *O* and *R*). For these groups, b_{marg} was strongly positively associated with Ω (Fig. 2 *N* and *Q*). This positive association overwhelmed the negative association of b_{sync} with Ω to produce the overall positive association of b with Ω observed in Fig. 2 *M* and *P*. Thus, groups 3 and 4 results did not conflict with simulation results, but rather showed that other factors dominated. The change in time series marginal distributions for the chlorophyll-*a* data was not surprising, because these data were gathered across different depths, and chlorophyll-*a* density varies with depth in the ocean. *SI Appendix*, Fig. S99 is like Fig. 2 but identifies the species/groups/depths of plotted points; panels for the chlorophyll-*a* data show that depth probably played a role. Differing thermocline depths across groups 1–4 (*SI Appendix*, Fig. S101) may also have been important.

To examine in more detail the influence of synchrony on spatial TL in empirical data, we performed additional randomizations (*Methods*). Randomizations reduced or increased the synchrony in each of our 82 spatiotemporal population datasets while not modifying the marginal distributions in each sampling location. In virtually every case, increasing synchrony decreased b, whereas decreasing synchrony increased b (Fig. 3). The strength of the effect varied across datasets and was typically steeper for smaller values of synchrony. Values of b_{marg} correspond to the y-axis intercepts of the curves in Fig. 3. In a few cases, b appeared to depend in a ∪-shaped way on synchrony, as in some simulations, but the ∪ shape was modest when it occurred, also in agreement with simulations (i.e., only modest

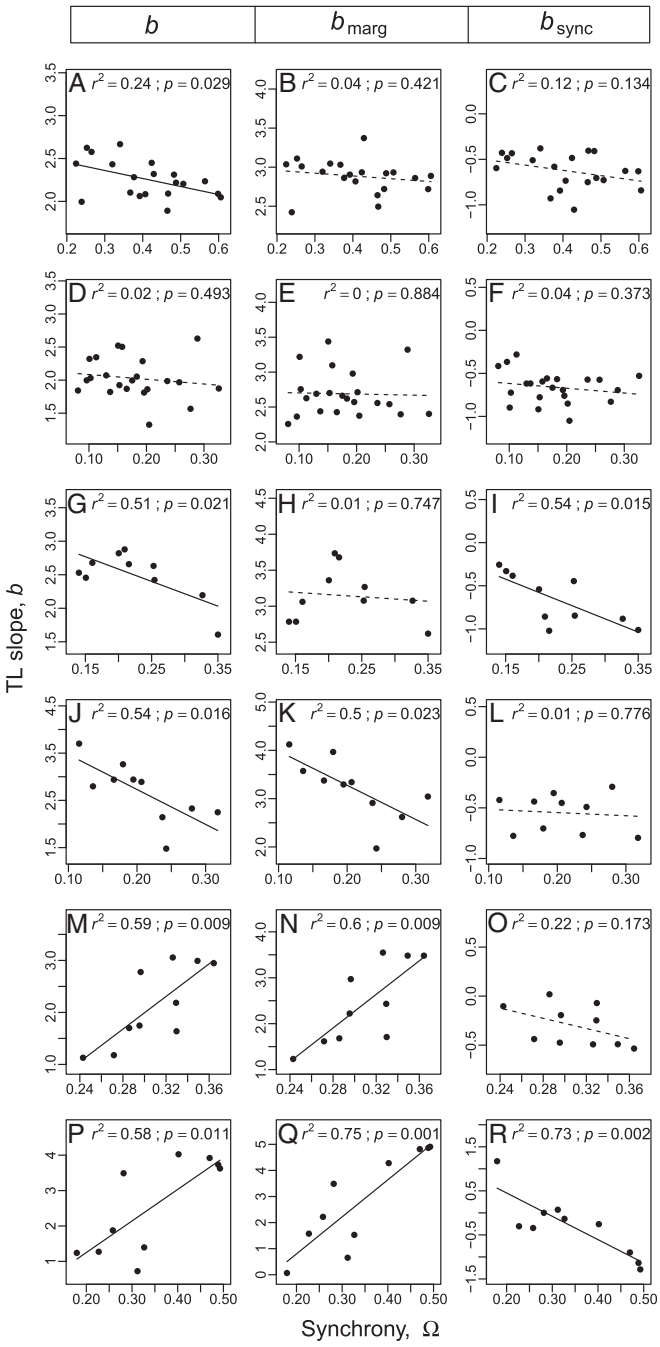

Fig. 2. Plots of TL slope b against synchrony Ω for (*A*) 20 species of aphid in the United Kingdom, (*D*) 22 plankton groups in the seas around the United Kingdom, and (*G*, *J*, *M*, and *P*) chlorophyll-*a* density time series measured at 10 depths in groups 1–4 (*Methods*), which are distance categories from shore. *A*, *D*, *G*, *J*, *M*, and *P* are paired with contributions to the slope, b, of (*B*, *E*, *H*, *K*, *N*, and *Q*) marginal distribution structure (b_{marg}) and (*C*, *F*, *I*, *L*, *O*, and *R*) synchrony (b_{sync}), respectively (*Methods*). Associations between synchrony and TL slope b can be due to associations between synchrony and b_{marg}, associations between synchrony and b_{sync}, or both, because $b = b_{marg} + b_{sync}$. *SI Appendix*, Fig. S99 shows another version of the figure that labels individual species/groups/depths.

increases in b with increasing Ω were observed in Fig. 3 *B*, *D*, and *F*). The linearity of TL was approximately supported across the range of synchrony values, except possibly for the highest synchrony values and the chlorophyll-*a* data in group 3 (*SI Appendix*, Figs. S97 and S98).

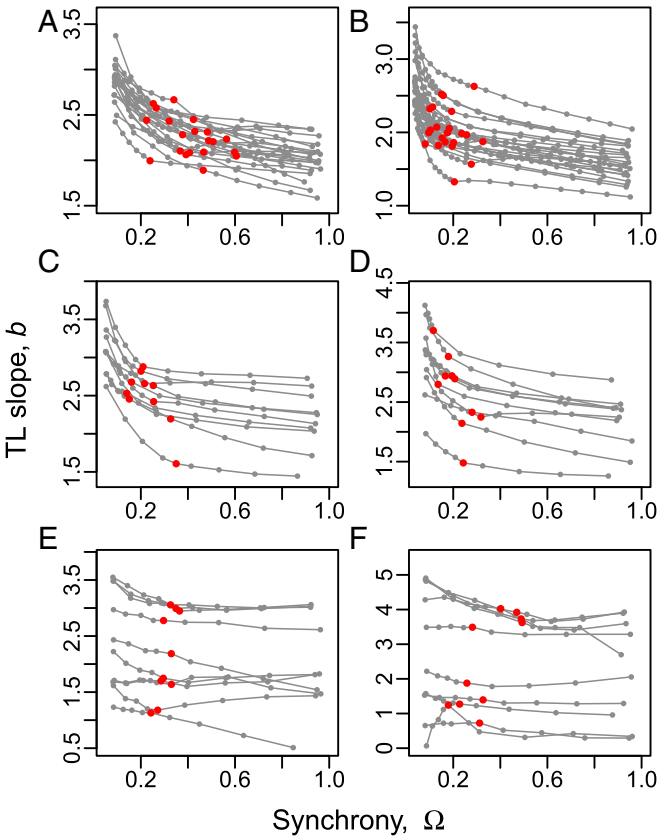

Fig. 3. The dependence of the spatial TL slope b on synchrony Ω, where synchrony was manipulated through randomizations or sorting of time series (*Methods*) for (*A*) aphid species, (*B*) plankton groups, and (*C–F*) a chlorophyll-*a* density index measured at 10 depths. *C* is for 19 group-1 locations, *F* is for 12 group-4 locations, and *D* and *E* are for 12 locations in each of two intermediate distance categories (groups 2 and 3) (*Methods*). Red points on plotted lines correspond to individual unrandomized (*A*) aphid species, (*B*) plankton groups, and (*C–F*) sampling depths detailed in *SI Appendix*, Table S1. Gray points are averages over randomizations or sortings (*Methods*). Values for individual randomizations are shown in *SI Appendix*, Fig. S100.

All results are summarized, with hyperlinks to supporting figures and derivations, in *SI Appendix*, Tables S3 and S4.

Discussion

Understanding the relationship of synchrony with TL is important, because both patterns are widespread in population ecology, and because TL and recent observed climate change-induced modifications in synchrony have applied importance (19, 21, 26–28).

We showed that the strength of synchrony substantially influences the log(variance) vs. log(mean) scatterplot, of which TL is one special form. It can destroy linearity of TL, but more commonly, it preserves linearity and changes the slope b of the plot. Synchrony influenced the slope of TL in essentially all of our analytic, numerical, empirical, and randomization-based examples. The one systematic exception occurred when the marginal distributions of time series in different locations were normally and identically distributed, so that a nonzero slope of TL was not expected with or without synchrony (15). As synchrony increased from zero, slope b almost always decreased quite sharply. For some theoretical and randomization examples, increasing synchrony starting from higher levels of synchrony increased the slope b modestly, but analogous increases were not seen in empirical examples when confounding changes in time series marginal distributions were controlled. Our analytic results generalize a theorem of Cohen and Xu (15). We provided a simple method of decomposing b into its contributions due to synchrony, b_{sync}, and due to time series marginal distributions, b_{marg}.

Ballantyne and Kerkhoff (14) and Eisler, et al. (section 3 in ref. 7) described interesting links between small-spatial-scale synchrony and temporal TL. To explain the basic idea, we construct an idealized example using aphids monitored by suction traps. Suppose trap i for $i = 1, \ldots, n$ has A_i agricultural fields that can produce aphids within its sampling range. Suppose traps are placed so that no fields contribute to more than one trap. Suppose field ij ($i = 1, \ldots, n$; $j = 1, \ldots, A_i$) contributes a random variable $V_{ij}(t)$ to trap i in year t, and suppose all of the $V_{ij}(t)$ are identically distributed with mean μ and variance σ^2. Then, if, for fixed i, $V_{ij}(t)$ are perfectly correlated so that all fields near i produce the same number of sampled aphids per year (this assumption constitutes very strong small-spatial-scale synchrony, the spatial scale being smaller than the spatial resolution of sampling), the mean of the number of aphids $\sum_j V_{ij}(t)$ sampled by trap i in year t is $\mu_i = A_i \times \mu$, and the variance is ${\sigma_i}^2 = {A_i}^2 \times \sigma^2$. Assuming that random variables for different times t are independent, the mean and variance across time of numbers of aphids sampled by trap i will converge almost surely, in the limit of long time series, to these same values (strong law of large numbers). Log transforming and doing basic algebra give $\ln({\sigma_i}^2) = 2 \times \ln(\mu_i) + C_1$ for a constant C_1; this equation demonstrates a temporal TL with slope two. If, for fixed i, $V_{ij}(t)$ are independent, then the mean of $\sum_j V_{ij}(t)$ is again $\mu_i = A_i \times \mu$, but the variance is now ${\sigma_i}^2 = A_i \times \sigma^2$. Log transforming and doing basic algebra give temporal TL with slope one. (This example shows, incidentally, that observing TL with slope one need not be evidence that the aphids or other organisms are Poisson distributed, although Poisson-distributed aphids or other organisms lead to TL with slope one.)

The above example differs in at least two important ways from our results. First, it concerns temporal TL, whereas we studied spatial TL. Second, the above example concerns synchrony at a different spatial scale from our study. Although dependence between numbers of aphids sampled at different traps seems likely to imply dependence between numbers contributed by fields within the range of individual traps, the reverse need not be true.

It seems worthwhile, in future research, to examine the possibly complex relationships between the above example (7, 14) and our study. Although Eisler, et al. (7) focus on temporal TL, they state without proof or details that many of their results also apply to TL more generally. Relationships between spatial and temporal TL have recently been examined (20) and may help connect the TL in the above example to the spatial TL of our study. Perhaps all of these versions of TL could be formally related to each other and synchrony.

Engen, et al. (25) produced a general model for analyzing a version of TL, in which each group of measurements of population density comes from plots of the same size, but different groups use different plot sizes (distinct from spatial and temporal TL). On p. 2,620 in ref. 25, they remind the reader that increasing population migration leads to increasing synchrony, which causes "the slope [of this version of TL] … to increase from 1 to 2 … as the migration increases." Engen, et al. (25) seem to indicate in the final sentences of their paper that their model could be extended to address spatial TL, possibly helping to illuminate connections among spatial, temporal, and their versions of TL and synchrony.

Cohen and Saitoh (20) examined relationships among synchrony and spatial and temporal TL in voles. Their example is consistent with our work and illustrates the value of our general results for understanding TL in specific systems. Using 31 y of population density data for the gray-sided vole, *Myodes rufocanus*, at 85 locations in Hokkaido, Japan, Cohen and Saitoh (20) verified that spatial and temporal TL held for the data as well as simulations of a previously validated Gompertz model of the dynamics of these populations. However, simulated time series had spatial and temporal TL slopes substantially steeper than

those from data. Cohen and Saitoh (20) observed that most pairs of vole populations were significantly temporally correlated and modified the Gompertz model accordingly. When density-independent perturbations in model dynamics were synchronized, inducing synchrony in simulated population time series, and when simulated populations with higher mean density had a reduced variance of density-independent perturbations, the modeled slopes of spatial and temporal TL were reduced to values similar to those of the data. Our results here account qualitatively for the effect on TL slopes of the first of these two modifications of the Gompertz model (i.e., the introduction of synchrony).

Our theoretical models and our randomizations kept the marginal distributions of time series fixed as synchrony changed to exclude confounding factors. In our empirical analyses, we identified the contribution of synchrony, b_{sync}, to the empirical TL slope b. In reality, synchrony may change jointly with marginal distributions across species, or depths, or some other axis of variation, as in some of our empirical data (Fig. 2). Covariation between changes in b_{sync} and b_{marg} should be context-dependent, may be biologically revealing, and is worth examining when multiple values of b are computed.

Increasing evidence shows that changing Moran effects, possibly due to climate change, modify synchrony (19, 21, 26–28). This work indicates that changed synchrony will modify the slope and possibly the validity of TL, with ramifications for applications of TL in many areas, including resource management (3), conservation (11), human demography (6), tornado outbreaks (8), and agriculture (2, 12, 13). Given the ubiquity of synchrony in nature (22), it seems highly likely that synchrony often affects values of TL slopes in real populations, as Hokkaido voles showed. It is important to understand better how TL is affected by synchrony and other factors.

Methods

Analytic and Numerical Methods. Full details of analytic results are in *SI Appendix, S1* and *S2*, and full details of numerical simulations are in *SI Appendix, S3–S6*.

Data. The Rothamsted Insect Survey runs a network of suction traps that sample flying aphids. Daily aphid counts are collected throughout the flight season for many species at multiple locations. Data were processed to produce annual total counts for 20 species (*SI Appendix*, Table S1) at 11 locations (*SI Appendix*, Table S2) for the years 1976–2010, forming 20 spatiotemporal population datasets.

The Continuous Plankton Recorder survey, now operated by the Sir Alister Hardy Foundation for Ocean Science, has sampled the seas around the United Kingdom for plankton abundances since before World War II using a sampling device towed behind commercial ships. Data were processed to produce annual abundance time series for 22 phytoplankton and zooplankton taxa (*SI Appendix*, Table S1) for 26 $2° \times 2^{\circ}$ areas around the United Kingdom for the years 1958–2013, forming 22 spatiotemporal population datasets.

The California Cooperative Oceanic Fisheries Investigations have surveyed the California Current System since 1949, measuring chlorophyll-*a* regularly since 1984. Time series of spring chlorophyll-*a* were based on measurements at 55 sites, which were divided into four groups based on distance from shore, with group 1 near to shore (average 87.7 km) and group 4 far from shore (average 539.3 km). For each site and sampling occasion, annual chlorophyll abundances were calculated for 0-, 10-, 20-, 30-, 50-, 75-, 100-, 125-, 150-, and 200-m depths, forming 10 spatiotemporal datasets for each group.

Additional data details are in *SI Appendix, S7*.

Randomizations and the Decomposition of *b*. Given a $T \times n$ matrix, with each column containing a time series of population size or density from one location (therefore, T is the length of the time series and n is the number of sampling locations), synchrony was reduced without affecting time series marginal distributions for the sampling locations by selecting k rows randomly and then randomly replacing the entries in those rows with randomly chosen (with replacement) values from the same column; this replacement was done independently within each column. Larger values of k destroy a larger fraction of any synchrony that was originally present in the time series. Setting $k = T$ completely eliminates synchrony by randomizing each complete time series independently. To increase the synchrony, starting from the original time series, k rows were again selected randomly. Within each column of this $k \times n$ submatrix separately, entries were sorted into increasing order. For each value of k, k rows were selected randomly in 100 ways, with values of b and Ω averaged for Fig. 3. The value b_{marg} was computed by randomizing time series with $k = T$ as described above to destroy synchrony and then computing $b = b_{\mathrm{marg}}$ for the randomized dataset.

ACKNOWLEDGMENTS. We thank contributors to the Continuous Plankton Recorder and the California Cooperative Oceanic Fisheries Investigations datasets; D. Stevens and P. Verrier for data extraction; J. Walter and T. Anderson for helpful suggestions; and Priscilla K. Rogerson for assistance. We also thank the staff of the Rothamsted Insect Survey (RIS), particularly James Bell. The RIS is a National Capability funded by Biotechnology and Biological Sciences Research Council. D.C.R., L.Z., and L.W.S. were partially supported by the University of Kansas, including Tier II and General Research Fund grants, as well as the James S. McDonnell Foundation. D.C.R. was partially supported by US National Science Foundation (NSF) Grant 1442595. J.E.C. was partially supported by NSF Grant DMS-1225529.

1. Taylor LR (1961) Aggregation, variance and the mean. *Nature* 189:732–735.
2. Döring TF, Knapp S, Cohen JE (2015) Taylor's power law and the stability of crop yields. *Field Crops Res* 183:294–302.
3. Kuo TC, Mandal S, Yamauchi A, Hsieh CH (2016) Life history traits and exploitation affect the spatial mean-variance relationship in fish abundance. *Ecology* 97: 1251–1259.
4. Xu M, Kolding J, Cohen JE (2017) Taylor's power law and fixed precision sampling: Application to abundance of fish sampled by gillnets in an African lake. *Can J Fish Aquat Sci* 74:87–100.
5. Taylor LR, Perry JN, Woiwod IP, Taylor RAJ (1988) Specificity of the spatial power-law exponent in ecology and agriculture. *Nature* 332:721–722.
6. Cohen JE, Xu M, Brunborg H (2013) Taylor's law applies to spatial variation in a human population. *Genus* 69:25–60.
7. Eisler Z, Bartos I, Kertész J (2008) Fluctuation scaling in complex systems: Taylor's law and beyond. *Adv Phys* 57:89–142.
8. Tippett MK, Cohen JE (2016) Tornado outbreak variability follows Taylor's power law of fluctuation scaling and increases dramatically with severity. *Nat Commun* 7:10668.
9. Fronczak A, Fronczak P (2010) Origins of Taylor's power law for fluctuation scaling in complex systems. *Phys Rev E Stat Nonlin Soft Matter Phys* 81:066112.
10. Giometto A, Formentin M, Rinaldo A, Cohen JE, Maritan A (2015) Sample and population exponents of generalized Taylor's law. *Proc Natl Acad Sci USA* 112:7755–7760.
11. Kalyuzhny M, et al. (2014) Temporal fluctuation scaling in populations and communities. *Ecology* 95:1701–1709.
12. Bechinski EJ, Pedigo LP (1981) Population dispersion and development of sampling plans for *Orius insidiosus* and *Nabis* spp. in soybeans. *Environ Entomol* 10:956–959.
13. Kogan M, Ruesink WG, McDowell K (1974) Spatial and temporal distribution patterns of the bean leaf beetle, *Cerotoma trifurcata* (Forester), on soybeans in Illinois. *Environ Entomol* 3:607–617.
14. Ballantyne F, 4th, Kerkhoff AJ (2005) Reproductive correlation and mean-variance scaling of reproductive output for a forest model. *J Theor Biol* 235:373–380.
15. Cohen JE, Xu M (2015) Random sampling of skewed distributions implies Taylor's power law of fluctuation scaling. *Proc Natl Acad Sci USA* 112:7749–7754.
16. Jørgensen B (1997) *The Theory of Dispersion Models* (Chapman & Hall, London).
17. Holyoak M, Lawler SP (1996) Persistence of an extinction-prone predator-prey interaction through metapopulation dynamics. *Ecology* 77:1867–1879.
18. Hanski I, Woiwod IP (1993) Spatial synchrony in the dynamics of moth and aphid populations. *J Anim Ecol* 62:656–668.
19. Post E, Forchhammer MC (2004) Spatial synchrony of local populations has increased in association with the recent Northern Hemisphere climate trend. *Proc Natl Acad Sci USA* 101:9286–9290.
20. Cohen JE, Saitoh T (2016) Population dynamics, synchrony, and environmental quality of Hokkaido voles lead to temporal and spatial Taylor's laws. *Ecology* 97:3402–3413.
21. Koenig WD, Liebhold AM (2016) Temporally increasing spatial synchrony of North American temperature and bird populations. *Nat Clim Chang* 6:614–617.
22. Liebhold A, Koenig WD, Bjørnstad ON (2004) Spatial synchrony in population dynamics. *Annu Rev Ecol Evol Syst* 35:467–490.
23. Micheli F, et al. (1999) The dual nature of community variability. *Oikos* 85:161–169.
24. Earn DJD, Levin SA, Rohani P (2000) Coherence and conservation. *Science* 290: 1360–1364.
25. Engen S, Lande R, Sæther BE (2008) A general model for analyzing Taylor's spatial scaling laws. *Ecology* 89:2612–2622.
26. Defriez EJ, Sheppard LW, Reid PC, Reuman DC (2016) Climate change-related regime shifts have altered spatial synchrony of plankton dynamics in the North Sea. *Glob Change Biol* 22:2069–2080.
27. Sheppard LW, Bell JR, Harrington R, Reuman DC (2016) Changes in large-scale climate alter synchrony of aphid pests. *Nat Clim Chang* 6:610–613.
28. Shestakova TA, et al. (2016) Forests synchronize their growth in contrasting Eurasian regions in response to climate warming. *Proc Natl Acad Sci USA* 113:662–667.
29. Brillinger DR (2001) *Time Series: Data Analysis and Theory* (SIAM, Philadelphia).
30. Snedecor G, Cochran W (1980) *Statistical Methods* (Iowa State Univ Press, Ames, IA), 7th Ed.
31. Oehlert GW (1992) A note on the delta method. *Am Stat* 46:27–29.
32. Fischer CH (1933) On correlation surfaces of sums with a certain number of random elements in common. *Ann Math Stat* 4:103–126.

Effects of synchrony on Taylor's law: Supporting information

Daniel C. Reuman, Lei Zhao, Lawrence W. Sheppard, Philip C. Reid, Joel E. Cohen

Section S1 states the general framework for the main mathematical analysis. Section S2 carries out the main analysis, which covers the case that the Y_i (see main text for a definition of Y_i) are identically distributed but not necessarily independent. Section S3 analyzes (via the results of section S2) and simulates case studies of distributions $Y = (Y_1, \ldots, Y_n)$ constructed by transforming multi-variate Gaussian random variables, and with identically distributed Y_i. Section S4 considers case studies of distributions constructed by transforming Gaussian variables so that the resulting distributions have non-identically distributed Y_i. Section S5 considers case studies using an alternate construction of Y with identically distributed Y_i. Section S6 has plotting methods. Section S7 has details of data. Sections S8-S10 contain plots associated with sections S3-S5. Remaining sections have additional figures and tables.

Contents

List of Figures

List of Tables

S1 Framework for mathematical analysis of spatial Taylor's law

Suppose the population size or density in location i at time t is modeled by the non-negative real-valued random variable $Y_i(t)$ for $i = 1, \ldots, n$. Assume that the stochastic process $Y(t) = (Y_1, \ldots, Y_n)$ is stationary and ergodic. Roughly speaking, a "stationary" stochastic process is one whose joint probability distribution is not affected by shifts in time, so that mechanisms of population dynamics are not shifting in time. And an "ergodic" process is one for which statistical characteristics can be deduced from a single, sufficiently long realization of the process, so that, for instance, long-term statistical outcomes are independent of initial conditions. Precise definitions are in standard texts [Brillinger, 2001]. These are common features or assumptions of ecological models [Nisbet and Gurney, 1982, Caswell, 2001, Turchin, 2003]. Define the spatial sample mean and sample variance as the random variables $m(t) = \frac{1}{n}\Sigma_{i=1}^{n} Y_i(t)$ and $v(t) = \frac{1}{n-1}\Sigma_{i=1}^{n}(Y_i(t) - \frac{1}{n}\Sigma_{j=1}^{n} Y_i(t))^2 = \frac{1}{n-1}\Sigma_{i=1}^{n} Y_i(t)^2 - \frac{n}{n-1}m(t)^2$, which are also ergodic stationary stochastic processes. We are interested in the $\log(v)$-versus-$\log(m)$ scatter plot for a finite-duration realization of these processes (ignoring times t for which $m(t)$ or $v(t)$ was zero), and particularly in the slope and intercept of an ordinary linear regression through such a plot,

$$b = \frac{\mathrm{cov}_t(\ln(m(t)), \ln(v(t)))}{\mathrm{var}_t(\ln(m(t)))}, \tag{1}$$

$$\ln(a) = \mathrm{E}_t(\ln(v(t))) - b\mathrm{E}_t(\ln(m(t))). \tag{2}$$

These are the basic quantities in spatial TL. The subscripts t indicate that the covariance, variance, and expected value (mean) are sample quantities computed through time for the finite-duration realization. By ergodicity of Y and consistency of the sample mean, variance, and covariance, for large samples, we instead consider

$$b = \frac{\mathrm{cov}(\ln(m), \ln(v))}{\mathrm{var}(\ln(m))}, \tag{3}$$

$$\ln(a) = \mathrm{E}(\ln(v)) - b\mathrm{E}(\ln(m)), \tag{4}$$

where the covariance, variance, and expected value are computed for the marginal distributions of the processes m and v conditional on positive values of these quantities. We assume these quantities are finite.

Suppose the population correlations $\rho_{ij} = \mathrm{cor}(Y_i, Y_j)$ exist for all $i, j = 1, \ldots, n$. These temporal correlations between populations represent spatial synchrony between locations i and j (again making use of ergodicity, and consistency of the sample covariance and variance). The synchrony $\Omega = \frac{1}{n^2}\Sigma_{ij}\rho_{ij}$ is an average correlation across all pairs of sampling locations (including comparisons of a location with itself, which give $\rho_{ii} = 1$), and is commonly used in empirical studies. We will analyze the influence of Ω on b.

Ω is naturally interpretable as a measure of average synchrony for the following additional reasons. First, letting $Z_i = Y_i/\sqrt{\text{var}(Y_i)}$, we have

$$\Omega = \frac{1}{n^2}\sum_{ij}\text{cor}(Y_i, Y_j) \tag{5}$$

$$= \frac{1}{n^2}\sum_{ij}\text{cor}(Z_i, Z_j) \tag{6}$$

$$= \frac{1}{n^2}\sum_{ij}\text{cov}(Z_i, Z_j) \tag{7}$$

$$= \frac{1}{n^2}\text{cov}\left(\sum_i Z_i, \sum_j Z_j\right) \tag{8}$$

$$= \text{var}\left(\frac{1}{n}\sum_i Z_i\right) \tag{9}$$

$$= \frac{\text{var}\left(\frac{1}{n}\sum_i Z_i\right)}{\frac{1}{n}\sum_i \text{var}(Z_i)}, \tag{10}$$

where equation (10) is the variance of a mean divided by the mean of the variances. This well known measure of synchrony is readily interpretable as the extent to which oscillations in local (normalized) time series reinforce each other or cancel in the average time series. Second, equation (10) and the definition of Ω show that $0 \leq \Omega \leq 1$. The value 0 occurs when the variability in the Z_i exactly cancels, i.e., $\text{var}\left(\frac{1}{n}\sum_i Z_i\right) = 0$ and $\frac{1}{n}\sum_i Z_i = \frac{1}{n}\sum_i \text{E}(Z_i)$, perfect asynchrony. The value 1 occurs when $Z_i = Z_j$ for all i, j, perfect synchrony. The summation $\frac{1}{n(n-1)}\Sigma_{i\neq j}\rho_{ij}$ is an alternative measure of synchrony but may be less natural because it can take negative values (its minimum is $-1/(n-1)$). The difference between this measure and Ω is essentially in whether 0 should represent perfect asynchrony (independence) or perfect antisynchrony (cancelation).

To understand the relationship between synchrony and TL for large samples under assumptions of stationarity and ergodicity, it is sufficient to work with the marginal distribution Y, instead of with the process $Y(t)$. We therefore consider families of distributions of the form $Y = (Y_1, \ldots, Y_n)$ such that for each i, all members of the family have the same marginals Y_i, and we consider how Ω and b covary through the family. In the theoretical development, marginals are kept constant to understand the influence of synchrony Ω in isolation from other potential influences on b.

To describe the intuition of the mathematical analyses that will be described in detail in section S2, we need a lemma, taken directly from Cohen and Xu [2015]. They cite Oehlert [1992] and Hosmer et al. [2008] pp. 355-358.

Lemma 1. *Let X be a real-valued random variable with finite mean $\text{E}(X)$ and finite variance $\text{var}(X)$. If a real-valued function f of real x is twice differentiable at $\text{E}(X)$, then the delta method gives*

$$f(X) \approx f(\text{E}(X)) + (X - \text{E}(X))f'(\text{E}(X)) \tag{11}$$

$$\text{E}(f(X)) \approx f(\text{E}(X)) + \frac{f''(\text{E}(X))}{2}\text{var}(X) \tag{12}$$

$$\text{var}(f(X)) \approx [f'(\text{E}(X))]^2\text{var}(X). \tag{13}$$

We now use the lemma with $f(x) = \ln(x)$:

$$\ln(m) \approx \ln(\mathrm{E}(m)) + \frac{m - \mathrm{E}(m)}{\mathrm{E}(m)} \tag{14}$$

$$\ln(v) \approx \ln(\mathrm{E}(v)) + \frac{v - \mathrm{E}(v)}{\mathrm{E}(v)} \tag{15}$$

$$\mathrm{var}(\ln(m)) = \frac{\mathrm{var}(m)}{\mathrm{E}(m)^2}, \tag{16}$$

where the approximation is good as long as m and v do not vary too much around $\mathrm{E}(m)$ and $\mathrm{E}(v)$, relative to the range of x for which first- and second-order Taylor expansions of $\ln(x)$ at $\mathrm{E}(m)$ and $\mathrm{E}(v)$ are good approximations. Therefore,

$$\frac{\mathrm{cov}(\ln(m), \ln(v))}{\mathrm{var}(\ln(m))} \approx \frac{\mathrm{E}(m)}{\mathrm{E}(v)} \frac{\mathrm{cov}(m, v)}{\mathrm{var}(m)}. \tag{17}$$

But $\mathrm{E}(v) = \frac{1}{n-1} \sum_{i=1}^{n} \mathrm{E}(Y_i^2) - \frac{n}{n-1}\mathrm{E}(m^2)$ and $\mathrm{var}(m) = \mathrm{E}(m^2) - \mathrm{E}(m)^2$, so $\mathrm{E}(m^2) = \mathrm{var}(m) + \mathrm{E}(m)^2$ and $\mathrm{E}(v) = \frac{1}{n-1} \sum_{i=1}^{n} \mathrm{E}(Y_i^2) - \frac{n}{n-1}(\mathrm{var}(m) + \mathrm{E}(m)^2) = \frac{n}{n-1}(A - \mathrm{var}(m))$ where $A = \frac{1}{n} \sum_{i=1}^{n} \mathrm{E}(Y_i^2) - \mathrm{E}(m)^2$. Thus

$$\frac{\mathrm{cov}(\ln(m), \ln(v))}{\mathrm{var}(\ln(m))} \approx \frac{(n-1)\mathrm{E}(m)}{n} \frac{\mathrm{cov}(m, v)}{(A - \mathrm{var}(m))\mathrm{var}(m)}. \tag{18}$$

The first factor on the right of this approximation depends only on n and the marginals Y_i and not on their correlations. The quantity A also depends only on marginals. The quantity $\mathrm{var}(m)$, however, equals $\frac{1}{n^2} \sum_{i,j} \mathrm{cov}(Y_i, Y_j)$, which relates to synchrony Ω and is similar in form to Ω. The expression in (18) therefore provides the intuition behind our analysis: if synchrony (Ω or $\mathrm{var}(m)$) changes and the marginals Y_i remain fixed, then (18) suggests that the slope b will be affected. Since the denominator of (18) is a $\cap$-shaped function of $\mathrm{var}(m)$, b may be a $\cup$-shaped function of synchrony, decreasing as synchrony increases for small values of synchrony, and increasing again for larger values of synchrony. These are hypotheses rather than conclusions because $\mathrm{cov}(m, v)$ in the numerator of (18) may also covary with synchrony.

S2 Mathematical analysis of the identically distributed case

S2.1 Setup of an identically distributed model

Assume the Y_i are all identically distributed (but not necessarily independent) with finite $\mathrm{E}(Y_i) = M > 0$ and finite $\mathrm{var}(Y_i) = V > 0$. Let $\mu_{ij} = \mathrm{E}((Y_i - M)(Y_j - M))$, $\mu_{ijk} = \mathrm{E}((Y_i - M)(Y_j - M)(Y_k - M))$, $\mu_{ijkl} = \mathrm{E}((Y_i - M)(Y_j - M)(Y_k - M)(Y_l - M))$, and assume these are all finite. Then $\rho_{ij} = \mathrm{cor}(Y_i, Y_j) = \frac{\mu_{ij}}{V}$. Also define $\rho_{ijk} = \frac{\mu_{ijk}}{\mu_{iii}}$. As in section S1, define $m = \frac{1}{n}\Sigma_{i=1}^{n} Y_i$ and $v = \frac{1}{n-1}\Sigma_{i=1}^{n}(Y_i - \frac{1}{n}\Sigma_{j=1}^{n} Y_i)^2 = \frac{1}{n-1}\Sigma_{i=1}^{n} Y_i^2 - \frac{n}{n-1}m^2$ to be the spatial sample mean and variance, and define $\Omega = \frac{1}{n^2}\Sigma_{ij}\rho_{ij}$ as synchrony. We aim to understand the influence of ρ_{ij} and Ω on the quantities

$$b = \frac{\mathrm{cov}(\ln(m), \ln(v))}{\mathrm{var}(\ln(m))}. \tag{19}$$

$$\ln(a) = \mathrm{E}(\ln(v)) - b\mathrm{E}(\ln(m)). \tag{20}$$

The following analytic development uses as a guide and generalizes the analysis in the supporting information of Cohen and Xu [2015]. The important generalization here is that we no longer assume independence (across space) of the random variables representing populations. Cohen and Xu [2015] also had unequal numbers of sites n_j measured for each time j, but we assume $n_j = n$ for all j.

S2.2 Preparatory lemmas

Lemma 2. *For the random variable m and $f(x) = \ln(x)$, the approximations from the delta method are*

$$\ln(m) \approx \ln(M) + \frac{m - M}{M} \tag{21}$$

$$\mathrm{E}(\ln(m)) \approx \ln(M) - \frac{1}{2M^2} V\Omega \tag{22}$$

$$\mathrm{var}(\ln(m)) \approx \frac{V\Omega}{M^2}, \tag{23}$$

where $\Omega = \frac{1}{n^2}\Sigma_{ij}\rho_{ij}$.

Proof. In the formulas of lemma 1, let $X = m$ and $f(x) = \ln(x)$. Then $f'(x) = \frac{1}{x}$, $f''(x) = \frac{-1}{x^2}$, $\mathrm{E}(m) = M$, and $\mathrm{var}(m) = \frac{1}{n^2}\Sigma_{ij}\mu_{ij} = V\Omega$. Plugging into the formulas gives the desired results. ■

If $\rho_{ij} = 0$ for all $i \neq j$ then $\Omega = \frac{1}{n}$ and the results of lemma 2 reduce to those of lemma 1 of Cohen and Xu [2015] with n_j set to n for all j.

Lemma 3. *For the random variable v and $f(x) = \ln(x)$, we have*

$$\mathrm{E}(v) = \frac{nV(1-\Omega)}{n-1} \tag{24}$$

$$\ln(v) \approx \ln(\mathrm{E}(v)) + \frac{v - \mathrm{E}(v)}{\mathrm{E}(v)} \tag{25}$$

$$\mathrm{E}(\ln(v)) \approx \ln(\mathrm{E}(v)) - \frac{(n-1)^2\mathrm{var}(v)}{2n^2V^2(1-\Omega)^2} \tag{26}$$

$$\mathrm{var}(\ln(v)) \approx \frac{(n-1)^2\mathrm{var}(v)}{n^2V^2(1-\Omega)^2} \tag{27}$$

$$\mathrm{var}(v) = \frac{n^2\sum_{ij}\mu_{iijj} - 2n\sum_{ijk}\mu_{iijk} + \sum_{ijkl}\mu_{ijkl}}{n^2(n-1)^2} - (\mathrm{E}(v))^2. \tag{28}$$

Proof.

$$\mathrm{E}(v) = \frac{1}{n-1}\Sigma_{i=1}^{n}\mathrm{E}(Y_i^2) - \frac{n}{n-1}\mathrm{E}(m^2) \tag{29}$$

$$= \frac{1}{n-1}\Sigma_{i=1}^{n}(V + M^2) - \frac{n}{n-1}(\mathrm{var}(m) + M^2) \tag{30}$$

$$= \frac{1}{n-1}\Sigma_{i=1}^{n}(V + M^2) - \frac{n}{n-1}(V\Omega + M^2) \tag{31}$$

$$= \frac{n}{n-1}(V + M^2) - \frac{n}{n-1}(V\Omega + M^2) \tag{32}$$

$$= \frac{Vn(1-\Omega)}{n-1}. \tag{33}$$

Now plugging into one of the formulas of lemma 1 with $X = v$ and $f(x) = \ln(x)$ gives the approximate equations for $\ln(v)$, $\mathrm{E}(\ln(v))$, and $\mathrm{var}(\ln(v))$ in terms of $\mathrm{var}(v)$. To work out $\mathrm{var}(v)$ in terms of the moments and co-moments of the Y_i, note

$$\mathrm{var}(v) = \mathrm{E}(v^2) - \mathrm{E}(v)^2 \tag{34}$$

$$= \mathrm{E}(v^2) - \left(\frac{nV(1-\Omega)}{n-1}\right)^2. \tag{35}$$

Define $Z_i = Y_i - M$. Then

$$v = \frac{1}{n-1}\sum_{i=1}^{n} Z_i^2 - \frac{n}{n-1}(\frac{1}{n}\sum_{i=1}^{n} Z_i)^2 \tag{36}$$

$$= \frac{n\sum_{i=1}^{n} Z_i^2 - (\sum_{i=1}^{n} Z_i)^2}{n(n-1)}. \tag{37}$$

Squaring this and taking the expectation gives

$$\mathrm{E}(v^2) = \frac{n^2\mathrm{E}((\sum_{i=1}^{n} Z_i^2)^2) - 2n\mathrm{E}((\sum_{i=1}^{n} Z_i^2)(\sum_{i=1}^{n} Z_i)^2) + \mathrm{E}((\sum_{i=1}^{n} Z_i)^4)}{n^2(n-1)^2} \tag{38}$$

$$= \frac{n^2\sum_{ij}\mu_{iijj} - 2n\sum_{ijk}\mu_{iijk} + \sum_{ijkl}\mu_{ijkl}}{n^2(n-1)^2}. \tag{39}$$

Plugging this into (35) gives the result for $\mathrm{var}(v)$. ■

If the Y_i are independent, then the results of lemma 3 reduce to those of lemma 2 of Cohen and Xu [2015] with n_j set to n for all j.

The approximations of lemmas 2 and 3 are better when the spreads of the random variables m and v are small relative to the curvature of the natural logarithm at $\mathrm{E}(m)$ and $\mathrm{E}(v)$, respectively. Typically, larger values of n will reduce the spread, but this spread will not necessarily decline to zero in the limit of large n. So approximations will not necessarily become arbitrarily good for larger n. For instance, $\mathrm{var}(m) = V\Omega = \frac{V}{n^2}\sum_{ij}\rho_{ij}$. If $\rho_{ij} = \rho$ for all $i \neq j$, this expression reduces to $\mathrm{var}(m) = \frac{V}{n^2}(n+n(n-1)\rho) = V(\frac{1}{n} + \frac{n-1}{n}\rho)$, which goes to $V\rho$ as n goes to infinity.

The delta method approximations (21) and (25) are considered "good" when $\sqrt{\mathrm{var}(m)}$ and $\sqrt{\mathrm{var}(v)}$ are smaller than a value proportional to one over the square root of the curvature of $\ln(x)$ at $\mathrm{E}(m)$ and $\mathrm{E}(v)$, respectively. The proportionality constant used here controls the "goodness" threshold desired. The curvature of $\ln(x)$ is asymptotically $1/x^2$ for large x, so comparing $\sqrt{\mathrm{var}(m)}$ and $\sqrt{\mathrm{var}(v)}$ to $\mathrm{E}(m)$ and $\mathrm{E}(v)$, respectively, indicates the quality of the delta method approximations. We have formulas for all these quantities. Approximations are asymptotically perfect in any limit which causes the ratios $\sqrt{\mathrm{var}(m)}/\mathrm{E}(m) = \sqrt{V\Omega}/M$ and $\sqrt{\mathrm{var}(v)}/\mathrm{E}(v)$ to decline to zero.

Lemma 4. *The covariance of m and v is*

$$\mathrm{cov}(m, v) = \frac{1}{n(n-1)}\left(\Sigma_{ij}\mu_{ijj} - \frac{1}{n}\Sigma_{ijk}\mu_{ijk}\right). \tag{40}$$

Proof. In the iid case, the result is $\mathrm{cov}(m, v) = \frac{\mu_{iii}}{n}$, as proved (though not originally) by Zhang [2007] and cited by Cohen and Xu [2015] (their lemma 3). The quantity μ_{iii} does not depend on i because the Y_i are identically distributed. Cohen and Xu [2015] denote this quantity μ_3. The beginning of the proof of Zhang [2007] also holds in our non-independent case: $\mathrm{cov}(m, v) = \frac{1}{n(n-1)}(I_1 - I_2)$, where I_1 and I_2 are defined by Zhang [2007] as

$$I_1 = \mathrm{E}(\Sigma_{i=1}^{n} Z_i \Sigma_{j=1}^{n} Z_j^2) \tag{41}$$

$$I_2 = \frac{1}{n}\mathrm{E}(\Sigma_{i=1}^{n} Z_i (\Sigma_{j=1}^{n} Z_j)^2) \tag{42}$$

where $Z_i = Y_i - M$. We then compute

$$I_1 - I_2 = \Sigma_{ij}\mathrm{E}(Z_i Z_j^2) - \frac{1}{n}\Sigma_{ijk}\mathrm{E}(Z_i Z_j Z_k), \tag{43}$$

and therefore (40) holds. This expression reduces to the earlier result of Cohen and Xu [2015] in the iid case. ■

S2.3 The main theorem and interpretation

Theorem 5. *Given the definitions and assumptions listed in section S2.1, and with the expression for* $\mathrm{var}(v)$ *given in lemma 3,*

$$b \approx \tilde{b} \equiv \left(\frac{M\mu_{iii}}{V^2}\right)\left(\frac{\Sigma_{ij}\rho_{ijj} - \frac{1}{n}\Sigma_{ijk}\rho_{ijk}}{n^2(1-\Omega)\Omega}\right) \tag{44}$$

$$= \left(\frac{M\mu_{iii}}{V^2}\right)\left(\frac{n-1}{n^2(1-\Omega)\Omega}\right)\left(\frac{1}{n-1}\Sigma_{ij}\rho_{ijj} - \frac{1}{n(n-1)}\Sigma_{ijk}\rho_{ijk}\right) \tag{45}$$

$$= \frac{M}{V^2}\left(\frac{\mathrm{E}\left(\sum_i (Y_i - M)\sum_j (Y_j - M)(Y_j - m)\right)}{n^2(1-\Omega)\Omega}\right) \tag{46}$$

$$\ln(a) \approx \ln\left(\frac{nV(1-\Omega)}{n-1}\right) - \frac{(n-1)^2\mathrm{var}(v)}{2n^2V^2(1-\Omega)^2} - \tilde{b}\left(\ln(M) - \frac{1}{2M^2}V\Omega\right). \tag{47}$$

Approximations are better, respectively asymptotically perfect, when the delta method approximations (21) and (25) are better, respectively asymptotically perfect, and this occurs as described in the text following lemma 3.

The first factor of (44) is the iid result for b of Cohen and Xu [2015]. In the iid case, $\rho_{ij} = 0$ for all $i \neq j$, and $\rho_{ijk} = 0$ whenever i, j and k are not all equal, and (44) reduces to

$$b \approx \left(\frac{M\mu_{iii}}{V^2}\right)\frac{n - \frac{1}{n}n}{n^2(1-\frac{1}{n})\frac{1}{n}} = \frac{M\mu_{iii}}{V^2} \tag{48}$$

which is the result of Cohen and Xu [2015]. This result holds for weaker assumptions than the full independence assumed by Cohen and Xu [2015], namely, $\rho_{ij} = 0$ for $i \neq j$, $\rho_{ijk} = 0$ for i, j, k not all equal. The denominator of the second factor of (44) depends only on synchrony, and therefore suggests how synchrony affects the TL slope. The numerator of the second factor of (44) depends only on the third-order moments and co-moments. The iid result of Cohen and Xu [2015] shows that third-order moments affect TL slope, but our result shows that co-moments are also involved when they are non-zero.

Equation (45) emphasizes the separate effects of synchrony (Ω) and the third-order co-moments, as follows. If $\rho_{ij} = 0$ for all $i \neq j$ (no synchrony) then the second factor in (45) is 1. If $\rho_{ijk} = 0$ whenever i, j, and k are not all equal, then the third factor in (45) is 1. So the second factor gives the effects of synchrony on TL slope and the third factor gives the effects of higher moments. The second factor of (45) has its minimum for $\Omega = \frac{1}{2}$. So (45) may suggest that TL slope may be shallower for larger values of synchrony up to $\Omega = \frac{1}{2}$, and then for $\Omega > \frac{1}{2}$, TL slope should get steeper again. However, this will hold only if the ρ_{ijk} do not change simultaneously to counteract the effects of Ω, which they can (see Results and below for examples).

Equation (46) offers an alternative interpretation and is in some ways more intuitive because only two subscript indices appear explicitly instead of the three in (44) and (45). The expression $\sum_i (Y_j - M)(Y_j - m)$ is proportional to a hybrid form of the sample variance: typically sample variance uses M in both factors or m in both factors, whereas this expression uses one of each.

Our theorem provides some simple intuition about why higher synchrony reduced the spatial TL slope b. Independent draws $y_1, \ldots, y_n$ from a right-skewed probability density function $\psi(y)$ will tend to produce larger sample variances when they produce larger sample means [Cohen and Xu, 2015] because the probability mass in the right portion of the distribution is more "spread out" than that in the left portion. For instance, as a simplified illustration, consider n independent draws conditional on all values being smaller than the median M_d of $\psi(y)$; compared to n independent draws conditional on all values being bigger than M_d. This is the same as drawing instead from the distributions $\psi_<(y)$ or $\psi_>(y)$, where the subscripts refer to density functions that are proportional to $\psi(y)$ below (respectively, above) M_d,

but that have been set to zero above (respectively, below) M_d. The right skew of $\psi(y)$ means that not only the mean but also the variance of $\psi_<(y)$ should be less than the mean and variance, respectively, of $\psi_>(y)$. This thought experiment shows that synchrony mitigates the influence of higher means on higher variances by forcing the points $y_1, \ldots, y_n$ to be positively correlated, reducing the variance of the sample when the mean is larger. If the range of variation of the sample mean is small (e.g., because the variability of the sample mean decreases as the sample size increases), the log(variance)-versus-log(mean) plot should be linear as a tangent approximation to whatever the smooth underlying non-linear relation may be, as Cohen and Xu [2015] pointed out.

Proof. Starting with the numerator of (19), by lemmas 2 and 3, we have

$$\begin{aligned}
\operatorname{cov}(\ln(m), \ln(v)) &\approx \operatorname{cov}\left(\ln(M) + \frac{m-M}{M}, \ln\left(\frac{nV(1-\Omega)}{n-1}\right) + \frac{v - \frac{nV(1-\Omega)}{n-1}}{\frac{nV(1-\Omega)}{n-1}}\right) && (49)\\
&\approx \operatorname{cov}\left(\frac{m-M}{M}, \frac{v - \frac{nV(1-\Omega)}{n-1}}{\frac{nV(1-\Omega)}{n-1}}\right) && (50)\\
&= \frac{n-1}{MnV(1-\Omega)} \operatorname{cov}\left(m - M, v - \frac{nV(1-\Omega)}{n-1}\right) && (51)\\
&= \frac{n-1}{MnV(1-\Omega)} \operatorname{cov}(m, v). && (52)
\end{aligned}$$

By lemma 4, this is

$$\operatorname{cov}(\ln(m), \ln(v)) \approx \frac{\Sigma_{ij}\mu_{ijj} - \frac{1}{n}\Sigma_{ijk}\mu_{ijk}}{Mn^2V(1-\Omega)}. \quad (53)$$

The denominator of (19) was given in lemma 2, so

$$\begin{aligned}
b &\approx \frac{\Sigma_{ij}\mu_{ijj} - \frac{1}{n}\Sigma_{ijk}\mu_{ijk}}{Mn^2V(1-\Omega)\operatorname{var}(\ln(m))} && (54)\\
&\approx \frac{M(\Sigma_{ij}\mu_{ijj} - \frac{1}{n}\Sigma_{ijk}\mu_{ijk})}{n^2V^2(1-\Omega)\Omega} && (55)\\
&= \left(\frac{M}{V^2}\right)\left(\frac{\Sigma_{ij}\mu_{ijj} - \frac{1}{n}\Sigma_{ijk}\mu_{ijk}}{n^2(1-\Omega)\Omega}\right) && (56)\\
&= \left(\frac{M\mu_{iii}}{V^2}\right)\left(\frac{\Sigma_{ij}\rho_{ijj} - \frac{1}{n}\Sigma_{ijk}\rho_{ijk}}{n^2(1-\Omega)\Omega}\right), && (57)
\end{aligned}$$

giving (44). Then (45) follows by algebraic manipulation and (46) follows from

$$\sum_{ij}\mu_{ijj} - \frac{1}{n}\sum_{ijk}\mu_{ijk} = \frac{1}{n}\sum_{ijk}\mu_{ijj} - \frac{1}{n}\sum_{ijk}\mu_{ijk} = \frac{1}{n}\sum_{ijk}(\mu_{ijj} - \mu_{ijk}). \quad (58)$$

But

$$\begin{aligned}
\mu_{ijj} - \mu_{ijk} &= \mathrm{E}\left((Y_i - M)[(Y_j - M)^2 - (Y_j - M)(Y_k - M)]\right) && (59)\\
&= \mathrm{E}\left((Y_i - M)(Y_j - M)[(Y_j - M) - (Y_k - M)]\right) && (60)\\
&= \mathrm{E}\left((Y_i - M)(Y_j - M)(Y_j - Y_k)\right). && (61)
\end{aligned}$$

Therefore

$$\sum_{ij}\mu_{ijj} - \frac{1}{n}\sum_{ijk}\mu_{ijk} = \frac{1}{n}\sum_{ijk}(\mu_{ijj} - \mu_{ijk}) \tag{62}$$

$$= \mathrm{E}\left(\sum_{i}(Y_i - M)\sum_{j}(Y_j - M)\frac{1}{n}\sum_{k}(Y_j - Y_k)\right) \tag{63}$$

$$= \mathrm{E}\left(\sum_{i}(Y_i - M)\sum_{j}(Y_j - M)(Y_j - m)\right). \tag{64}$$

Plugging this in to (56) gives (46). The expression for $\ln(a)$ follows by plugging results of lemmas 2 and 3 into (20). ■

S3 Cases: Distributions constructed using Gaussian copulas and identically distributed marginals

We want to construct a multivariate random variable $(Y_1, \ldots, Y_n)$ such that the Y_i are identically distributed with some given distribution, and such that we can control the correlation between Y_i and Y_j, for all $i \neq j$, with a parameter, ρ. One of many ways to do this follows. Let $X = (X_1, \ldots, X_n)$ be a multivariate normal random variable with mean $(0, \ldots, 0)$ and covariance matrix with diagonal entries 1 and off-diagonal entries $\rho \geq 0$. We let $Y_i = \varphi(X_i)$, where φ is a transformation that transforms a standard normal variable to one distributed as desired. By construction the Y_i are identically distributed, and larger values of ρ mean larger values of $\mathrm{cor}(Y_i, Y_j)$, which is common to all pairs i, j with $i \neq j$. This amounts to controlling the dependence among the Y_i using Gaussian copulas. Simulating draws from $(Y_1, \ldots, Y_n)$ is straightforward and reasonably efficient within any computing system containing a multivariate random normal distribution sampler (e.g., the R programming language, which has the function rmvnorm in the package mvtnorm). Simulations were thus used to evaluate the relationship between mean-variance relationships (e.g., TL) and synchrony for Y_i Poisson, negative binomial, gamma, exponential, chi-squared, normal, and log-normal distributions. Plots were generated as described in section S6, see figures S1 on page 23 to S32 on page 54. These are discussed in batches by marginal distribution family below. There are multiple parameterizations of the negative binomial and gamma distributions. For the negative binomial distribution, we used the probability density function (pdf) $\psi(k) = \binom{k+r-1}{k}(1-p)^r p^k$. For the gamma distribution, we used $\psi(x) = \frac{\beta^\alpha}{\Gamma(\alpha)}x^{\alpha-1}\exp(-\beta x)$, for shape and rate parameters α and β.

For Poisson and negative binomial marginals (figures S1 on page 23 through S10 on page 32), although substantial curvature and heteroskedasticity and noticeable granularity in $\log(v)$-versus-$\log(m)$ plots were evident for marginal distributions with small means, TL was typically otherwise approximately valid, i.e., $\log(v)$-versus-$\log(m)$ were reasonably linear. There was a general tendency for b to be smaller for larger values of ρ.

For Y_i a gamma distribution (or other continuous distributions - see below), approximate partially analytic results can also be obtained using (56). The moments M, V, and μ_{iii} are well known in this case. The moments μ_{ij}, μ_{ijj} and μ_{ijk}, for i, j, k distinct, were computed numerically by evaluating the integrals corresponding to their definitions, for instance,

$$\mu_{ijk} = \mathrm{E}((Y_i - M)(Y_j - M)(Y_k - M)) \tag{65}$$

$$= \int_{-\infty}^{\infty}\int_{-\infty}^{\infty}\int_{-\infty}^{\infty}(\varphi(x_i) - M)(\varphi(x_j) - M)(\varphi(x_k) - M)\Psi(x_i, x_j, x_k)dx_i dx_j dx_k, \tag{66}$$

where Ψ is the pdf of X. This calculation used the function cuhre in the R2Cuba package in the R programming language. That function reports estimates of error in its computations, which were retained

and propagated through subsequent algebraic manipulations to yield estimates of the resulting error in calculating (56). Typically errors were very small. A similar approach could not easily have been used for the Poisson or negative binomial distributions (above), because the performance of the R2Cuba package for non-continuous pdfs was not expected to be sufficient.

For gamma marginals (figures S11 on page 33 to S16 on page 38), the approximation (56) always captured the decline in the slope b with larger values of ρ. The approximation was quantitatively accurate for larger values of α and smaller values of ρ. Statistically significant curvature or heteroskedasticity were sometimes evident in $\log(v)$-versus-$\log(m)$ for smaller values of α and larger values of ρ, but curvature was a much smaller feature of $\log(v)$-versus-$\log(m)$ plots than was the overall trend. In all cases the slope b was markedly smaller for larger values of ρ.

Results for distributions with exponential marginals (figures S17 on page 39 to S18 on page 40) were similar to the gamma results in all respects, except that modest, statistically significant curvature or heteroskedasticity of the $\log(v)$-versus-$\log(m)$ relationship was detectable for all values of the exponential parameter λ considered, except at the lowest values of ρ. The approximation (56) always captured the decline in the slope b with larger values of ρ, but it was quantitatively accurate only for the smallest values of ρ.

Results for distributions with chi-squared marginals (figures S19 on page 41 to S20 on page 42) were similar to the gamma results in all respects, as expected since the chi-squared is a special case of the gamma. Modest but significant curvature and heteroskedasticity of the $\log(v)$-versus-$\log(m)$ relationship was visible for smaller degrees of freedom, k.

For Y_i a normal or log-normal distribution, the moments M, V, μ_{iii}, μ_{ij}, μ_{ijj} and μ_{ijk} for i, j, k distinct are known in closed form, facilitating approximate analytic results via (56). These moments for Y_i a normal distribution are in standard statistics texts, and lead to $b \approx 0$ via equation (56). For the log-normal distribution obtained using $\varphi(x) = \exp(\mu+\sigma x)$, it is well-known that $M = \exp(\mu+\sigma^2/2)$, $V = (\exp(\sigma^2)-1)\exp(2\mu+\sigma^2)$, and $\mu_{iii} = \exp(3\mu+3\sigma^2/2)(\exp(\sigma^2)-1)^2(\exp(\sigma^2)+2)$. Letting $Z_i = \mu+\sigma X_i$, it is also well known that the moment generating function for $Z = (Z_1, \ldots, Z_n)$ is $M_Z(t_n) = \mathrm{E}(\exp(t_n^T Z)) = \exp(t_n^T \vec{\mu} + \frac{1}{2} t_n^T \Sigma t_n)$, where t_n is an n-dimensional vector of non-negative integers, $\vec{\mu} = (\mu, \ldots, \mu)$, a superscript T denotes transpose, and Σ is the covariance matrix of Z (an n-by-n matrix with diagonal entries σ^2 and off-diagonal entries $\sigma^2\rho$). Applying the earlier expression for $\mathrm{E}(Y_i) = M = \exp(\mu + \sigma^2/2)$ and using the moment generating function,

$$
\begin{aligned}
\mu_{ij} &= \mathrm{E}((Y_i - \mathrm{E}(Y_i))(Y_j - \mathrm{E}(Y_j))) && (67)\\
&= \mathrm{E}(Y_i Y_j) - \mathrm{E}(Y_i)\mathrm{E}(Y_j) && (68)\\
&= \mathrm{E}(Y_i Y_j) - \exp(2\mu + \sigma^2) && (69)\\
&= \mathrm{E}(\exp(Z_i)\exp(Z_j)) - \exp(2\mu + \sigma^2) && (70)\\
&= \mathrm{E}(\exp(Z_i + Z_j)) - \exp(2\mu + \sigma^2) && (71)\\
&= \mathrm{E}(\exp((e_i + e_j)^T Z)) - \exp(2\mu + \sigma^2) && (72)\\
&= \exp((e_i + e_j)^T \vec{\mu} + \frac{1}{2}(e_i + e_j)^T \Sigma (e_i + e_j)) - \exp(2\mu + \sigma^2) && (73)\\
&= \exp(2\mu + \sigma^2)[\exp(\sigma^2\rho) - 1], && (74)
\end{aligned}
$$

where e_i is the n-dimensional vector consisting of all zeros except for a 1 in the ith component. We use

the same techniques to calculate μ_{ijk}. For i, j, k distinct and skipping algebraic manipulations, we have

$$\begin{aligned}
\mu_{ijk} &= \mathrm{E}((Y_i - \mathrm{E}(Y_i))(Y_j - \mathrm{E}(Y_j))(Y_k - \mathrm{E}(Y_k))) && (75)\\
&= \mathrm{E}(Y_iY_jY_k) - \mathrm{E}(Y_iY_j)\mathrm{E}(Y_k) - \mathrm{E}(Y_iY_k)\mathrm{E}(Y_j) - \mathrm{E}(Y_jY_k)\mathrm{E}(Y_i) + 2\mathrm{E}(Y_i)\mathrm{E}(Y_j)\mathrm{E}(Y_k) && (76)\\
&= \mathrm{E}(Y_iY_jY_k) - 3\mathrm{E}(Y_iY_j)\mathrm{E}(Y_k) + 2\exp(3\mu + 3\sigma^2/2) && (77)\\
&= \mathrm{E}(Y_iY_jY_k) - 3\exp((e_i+e_j)^T\vec{\mu} + \frac{1}{2}(e_i+e_j)^T\Sigma(e_i+e_j))\exp(\mu+\sigma^2/2) + 2\exp(3\mu+3\sigma^2/2) && (78)\\
&= \mathrm{E}(Y_iY_jY_k) - 3\exp(2\mu+\sigma^2+\rho\sigma^2)\exp(\mu+\sigma^2/2) + 2\exp(3\mu+3\sigma^2/2), && (79)
\end{aligned}$$

where

$$\begin{aligned}
\mathrm{E}(Y_iY_jY_k) &= \mathrm{E}(\exp(Z_i+Z_j+Z_k)) && (80)\\
&= \exp((e_i+e_j+e_k)^T\vec{\mu} + \frac{1}{2}(e_i+e_j+e_k)^T\Sigma(e_i+e_j+e_k)) && (81)\\
&= \exp(3\mu + (3\sigma^2+6\rho\sigma^2)/2). && (82)
\end{aligned}$$

Combining gives $\mu_{ijk} = \exp(3\mu+(3\sigma^2+6\rho\sigma^2)/2) - 3\exp(2\mu+\sigma^2+\rho\sigma^2)\exp(\mu+\sigma^2/2) + 2\exp(3\mu+3\sigma^2/2)$. Using the same approach, it is straightforward to compute, for $i \neq j$, $\mu_{ijj} = \exp(3\mu+5\sigma^2/2+2\rho\sigma^2) - 2\exp(3\mu+3\sigma^2/2+\rho\sigma^2) - \exp(3\mu+5\sigma^2/2) + 2\exp(3\mu+3\sigma^2/2)$. This leads to

$$b \approx \left(\frac{1}{n\Omega}\right)\left(\frac{\exp(\sigma^2(\rho+1)) - 2\exp(2\rho\sigma^2) - n + \exp(2\sigma^2) + n\exp(2\rho\sigma^2)}{(\exp(\sigma^2)-1)(\exp(\sigma^2)+2)}\right), \quad (83)$$

the first factor of which indicates that b decreases as Ω increases as long as the numerator of the second factor does not modify or eliminate that apparent relationship.

Results for distributions with normal marginals (figures S21 on page 43 through S26 on page 48) always showed no relationship between $\log(v)$ and $\log(m)$. The value $b \approx 0$ was always obtained, as expected.

Results for distributions with log-normal marginals (figures S27 on page 49 through S32 on page 54) always supported TL (the $\log(v)$-versus-$\log(m)$ relationship was always approximately linear, with statistical tests generally failing to reject the hypotheses of linearity and homoskedasticity), and b was smaller for larger values of ρ. For $\sigma = 0.1$, (56) was a qualitatively and quantitatively good approximation. For $\sigma = 0.5$, equation (56) qualitatively reflected the same dependence of b on ρ as simulations, but was not quantitatively accurate. For larger values of σ, (56) was neither qualitatively nor quantitatively accurate.

We carried out independent tests of the accuracy of the delta method approximations for the continuous distributions considered above using the ideas in the text immediately preceding lemma 4. As explained there, the delta method approximations were considered "good" when $\sqrt{\mathrm{var}(m)} = \sqrt{V\Omega}$ and $\sqrt{\mathrm{var}(v)}$ are smaller than values proportional to $\mathrm{E}(m) = M$ and $\mathrm{E}(v)$, respectively, where the level of "goodness" required is determined by the choice of the constant of proportionality. We used proportionality constant 0.5, requiring $\sqrt{V\Omega} \leq M/2$ and $\sqrt{\mathrm{var}(v)} \leq \mathrm{E}(v)/2$ for the approximation to be deemed adequate. All the quantities in these inequalities are simple functions of the moments already computed as described in the previous paragraphs, except for $\mathrm{var}(v)$. Rather than using lemma 3 to approximate $\mathrm{var}(v)$, which would have required that we compute fourth-order moments numerically, we used the sample variance of all sample variances computed in the numeric analysis (see section S6). A second, numeric method of assessing the accuracy of the delta method approximations was also used, described in section S6. Results of assessing the accuracy of delta method approximations are shown on plots in sections S8 and S10, as described in section S6.

S4 Cases: Distributions constructed using Gaussian copulas and non-identically distributed marginals

As in section S3, we constructed a multivariate random variable $Y = (Y_1, \ldots, Y_n)$ using techniques that amount to the use of Gaussian copulas, but we no longer required that the Y_i are identically distributed. We did require that they all come from the same family of distributions, e.g., they are all normally distributed, or all gamma distributed, etc.

Letting $X = (X_1, \ldots, X_n)$ be a multivariate normal random variable with mean $(0, \ldots, 0)$ and covariance matrix with diagonal entries 1 and off-diagonal entries ρ, we let $Y_i = \varphi_i(X_i)$, where φ_i are transformations that produce the desired marginal distributions. The parameter ρ controls the degree of synchrony. Simulations were used to evaluate the effects of synchrony on $\log(v)$-versus-$\log(m)$ relationships for Y_i obeying gamma, normal, exponential, log-normal, chi-squared, Poisson, and negative binomial distributions.

The initial general procedure for gamma, normal, exponential, and log-normal marginals was to consider Y such that Y_i is distributed in the same way as $f_i Y_1$ for $f_i > 0$ for $i = 2, \ldots, n$. For each of these families of distributions, requiring that Y_1 is in the family is sufficient to guarantee that Y_i is also in the family. This is not true for the negative binomial, Poisson, or chi-squared families. They are treated in different ways, described below.

For gamma distributions, for a variety of different Y_1, we used $f_i = 1 + (i-1)/4$ (results in figures S35 on page 57 through S40 on page 62). For exponential distributions, for a variety of different Y_1, we used $f_i = i$ (results in figure S41 on page 63 through S42 on page 64). We also used $f_i = i$ for normal distributions (results in figures S45 on page 67 through S50 on page 72) and for log-normal distributions (results in figures S51 on page 73 through S56 on page 78).

In all cases, TL was qualitatively validated: although more than 5% of tests for heteroskedasticity or curvature often rejected their null hypotheses with 95% confidence, curvature and heteroskedasticity were modest, and visually undetectable in most $\log(v)$-versus-$\log(m)$ plots. In all cases, TL slope initially decreased as ρ increased from 0. For larger values of n, this initial decrease was steeper. For $\rho \gg 0$, $\log(v)$-versus-$\log(m)$ simulations clustered very tightly around a linear regression line, i.e., residuals were very small.

For all the distributions, in the limit as $\rho \to 1$, we approach the case $Y_i = f_i Y_1$. In this case, $m = \text{mean}_i(Y_i) = \text{mean}_i(f_i Y_1) = Y_1 \text{mean}_i(f_i)$, and $v = \text{var}_i(Y_i) = \text{var}_i(f_i Y_1) = Y_1^2 \text{var}_i(f_i)$. Therefore, $\log(v) = 2\log(Y_1) + \log(\text{var}_i(f_i))$, $\log(m) = \log(Y_1) + \log(\text{mean}_i(f_i))$, and $\log(v) = 2\log(m) - 2\log(\text{mean}_i(f_i)) + \log(\text{var}_i(f_i))$. Thus in the limit as $\rho \to 1$, we expect a perfect TL, with slope 2, as the plots cited above showed: middle panels in plots showed TL slopes approaching 2, while TL root mean square errors approached zero, as ρ approached 1. Sometimes the TL slope approached 2 from above, sometimes from below. Sometimes the overall pattern of dependence of TL slope on ρ was $\cup$-shaped, i.e., exhibiting an initial decrease, followed by a minimum, followed by an increase. Sometimes the overall pattern was a monotonic decline.

For the negative binomial distribution, it is not true that if Y_1 is in the family, then $f_i Y_1$ is in the family for a positive constant f_i. To provide examples with negative binomial marginals, we constructed negative binomial distributions Y_i with means μ_i and standard deviations σ_i such that $\mu_i = f_i \mu_1$ and $\sigma_i = f_i \sigma_1$ for positive constants f_i, $i = 2, \ldots, n$. For a variety of negative binomial distributions Y_1 (with parameters r_1 and p_1) in separate runs, we used the well-known formulas for the mean and standard deviation of a negative binomial distribution, $\mu_1 = \frac{r_1 p_1}{1-p_1}$ and $\sigma_1 = \frac{\sqrt{r_1 p_1}}{1-p_1}$. We then assigned $\mu_i = \mu_1 + (i-1)/4$ for $i = 2, \ldots, n$ when n was 25, and $\mu_i = \mu_1 + (i-1)/16$ for $i = 2, \ldots, n$ when n was 100, implicitly defining the $f_i = \mu_i/\mu_1$. We then defined $\sigma_i = f_i \sigma_1$, and let Y_i be the negative binomial distribution with mean μ_i and standard deviation σ_i, for $i = 1, \ldots, n$. It is straightforward to show that there is exactly one such a negative binomial distribution. Results are in figures S57 on page 79 to S64 on page 86.

It is not possible to have Poisson or chi-squared distributions Y_i with $\mu_i = f_i \mu_1$ and $\sigma_i = f_i \sigma_1$. This would make μ_i proportional to σ_i. But for the Poisson family, $\mu_i = \lambda_i$ and $\sigma_i = \sqrt{\lambda_i}$, so $\sigma_i = \sqrt{\mu_i}$, and for

the chi-squared family, $\mu_i = k_i$ and $\sigma_i = \sqrt{2k_i}$, so $\sigma_i = \sqrt{2\mu_i}$, showing that proportionality does not occur in these families. If Y_1 is a chi-squared distribution, and therefore is also a gamma distribution, then $f_i Y_1$ is a gamma distribution; but it is not necessarily also a chi-squared distribution. We nevertheless tried Poisson distributions with a variety of choices for λ_1 and with $\lambda_i = \lambda_1 + i - 1$. Results are in figures S33 on page 55 to S34 on page 56. We also tried chi-squared distributions with a variety of choices for k_1 and with $k_i = k_1 + i - 1$. Results are in figures S43 on page 65 to S44 on page 66.

For Poisson and chi-squared examples, TL was a reasonable approximation, and the slope b declined steeply as ρ increased from 0 and continued to decline across the whole range of ρ. Negative binomial examples often strongly violated the linear hypothesis of TL for larger values of ρ.

S5 Cases: Distributions constructed using sums and identically distributed marginals

We applied the well-known "common elements" method [Fischer, 1933] of constructing a multivariate random variable $(Y_1, \ldots, Y_n)$ such that the Y_i are identically distributed according to some specified distribution, and such that $\mathrm{cor}(Y_i, Y_j) = \rho$ for $i \neq j$. For several common distributions, we defined independent random variables X, X_i, for $i = 1, \ldots, n$ and let $Y_i = X + X_i$. Because X is a summand in all the Y_i, the Y_i are correlated as desired. The approach leads to analytic results about the relationship between the $\log(v)$-versus-$\log(m)$ relationship and synchrony.

To generate Poisson-distributed Y_i with parameters $\mathrm{E}(Y_i) = \mathrm{var}(Y_i) = \lambda$ for all i, let X and X_i for $i = 1, \ldots, n$ be independent Poisson random variables with parameters $\mathrm{E}(X) = \mathrm{var}(X) = \lambda\rho$ and $\mathrm{E}(X_i) = \mathrm{var}(X_i) = \lambda(1 - \rho)$, respectively. Defining $Y_i = X + X_i$, it is well-known that Y_i is Poisson distributed, because the summands are independent, and $\mathrm{E}(Y_i) = \mathrm{E}(X) + \mathrm{E}(X_i) = \lambda\rho + \lambda(1 - \rho) = \lambda$, as desired. Also, for $i \neq j$,

$$\mathrm{cor}(Y_i, Y_j) = \frac{\mathrm{cov}(Y_i, Y_j)}{\lambda} = \frac{\mathrm{cov}(X + X_i, X + X_j)}{\lambda} = \frac{\mathrm{E}(X)}{\lambda} = \rho, \tag{84}$$

as desired. Simulating draws from $(Y_1, \ldots, Y_n)$ is straightforward and computationally efficient.

To evaluate the formulas of theorem 5, we need the moments M, V, μ_{ij}, μ_{iii}, μ_{ijj}, and μ_{ijk} for i, j, and k distinct. By construction, $M = V = \lambda$ and $\mu_{ij} = \rho\lambda$. The third central moment of a Poisson distribution of mean λ is well known, $\mu_{iii} = \lambda$. The moments

$$\mu_{ijj} = \rho \tag{85}$$

$$\mu_{ijk} = \rho \tag{86}$$

were computed by starting with the definitions $\mu_{ijj} = \mathrm{E}((Y_i - \lambda)(Y_j - \lambda)^2)$ and $\mu_{ijk} = \mathrm{E}((Y_i - \lambda)(Y_j - \lambda)(Y_k - \lambda))$, substituting $Y_i = X_i + X$, and using the Matlab symbolic mathematics toolbox.

Plugging the moments into (56) and simplifying gives

$$b \approx \left(\frac{M\mu_{iii}}{V^2}\right)\left(\frac{1}{n\Omega}\right) = \frac{1}{n\Omega}, \tag{87}$$

which decreases with increasing Ω. The decline of b with increasing Ω is more rapid for larger values of n.

We assessed the accuracy of the delta method approximations analytically. As explained in the text immediately preceding lemma 4, we say that the delta method approximations are "good" when $\sqrt{\mathrm{var}(m)} = \sqrt{V\Omega}$ and $\sqrt{\mathrm{var}(v)}$ are smaller than values proportional to $\mathrm{E}(m) = M = \lambda$ and $\mathrm{E}(v)$, respectively, where the level of "goodness" required is determined by the choice of the constant of proportionality. We used proportionality constant 0.5, requiring $\sqrt{V\Omega} \leq M/2$ and $\sqrt{\mathrm{var}(v)} \leq \mathrm{E}(v)/2$ for the approximation to be deemed adequate. The first inequality becomes $\Omega \leq \lambda/4$ and the second becomes $\mathrm{var}(v) \leq \mathrm{E}(v)^2/4$. To analyze the second inequality, we produced analytic expressions for the moments

μ_{iiii}, μ_{iijj}, μ_{iiij}, μ_{iijk} and μ_{ijkl} (for i, j, k, l distinct) appearing in (28) for $\mathrm{var}(v)$, beginning from the definitions of these quantities, and using the Matlab symbolic mathematics toolbox. Moments were

$$\mu_{iiii} = \lambda(3\lambda + 1) \tag{88}$$
$$\mu_{iijj} = \lambda(2\lambda\rho^2 + \rho + \lambda) \tag{89}$$
$$\mu_{iiij} = \lambda\rho(3\lambda + 1) \tag{90}$$
$$\mu_{iijk} = \lambda\rho(\lambda + 2\lambda\rho + 1) \tag{91}$$
$$\mu_{ijkl} = \lambda\rho(3\lambda\rho + 1). \tag{92}$$

We plugged these into (28) and simplified, obtaining $(\lambda(1-\rho)(n + 2\lambda n - 2\lambda n\rho - 1))/(n(n-1)) \leq (\lambda(1-\rho))^2/4$ as an explicit form of the inequality $\mathrm{var}(v) \leq \mathrm{E}(v)^2/4$. For verification, we also assessed the accuracy of the delta method approximations numerically, as described in section S6.

Plots for Poisson examples are in figures S65 on page 87 to S66 on page 88. We conclude that 1) the analytic approximation illustrates the overall shape of the relationship between b and Ω, 2) larger values of synchrony Ω decreased values of the slope b of the $\log(v)$-versus-$\log(m)$ relationship, 3) the slope b goes to zero for large Ω, and 4) the decrease in b with increasing Ω happens faster for larger n, as predicted by the analytic results.

However, additional observations eclipsed these. Simulations often did not obey TL for $\Omega > 0$: the relationship between $\log(v)$ and $\log(m)$ was, for many parameters, nonlinear and/or heteroskedastic. The above conclusions pertain to the $\log(v)$-versus-$\log(m)$ relationship, which was often not described by TL (which postulates linearity). The example $\log(v)$-versus-$\log(m)$ plots in figures S65 on page 87 to S66 on page 88 show that values of $\Omega > 0$ modified the TL pattern that occurs for $\Omega = 0$ by smearing points rightward in $\log(v)$-versus-$\log(m)$ space, decreasing b.

The same analytic strategy was applied to other distributions. Let X be negative binomially distributed with parameters $r_X = \rho r$ and p, and let the X_i be independent (with respect to each other and X) negative binomials with parameters $r_i = r - r_X = r(1-\rho)$ and p. Defining $Y_i = X + X_i$, it is known that Y_i is negative binomial with parameters $r_X + r_i = r$ and p, as desired; it is also easy to show, since the variance of a negative binomial with parameters r and p is $pr/(1-p)^2$, that $\mathrm{cor}(Y_i, Y_j) = \rho$, as desired. Simulating draws from $(Y_1, \ldots, Y_n)$ is straightforward and computationally efficient. Standard formulas for negative binomial moments provide

$$M = pr/(1-p) \tag{93}$$
$$V = pr/(p-1)^2 \tag{94}$$
$$\mu_{iii} = (pr(p+1))/(1-p)^3 \tag{95}$$
$$\mu_{iiii} = pr(4p + 3pr + p^2 + 1)/(p-1)^4. \tag{96}$$

Additional moments were computed by starting with their definitions, inserting $Y_i = X_i + X$, and using the Matlab symbolic mathematics toolbox,

$$\mu_{ij} = (pr\rho)/(p-1)^2 \tag{97}$$
$$\mu_{ijk} = (pr\rho(p+1))/(1-p)^3 \tag{98}$$
$$\mu_{ijj} = (pr\rho(p+1))/(1-p)^3 \tag{99}$$
$$\mu_{iijj} = pr(p^2\rho + 2rp\rho^2 + 4p\rho + rp + \rho)/(p-1)^4 \tag{100}$$
$$\mu_{iiij} = pr\rho(4p + 3pr + p^2 + 1)/(p-1)^4 \tag{101}$$
$$\mu_{iijk} = pr\rho(4p + pr + p^2 + 2pr\rho + 1)/(p-1)^4 \tag{102}$$
$$\mu_{ijkl} = pr\rho(4p + p^2 + 3pr\rho + 1))/(p-1)^4, \tag{103}$$

where i, j, k, l are distinct. These formulas were substituted into (56) and the result was algebraically simplified to

$$b \approx \left(\frac{M\mu_{iii}}{V^2}\right)\left(\frac{1}{n\Omega}\right) = \frac{p+1}{n\Omega}, \tag{104}$$

which again displays a decreasing dependence on synchrony, with a faster decrease for larger values of n. The above expressions were also substituted into $\mathrm{var}(m) \leq \mathrm{E}(m)^2/4$ and $\mathrm{var}(v) \leq \mathrm{E}(v)^2/4$ to obtain the following constraints required for adequate accuracy of the delta method approximations:

$$\frac{pr(n\rho - \rho + 1)}{n(p-1)^2} \leq \left(\frac{pr}{2(1-p)}\right)^2 \tag{105}$$

$$\frac{pr(1-\rho)(n - 4p + 4np + np^2 - p^2 + 2npr - 2npr\rho - 1)}{n(n-1)(p-1)^4} \leq \left(\frac{pr(1-\rho)}{2(p-1)^2}\right)^2. \tag{106}$$

The same numeric and plotting code (see section S6) that was applied to the Poisson distribution was also applied to the negative binomial. Figures S67 on page 89 to S74 on page 96 lead to similar conclusions about the relationship between b and Ω, but, as in the Poisson case, simulations often did not obey TL for $\Omega > 0$, and larger values of Ω destroyed the TL pattern by smearing points right in $\log(v)$-versus-$\log(m)$ space instead of modifying the slope while preserving linearity.

The same analytic strategy was applied to the gamma distribution. Let X be gamma distributed with shape and rate parameters $\rho\alpha$ and β, and let the X_i be independent (with respect to each other and X) gammas with parameters $\alpha(1-\rho)$ and β. It is known that that $Y_i = X + X_i$ is gamma distributed, with shape parameter equal to the sum of the shape parameters of X and X_i, α, and rate parameter equal to the common rate parameter for the summands, β. It is straightforward to see that $\mathrm{cor}(Y_i, Y_j) = \rho$ for $i \neq j$, as desired. Simulating draws from $(Y_1, \ldots, Y_n)$ is again straightforward and computationally efficient. Moments were from standard formulas or were computed by inserting $Y_i = X + X_i$ into the moment definitions and computing:

$$M = \alpha/\beta \tag{107}$$

$$V = \alpha/\beta^2 \tag{108}$$

$$\mu_{ij} = \alpha\rho/\beta^2 \tag{109}$$

$$\mu_{iii} = 2\alpha/\beta^3 \tag{110}$$

$$\mu_{ijk} = 2\alpha\rho/\beta^3 \tag{111}$$

$$\mu_{ijj} = 2\alpha\rho/\beta^3 \tag{112}$$

$$\mu_{iiii} = 3\alpha(\alpha+2)/\beta^4 \tag{113}$$

$$\mu_{iijj} = \alpha(2\alpha\rho^2 + 6\rho + \alpha)/\beta^4 \tag{114}$$

$$\mu_{iiij} = 3\alpha\rho(\alpha+2)/\beta^4 \tag{115}$$

$$\mu_{iijk} = \alpha\rho(\alpha + 2\alpha\rho + 6)/\beta^4 \tag{116}$$

$$\mu_{ijkl} = 3\alpha\rho(\alpha\rho+2)/\beta^4. \tag{117}$$

In these formulas, i, j, k and l are distinct. The moments were substituted into (56) and the result was algebraically simplified to give

$$b \approx \left(\frac{M\mu_{iii}}{V^2}\right)\left(\frac{1}{n\Omega}\right) = \frac{2}{n\Omega}, \tag{118}$$

which again displays a decreasing dependence on synchrony, with a faster decrease for larger values of n. The above expressions were also substituted into $\mathrm{var}(m) \leq \mathrm{E}(m)^2/4$ and $\mathrm{var}(v) \leq \mathrm{E}(v)^2/4$ to obtain the

constraints required for adequate accuracy of the delta method approximations:

$$\frac{\alpha(n\rho-\rho+1)}{\beta^2 n} \leq \frac{\alpha^2}{4\beta^2} \tag{119}$$

$$\frac{2\alpha(1-\rho)(3n+\alpha n-\alpha n\rho-3)}{\beta^4 n(n-1)} \leq \left(\frac{\alpha(1-\rho)}{2\beta^2}\right)^2. \tag{120}$$

The same numeric and plotting code (section S6) yielded outputs in figures S75 on page 97 to S80 on page 102.

It is well known that the exponential and chi-squared distributions are special cases of the gamma distribution, therefore these cases were explored with the same formulas and plotting code described above, with outputs in figures S81 on page 103 to S84 on page 106. The same conclusions about the dependence of b on Ω as for the Poisson and negative binomial distributions hold here. However, as in those cases, simulations often did not obey TL for $\Omega > 0$, and increasing synchrony destroyed TL by smearing points toward the right in $\log(v)$-versus-$\log(m)$ space, producing smaller values of b.

The same analytic strategy was applied to the normal distribution (parameters μ, the mean, and σ, the standard deviation). The results were, for distinct i, j, k,

$$M = \mu \tag{121}$$

$$V = \sigma^2 \tag{122}$$

$$\mu_{ij} = \rho\sigma^2 \tag{123}$$

$$\mu_{iii} = 0 \tag{124}$$

$$\mu_{ijk} = 0 \tag{125}$$

$$\mu_{ijj} = 0 \tag{126}$$

$$\mu_{iiii} = 3\sigma^4 \tag{127}$$

$$\mu_{iijj} = \sigma^4(2\rho^2+1) \tag{128}$$

$$\mu_{iiij} = 3\rho\sigma^4 \tag{129}$$

$$\mu_{iijk} = \rho\sigma^4(2\rho+1) \tag{130}$$

$$\mu_{ijkl} = 3\rho^2\sigma^4 \tag{131}$$

$$b \approx 0, \tag{132}$$

subject to the requirements

$$\frac{\sigma^2(n\rho-\rho+1)}{n} \leq \mu^2/4 \tag{133}$$

$$\frac{2\sigma^4(\rho-1)^2}{n-1} \leq \frac{\sigma^4(1-\rho)^2}{4} \tag{134}$$

for the delta method approximations to be adequate. This result reflects the fact, evident from (56), that TL slope is zero whenever there is no skewness in the common marginal distribution Y_i. Plots for the normal distribution are in figures S85 on page 107 to S90 on page 112.

The following result encompasses the examples described above and illuminates them.

Proposition 6. *Let $P \subseteq [0,1)$ and suppose we have independent random variables $X(\rho)$, $X_i(\rho)$ for $\rho \in P$ and $i = 1,\ldots,n$ such that for each ρ the $X_i(\rho)$ for $i = 1,\ldots,n$ are identically distributed. Let $Y_i(\rho) = X(\rho) + X_i(\rho)$ and assume $\mathrm{cor}(Y_i(\rho), Y_j(\rho)) = \rho$ and $\mathrm{E}(Y_i(\rho)) = M$ and $\mathrm{var}(Y_i(\rho)) = V$ for all ρ and $i \neq j$, for constants M and V. Let $m(\rho) = \mathrm{mean}_i(Y_i(\rho))$ and $v(\rho) = \mathrm{var}_i(Y_i(\rho))$ be the sample mean and variance. Then $\mathrm{E}(v(\rho))$ decreases and $\mathrm{var}(m(\rho))$ increases as ρ increases. Furthermore,*

$$b(\rho) \approx \frac{M(n-1)\mu_3^{(X_i(\rho))}}{n^2V^2(1-\Omega(\rho))\Omega(\rho)} \tag{135}$$

where $b(\rho)$ and $\Omega(\rho)$ are the TL slope and synchrony defined previously, and $\mu_3^{(X_i(\rho))}$ is the third central moment of $X_i(\rho)$. If $\mu_3^{(X_i(\rho))}$ is proportional to $1-\rho$ then $b(\rho)$ is approximately proportional to $\frac{1}{\Omega(\rho)}$.

Proof. We omit the explicit dependence of X, X_i, Y_i, etc. on ρ. Using the independence of the X, X_i and the assumption that the X_i for $i = 1, \ldots, n$ are identically distributed for any given ρ,

$$\begin{aligned}
\mathrm{cor}(Y_i, Y_j) &= \frac{\mathrm{cov}(Y_i, Y_j)}{\sqrt{\mathrm{var}(Y_i)\mathrm{var}(Y_j)}} && (136)\\
&= \frac{\mathrm{var}(X)}{\mathrm{var}(Y_i)} && (137)\\
&= \frac{\mathrm{var}(X)}{V} && (138)\\
&= \rho, && (139)
\end{aligned}$$

so $\mathrm{var}(X) = \rho V$. Also by independence, $V = \mathrm{var}(Y_i) = \mathrm{var}(X + X_i) = \mathrm{var}(X) + \mathrm{var}(X_i)$, so $\mathrm{var}(X_i) = V - \rho V = V(1-\rho)$. Thus $\mathrm{E}(v) = \mathrm{E}(\mathrm{var}_i(Y_i)) = \mathrm{E}(\mathrm{var}_i(X + X_i)) = \mathrm{E}(\mathrm{var}_i(X_i)) = \mathrm{var}(X_i) = V(1-\rho)$, which decreases as ρ increases. Next,

$$\begin{aligned}
\mathrm{var}(m) &= \mathrm{var}(\mathrm{mean}_i(Y_i)) && (140)\\
&= \mathrm{var}(\mathrm{mean}_i(X + X_i)) && (141)\\
&= \mathrm{var}(X + \mathrm{mean}_i(X_i)) && (142)\\
&= \mathrm{var}(X) + \mathrm{var}(\mathrm{mean}_i(X_i)) && (143)\\
&= \mathrm{var}(X) + \frac{1}{n^2}\sum_{i=1}^{n} \mathrm{var}(X_i) && (144)\\
&= \frac{V}{n}((n-1)\rho + 1), && (145)
\end{aligned}$$

which increases as ρ increases.

Combining (19) and (52),

$$b \approx \frac{n-1}{MnV(1-\Omega)} \frac{\mathrm{cov}(m, v)}{\mathrm{var}(\ln(m))}. \tag{146}$$

By lemma 2, this becomes

$$b \approx \frac{M(n-1)\mathrm{cov}(m, v)}{nV^2(1-\Omega)\Omega}. \tag{147}$$

But

$$\begin{aligned}
\mathrm{cov}(m, v) &= \mathrm{cov}(X + \mathrm{mean}_i(X_i), \mathrm{var}_i(X_i)) && (148)\\
&= \mathrm{cov}(m_{X_i}, v_{X_i}), && (149)
\end{aligned}$$

where $m_{X_i} = \mathrm{mean}_i(X_i)$ and $v_{X_i} = \mathrm{var}_i(X_i)$. Because the X_i are independent and identically distributed, it is known [Zhang, 2007, Cohen and Xu, 2015] that $\mathrm{cov}(m_{X_i}, v_{X_i}) = \frac{\mu_3^{(X_i)}}{n}$. Therefore $\mathrm{cov}(m, v) = \frac{\mu_3^{(X_i)}}{n}$, and combining this expression with (147) gives (135). The last statement of the theorem follows because

$$\begin{aligned}
1 - \Omega &= 1 - \frac{1}{n^2}\sum_{ij} \mathrm{cor}(Y_i, Y_j) && (150)\\
&= \left(\frac{n-1}{n}\right)(1-\rho). && (151)
\end{aligned}$$

■

The theorem pertains in its entirety to the Poisson, negative binomial, gamma, and normal examples examined above because in these cases, $\mu_3^{(X_i)}$ is $\lambda(1-\rho)$, $\frac{(1+p)pr(1-\rho)}{(1-p)^3}$, $\frac{2\alpha(1-\rho)}{\beta^3}$, and 0, respectively, each of which is proportional to $1-\rho$. The "rightward smearing" of points in $\log(v)$-versus-$\log(m)$ space that occurred as synchrony increased from 0 in the examples above corresponds to the increases in $\text{var}(m)$ with increasing ρ in proposition 6.

The analytic strategy we applied above to Poisson, negative binomial, gamma, and normal examples cannot be applied to the log-normal distribution because it is not true that the sum of two independent log-normally distributed random variables is another log-normally distributed random variable. However, a slightly modified strategy could be applied, because the product of two independent log-normally distributed random variables is another log-normally distributed random variable. We did not carry out such an analysis.

For the examples considered in this section, $\mu_{ijj} = \mu_{ijk}$ (for the Poisson, see (85) and (86); for the negative binomial, see (98) and (99); for the gamma, which encompasses chi-squared and exponential, see (111) and (112); for the normal, see (125) and (126)). More generally:

Proposition 7. *Let X and X_i for $i = 1, \ldots, n$ be independent random variables and let the X_i be identically distributed. Let $Y_i = X + X_i$. Then $\mu_{ijj} = \mu_{ijk}$ for all i, j, k distinct.*

Proof. Using the definitions

$$\mu_{ijj} = \text{E}((Y_i - \text{E}(Y_i))(Y_j - \text{E}(Y_j))(Y_j - \text{E}(Y_j))) \tag{152}$$
$$\mu_{ijk} = \text{E}((Y_i - \text{E}(Y_i))(Y_j - \text{E}(Y_j))(Y_k - \text{E}(Y_k))) \tag{153}$$

and substituting $Y_i = X + X_i$ and using the Matlab symbolic manipulation toolbox, we get

$$\mu_{ijj} = 2\text{E}(X)^3 - 3\text{E}(X^2)\text{E}(X) + \text{E}(X^3) \tag{154}$$
$$\mu_{ijk} = 2\text{E}(X)^3 - 3\text{E}(X^2)\text{E}(X) + \text{E}(X^3). \tag{155}$$

■

S6 Methods for the omnibus plots

For all distributions Y considered, simulation-based results were generated and plotted, and for some of them approximate analytic or semi-analytic results were also plotted. The assumption of TL that the $\log(v)$-versus-$\log(m)$ relationship is linear was also tested. An omnibus plot summarizing these results was generated for each example considered. Components of the plot are described here.

Simulation-based results. Given a random vector $Y(\rho) = (Y_1(\rho), \ldots, Y_n(\rho))$ for a fixed ρ, 5000 independent realizations were generated in 50 blocks of $N = 100$ realizations each. For each realization, the sample mean, m, and the sample variance, v, were computed, producing 50 blocks of 100 pairs (m, v). For each of a few example values of ρ (e.g., 0, 0.1, 0.5, 0.9), $\log(v)$ was plotted as a function of $\log(m)$ using all 5000 pairs (m, v) except those for which either m or v was 0. The plots were placed at the top of the omnibus plot. Axes were the same on all top panels within a plot, to facilitate comparison. Axis number labels are only shown on alternate top panels within a plot.

For each block separately, the slope b was computed through ordinary linear regression of $\log(v)$ against $\log(m)$, again omitting pairs for which m or v was 0. The value of Ω was also computed for each block (separately) as the average Pearson correlation coefficient between realizations of Y_i and Y_j in that block, the average being computed over pairs i and j, including cases with $i = j$ (which necessarily produced a correlation of 1). The average (across blocks) b value was plotted against the average (across blocks) Ω value, as ρ ranged from 0 to 0.9 in increments of 0.1, with error bars plotted for both quantities based on standard deviations (across blocks). For each block, residuals of the $\log(v)$-versus-$\log(m)$ regression were

computed and used to generate a root mean squared error (RMSE). The mean (across blocks) RMSE was plotted against Ω. Both b and RMSE were plotted against Ω in the central panel of the omnibus plot.

Analytic results. When possible (e.g., figures S11 on page 33 through S32 on page 54), the approximation (56) was computed for each value of ρ, either analytically or semi-analytically (here "semi-analytic" refers to calculations for which the constituent moments of (56) were calculated numerically, though with negligible error, see, e.g., (66)), and plotted against ρ in red on the central panel of the omnibus plot. Whether the approximation (56) could be computed depended on whether the moments in that expression could be evaluated either analytically or numerically. Calculation of moments from samples was not used because it is unreliable for reasonable numbers of samples for some of the required moments and distributions. How we evaluated moments, when available, is described on a case-by-case basis in sections above. When the inequalities $\sqrt{\mathrm{var}(m)} \leq \mathrm{E}(m)/2$ and $\sqrt{\mathrm{var}(v)} \leq \mathrm{E}(v)/2$ were satisfied (see section S3), a red downward-pointing triangle was superimposed on the point, indicating an independent validation of the approximations underlying (56) for that point. The quality of the delta-method approximations underlying (56) was also evaluated numerically by testing the quality of the approximations (21) and (25). When the correlations of the left and right sides of those formulas, across all 5000 samples from Y, were greater than 0.75, a red upward-pointing triangle was superimposed on the point.

Assumptions of Taylor's law. For each value of ρ, the fraction of 5000 samples from Y producing $m = 0$ was plotted on the bottom panel of the omnibus plot, as was the fraction of samples producing $v = 0$. Samples with either $m = 0$ or $v = 0$ were omitted from the estimation and testing of Taylor's law. The $\log(v)$-versus-$\log(m)$ relationship is conditional on positive m and v.

TL postulates a linear relationship between $\log(v)$ and $\log(m)$, so linearity was evaluated. For each block, the linear relationship $\log(v) = b\log(m) + c$ was tested against a quadratic alternative, $\log(v) = a\log(m)^2 + b\log(m) + c$ using a standard F-test, and the p-value was recorded. The fraction of blocks for which this p-value was less than 0.05 was plotted against Ω on the bottom panel of the omnibus plot. When this value substantially exceeded the type-I error rate of 0.05, significant curvature existed in the $\log(v)$-versus-$\log(m)$ relationship. This curvature could be modest (assessed visually through the example panels at the top of the omnibus plot) even when significant.

Homoskedasticity of the $\log(v)$-versus-$\log(m)$ relationship was also tested. For each block, absolute residuals from the regression $\log(v) = b\log(m) + c$ were computed and regressed against predictions of the same linear model. The p-value was recorded for the test of the null hypothesis that the slope of this latter regression was 0, a non-zero slope indicating heteroskedasticity. The fraction of blocks for which this p-value was less than 0.05 was plotted against ρ on the bottom panel of the omnibus plot. When this value substantially exceeded 0.05, significant heteroskedasticity existed in the $\log(v)$-versus-$\log(m)$ relationship.

S7 Data details

Rothamsted Insect Survey (RIS) runs a network of suction traps that sample flying aphids [Macaulay et al., 1988, Harrington, 2014, Bell et al., 2015]. Daily aphid counts are collected throughout the flight season for many species at multiple locations. Twenty species (table S1) and 11 locations (table S2) were selected in advance of any analyses. Species were selected for their commonness (necessary for analyses of synchrony) and their importance as pests and as models for studies of population dynamics. Locations were selected for long duration of operation. The total count for a species over all days for a year was taken as the count for that species and year. RIS suction trap locations were chosen decades ago to give optimal coverage of the UK, subject to resource limitations. Nevertheless, relative to the whole UK, there are some gaps in the network of 11 traps we used, in Wales, Northern Ireland, and central southern England. After processing, time series were annual, from 1976 through 2010. See Sheppard et al. [2015] for additional details.

The Continuous Plankton Recorder (CPR) survey, now operated by the Sir Alister Hardy Foundation for Ocean Science (SAHFOS), has sampled the seas around the UK and elsewhere for plankton abundances

since before World War II, using a sampling device towed behind commercial ships [Batten et al., 2003, Beaugrand and Reid, 2003, Raitsos et al., 2013]. The device is towed at about 7 m depth. Water is filtered through a moving band of silk, which is later cut into sections representing samples of 3 cubic meters of sea water over 10 nautical miles, thereby producing spatiotemporal data through repeat tows. Minimal changes have been made to the sampling device and analysis procedure over the history of the survey, to ensure consistency [Batten et al., 2003]. The resulting database contains estimates of the abundance of more than 500 taxa on a very large number of transects. We examined 22 phytoplankton and zooplankton taxa (table S1), selected prior to any analyses for their common occurrence and their importance for marine ecosystems. Samples are typically taken along standard routes approximately once a month, but precise times and locations are irregular, being influenced by ship availability and weather. Samples were compiled into 26 annual time series for 2×2 degree areas of sea around the UK. Time series were from 1958 through 2013.

The California Cooperative Oceanic Fisheries Investigations (CalCOFI) has surveyed the California Current System off southern California since 1949 on a monthly-to-quarterly basis. Chlorophyll-a has been regularly measured since 1984 [Mantayla et al., 2008]. Time series from spring sampling for the 28 years from 1984 to 2011 were used (average of March-May sampling). Eighteen of 73 sampling stations were omitted, including 7 coastal stations and another 11 stations which are too shallow or have too many gaps in the time series. The remaining 55 sites were divided into four groups based on distance from shore, with group 1 near to shore (average 87.7 km) and group 4 far from shore (average 539.3 km). For each site and sampling occasion, chlorophyll samples were drawn from 0, 10, 20, 30, 50, 75, 100, 125, 150, and 200 m depths. Samples were filtered through Whatman GF/F filters and cold-extracted in a 90% acetone solution in the dark and under refrigeration and then measured fluorometrically using an acidification technique. Sampling and measuring protocols are described in detail on the CalCOFI web site (`http://calcofi.org/ccpublications/calcofi-methods.html`).

CalCOFI data can be downloaded from their website. SAHFOS and RIS data can be obtained by contacting those institutes and going through their long-established data sharing procedures.

S8 Figures, distributions constructed using Gaussian copulas and identically distributed marginals

A, B

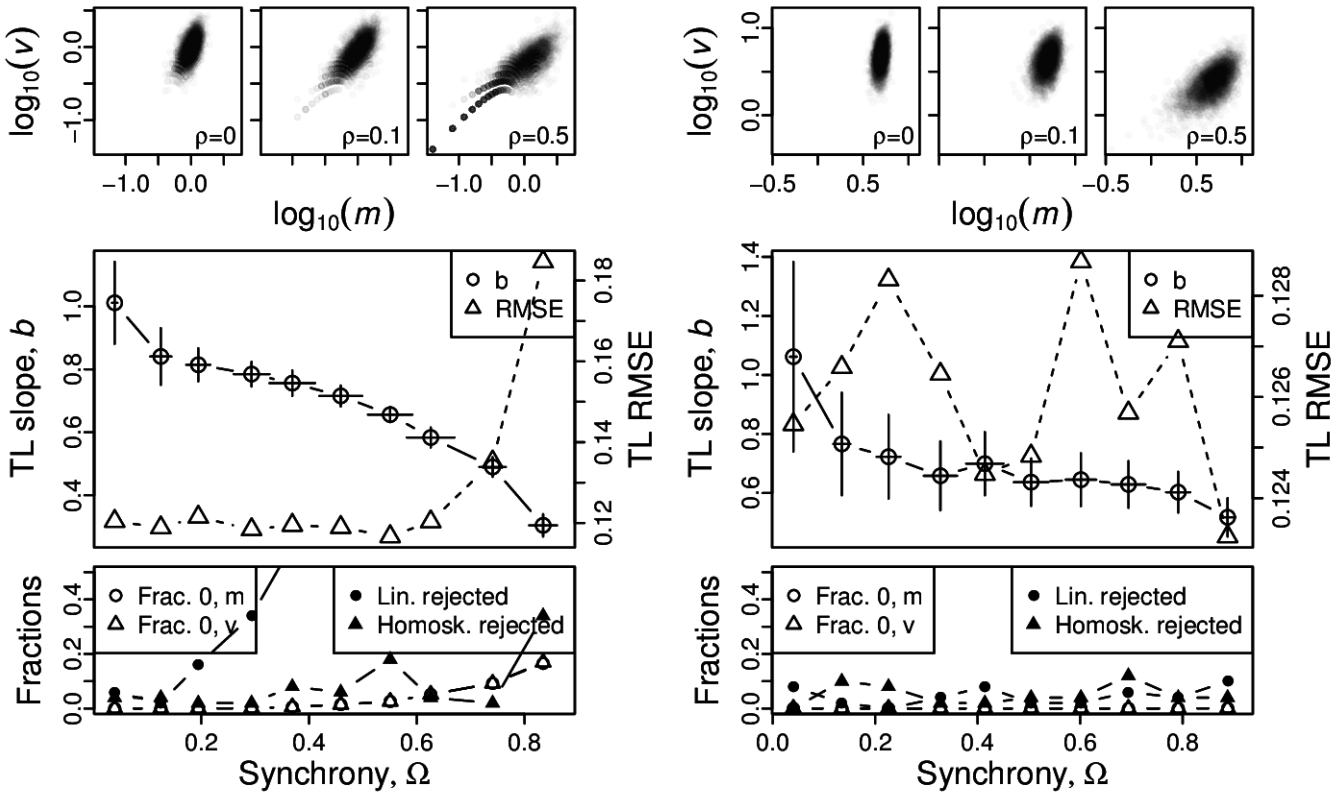

C, D

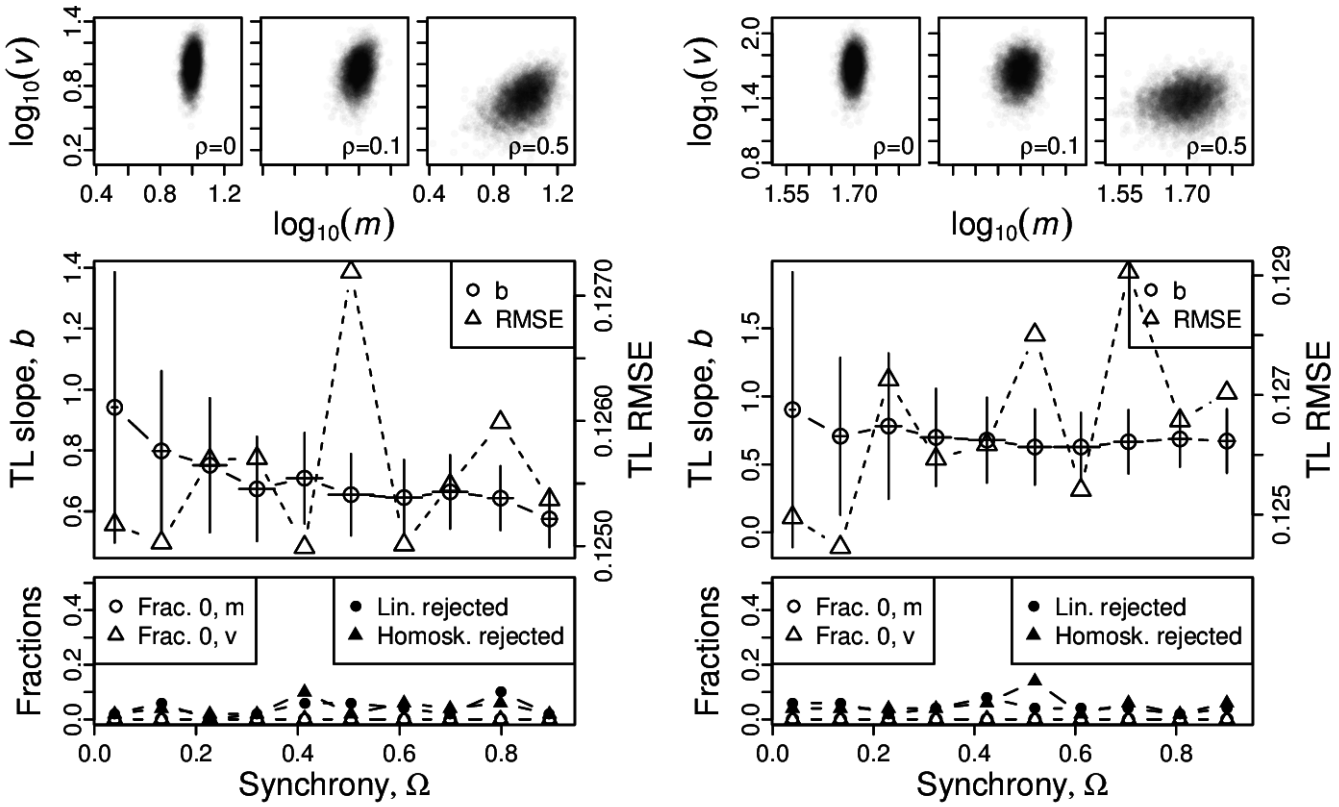

Figure S1: Omnibus plots (see section S6) for identically distributed Poisson marginals under the set up of section S3, for $n = 25$, for $\lambda = 1$ (A), $\lambda = 5$ (B), $\lambda = 10$ (C), and $\lambda = 50$ (D).

A, B

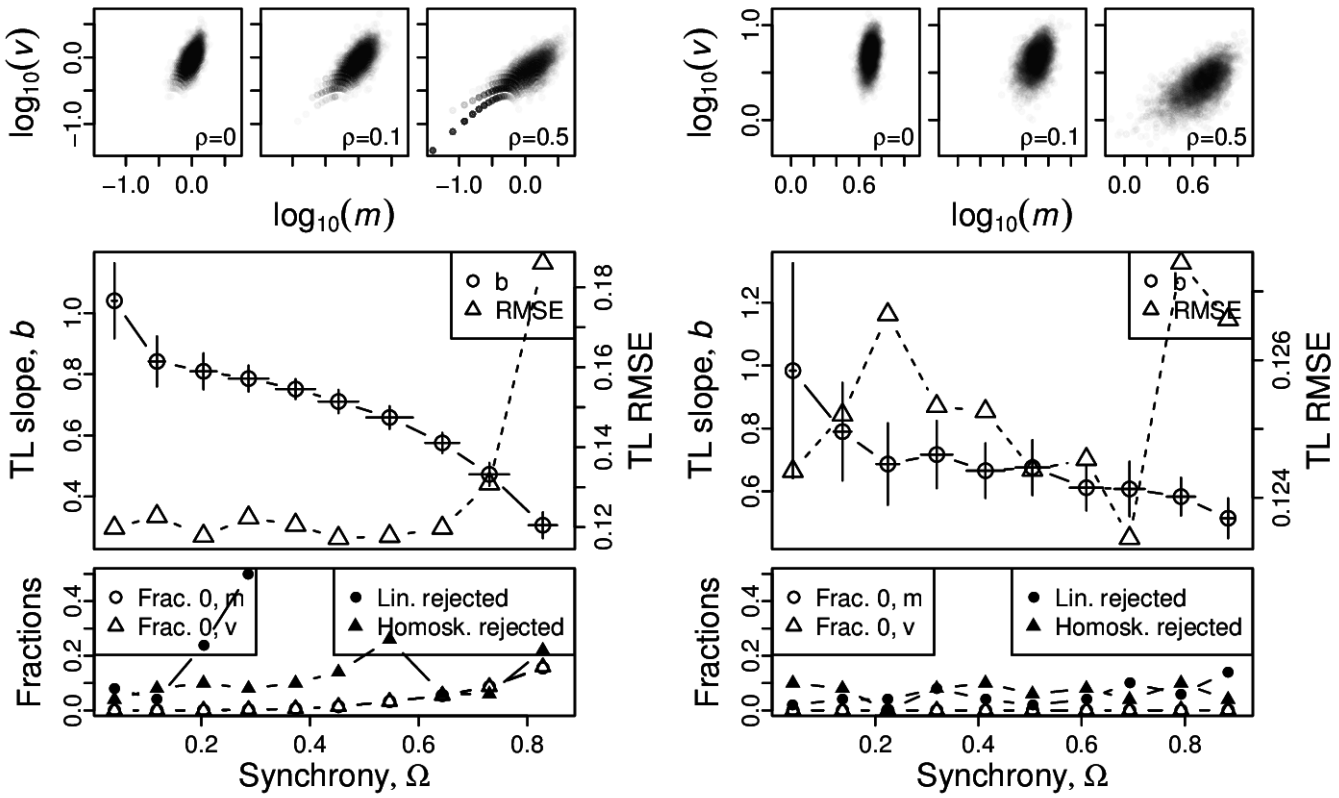

C, D

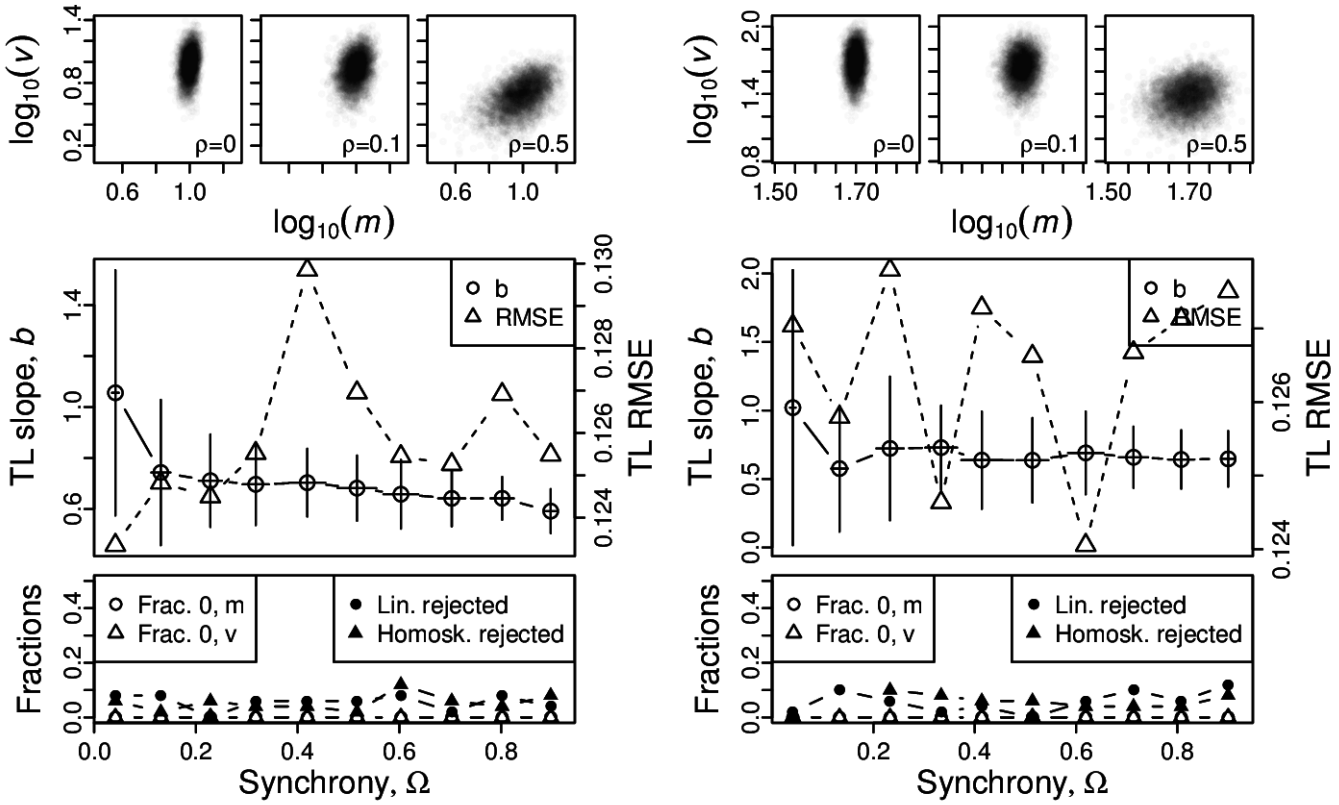

Figure S2: Omnibus plots (see section S6) for identically distributed Poisson marginals under the set up of section S3, for $n = 100$, for $\lambda = 1$ (A), $\lambda = 5$ (B), $\lambda = 10$ (C), and $\lambda = 50$ (D).

A, B

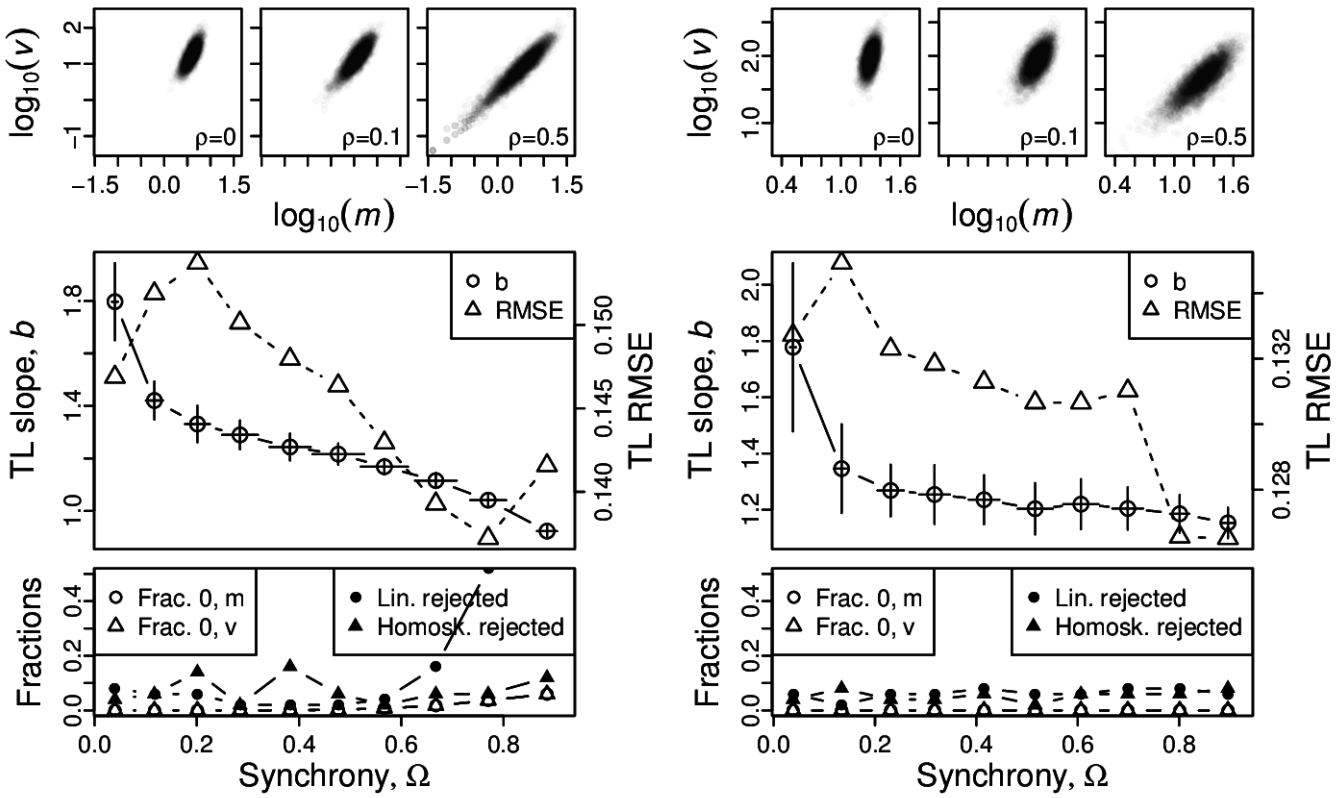

C, D

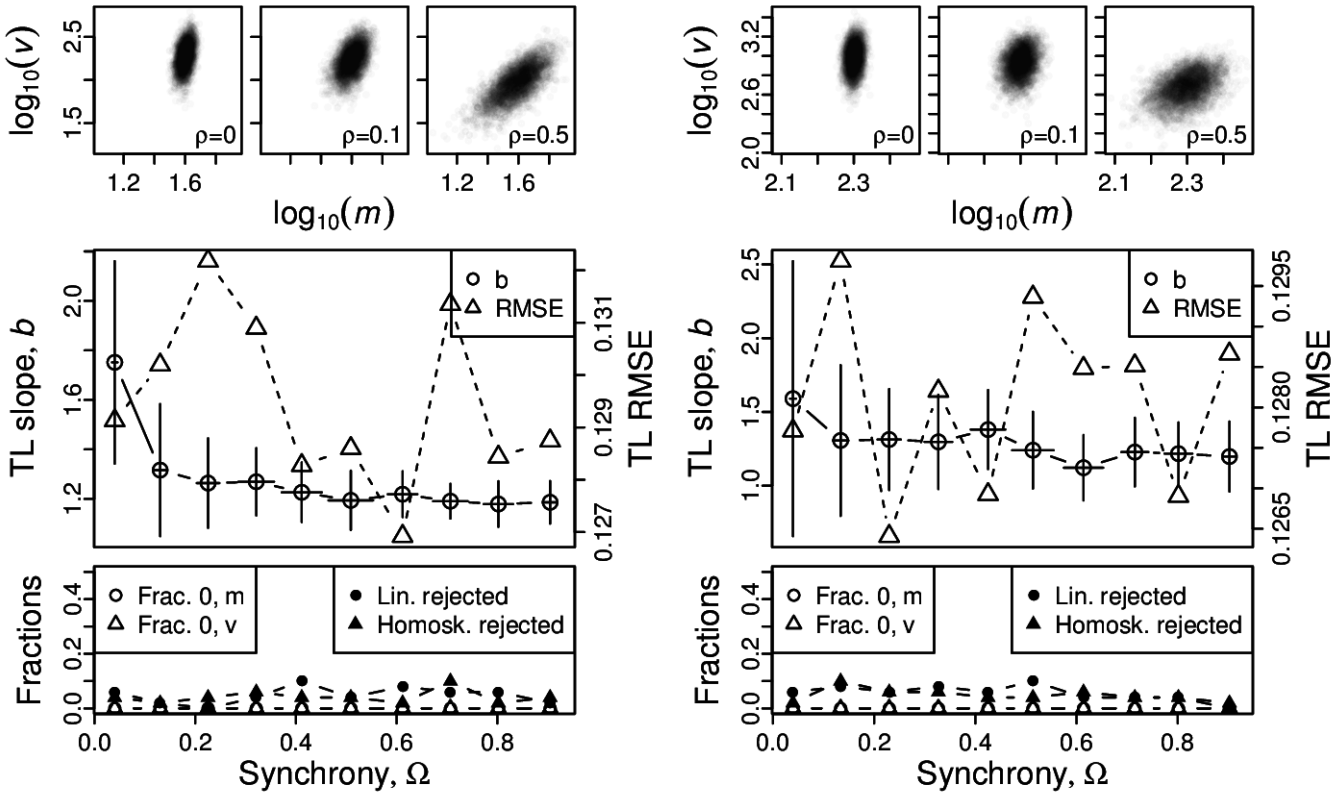

Figure S3: Omnibus plots (see section S6) for identically distributed negative binomial marginals under the set up of section S3, for $n = 25$ and $p = 0.2$, for $r = 1$ (A), $r = 5$ (B), $r = 10$ (C), and $r = 50$ (D).

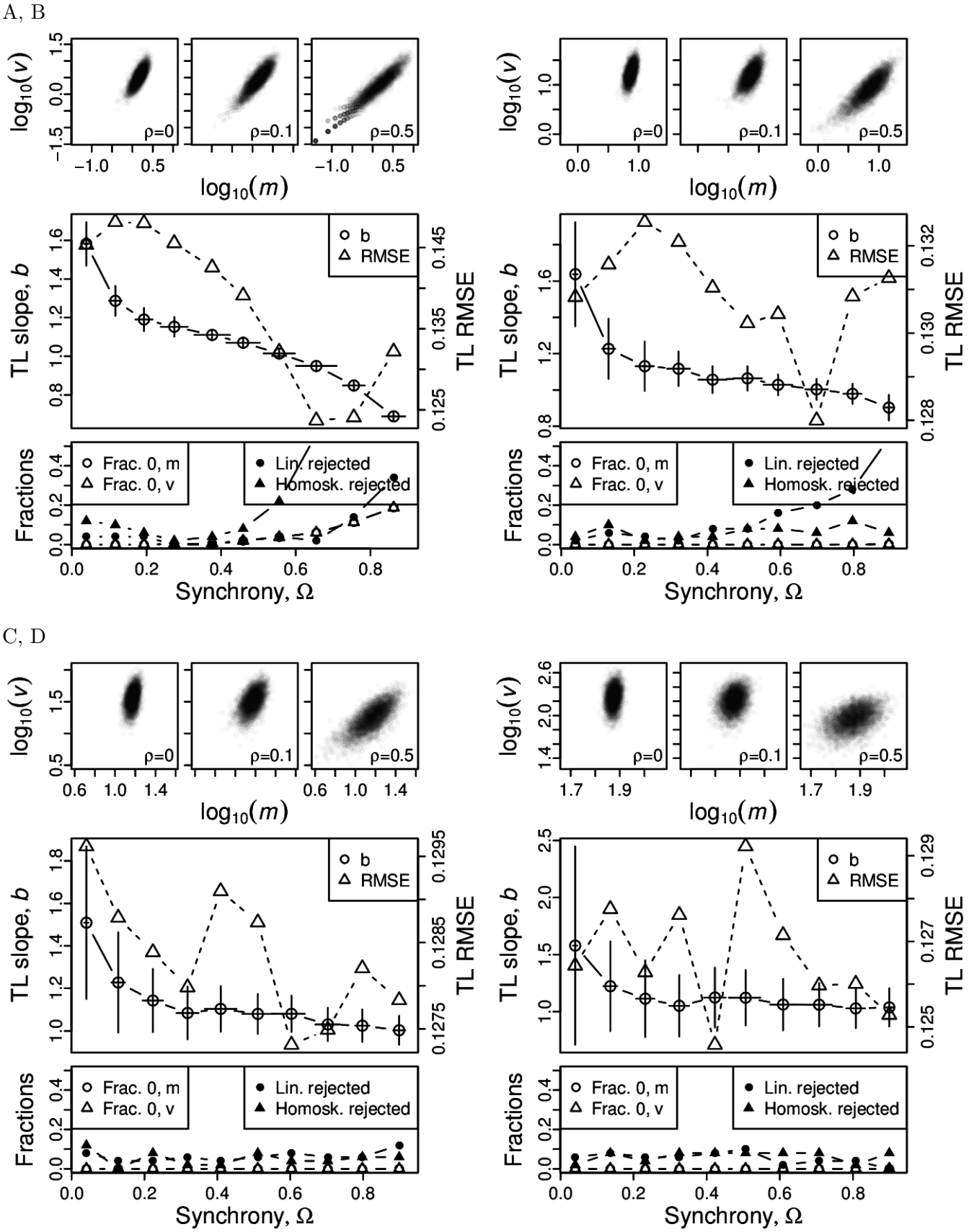

Figure S4: Omnibus plots (see section S6) for identically distributed negative binomial marginals under the set up of section S3, for $n = 25$ and $p = 0.4$, for $r = 1$ (A), $r = 5$ (B), $r = 10$ (C), and $r = 50$ (D).

A, B

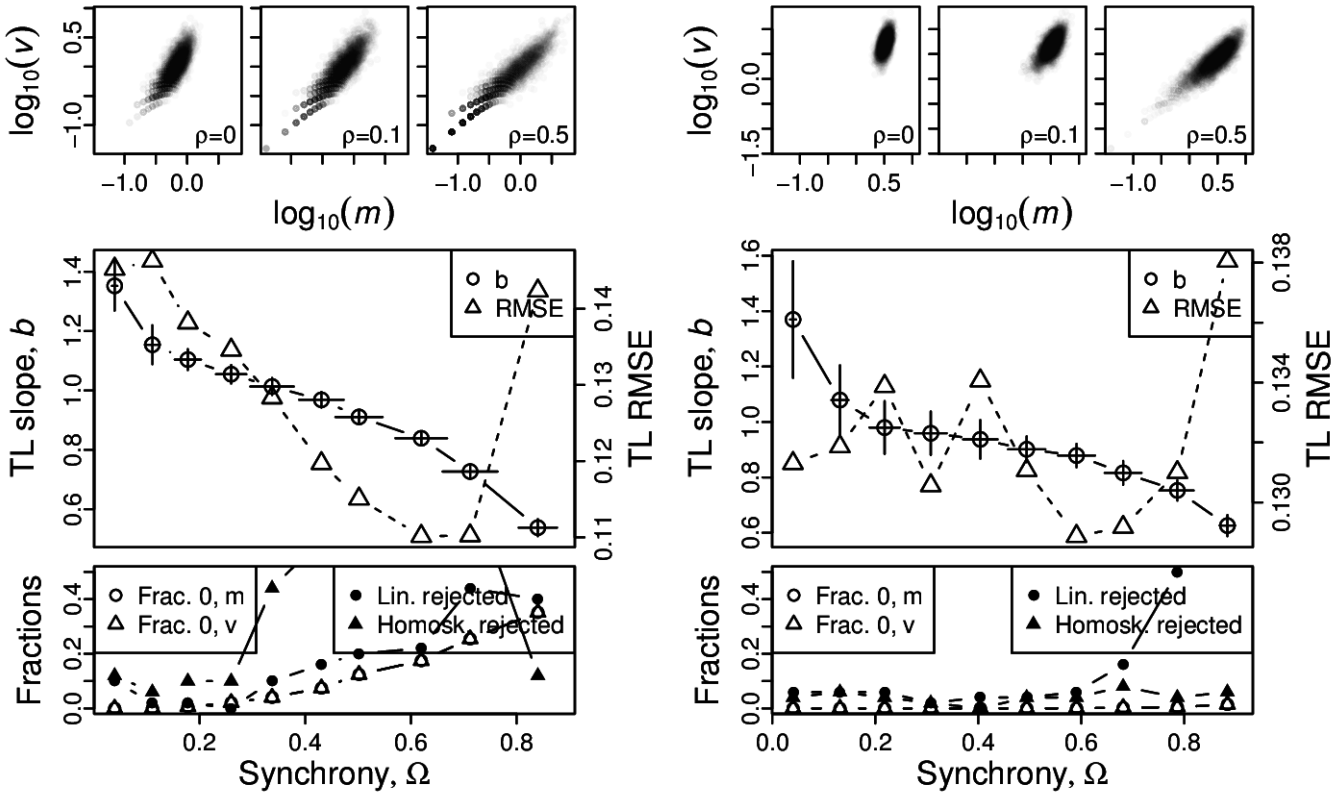

C, D

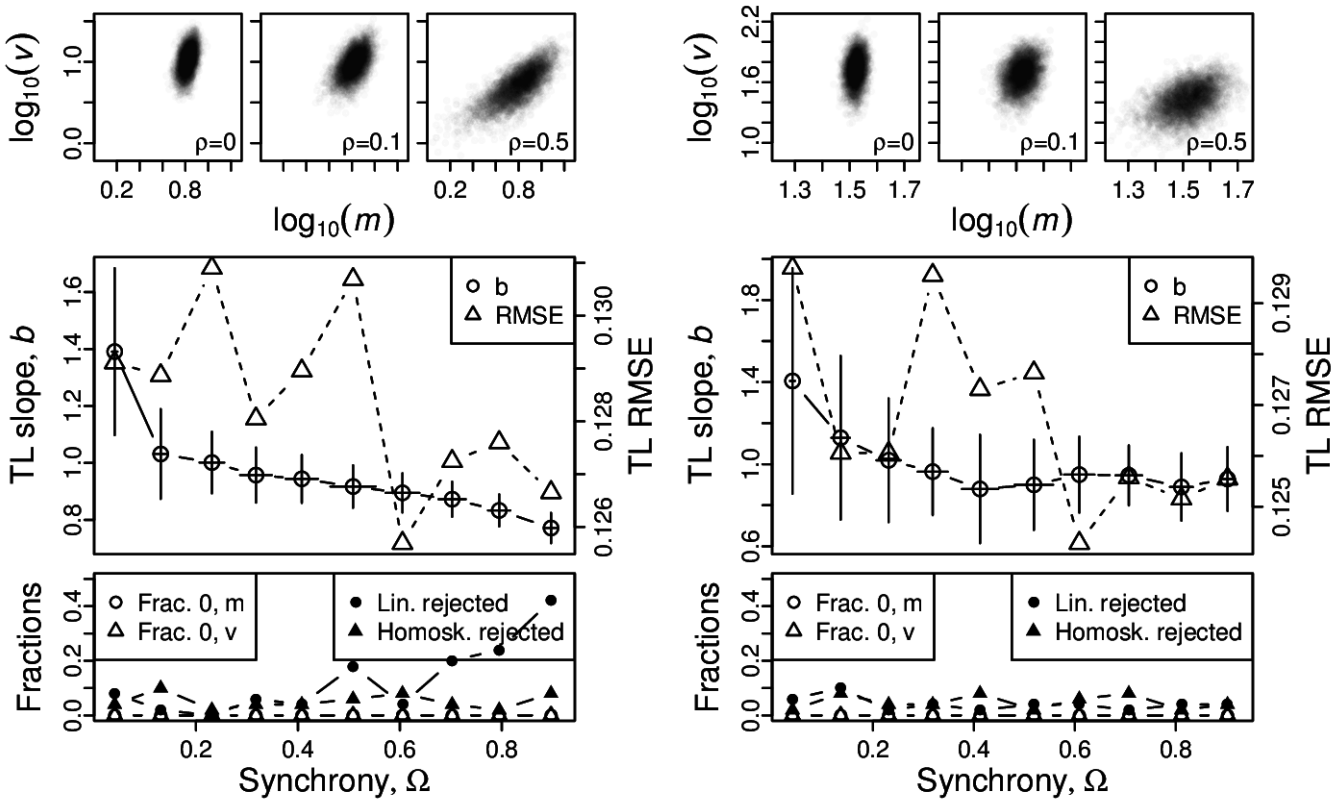

Figure S5: Omnibus plots (see section S6) for identically distributed negative binomial marginals under the set up of section S3, for $n = 25$ and $p = 0.6$, for $r = 1$ (A), $r = 5$ (B), $r = 10$ (C), and $r = 50$ (D).

A, B

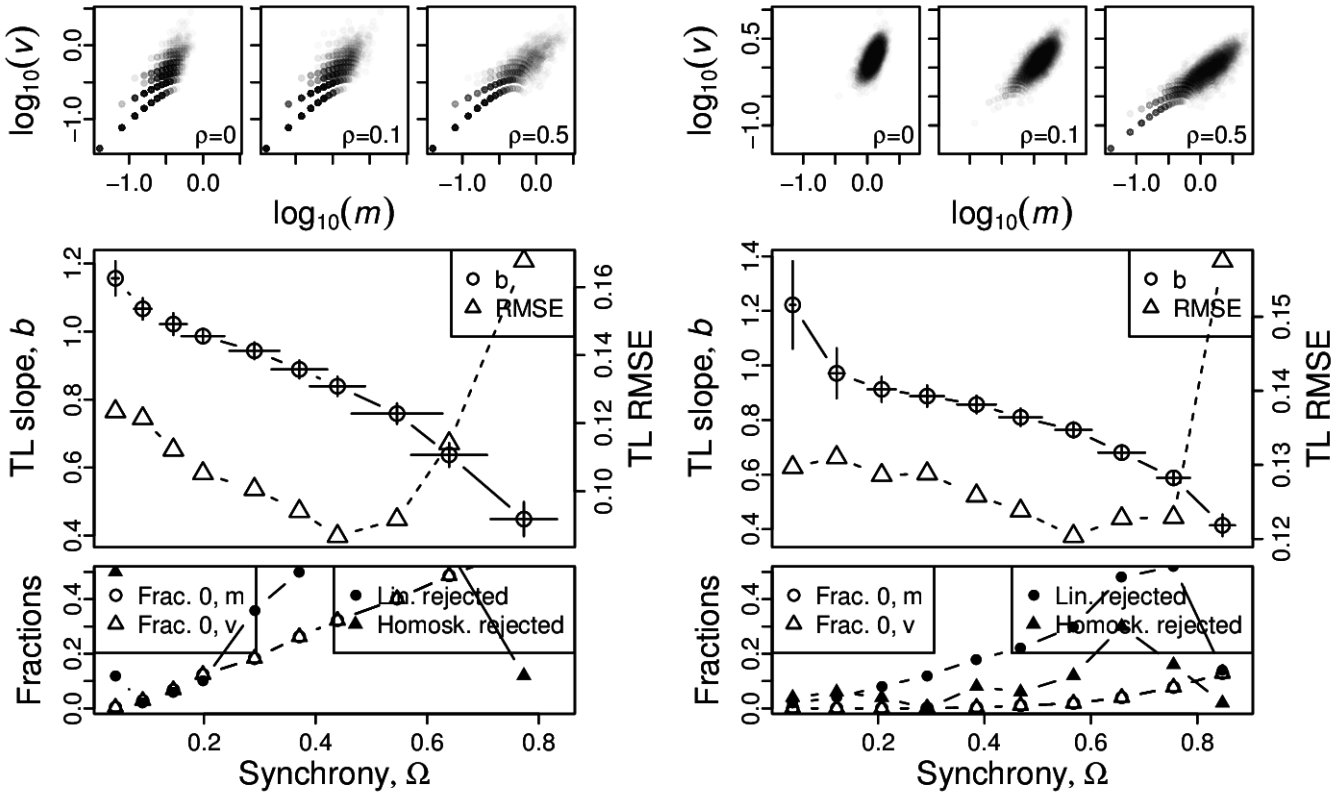

C, D

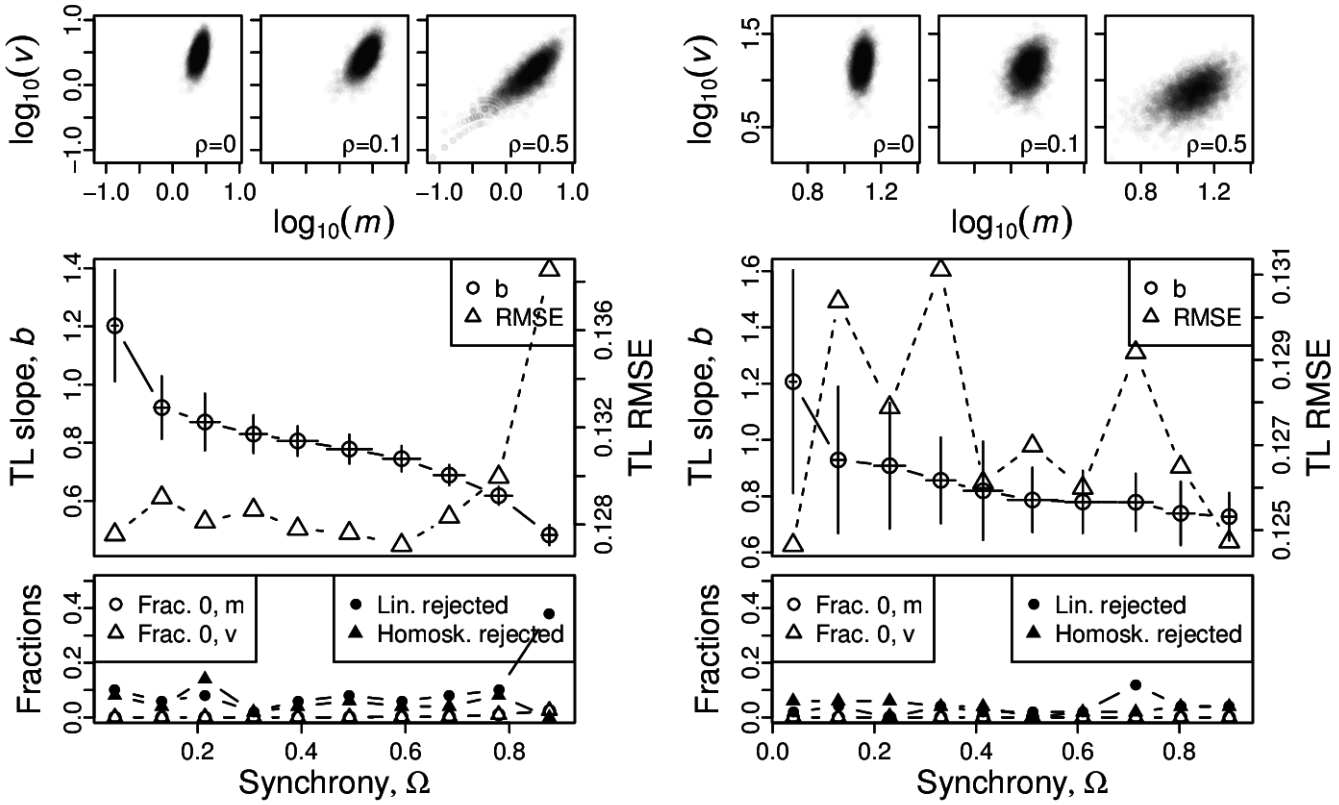

Figure S6: Omnibus plots (see section S6) for identically distributed negative binomial marginals under the set up of section S3, for $n = 25$ and $p = 0.8$, for $r = 1$ (A), $r = 5$ (B), $r = 10$ (C), and $r = 50$ (D).

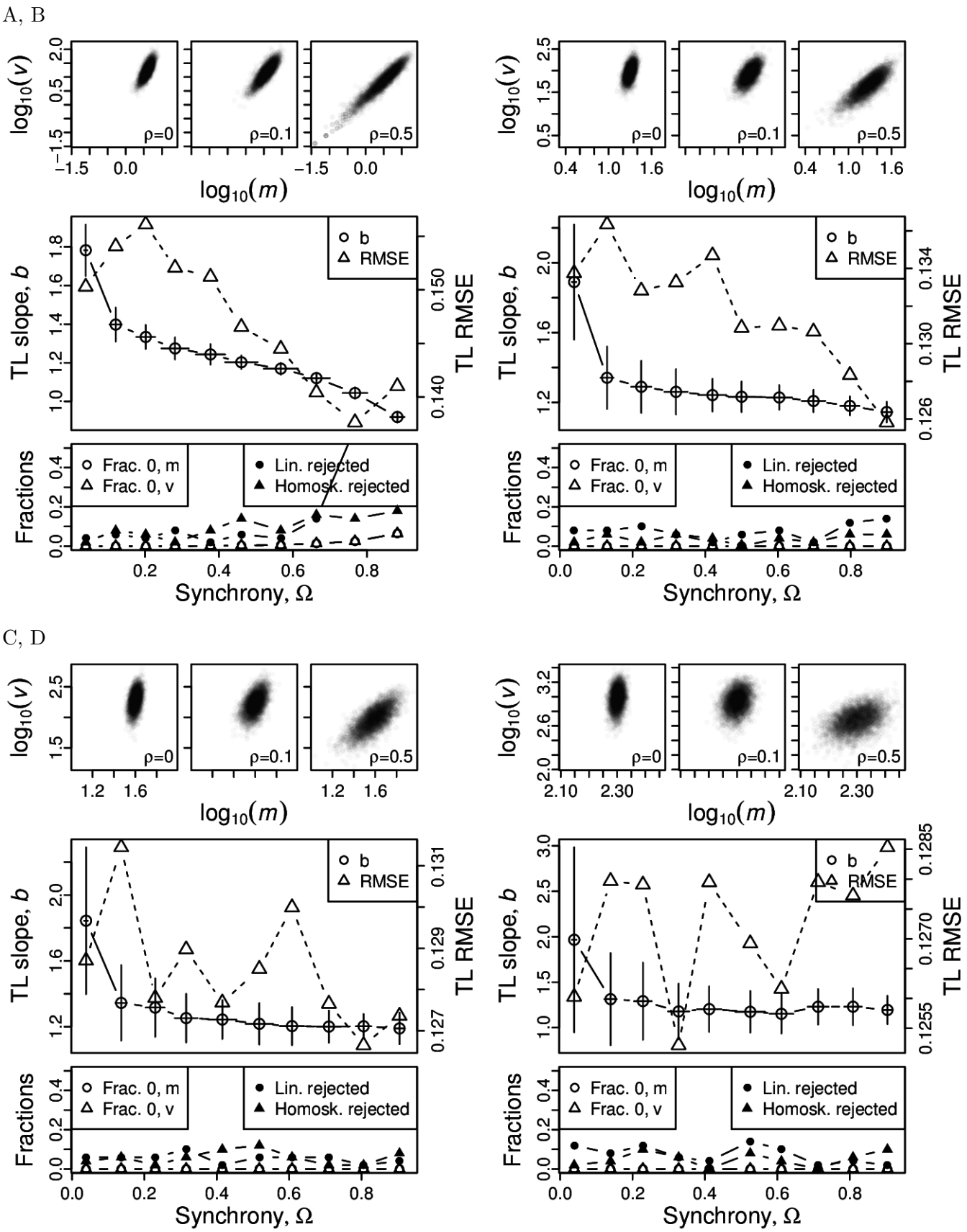

Figure S7: Omnibus plots (see section S6) for identically distributed negative binomial marginals under the set up of section S3, for $n = 100$ and $p = 0.2$, for $r = 1$ (A), $r = 5$ (B), $r = 10$ (C), and $r = 50$ (D).

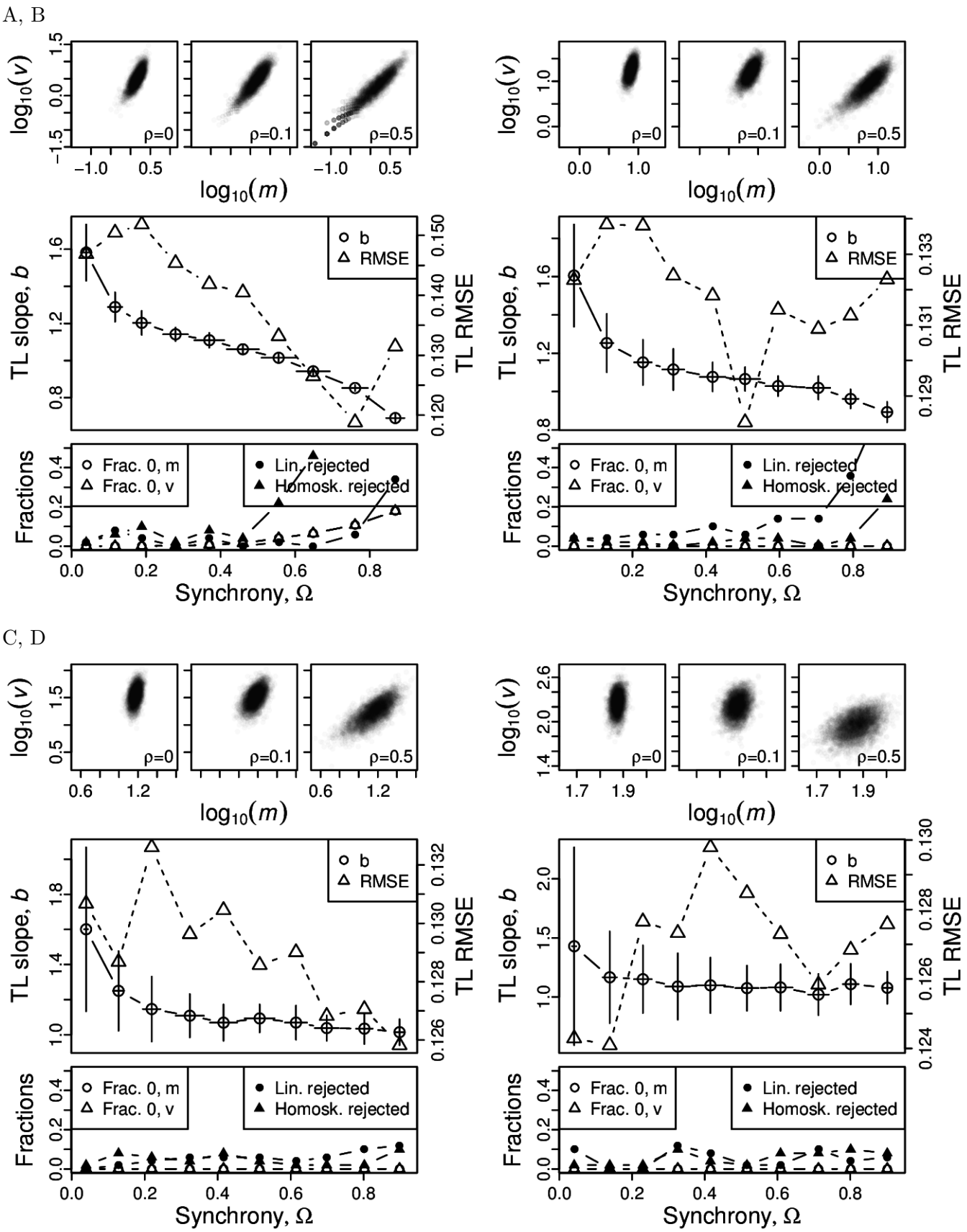

Figure S8: Omnibus plots (see section S6) for identically distributed negative binomial marginals under the set up of section S3, for $n = 100$ and $p = 0.4$, for $r = 1$ (A), $r = 5$ (B), $r = 10$ (C), and $r = 50$ (D).

A, B

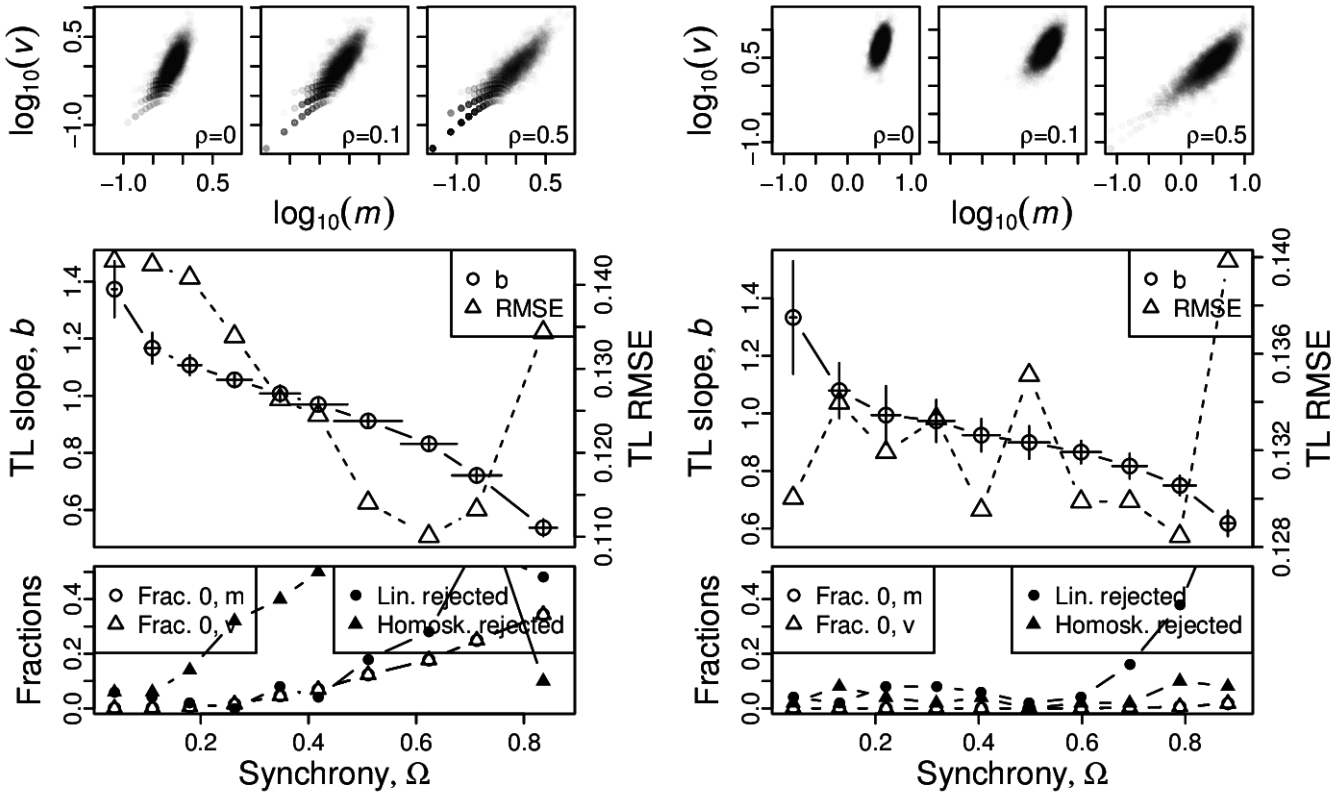

C, D

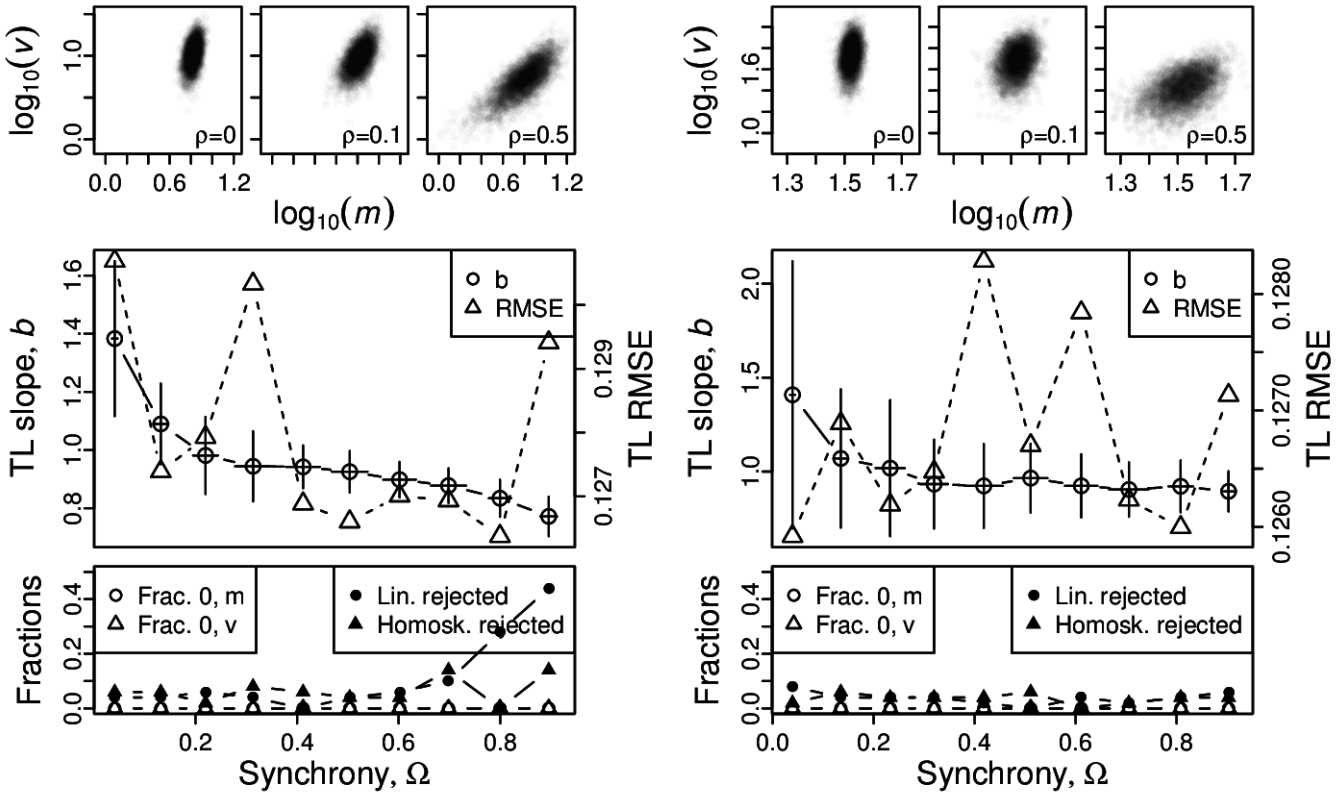

Figure S9: Omnibus plots (see section S6) for identically distributed negative binomial marginals under the set up of section S3, for $n = 100$ and $p = 0.6$, for $r = 1$ (A), $r = 5$ (B), $r = 10$ (C), and $r = 50$ (D).

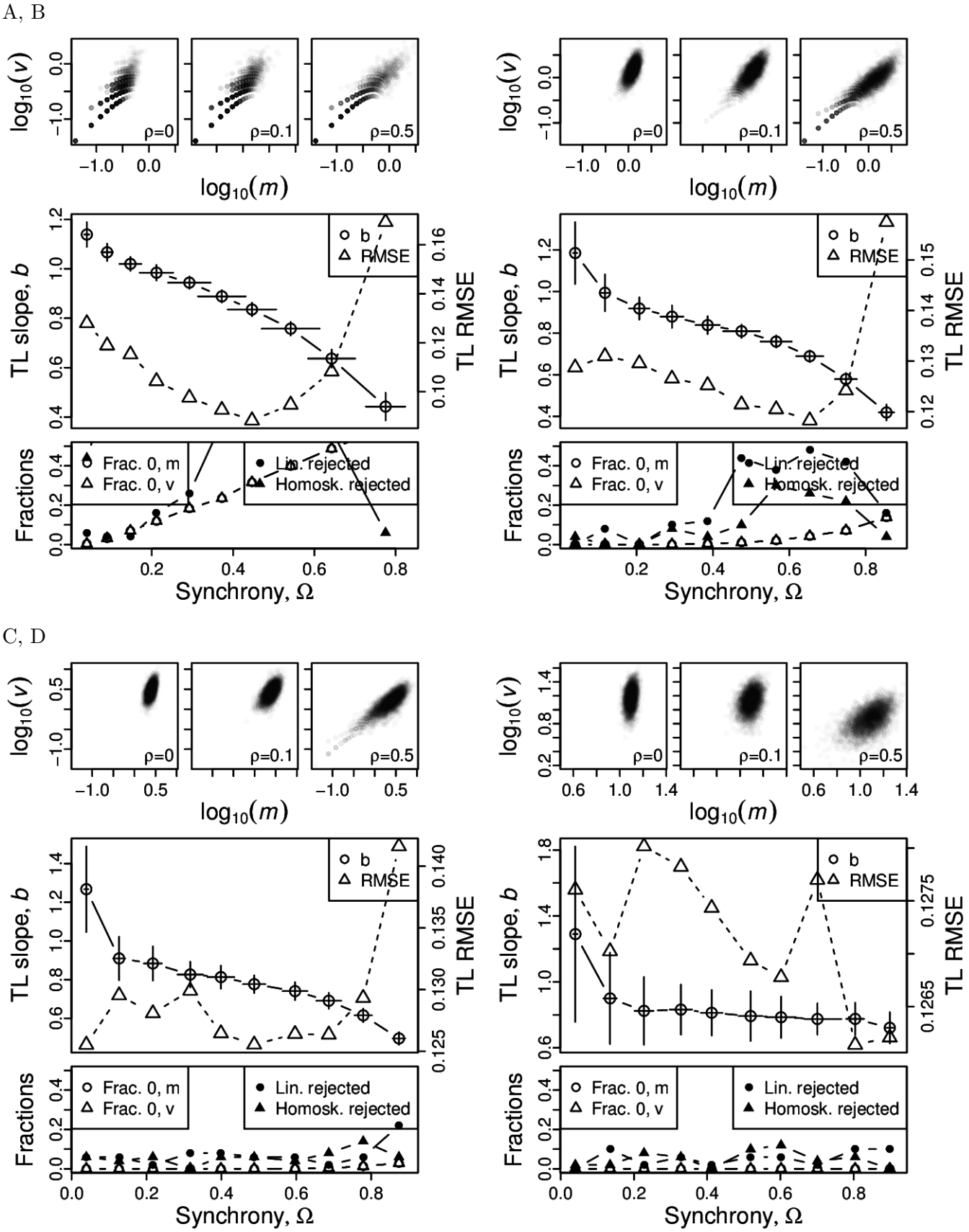

Figure S10: Omnibus plots (see section S6) for identically distributed negative binomial marginals under the set up of section S3, for $n = 100$ and $p = 0.8$, for $r = 1$ (A), $r = 5$ (B), $r = 10$ (C), and $r = 50$ (D).

A, B

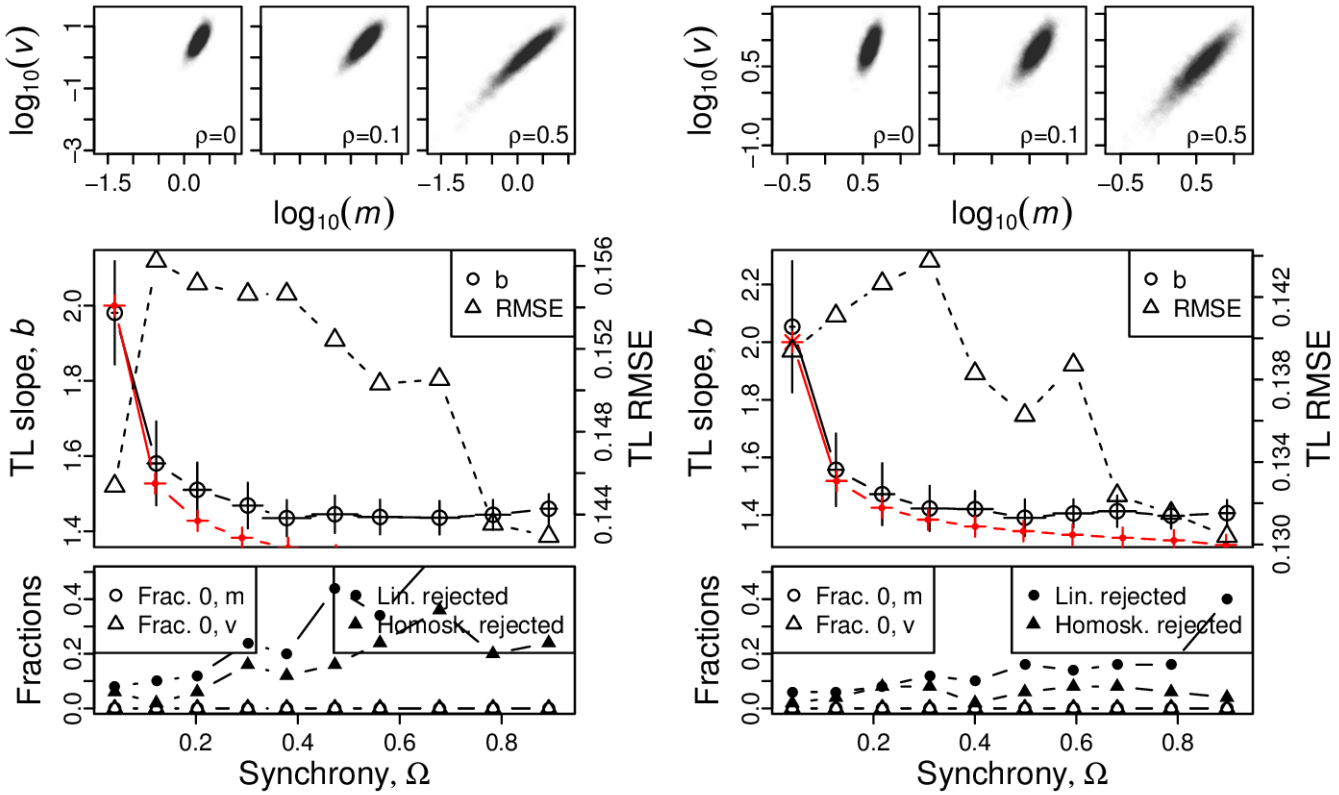

C, D

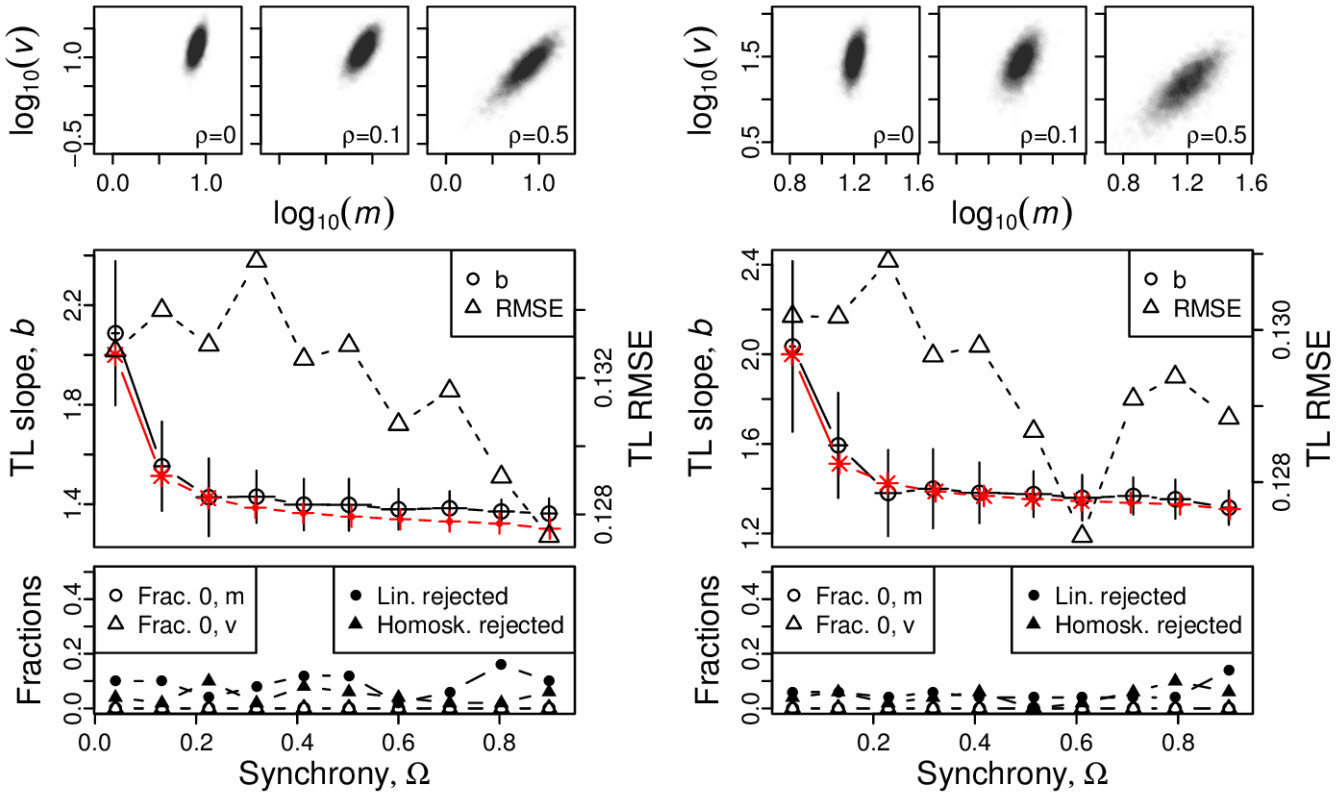

Figure S11: Omnibus plots (see section S6) for identically distributed gamma marginals under the set up of section S3, for $n = 25$ and $\beta = 0.5$, for $\alpha = 1$ (A), $\alpha = 2$ (B), $\alpha = 4$ (C), and $\alpha = 8$ (D).

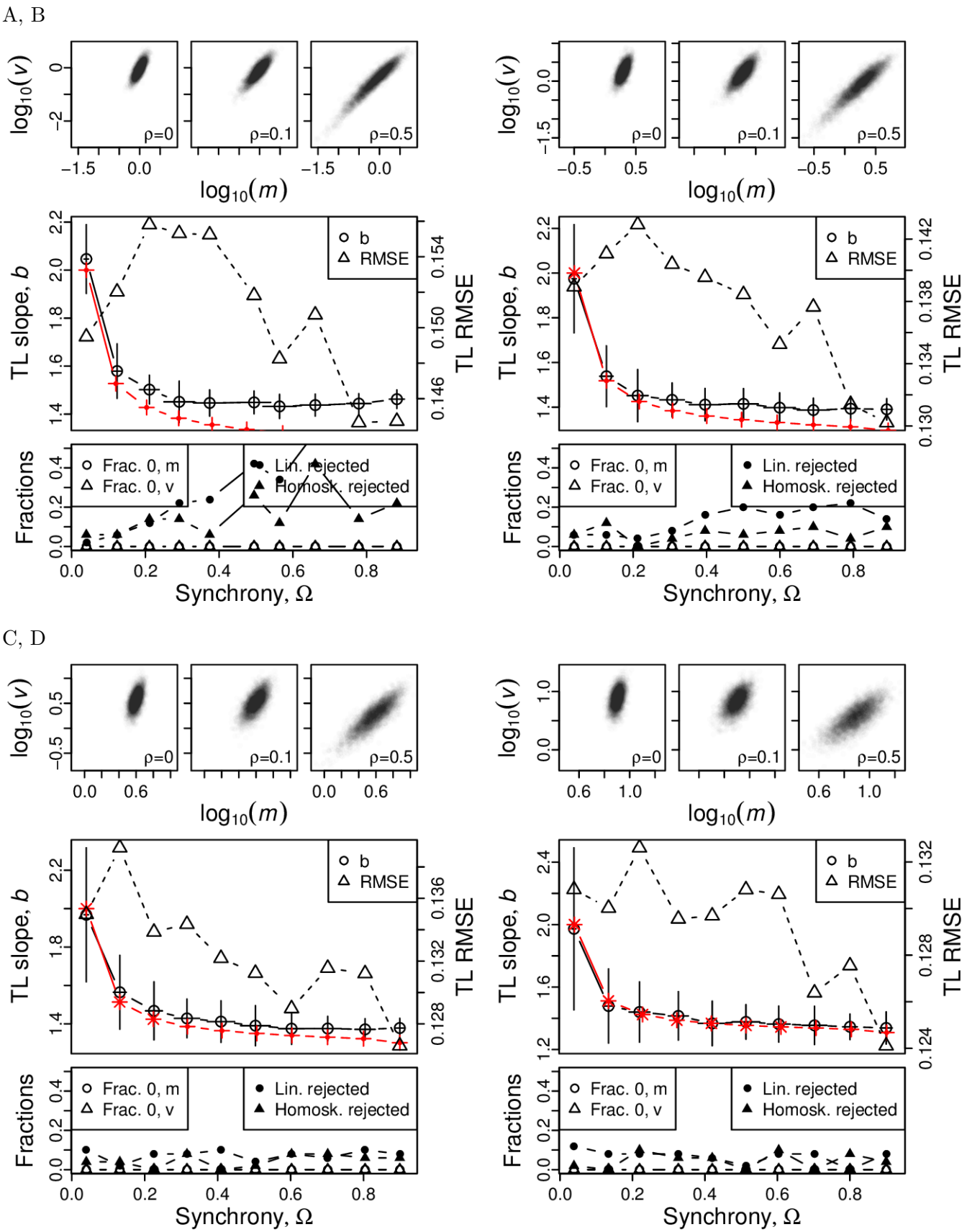

Figure S12: Omnibus plots (see section S6) for identically distributed gamma marginals under the set up of section S3, for $n = 25$ and $\beta = 1$, for $\alpha = 1$ (A), $\alpha = 2$ (B), $\alpha = 4$ (C), and $\alpha = 8$ (D).

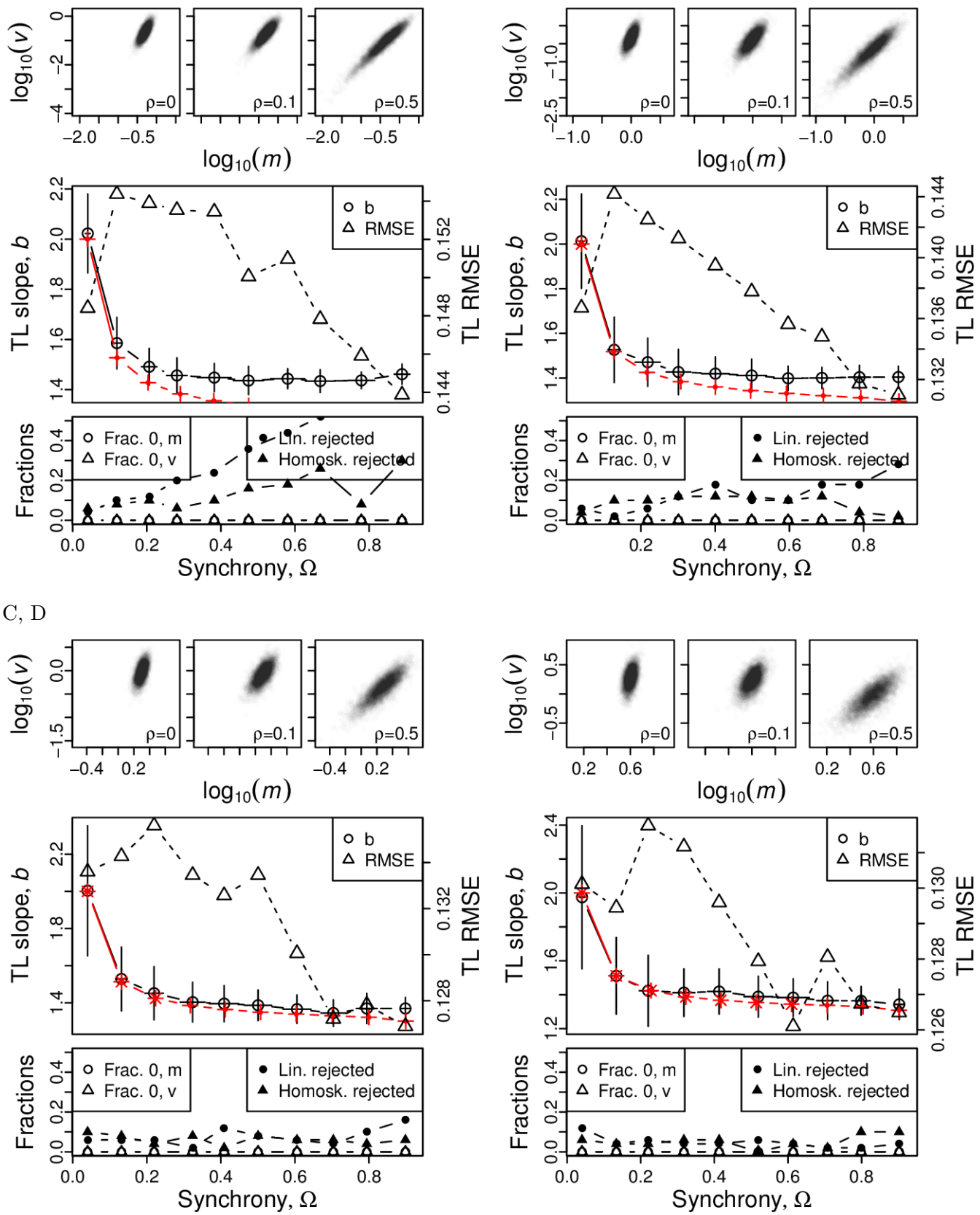

Figure S13: Omnibus plots (see section S6) for identically distributed gamma marginals under the set up of section S3, for $n = 25$ and $\beta = 2$, for $\alpha = 1$ (A), $\alpha = 2$ (B), $\alpha = 4$ (C), and $\alpha = 8$ (D).

A, B

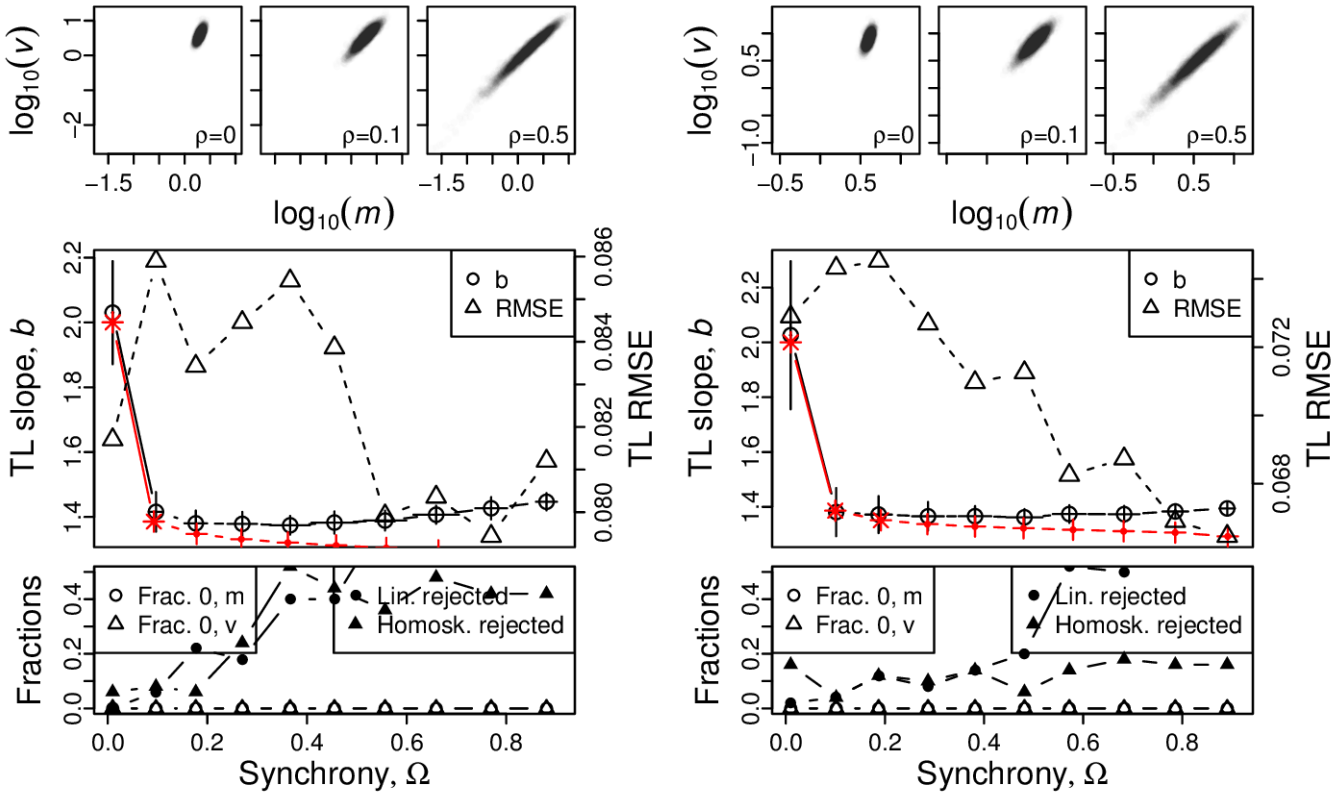

C, D

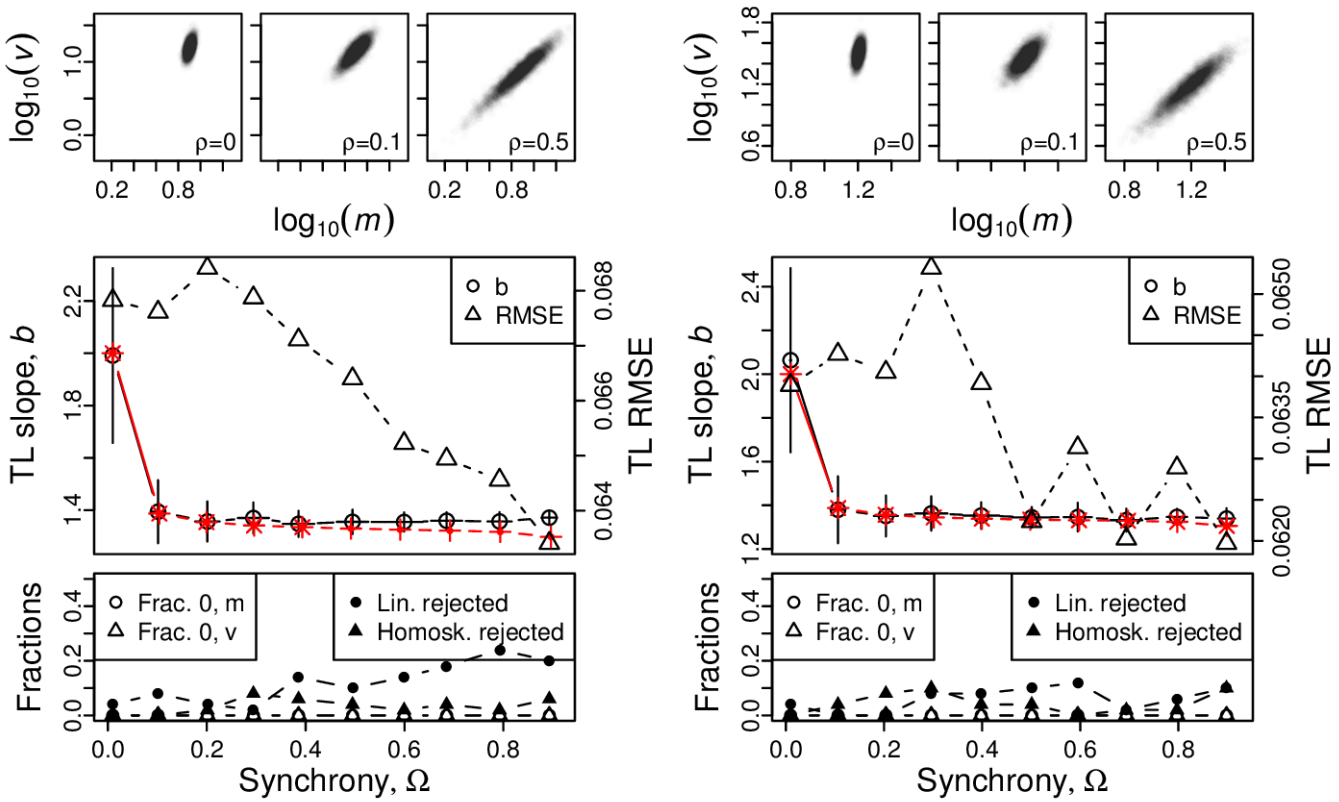

Figure S14: Omnibus plots (see section S6) for identically distributed gamma marginals under the set up of section S3, for $n = 100$ and $\beta = 0.5$, for $\alpha = 1$ (A), $\alpha = 2$ (B), $\alpha = 4$ (C), and $\alpha = 8$ (D).

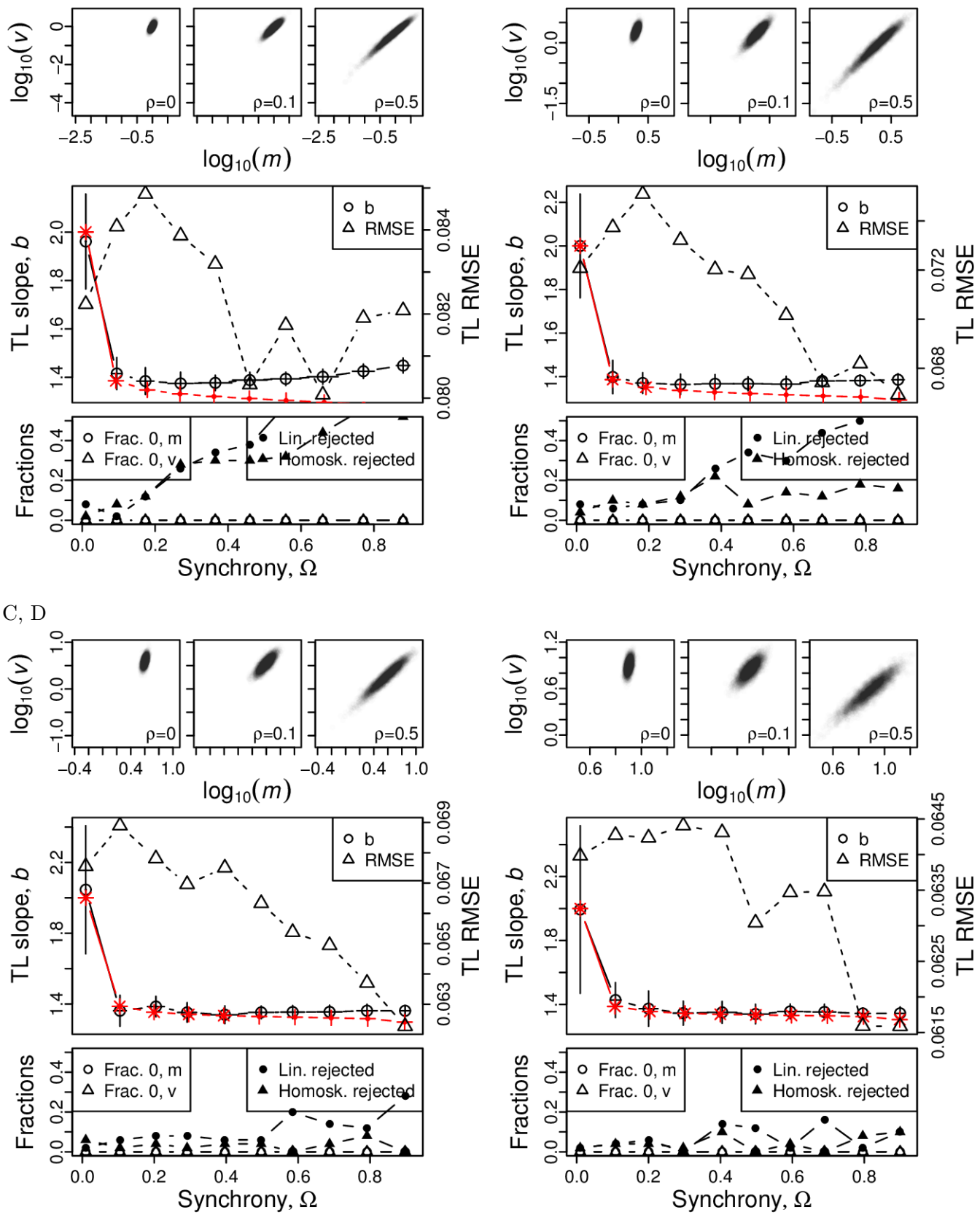

Figure S15: Omnibus plots (see section S6) for identically distributed gamma marginals under the set up of section S3, for $n = 100$ and $\beta = 1$, for $\alpha = 1$ (A), $\alpha = 2$ (B), $\alpha = 4$ (C), and $\alpha = 8$ (D).

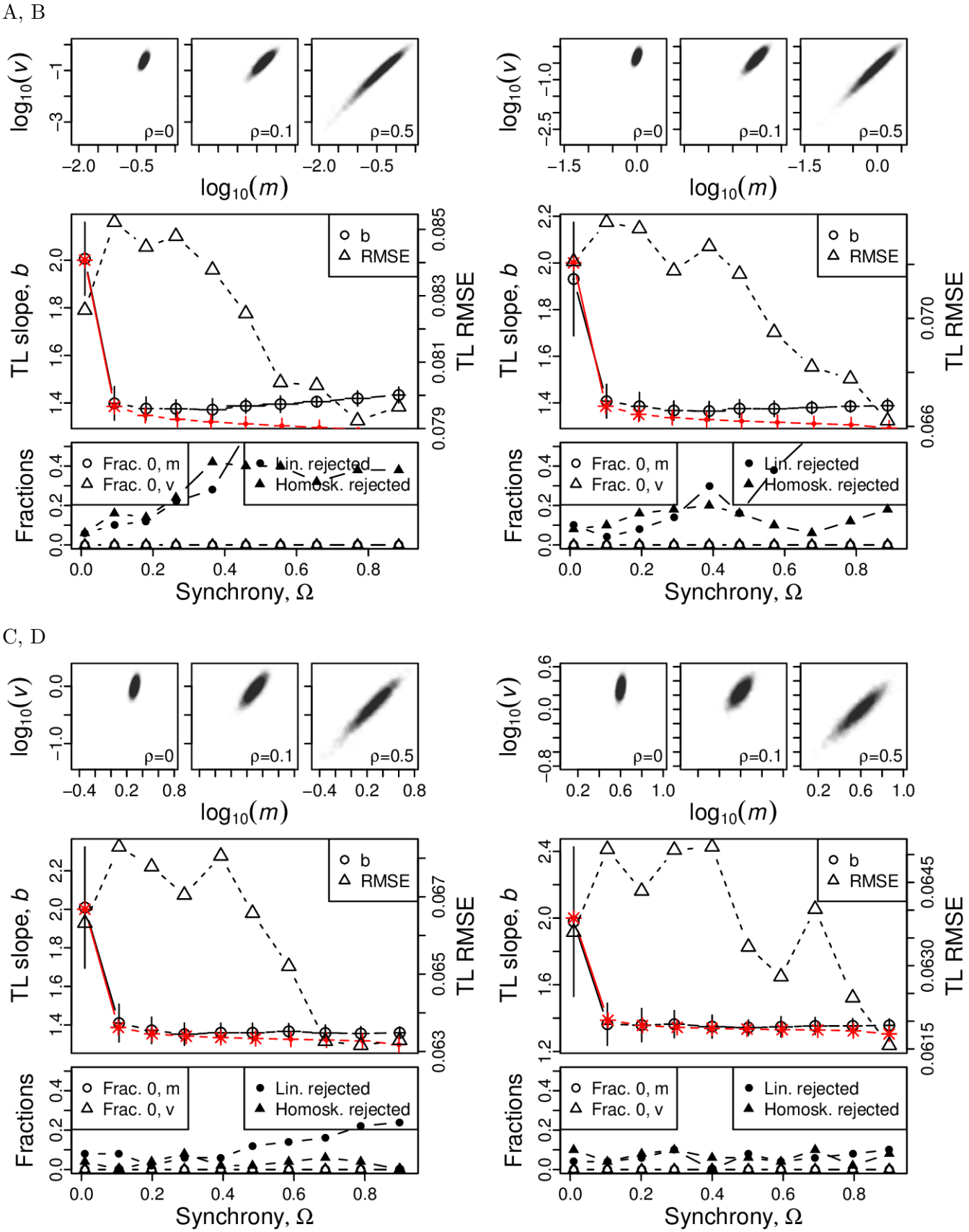

Figure S16: Omnibus plots (see section S6) for identically distributed gamma marginals under the set up of section S3, for $n = 100$ and $\beta = 2$, for $\alpha = 1$ (A), $\alpha = 2$ (B), $\alpha = 4$ (C), and $\alpha = 8$ (D).

A, B

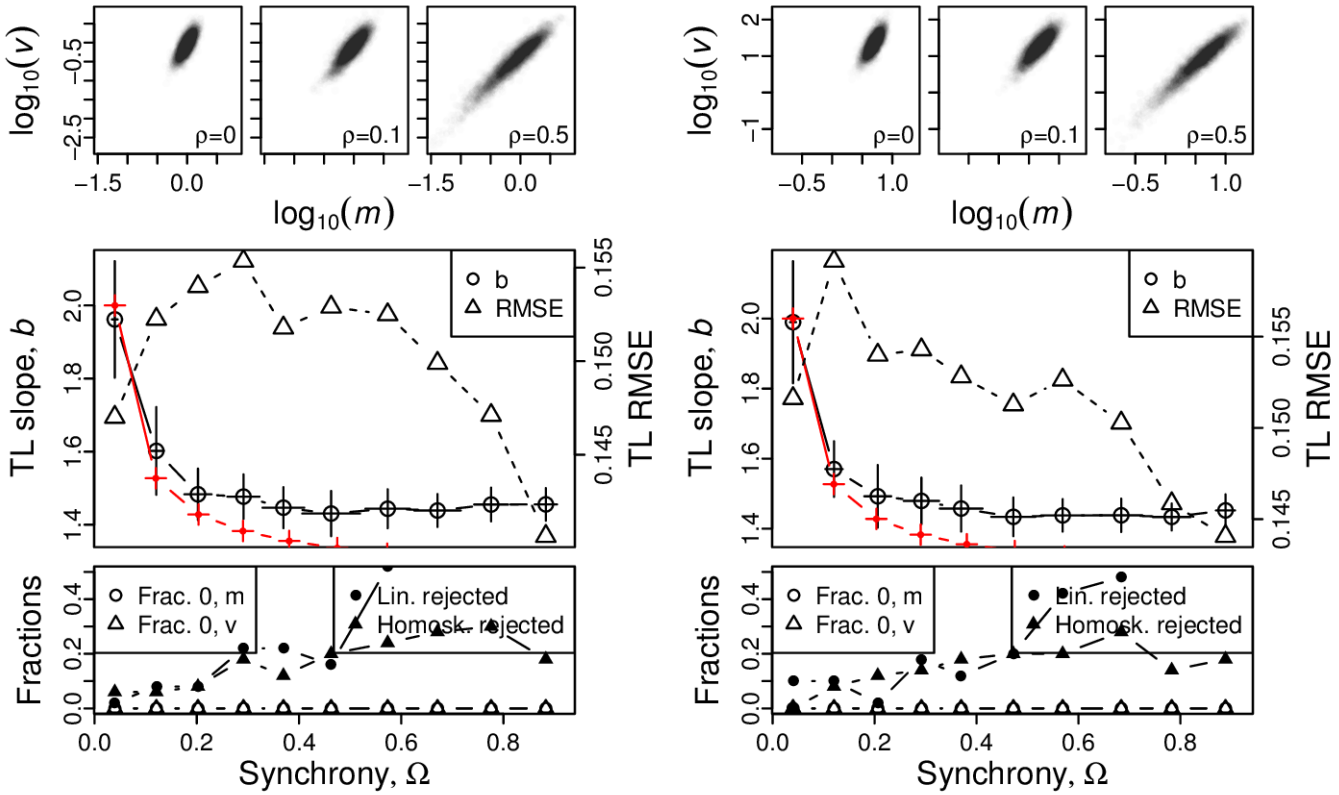

C, D

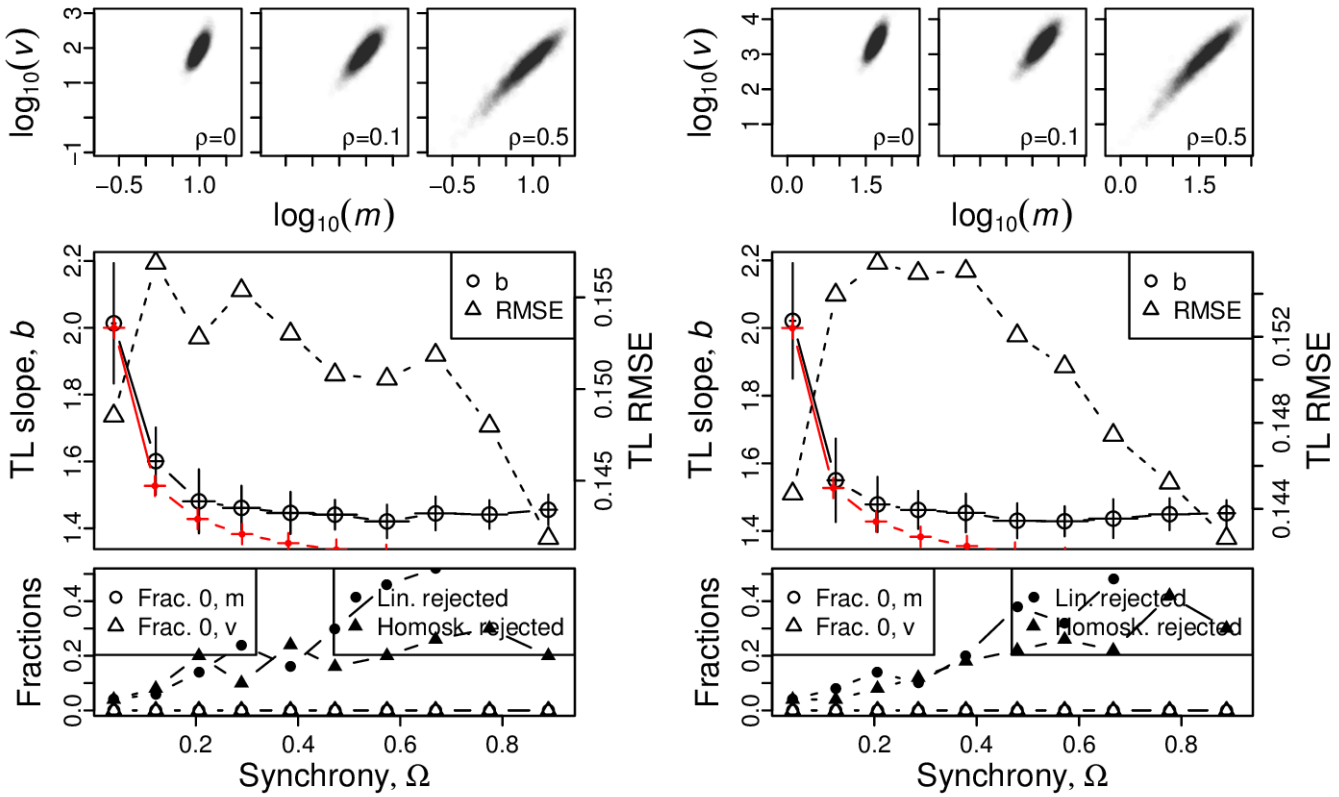

Figure S17: Omnibus plots (see section S6) for identically distributed exponentially distributed marginals under the set up of section S3, for $n = 25$, for $1/\lambda = 1$ (A), $1/\lambda = 5$ (B), $1/\lambda = 10$ (C), and $1/\lambda = 50$ (D).

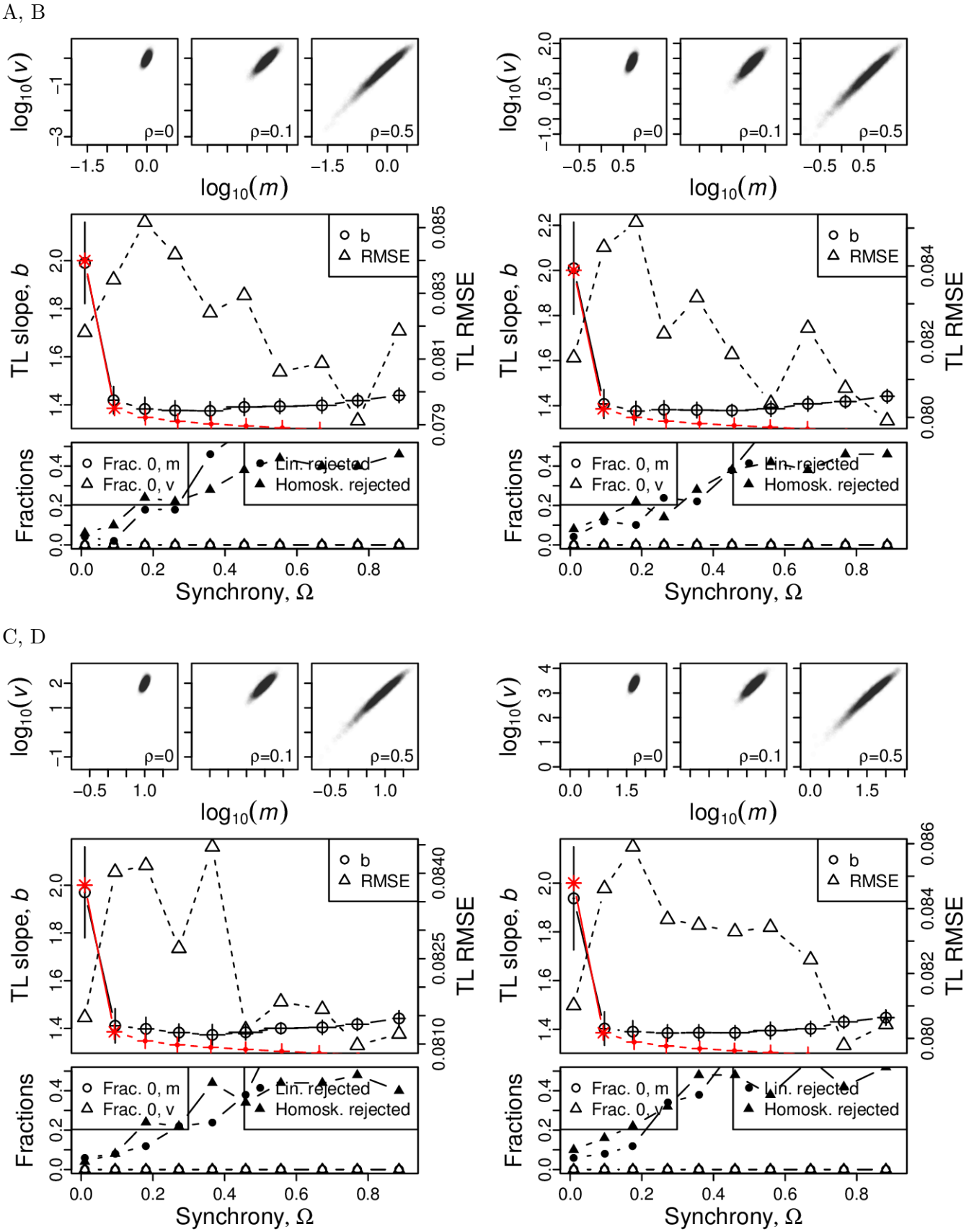

Figure S18: Omnibus plots (see section S6) for identically distributed exponentially distributed marginals under the set up of section S3, for $n = 100$, for $1/\lambda = 1$ (A), $1/\lambda = 5$ (B), $1/\lambda = 10$ (C), and $1/\lambda = 50$ (D).

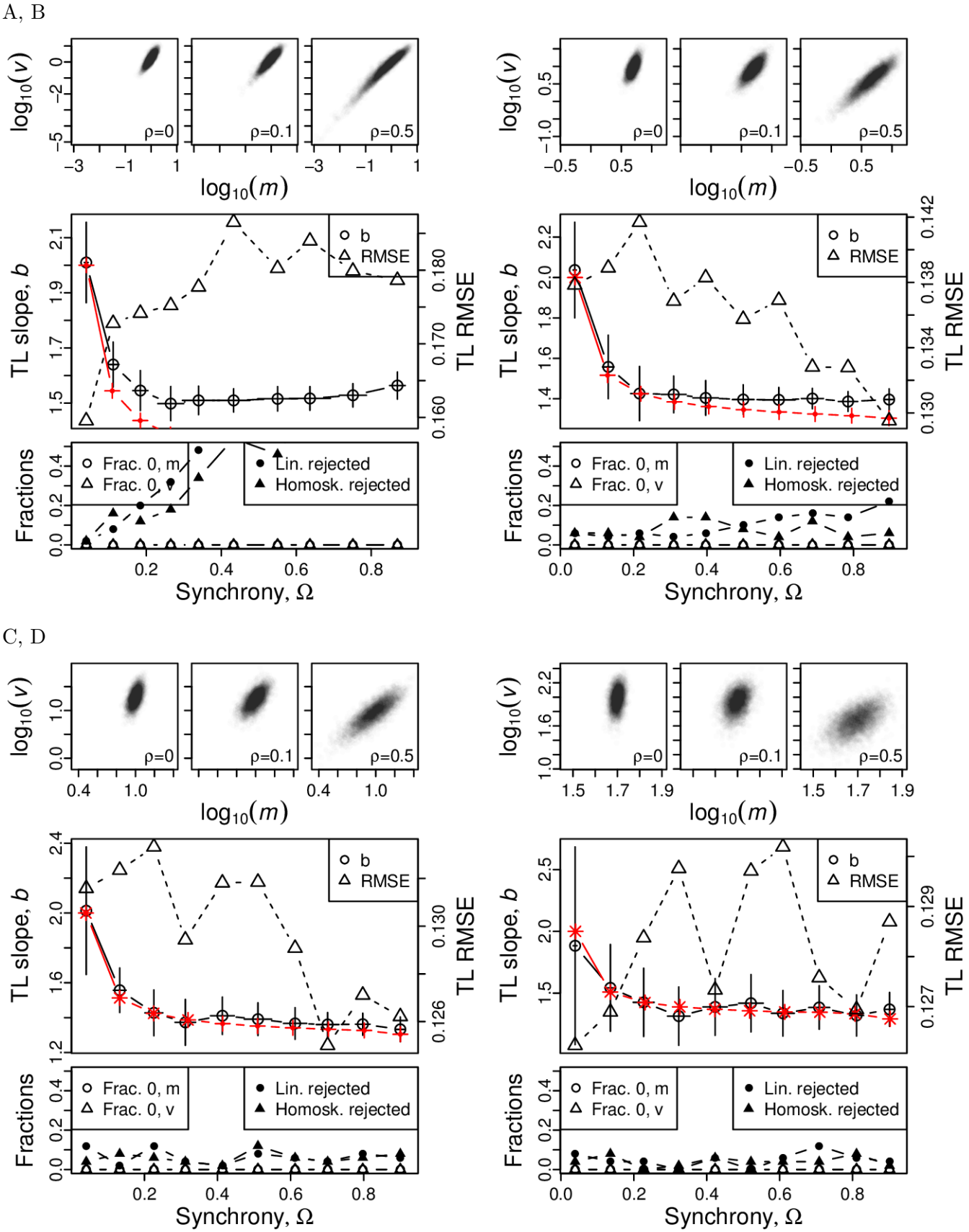

Figure S19: Omnibus plots (see section S6) for identically distributed chi-squared marginals under the set up of section S3, for $n = 25$, for $k = 1$ (A), $k = 5$ (B), $k = 10$ (C), and $k = 50$ (D).

A, B

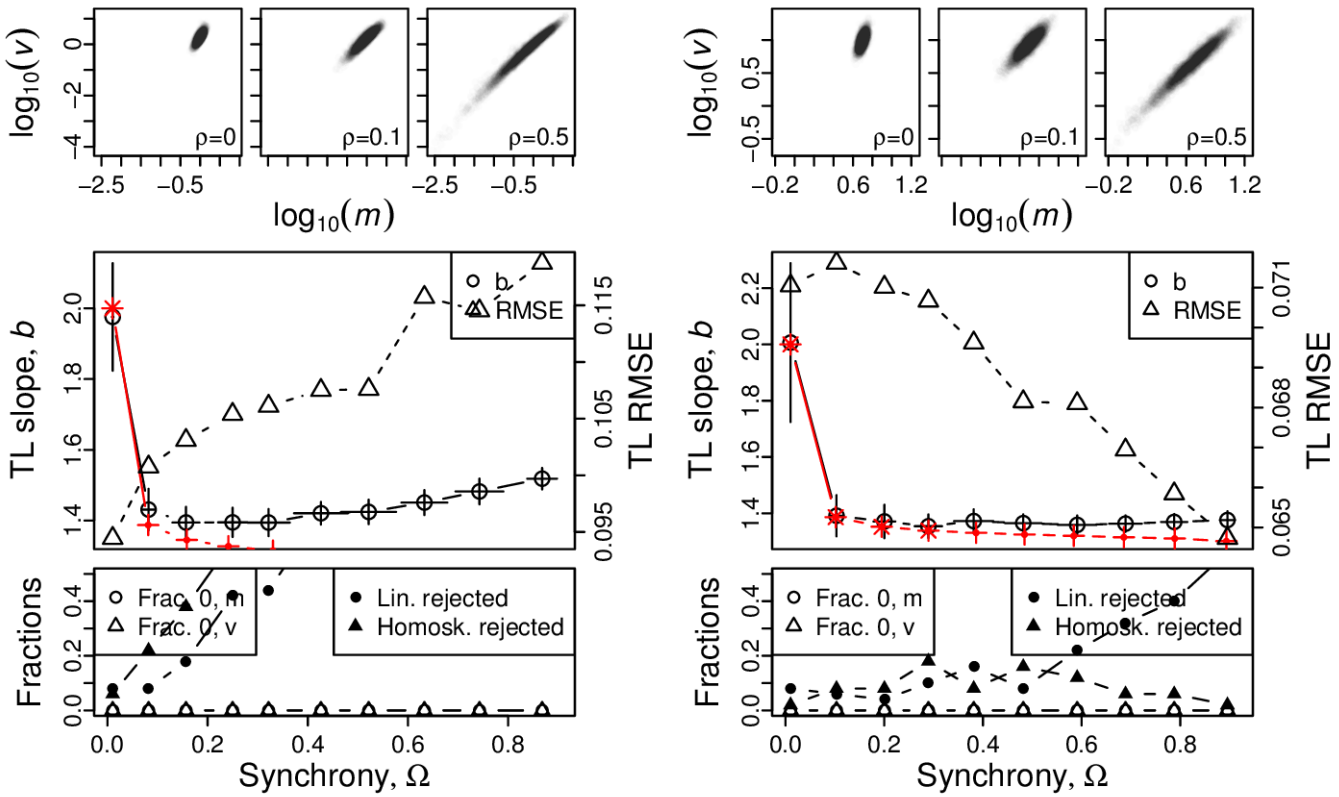

C, D

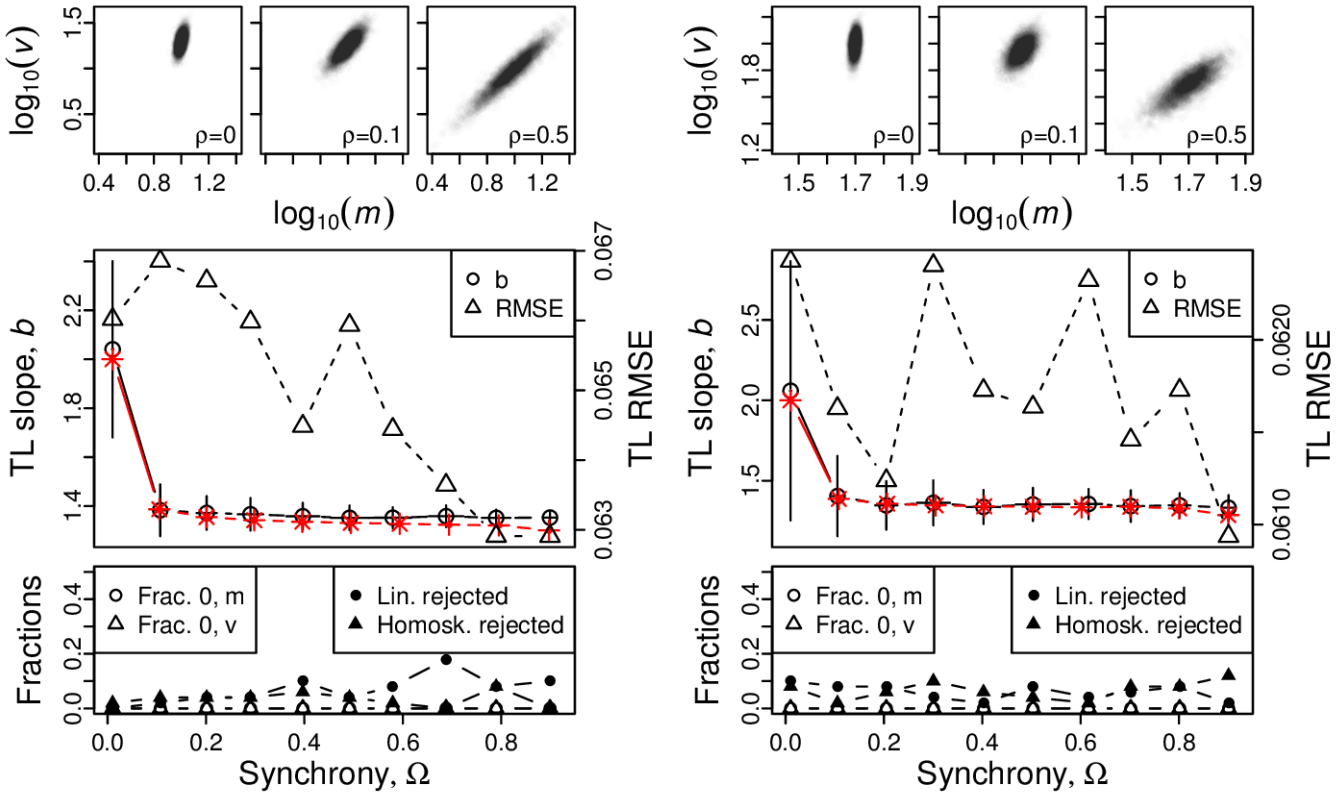

Figure S20: Omnibus plots (see section S6) for identically distributed chi-squared marginals under the set up of section S3, for $n = 100$, for $k = 1$ (A), $k = 5$ (B), $k = 10$ (C), and $k = 50$ (D).

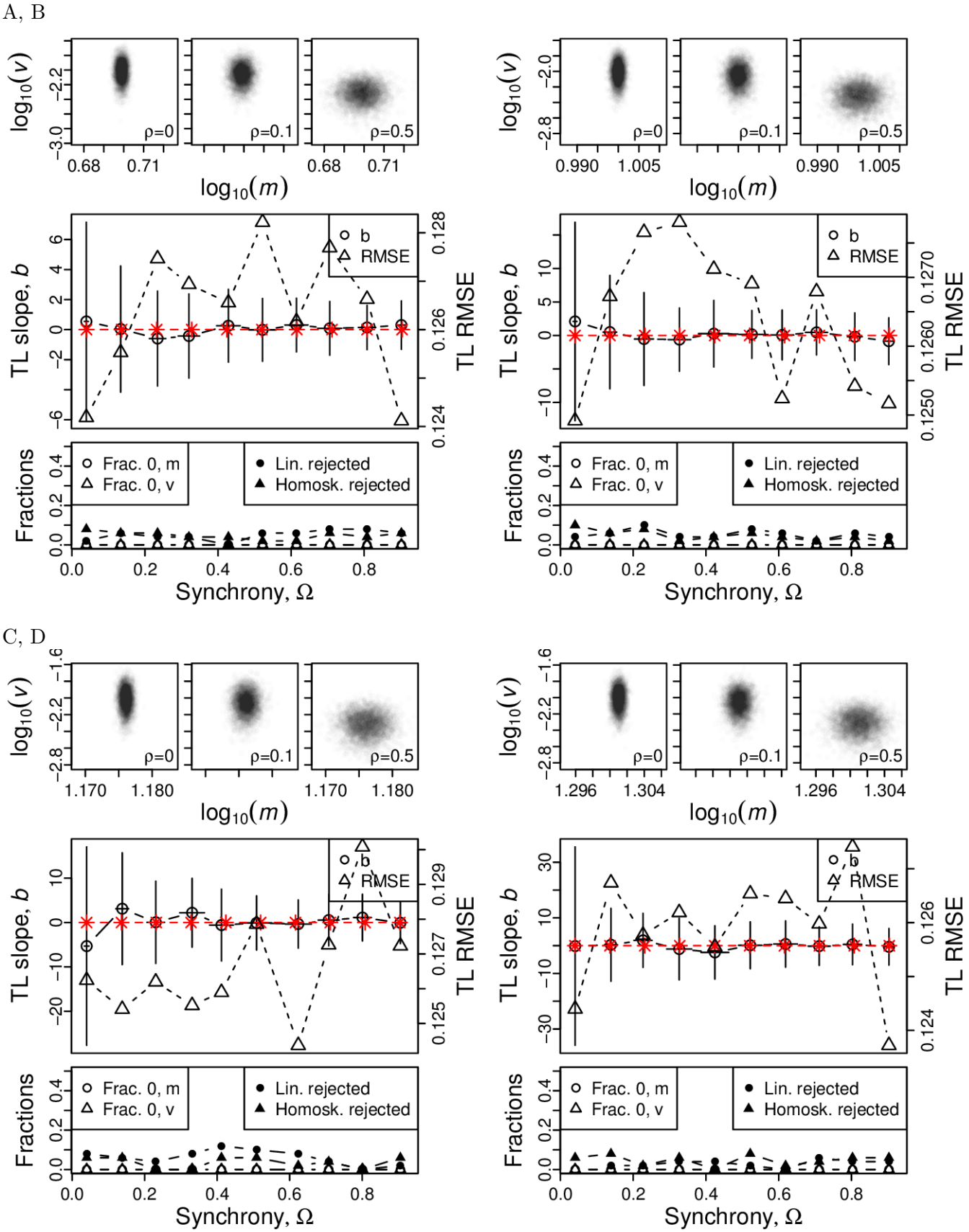

Figure S21: Omnibus plots (see section S6) for identically distributed normal marginals under the set up of section S3, for $n = 25$ and $\sigma = 0.1$, for $\mu = 5$ (A), $\mu = 10$ (B), $\mu = 15$ (C), and $\mu = 20$ (D).

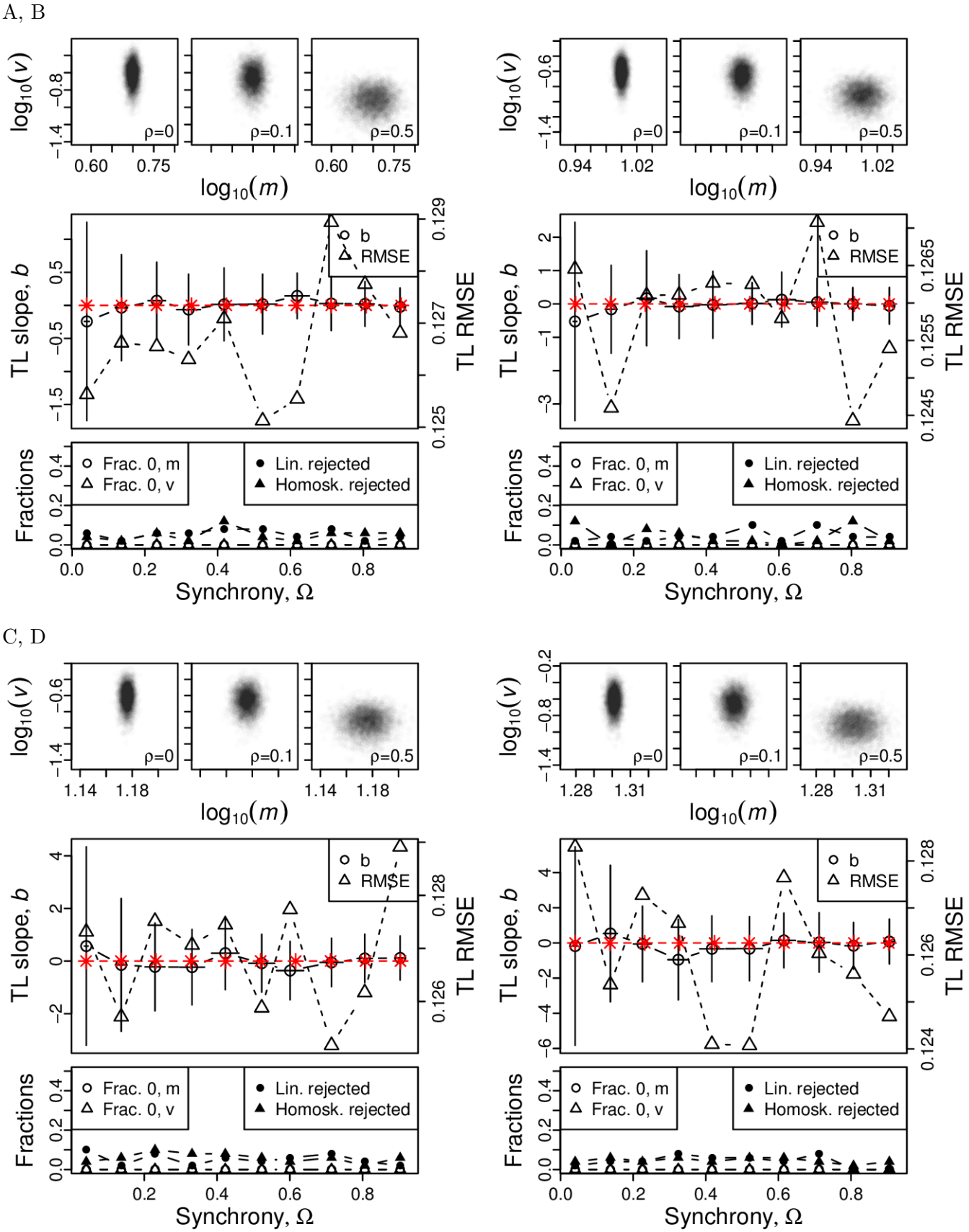

Figure S22: Omnibus plots (see section S6) for identically distributed normal marginals under the set up of section S3, for $n = 25$ and $\sigma = 0.5$, for $\mu = 5$ (A), $\mu = 10$ (B), $\mu = 15$ (C), and $\mu = 20$ (D).

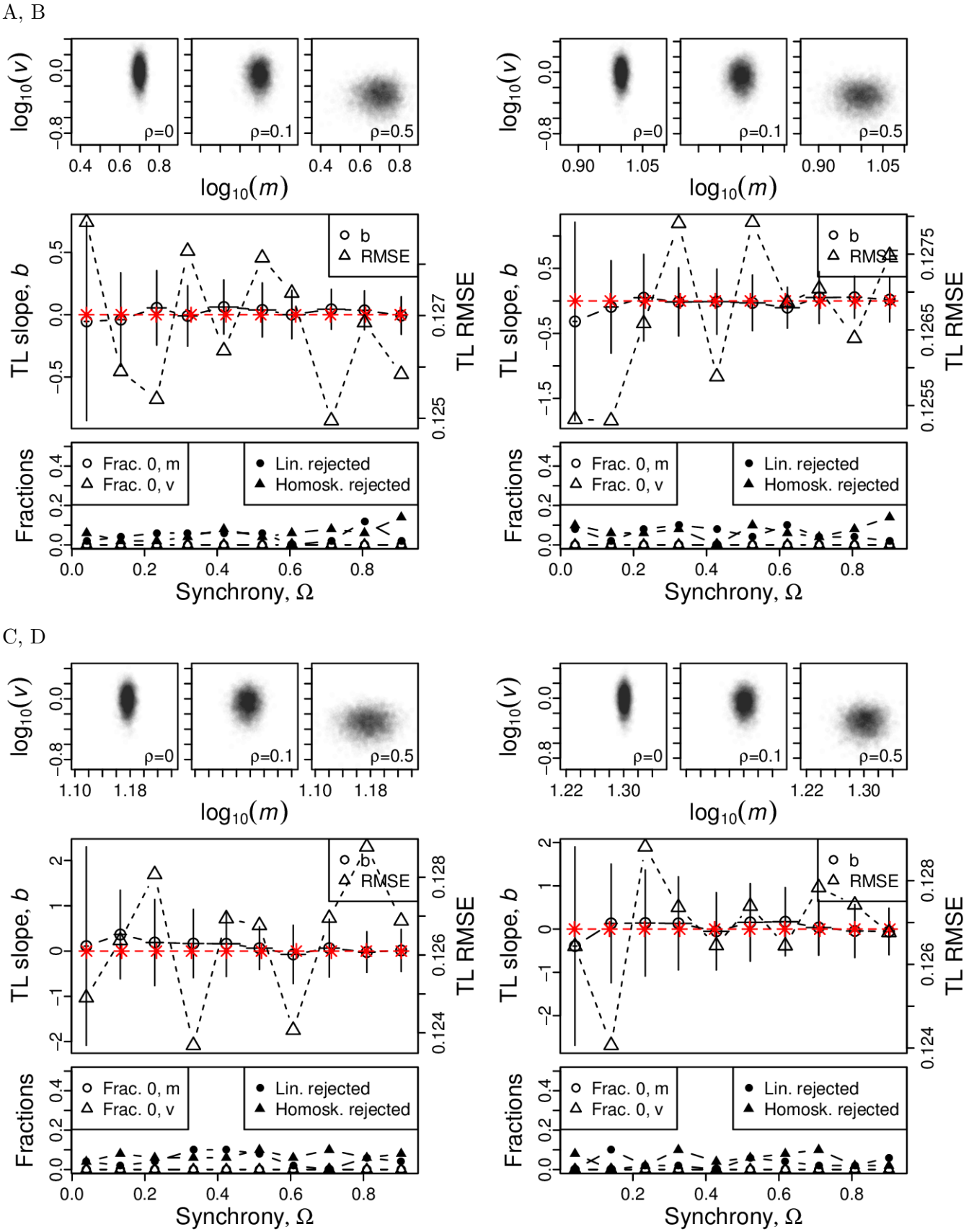

Figure S23: Omnibus plots (see section S6) for identically distributed normal marginals under the set up of section S3, for $n = 25$ and $\sigma = 1$, for $\mu = 5$ (A), $\mu = 10$ (B), $\mu = 15$ (C), and $\mu = 20$ (D).

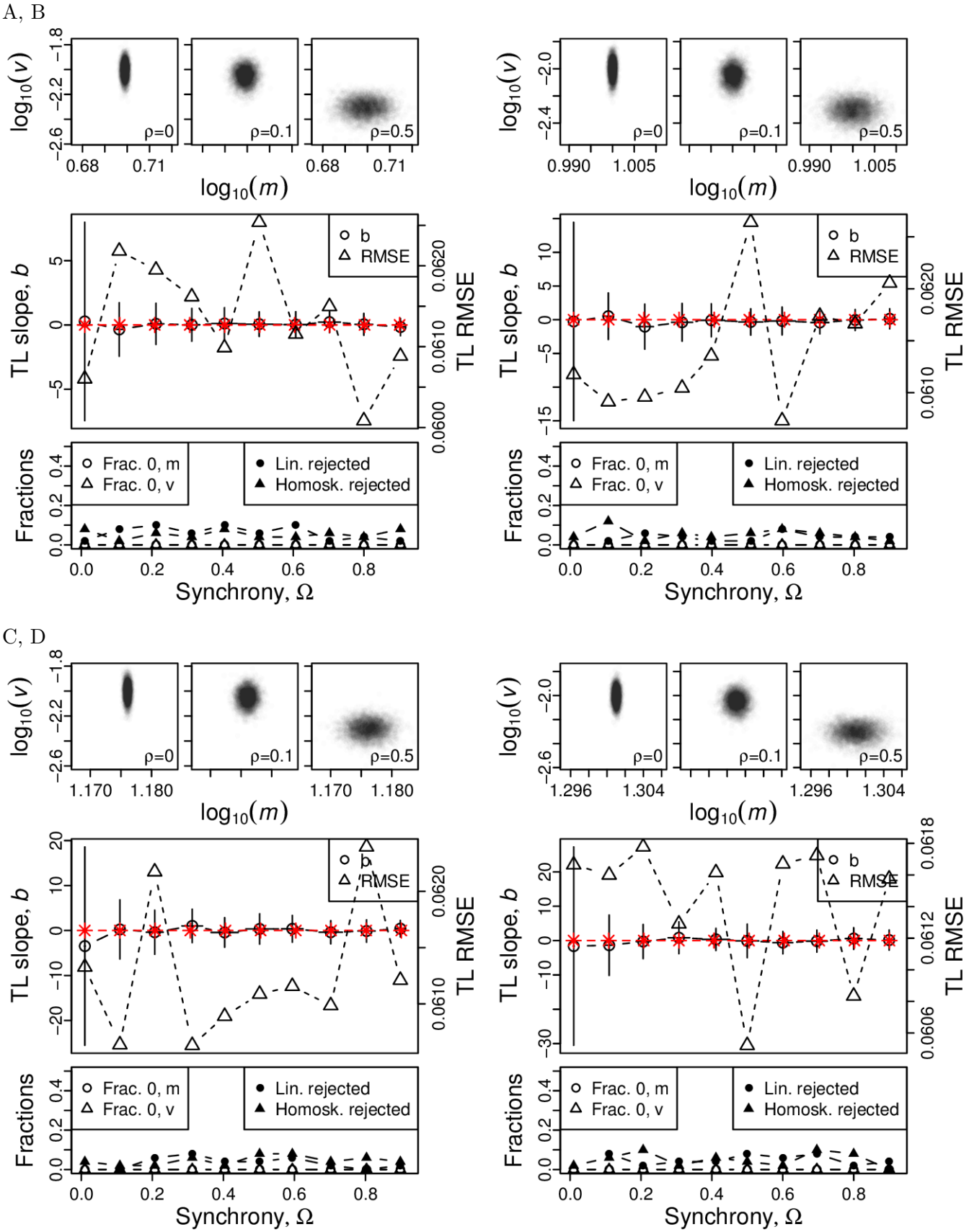

Figure S24: Omnibus plots (see section S6) for identically distributed normal marginals under the set up of section S3, for $n = 100$ and $\sigma = 0.1$, for $\mu = 5$ (A), $\mu = 10$ (B), $\mu = 15$ (C), and $\mu = 20$ (D).

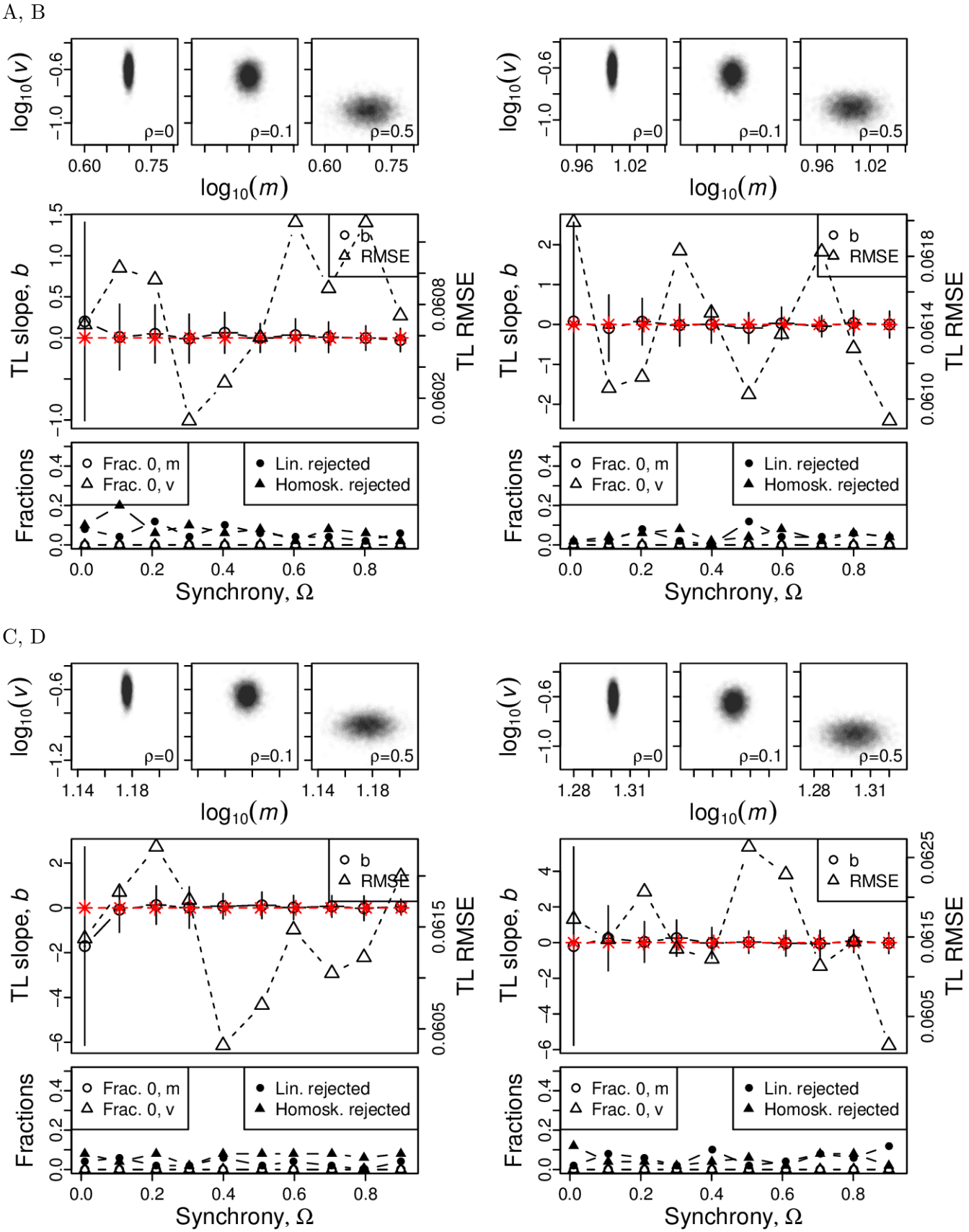

Figure S25: Omnibus plots (see section S6) for identically distributed normal marginals under the set up of section S3, for $n = 100$ and $\sigma = 0.5$, for $\mu = 5$ (A), $\mu = 10$ (B), $\mu = 15$ (C), and $\mu = 20$ (D).

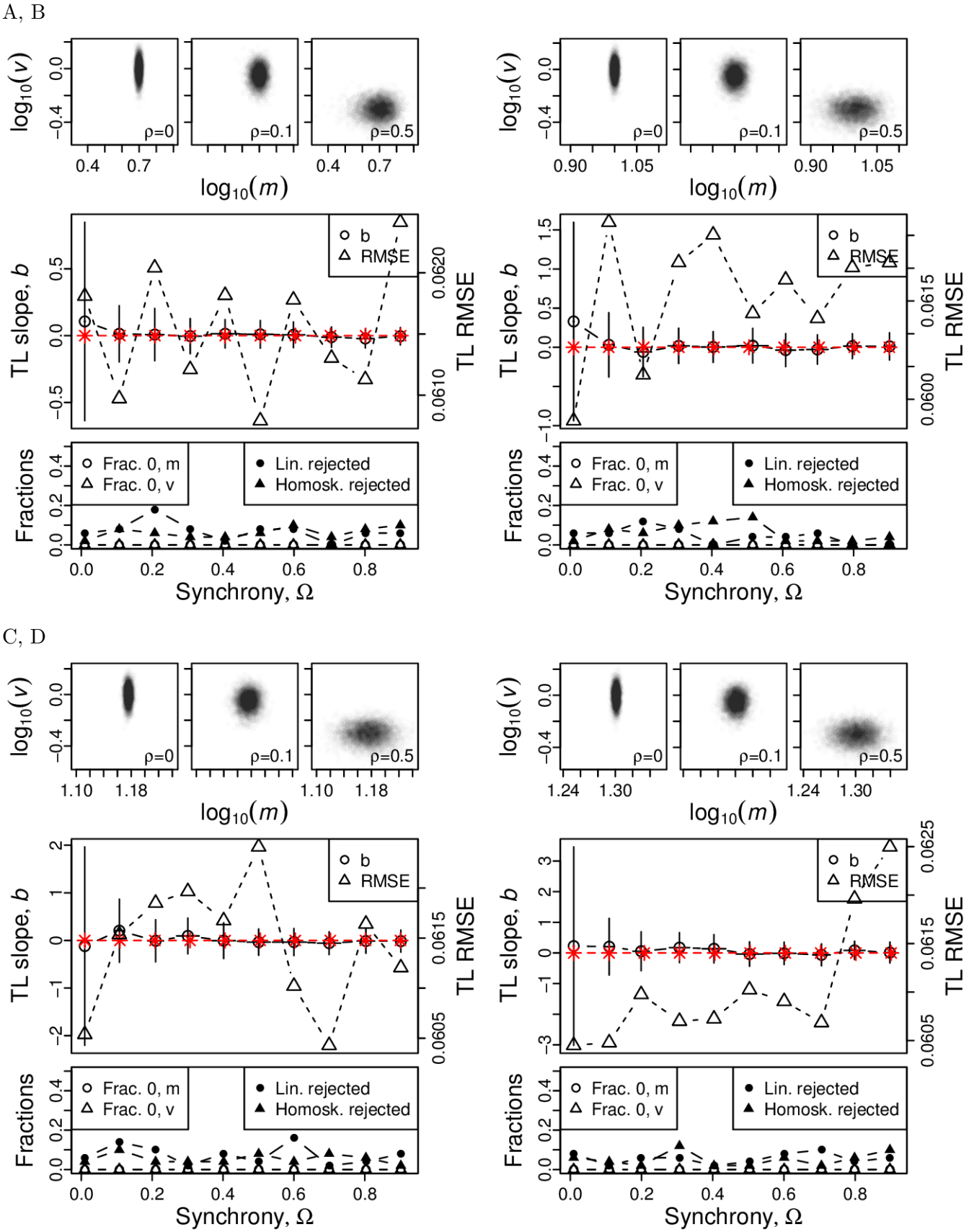

Figure S26: Omnibus plots (see section S6) for identically distributed normal marginals under the set up of section S3, for $n = 100$ and $\sigma = 1$, for $\mu = 5$ (A), $\mu = 10$ (B), $\mu = 15$ (C), and $\mu = 20$ (D).

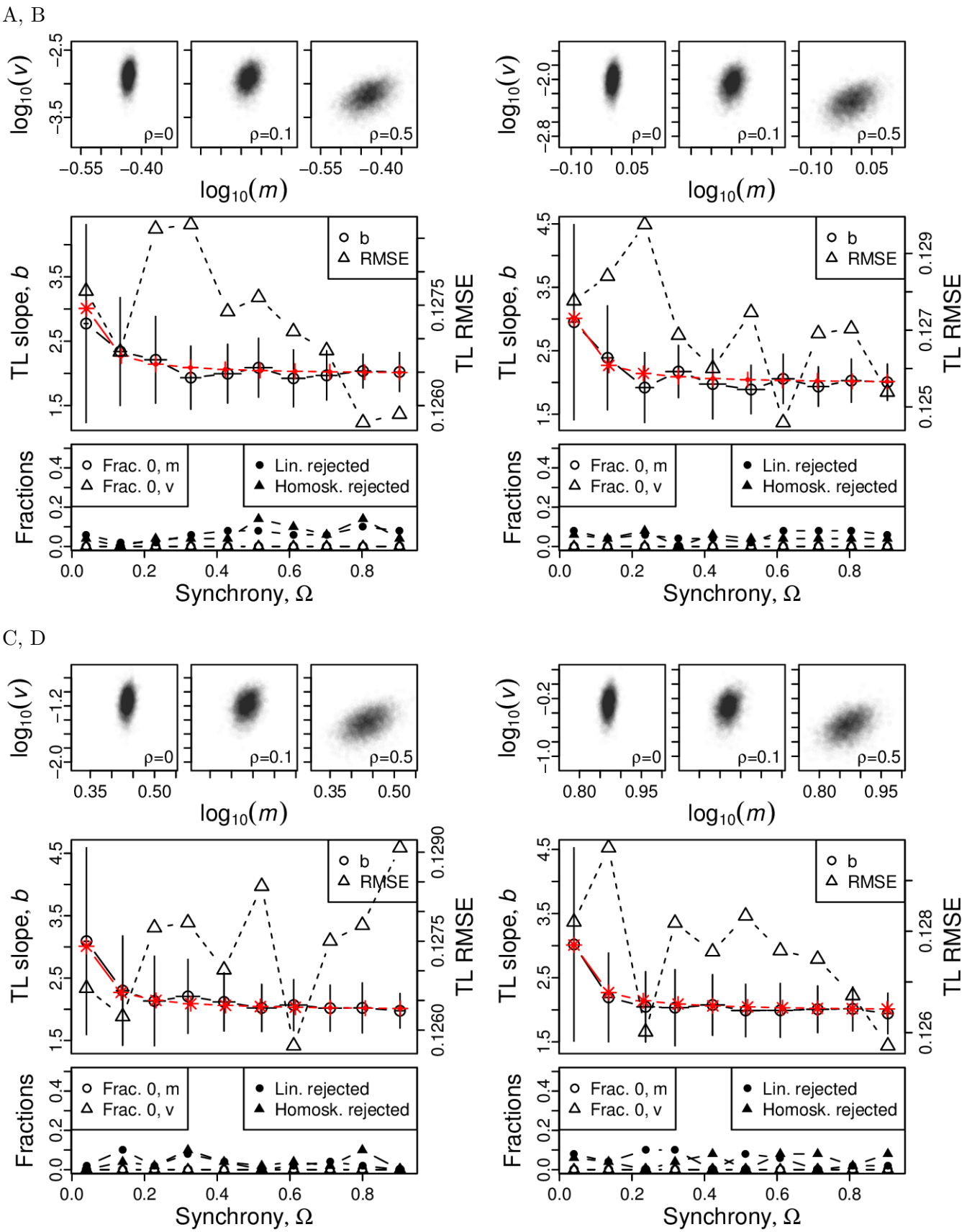

Figure S27: Omnibus plots (see section S6) for identically distributed log-normal marginals under the set up of section S3, for $n = 25$ and $\sigma = 0.1$, for $\mu = -1$ (A), $\mu = 0$ (B), $\mu = 1$ (C), and $\mu = 2$ (D).

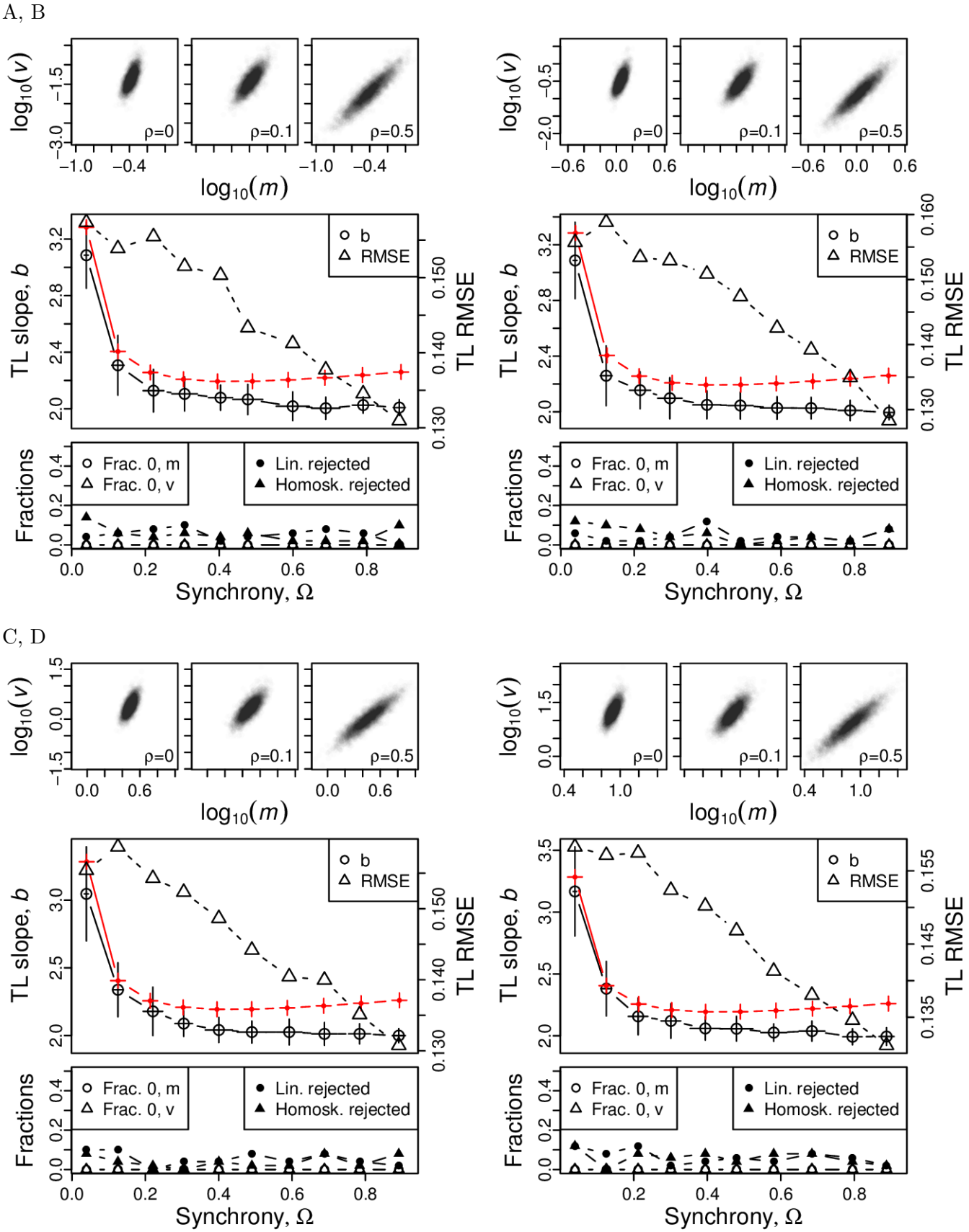

Figure S28: Omnibus plots (see section S6) for identically distributed log-normal marginals under the set up of section S3, for $n = 25$ and $\sigma = 0.5$, for $\mu = -1$ (A), $\mu = 0$ (B), $\mu = 1$ (C), and $\mu = 2$ (D).

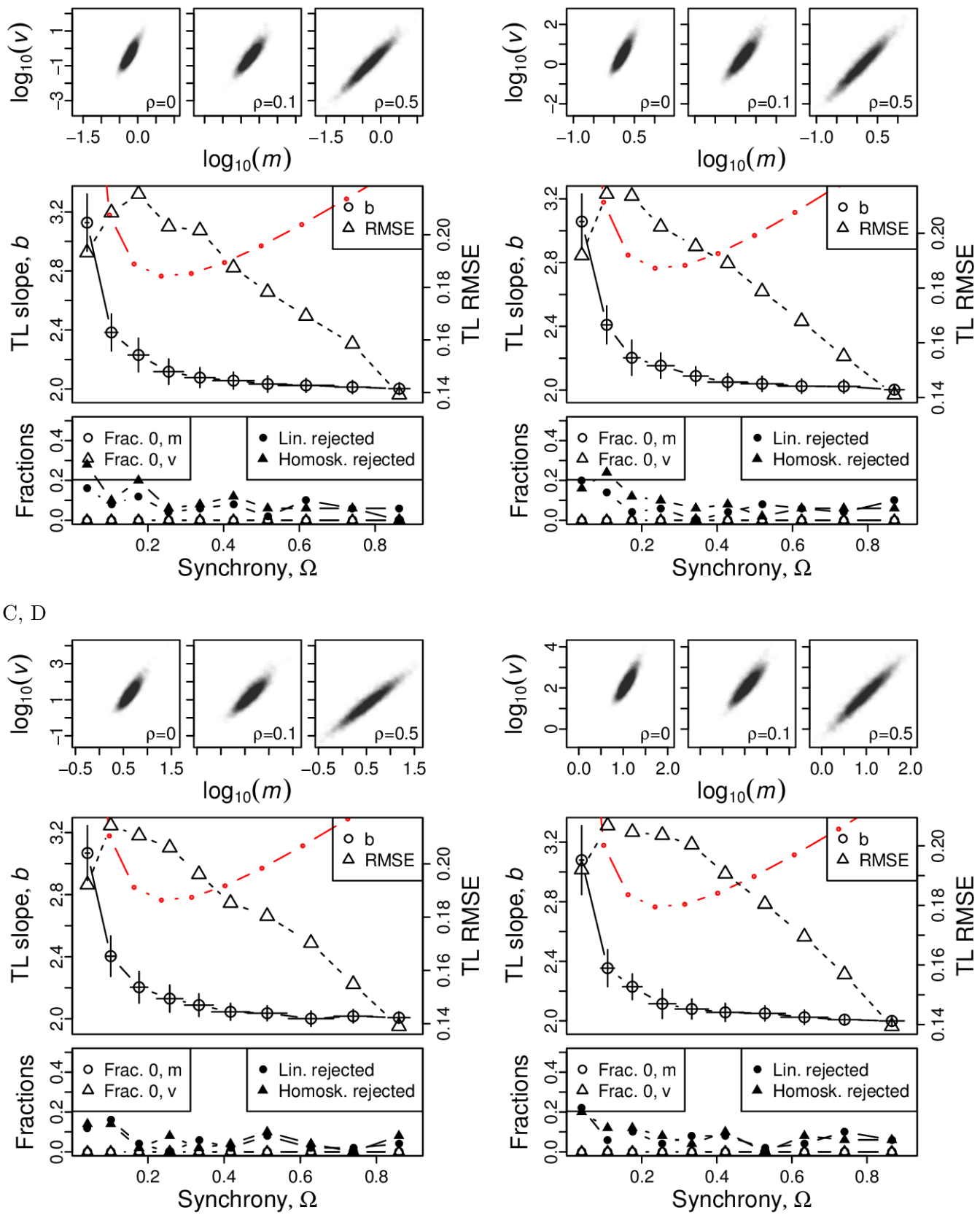

Figure S29: Omnibus plots (see section S6) for identically distributed log-normal marginals under the set up of section S3, for $n = 25$ and $\sigma = 1$, for $\mu = -1$ (A), $\mu = 0$ (B), $\mu = 1$ (C), and $\mu = 2$ (D).

A, B

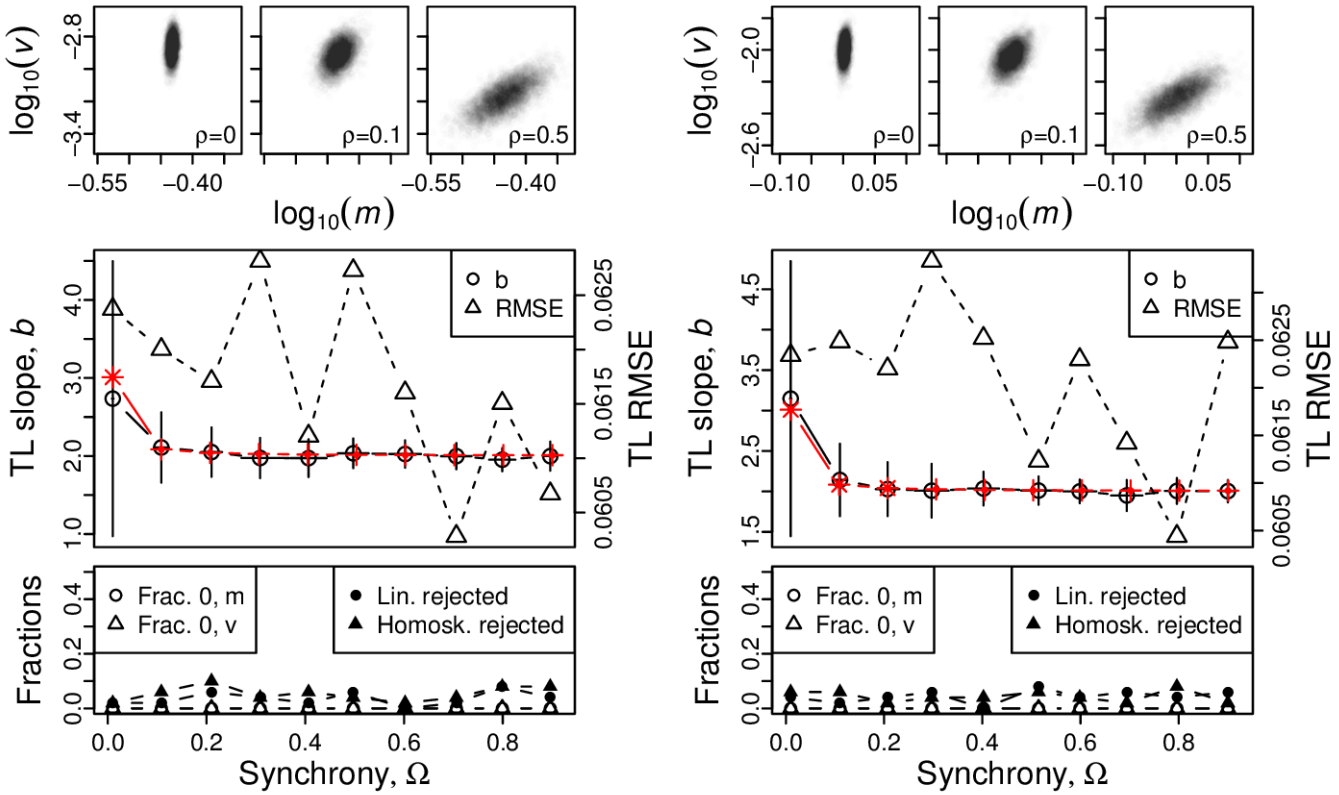

C, D

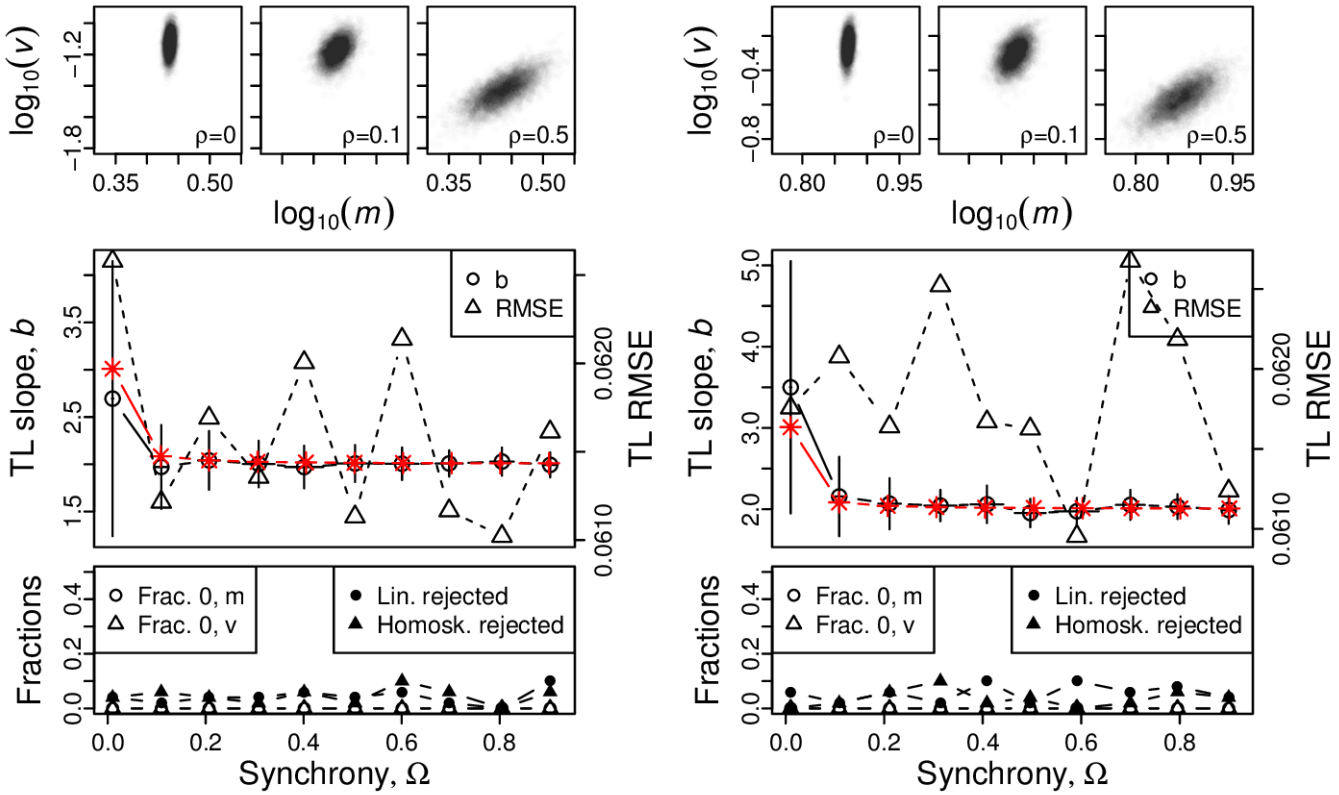

Figure S30: Omnibus plots (see section S6) for identically distributed log-normal marginals under the set up of section S3, for $n = 100$ and $\sigma = 0.1$, for $\mu = -1$ (A), $\mu = 0$ (B), $\mu = 1$ (C), and $\mu = 2$ (D).

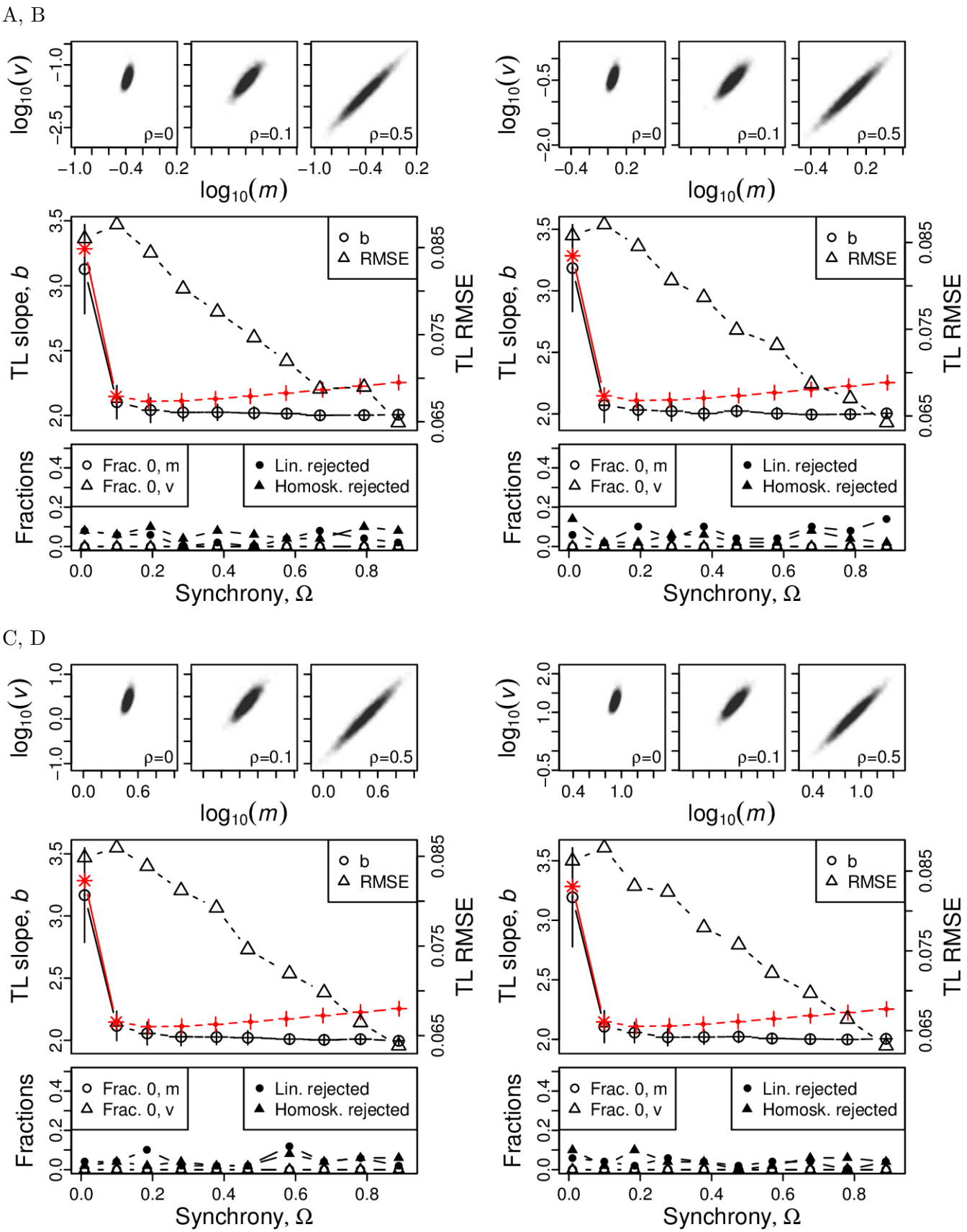

Figure S31: Omnibus plots (see section S6) for identically distributed log-normal marginals under the set up of section S3, for $n = 100$ and $\sigma = 0.5$, for $\mu = -1$ (A), $\mu = 0$ (B), $\mu = 1$ (C), and $\mu = 2$ (D).

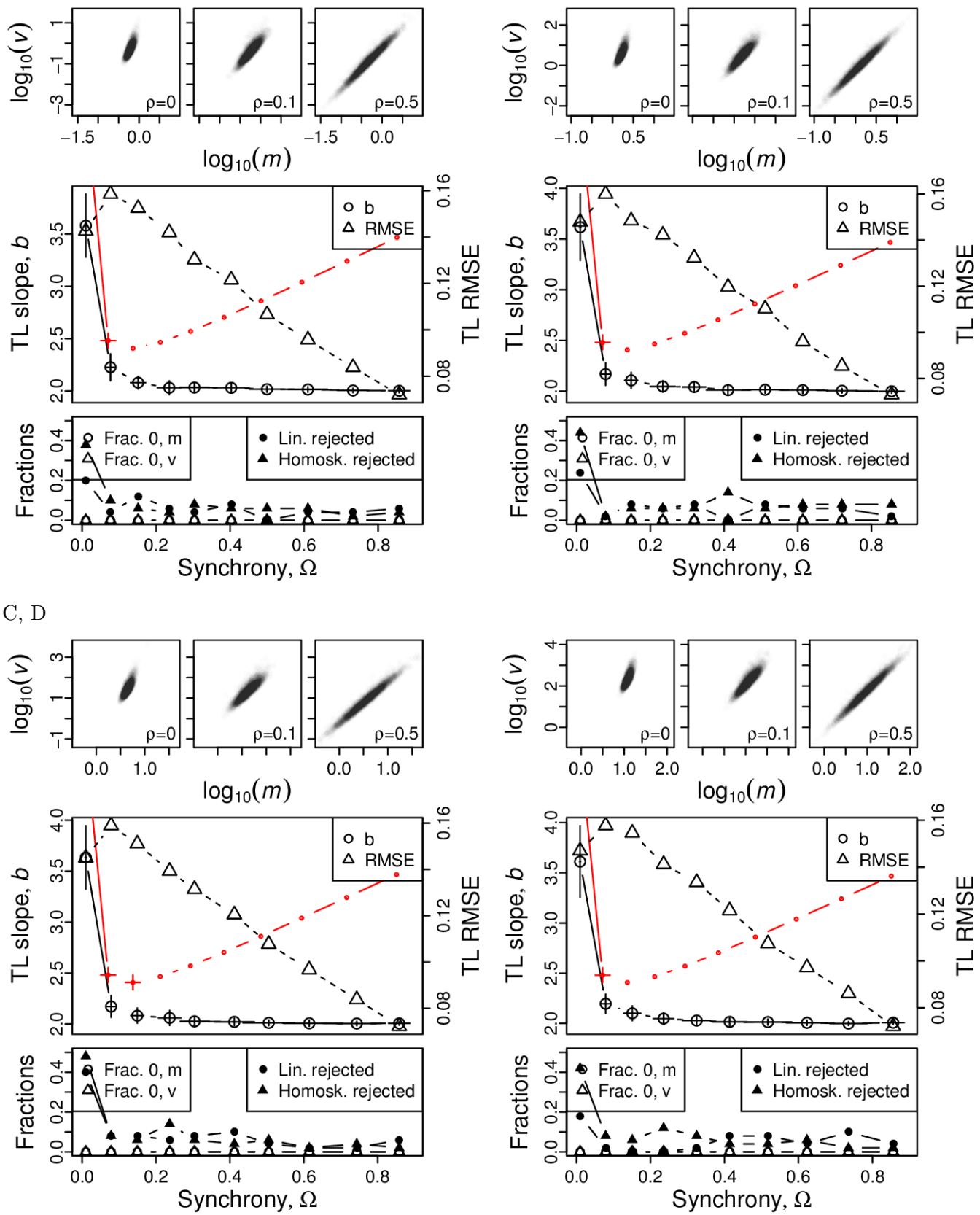

Figure S32: Omnibus plots (see section S6) for identically distributed log-normal marginals under the set up of section S3, for $n = 100$ and $\sigma = 1$, for $\mu = -1$ (A), $\mu = 0$ (B), $\mu = 1$ (C), and $\mu = 2$ (D).

S9 Figures, distributions constructed using Gaussian copulas and non-identically distributed marginals

A, B

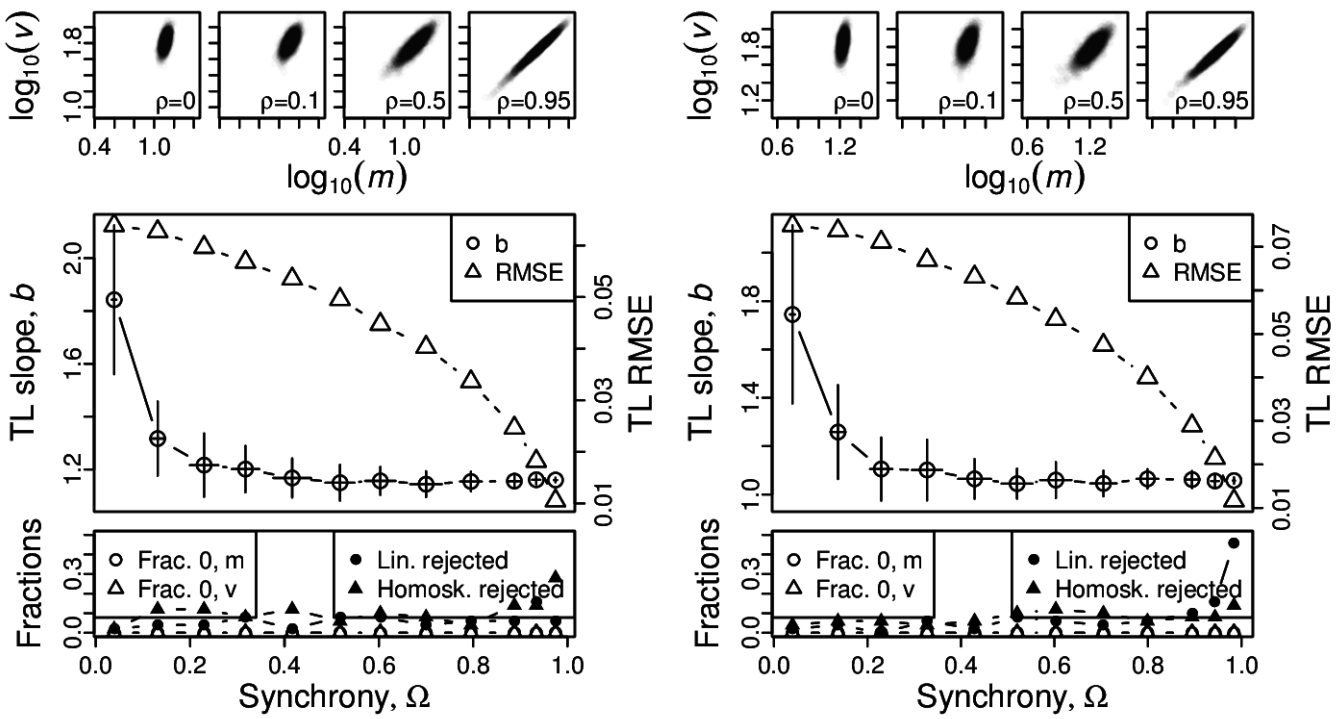

C, D

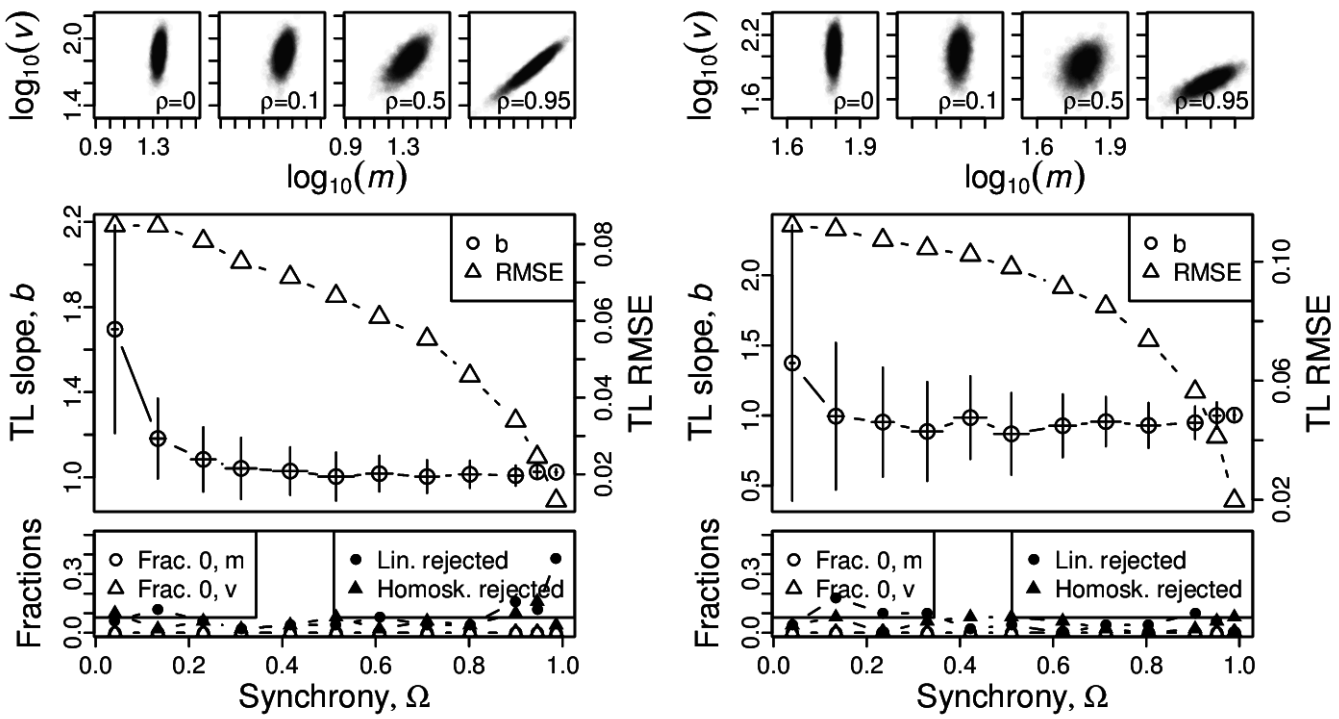

Figure S33: Omnibus plots (see section S6) for non-identically distributed Poisson marginals under the set up of section S4, for $n = 25$ and Y_1 with $\lambda = 1$ (A), $\lambda = 5$ (B), $\lambda = 10$ (C), and $\lambda = 50$ (D).

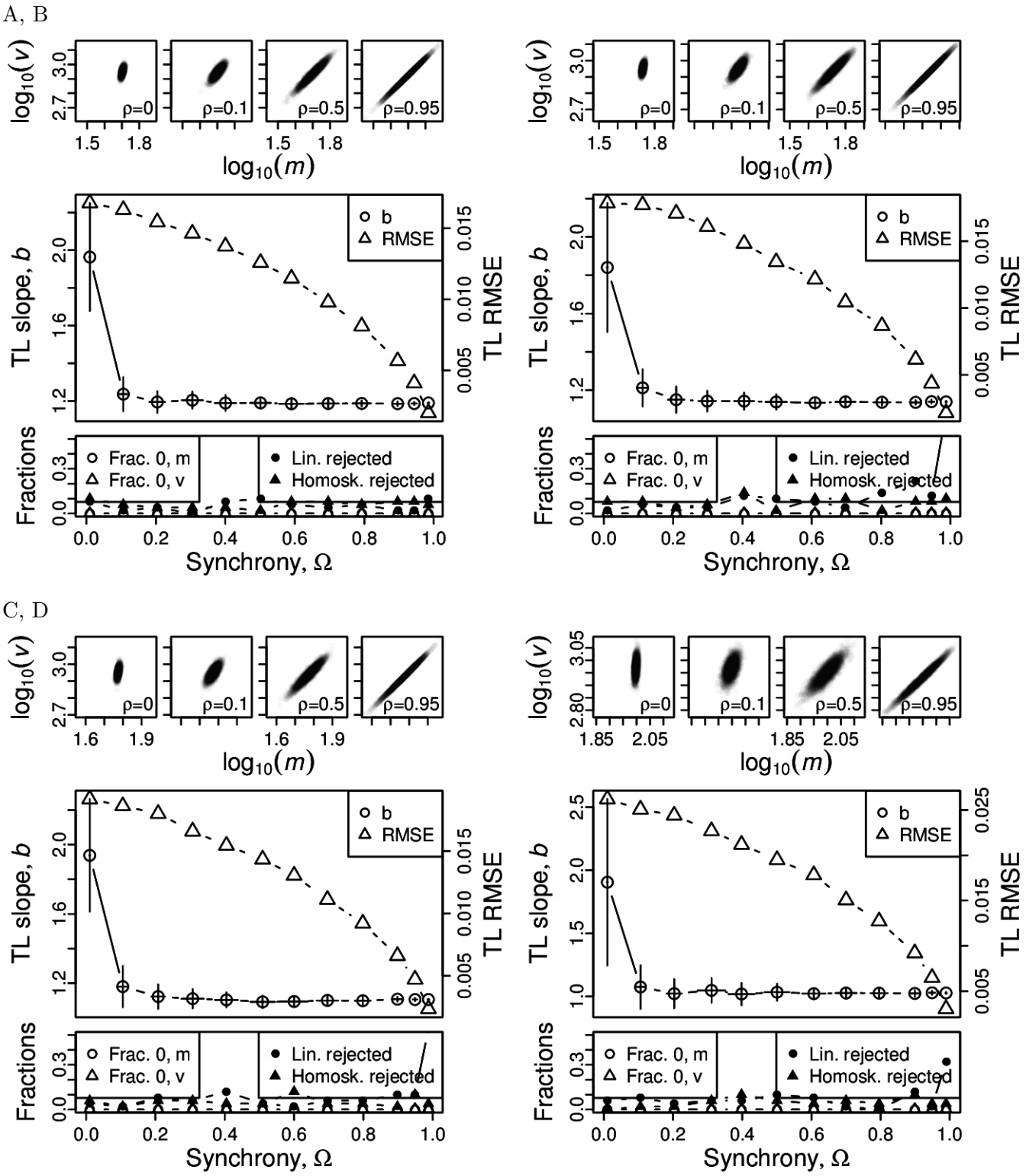

Figure S34: Omnibus plots (see section S6) for non-identically distributed Poisson marginals under the set up of section S4, for $n = 100$ and Y_1 with $\lambda = 1$ (A), $\lambda = 5$ (B), $\lambda = 10$ (C), and $\lambda = 50$ (D).

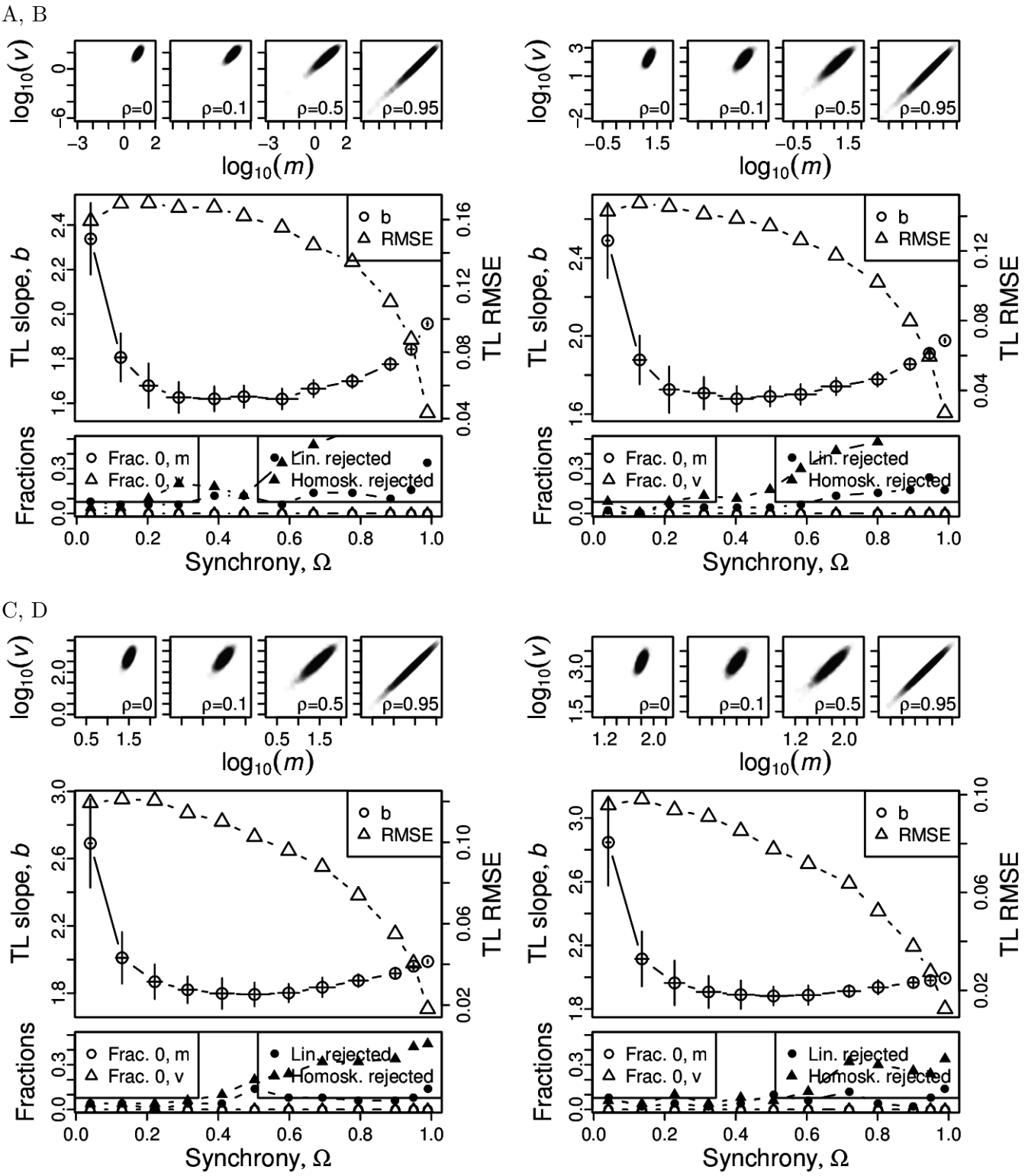

Figure S35: Omnibus plots (see section S6) for non-identically distributed gamma marginals under the set up of section S4, for $n = 25$ and Y_1 with $\beta = 0.5$ and $\alpha = 1$ (A), $\alpha = 2$ (B), $\alpha = 4$ (C), and $\alpha = 8$ (D).

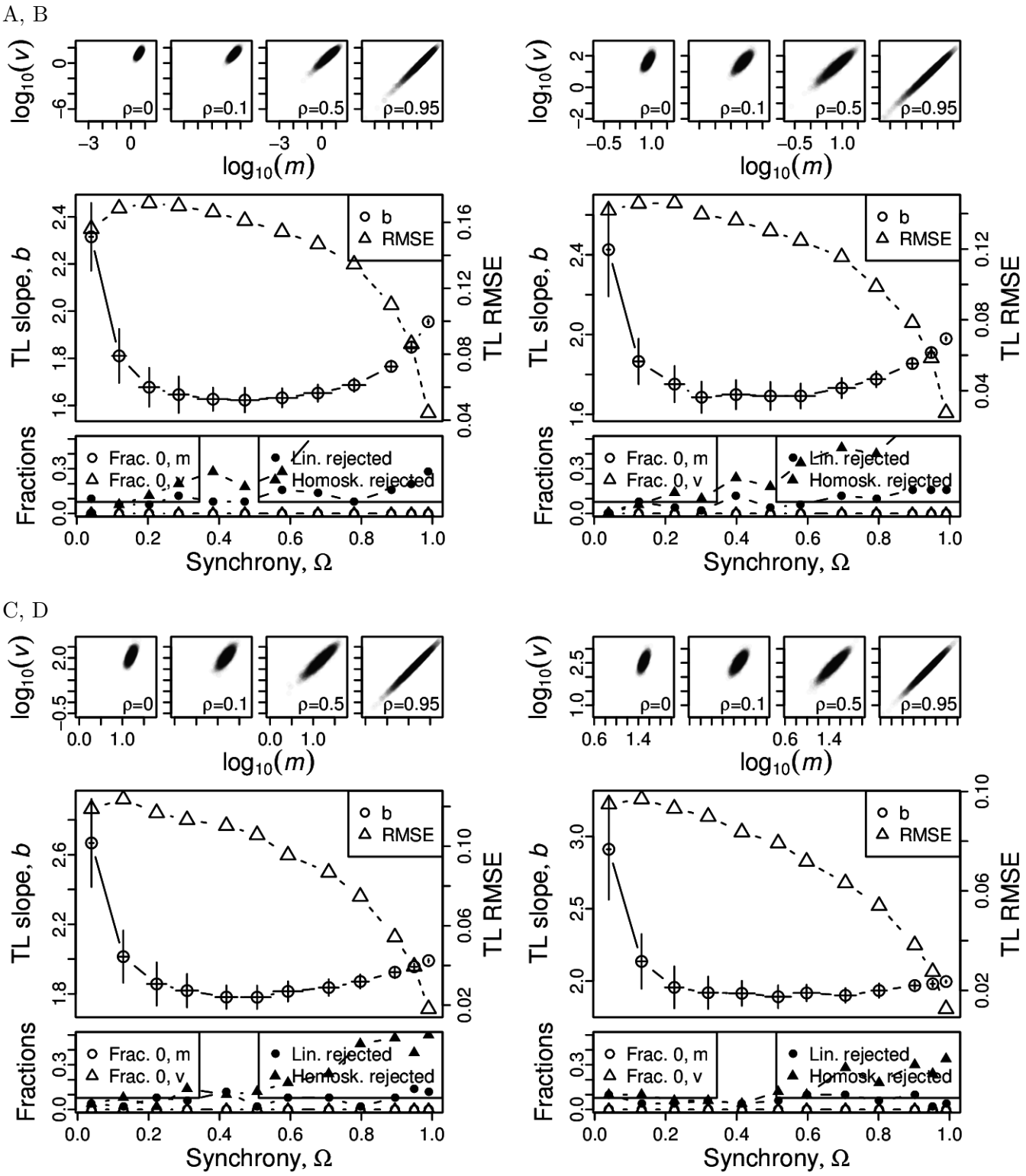

Figure S36: Omnibus plots (see section S6) for non-identically distributed gamma marginals under the set up of section S4, for $n = 25$ and Y_1 with $\beta = 1$ and $\alpha = 1$ (A), $\alpha = 2$ (B), $\alpha = 4$ (C), and $\alpha = 8$ (D).

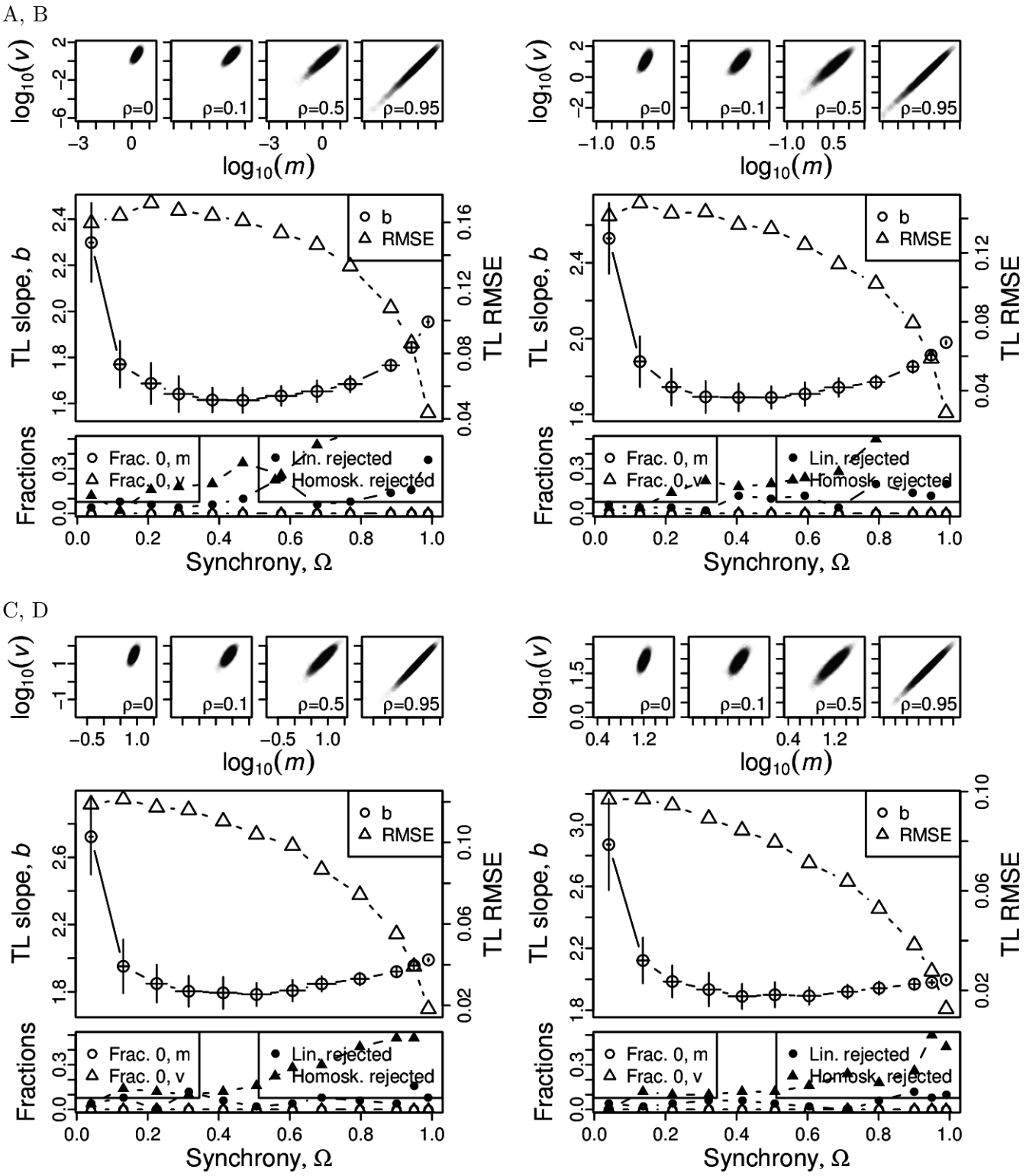

Figure S37: Omnibus plots (see section S6) for non-identically distributed gamma marginals under the set up of section S4, for $n = 25$ and Y_1 with $\beta = 2$ and $\alpha = 1$ (A), $\alpha = 2$ (B), $\alpha = 4$ (C), and $\alpha = 8$ (D).

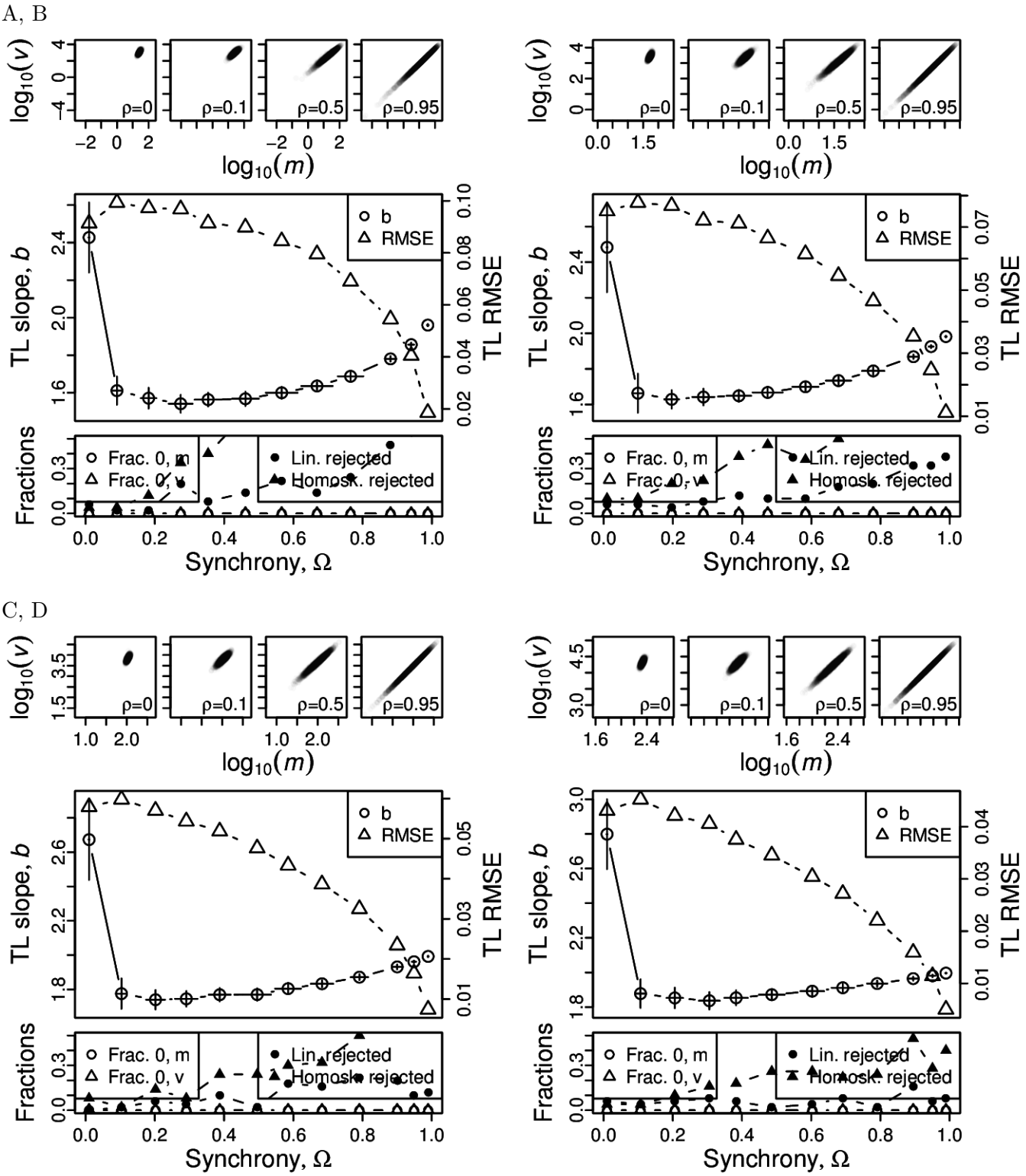

Figure S38: Omnibus plots (see section S6) for non-identically distributed gamma marginals under the set up of section S4, for $n = 100$ and Y_1 with $\beta = 0.5$ and $\alpha = 1$ (A), $\alpha = 2$ (B), $\alpha = 4$ (C), and $\alpha = 8$ (D).

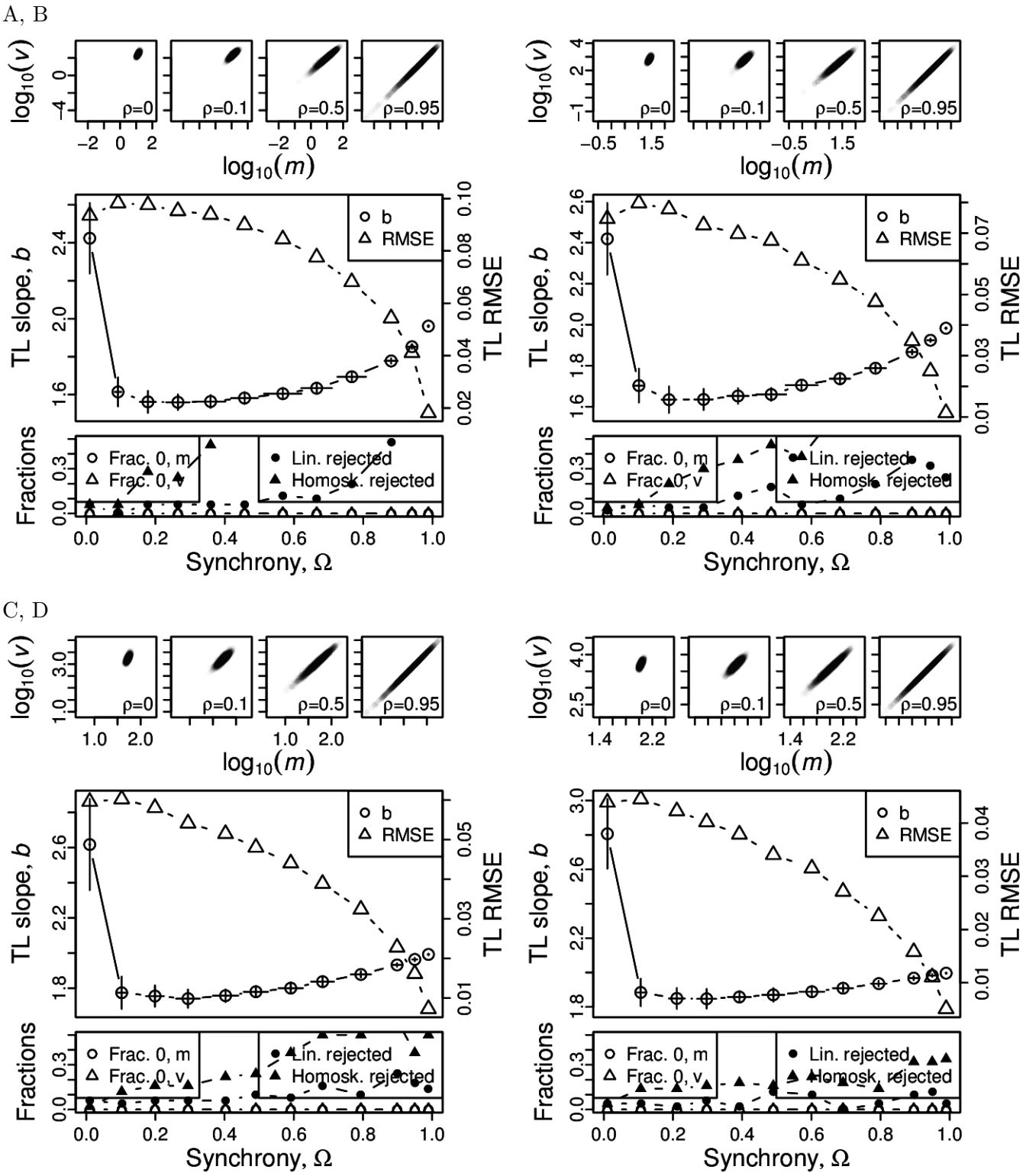

Figure S39: Omnibus plots (see section S6) for non-identically distributed gamma marginals under the set up of section S4, for $n = 100$ and Y_1 with $\beta = 1$ and $\alpha = 1$ (A), $\alpha = 2$ (B), $\alpha = 4$ (C), and $\alpha = 8$ (D).

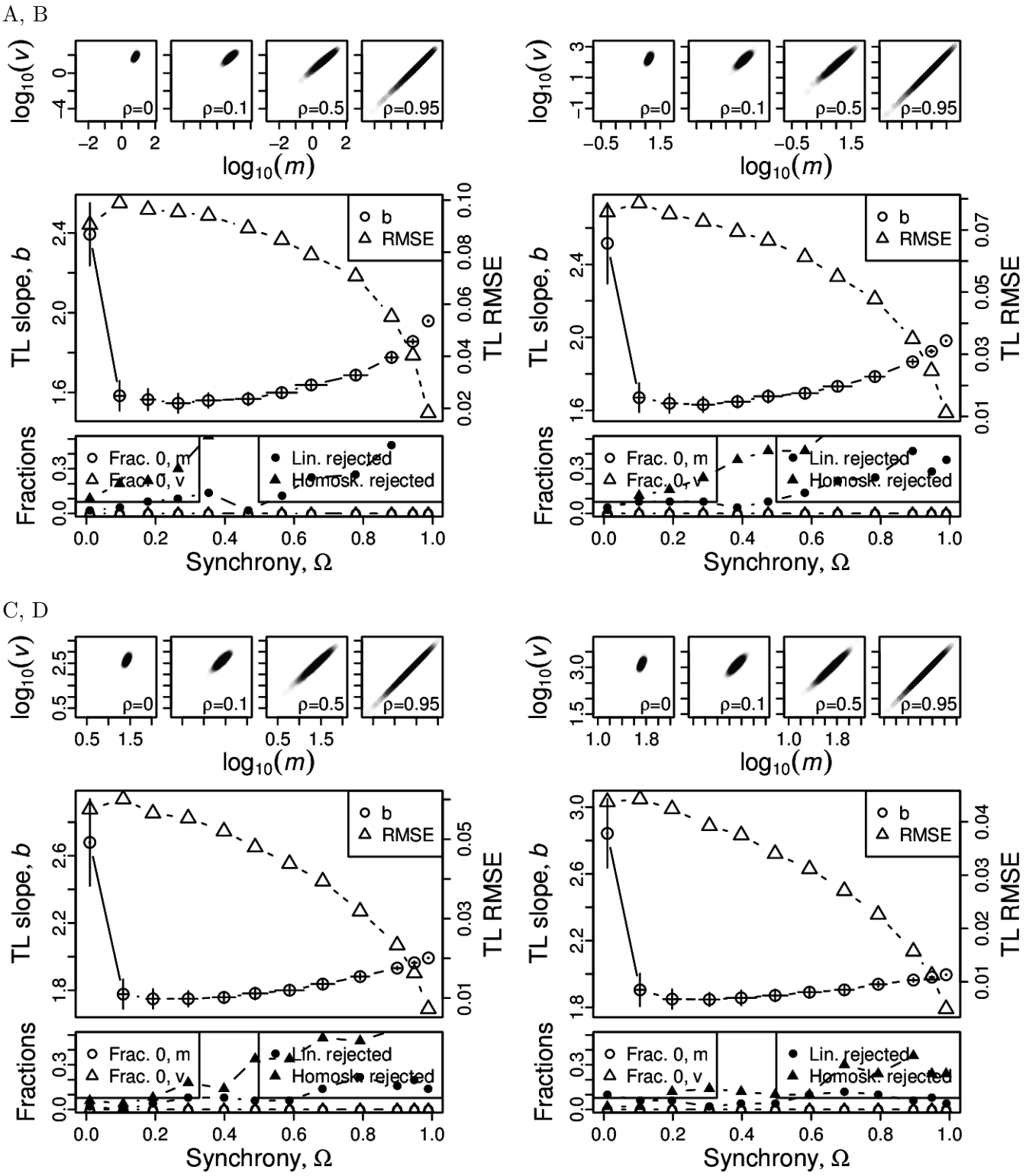

Figure S40: Omnibus plots (see section S6) for non-identically distributed gamma marginals under the set up of section S4, for $n = 100$ and Y_1 with $\beta = 2$ and $\alpha = 1$ (A), $\alpha = 2$ (B), $\alpha = 4$ (C), and $\alpha = 8$ (D).

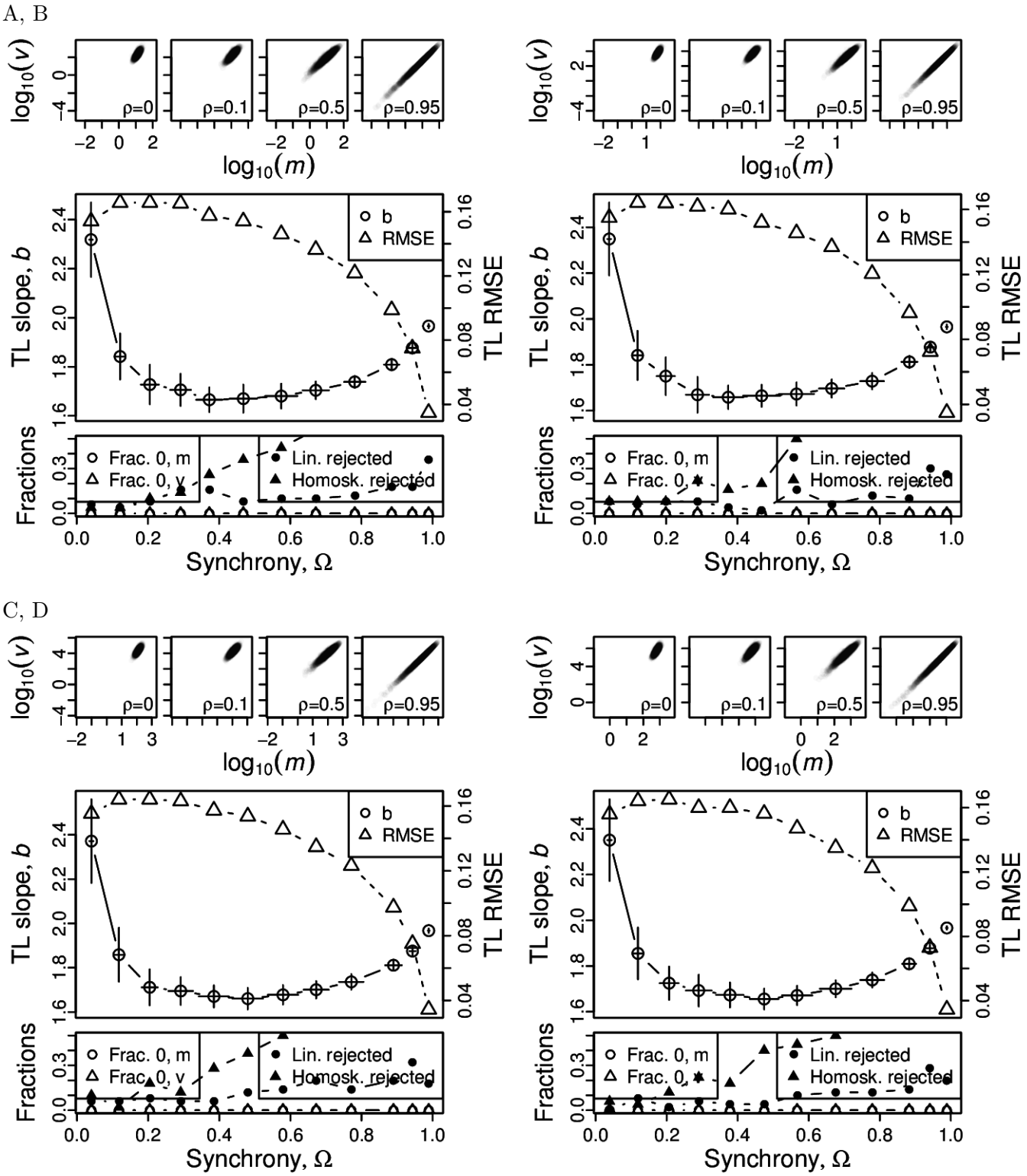

Figure S41: Omnibus plots (see section S6) for non-identically distributed exponentially distributed marginals under the set up of section S4, for $n = 25$ and Y_1 with $1/\lambda = 1$ (A), $1/\lambda = 5$ (B), $1/\lambda = 10$ (C), and $1/\lambda = 50$ (D).

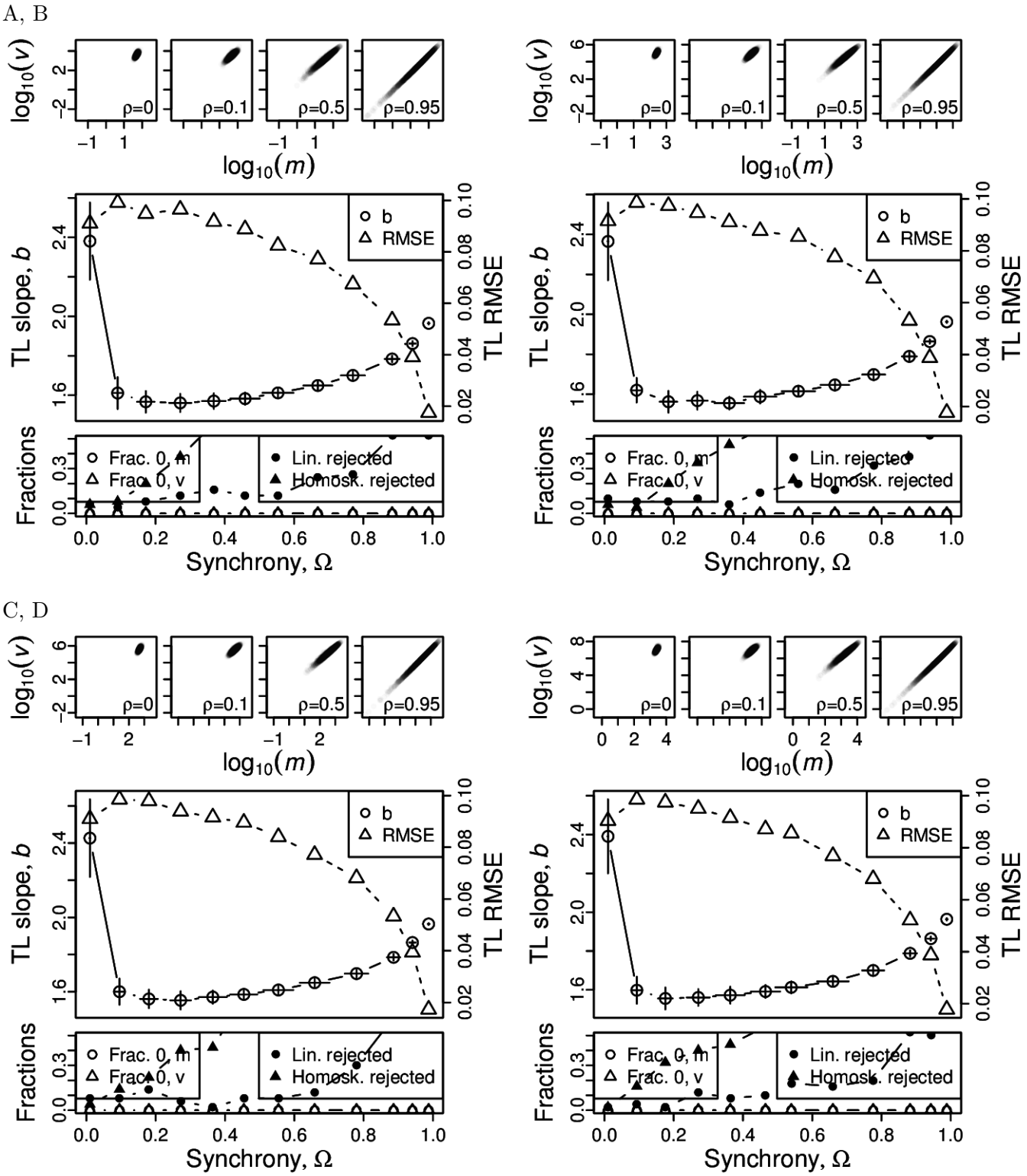

Figure S42: Omnibus plots (see section S6) for non-identically distributed exponentially distributed marginals under the set up of section S4, for $n = 100$ and Y_1 with $1/\lambda = 1$ (A), $1/\lambda = 5$ (B), $1/\lambda = 10$ (C), and $1/\lambda = 50$ (D).

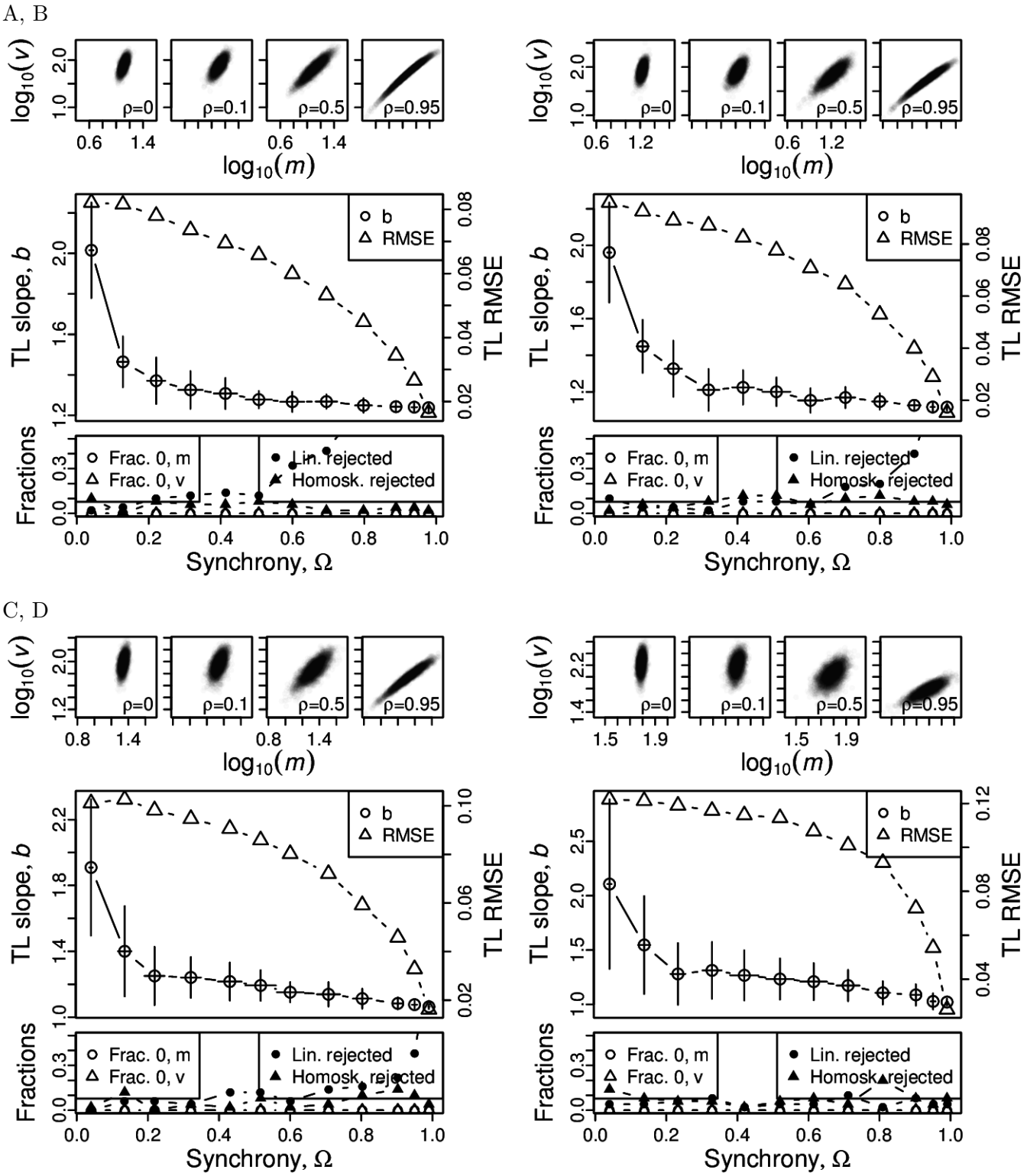

Figure S43: Omnibus plots (see section S6) for non-identically distributed chi-squared distributed marginals under the set up of section S4, for $n = 25$ and Y_1 with $k = 1$ (A), $k = 5$ (B), $k = 10$ (C), and $k = 50$ (D).

A, B

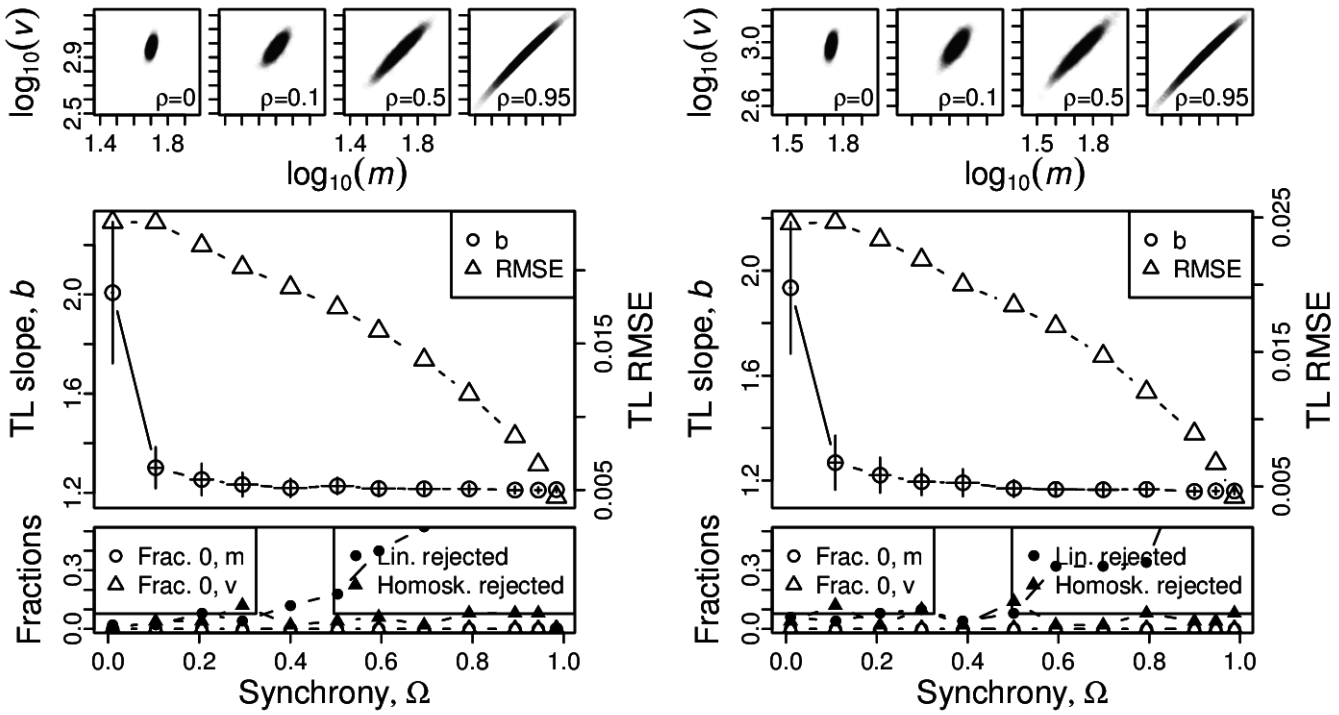

C, D

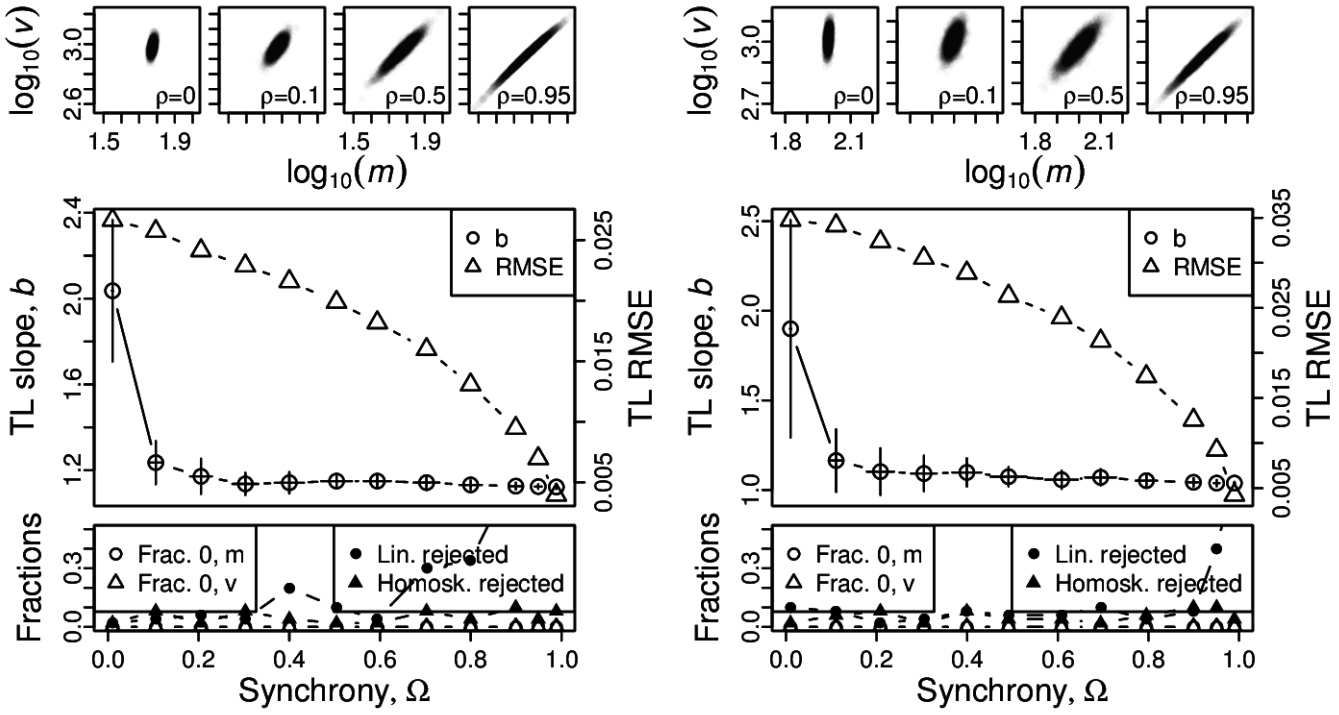

Figure S44: Omnibus plots (see section S6) for non-identically distributed chi-squared distributed marginals under the set up of section S4, for $n = 100$ and Y_1 with $k = 1$ (A), $k = 5$ (B), $k = 10$ (C), and $k = 50$ (D).

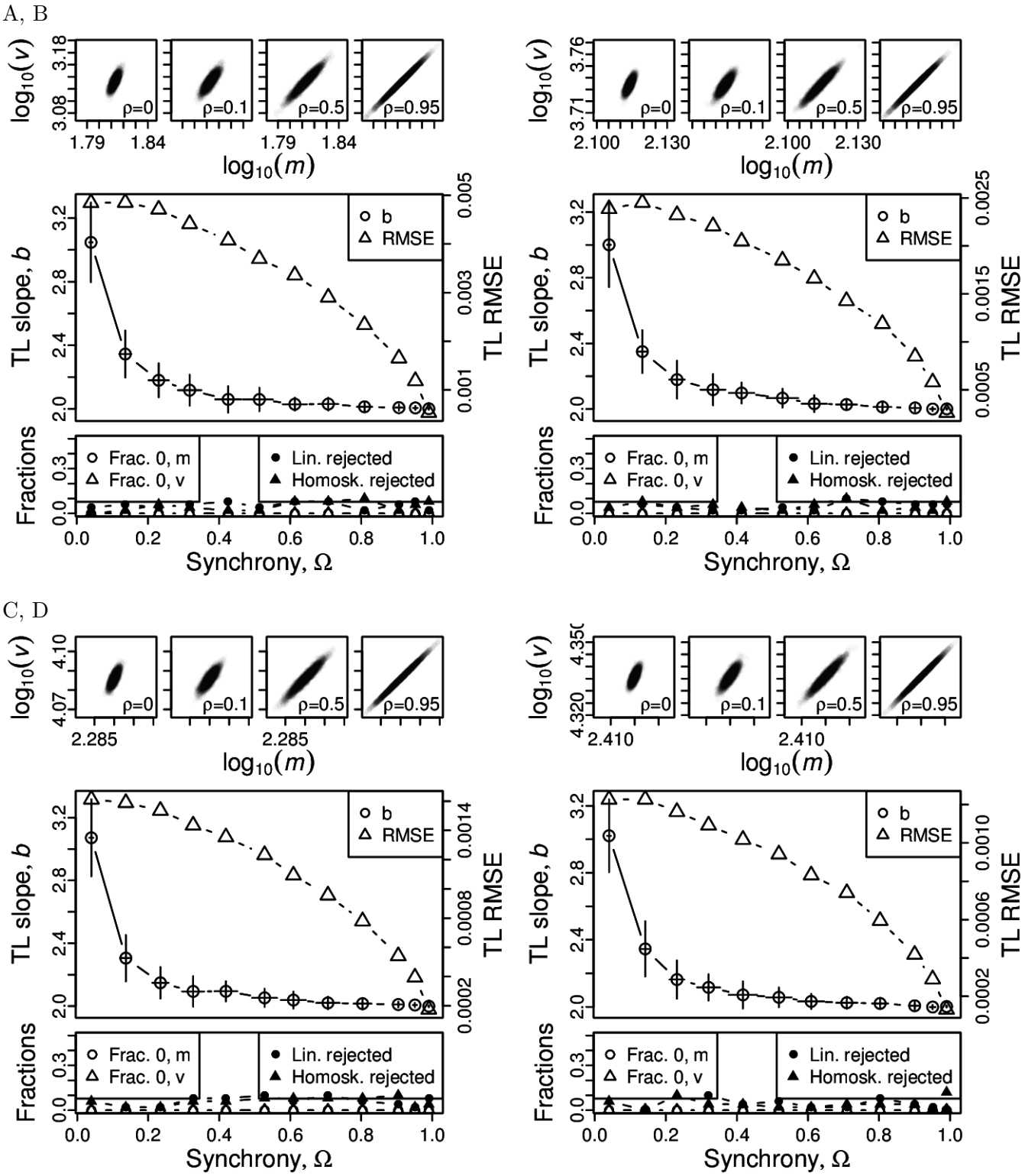

Figure S45: Omnibus plots (see section S6) for non-identically distributed normal marginals under the set up of section S4, for $n = 25$ and Y_1 with $\sigma = 0.1$ and $\mu = 5$ (A), $\mu = 10$ (B), $\mu = 15$ (C), and $\mu = 20$ (D).

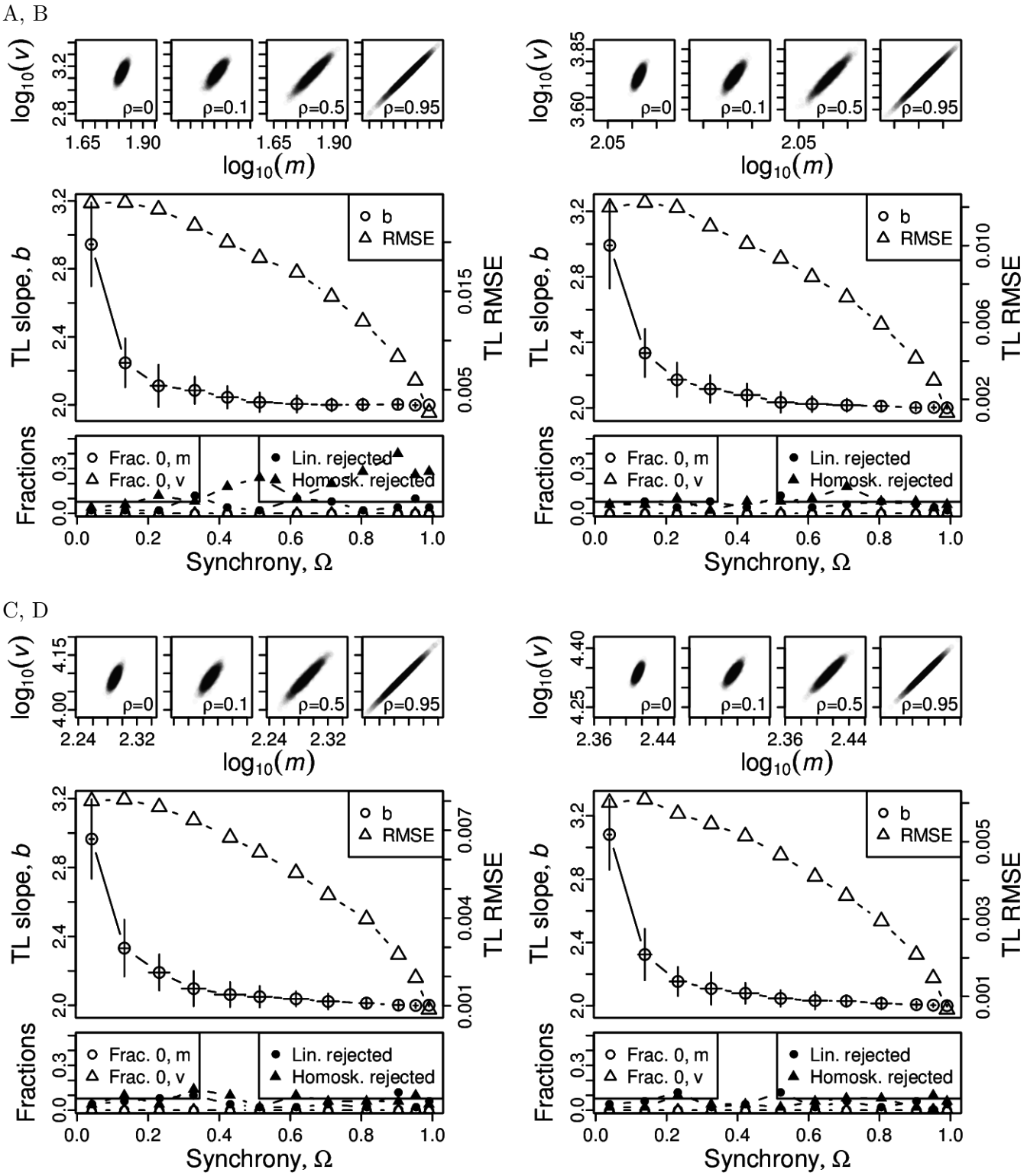

Figure S46: Omnibus plots (see section S6) for non-identically distributed normal marginals under the set up of section S4, for $n = 25$ and Y_1 with $\sigma = 0.5$ and $\mu = 5$ (A), $\mu = 10$ (B), $\mu = 15$ (C), and $\mu = 20$ (D).

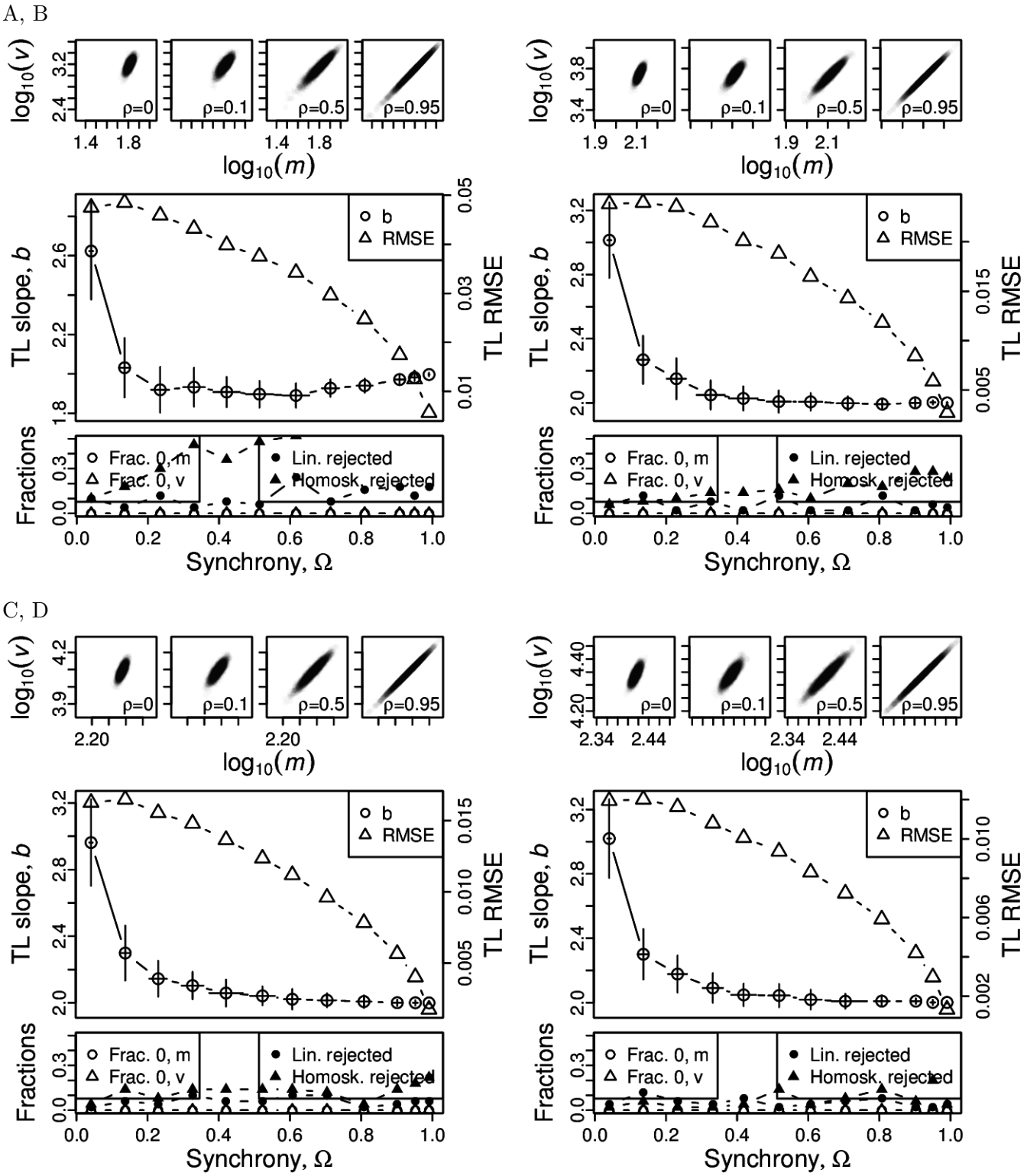

Figure S47: Omnibus plots (see section S6) for non-identically distributed normal marginals under the set up of section S4, for $n = 25$ and Y_1 with $\sigma = 1$ and $\mu = 5$ (A), $\mu = 10$ (B), $\mu = 15$ (C), and $\mu = 20$ (D).

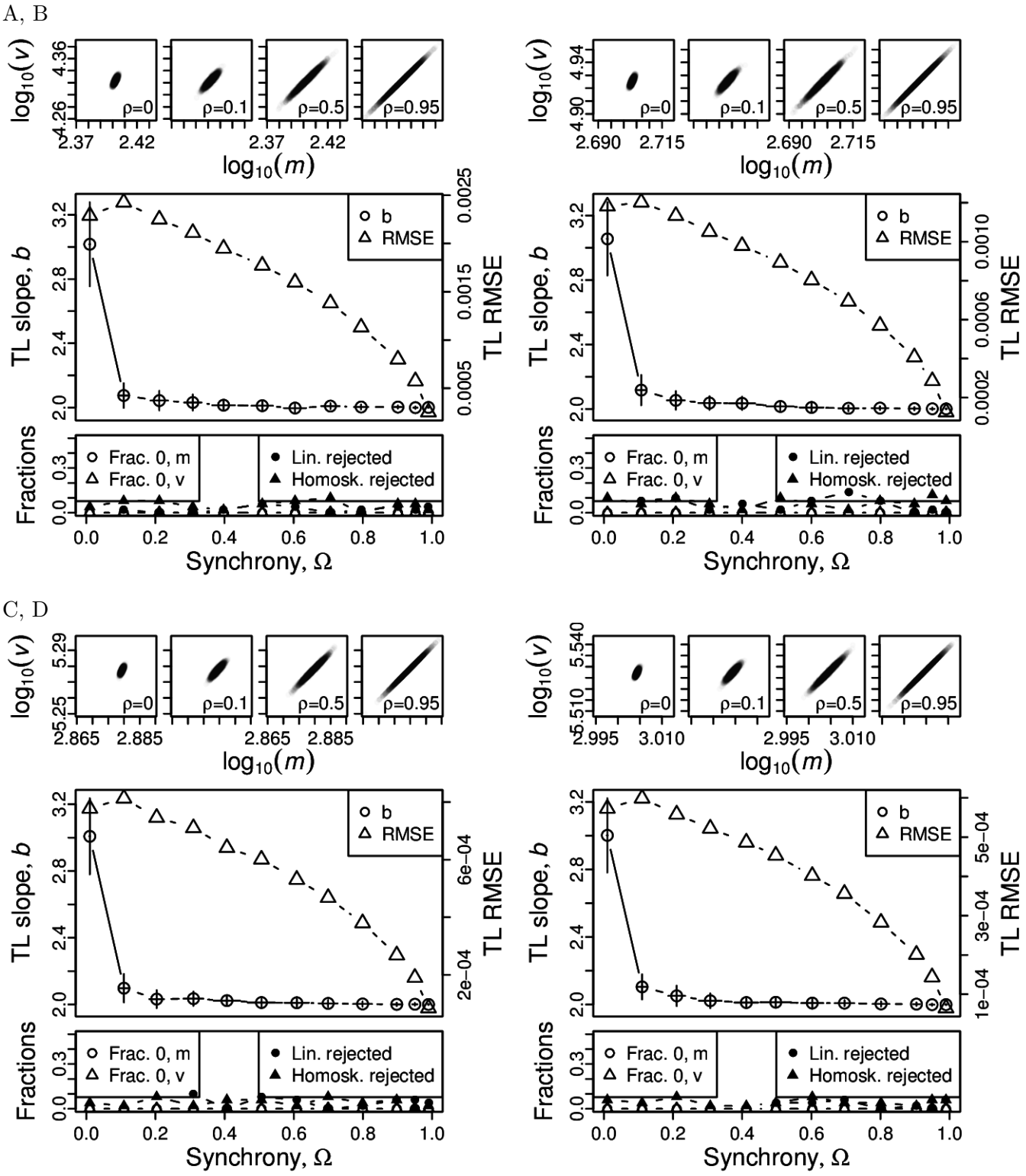

Figure S48: Omnibus plots (see section S6) for non-identically distributed normal marginals under the set up of section S4, for $n = 100$ and Y_1 with $\sigma = 0.1$ and $\mu = 5$ (A), $\mu = 10$ (B), $\mu = 15$ (C), and $\mu = 20$ (D).

A, B

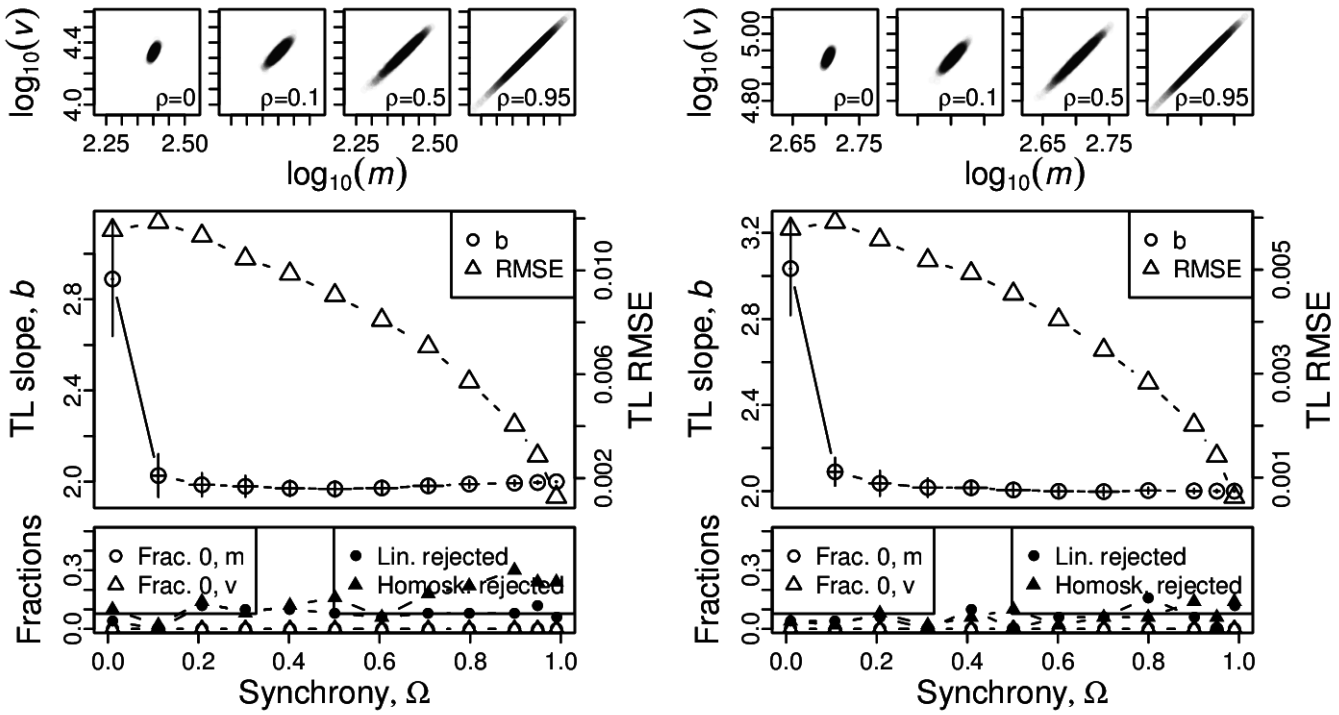

C, D

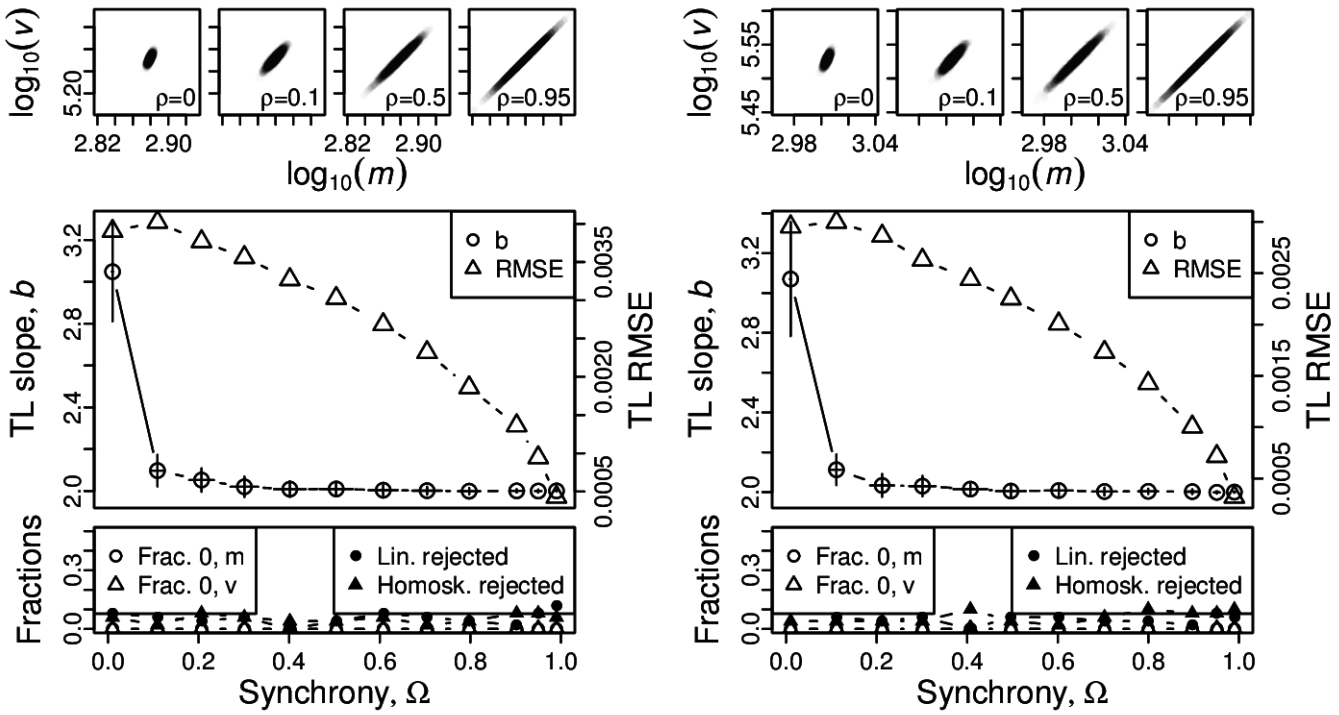

Figure S49: Omnibus plots (see section S6) for non-identically distributed normal marginals under the set up of section S4, for $n = 100$ and Y_1 with $\sigma = 0.5$ and $\mu = 5$ (A), $\mu = 10$ (B), $\mu = 15$ (C), and $\mu = 20$ (D).

A, B

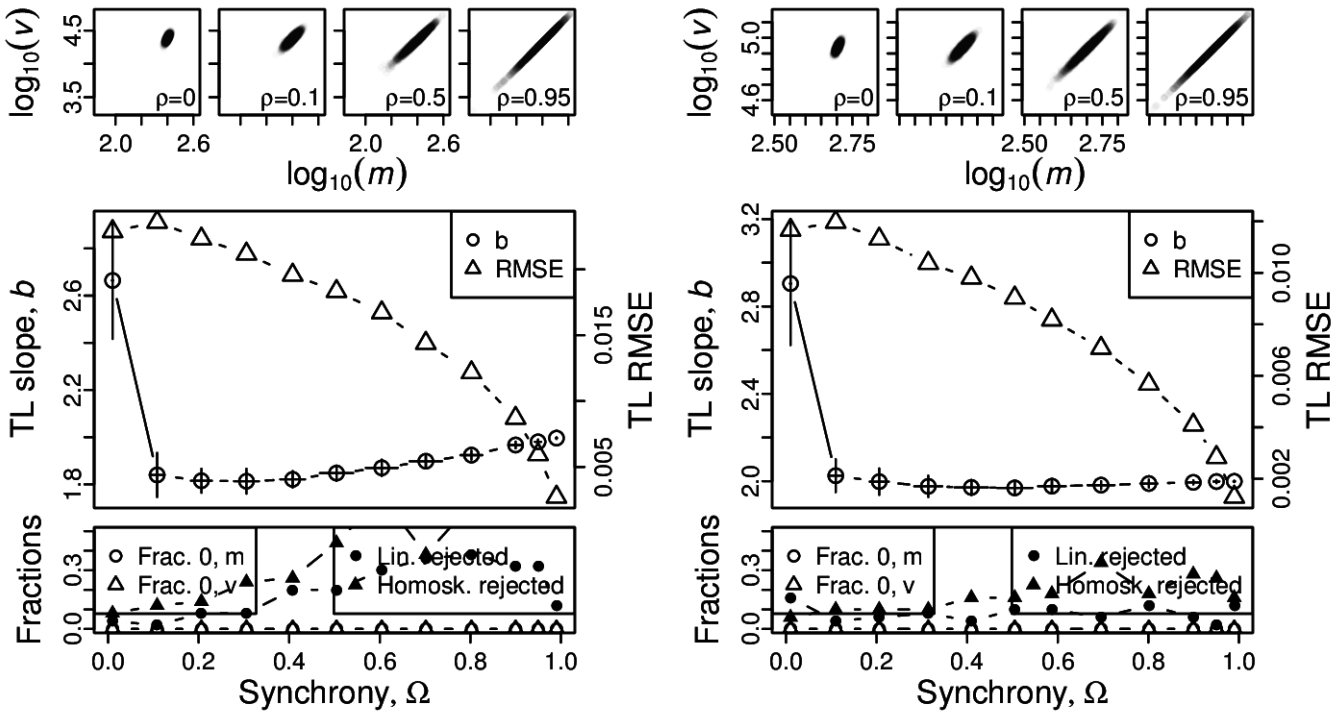

C, D

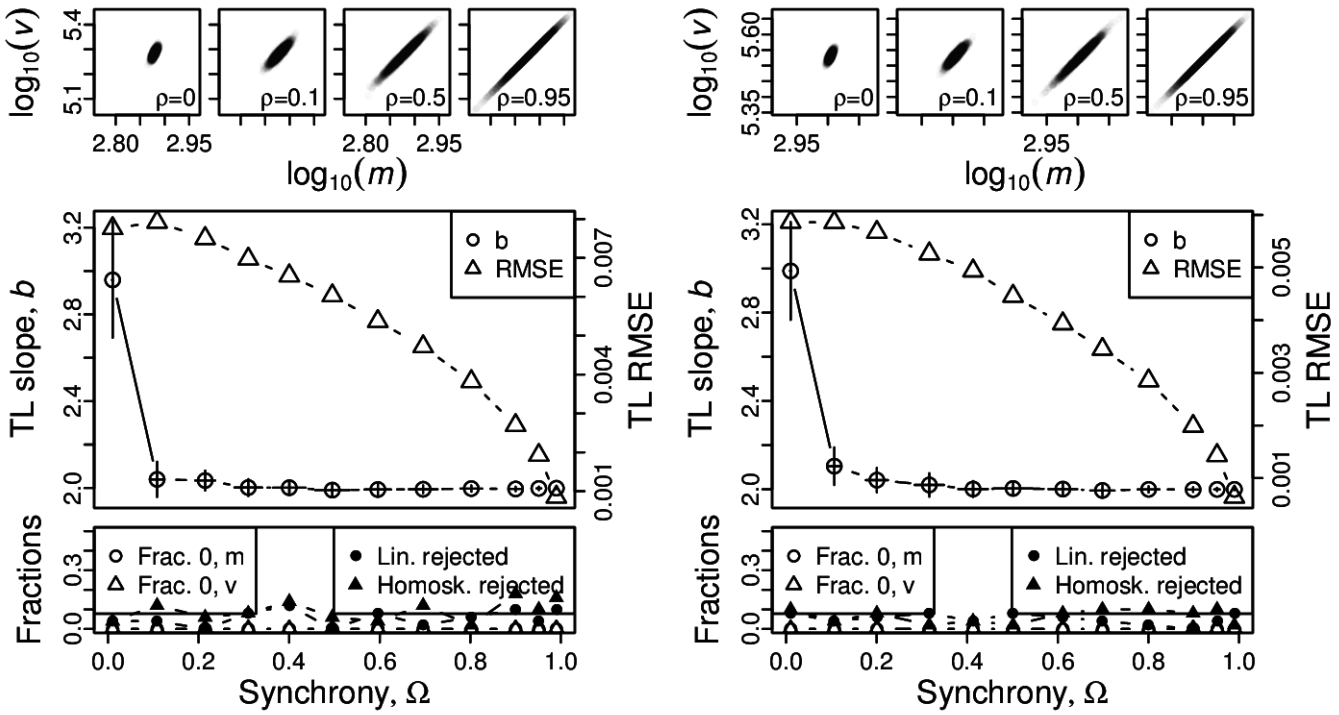

Figure S50: Omnibus plots (see section S6) for non-identically distributed normal marginals under the set up of section S4, for $n = 100$ and Y_1 with $\sigma = 1$ and $\mu = 5$ (A), $\mu = 10$ (B), $\mu = 15$ (C), and $\mu = 20$ (D).

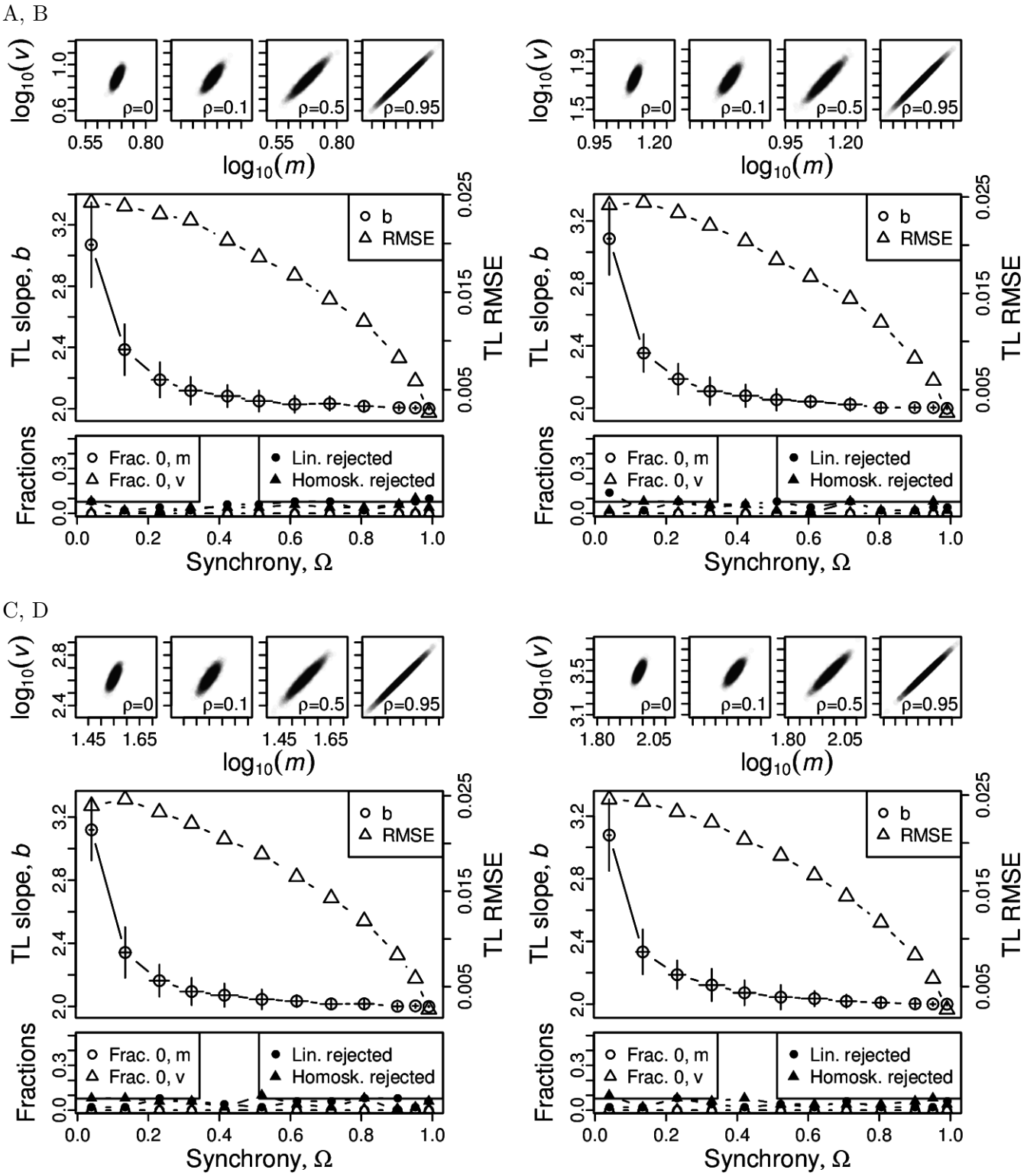

Figure S51: Omnibus plots (see section S6) for non-identically distributed log-normal marginals under the set up of section S4, for $n = 25$ and Y_1 with $\sigma = 0.1$ and $\mu = -1$ (A), $\mu = 0$ (B), $\mu = 1$ (C), and $\mu = 2$ (D).

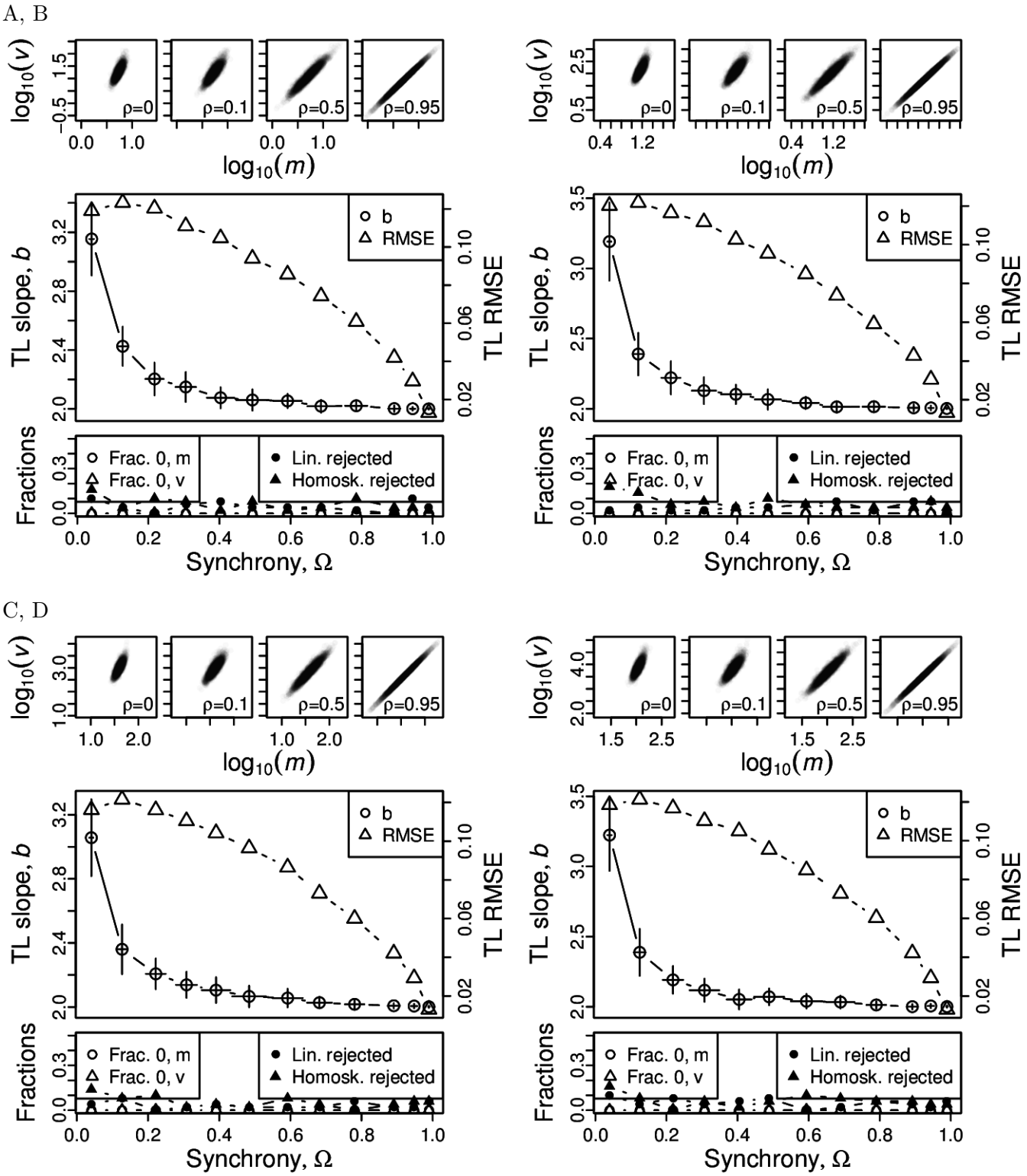

Figure S52: Omnibus plots (see section S6) for non-identically distributed log-normal marginals under the set up of section S4, for $n = 25$ and Y_1 with $\sigma = 0.5$ and $\mu = -1$ (A), $\mu = 0$ (B), $\mu = 1$ (C), and $\mu = 2$ (D).

A, B

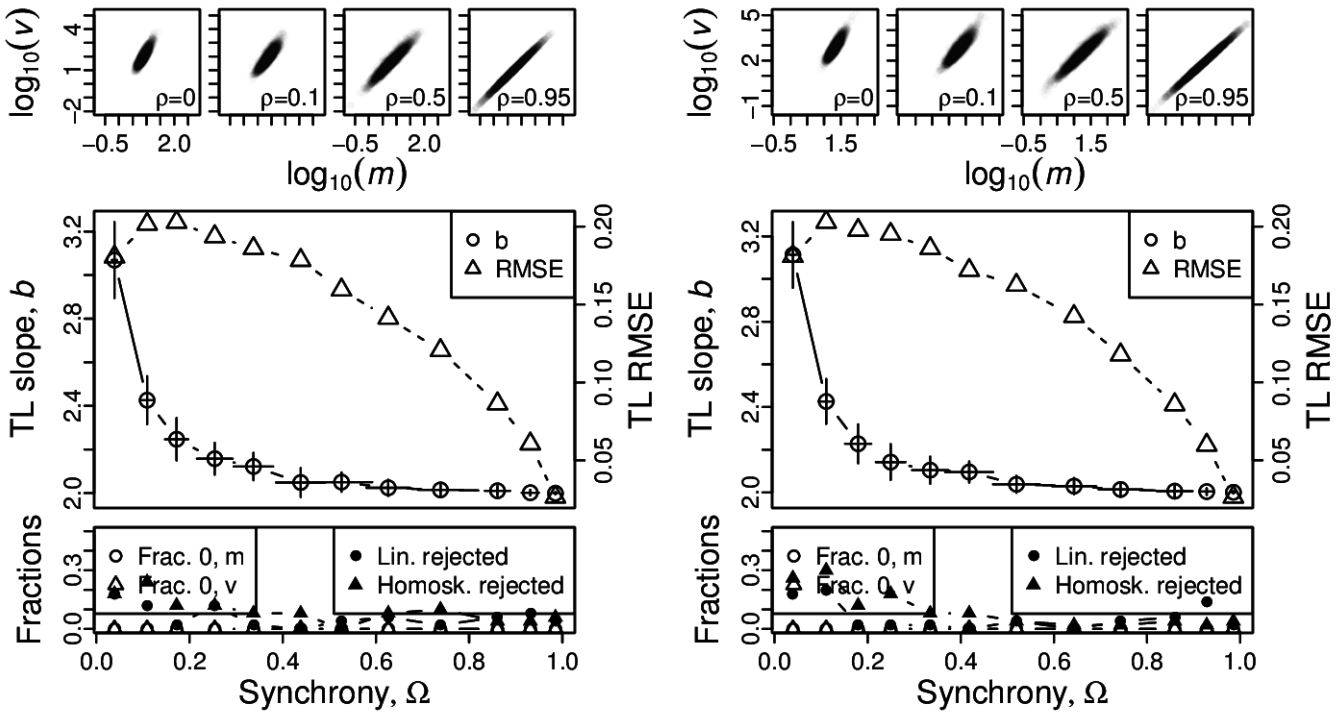

C, D

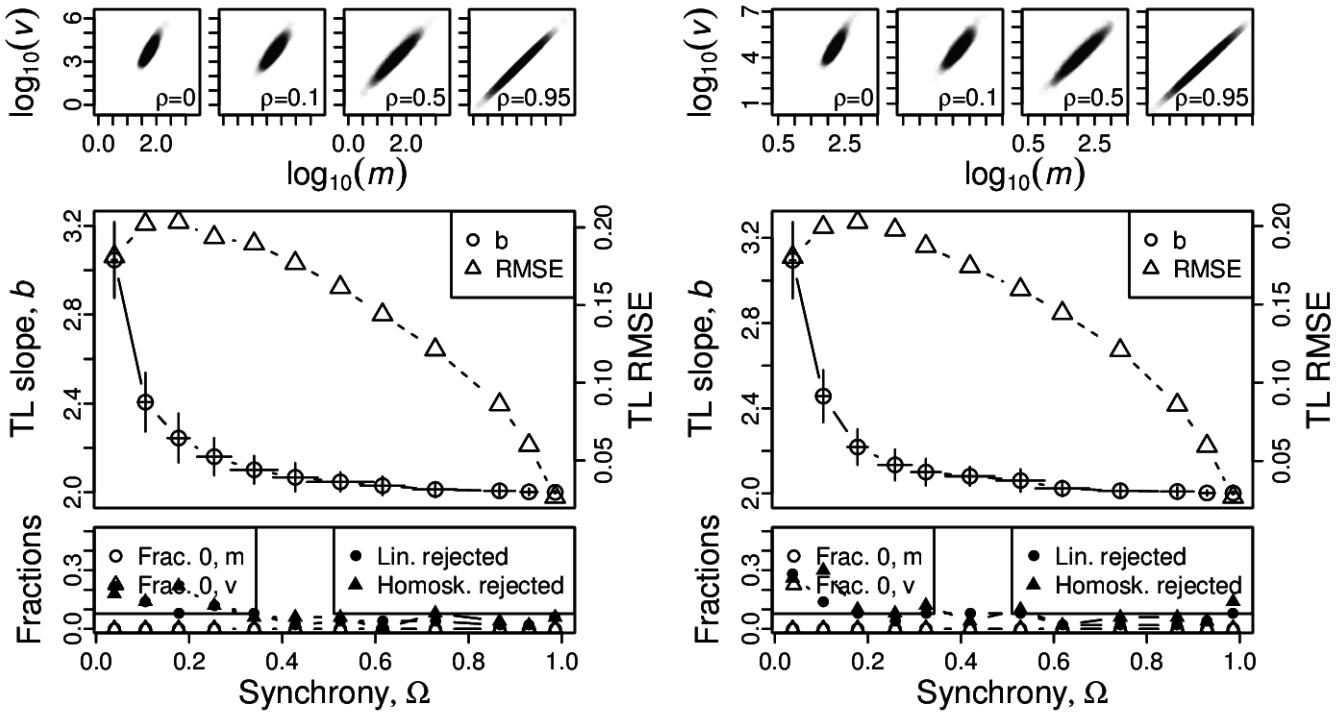

Figure S53: Omnibus plots (see section S6) for non-identically distributed log-normal marginals under the set up of section S4, for $n = 25$ and Y_1 with $\sigma = 1$ and $\mu = -1$ (A), $\mu = 0$ (B), $\mu = 1$ (C), and $\mu = 2$ (D).

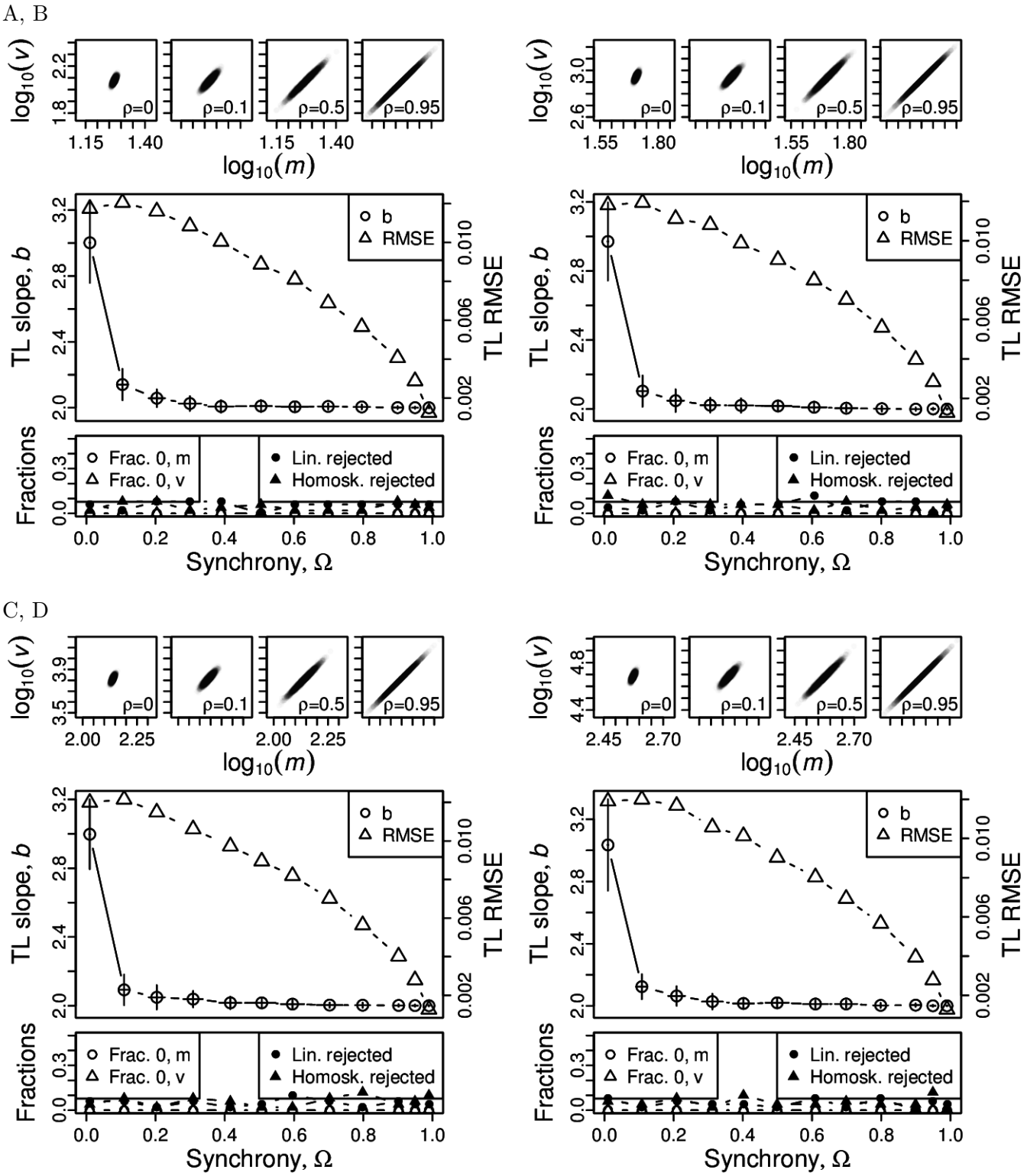

Figure S54: Omnibus plots (see section S6) for non-identically distributed log-normal marginals under the set up of section S4, for $n = 100$ and Y_1 with $\sigma = 0.1$ and $\mu = -1$ (A), $\mu = 0$ (B), $\mu = 1$ (C), and $\mu = 2$ (D).

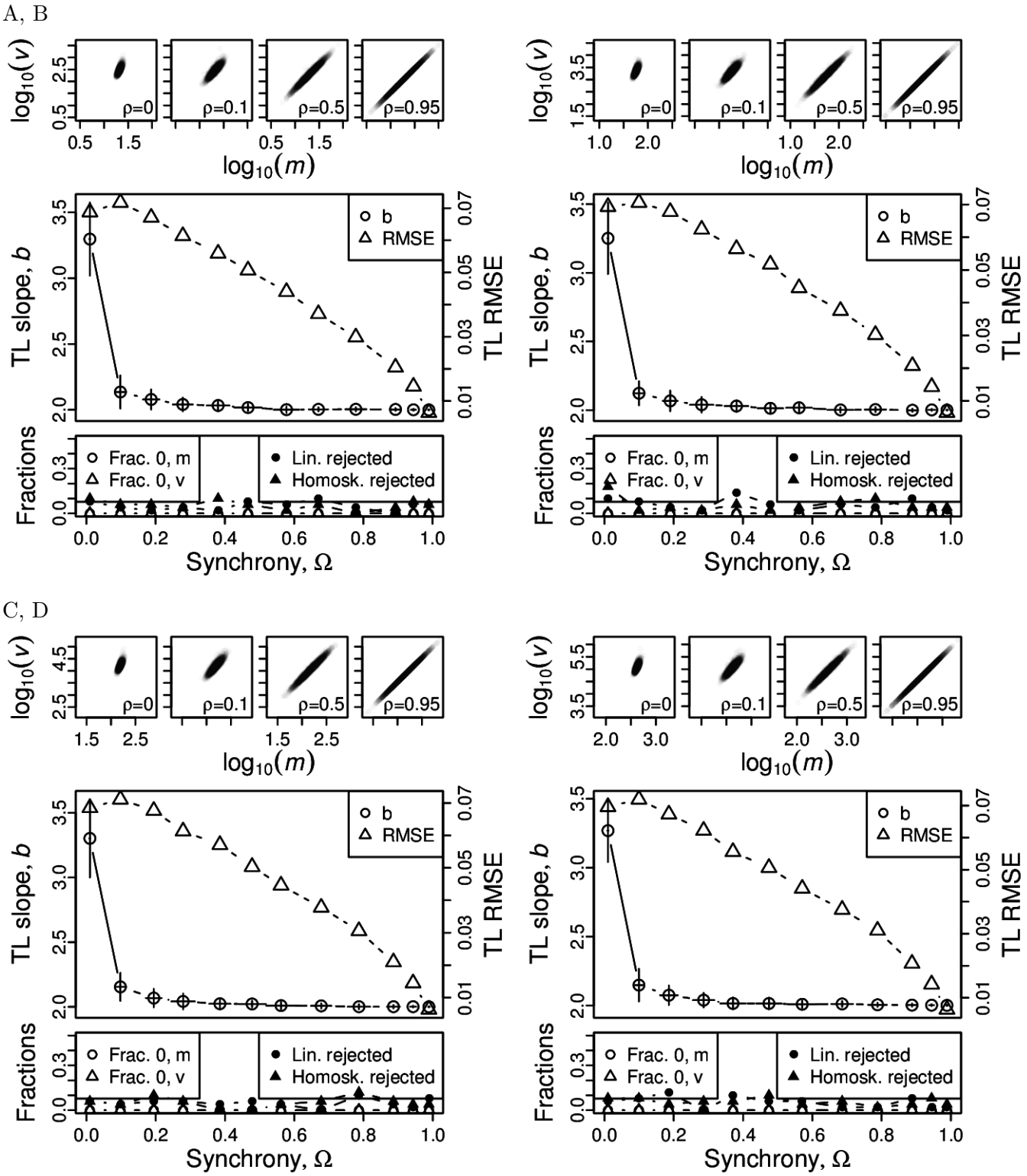

Figure S55: Omnibus plots (see section S6) for non-identically distributed log-normal marginals under the set up of section S4, for $n = 100$ and Y_1 with $\sigma = 0.5$ and $\mu = -1$ (A), $\mu = 0$ (B), $\mu = 1$ (C), and $\mu = 2$ (D).

A, B

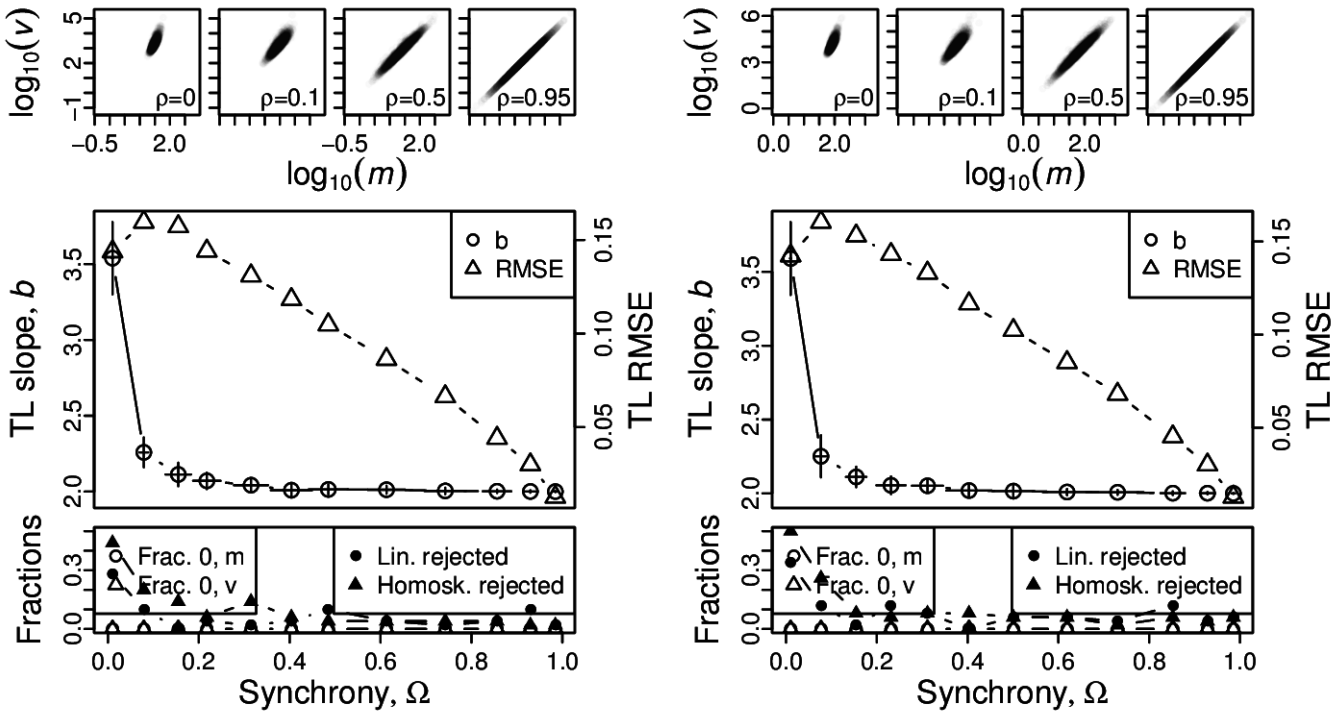

C, D

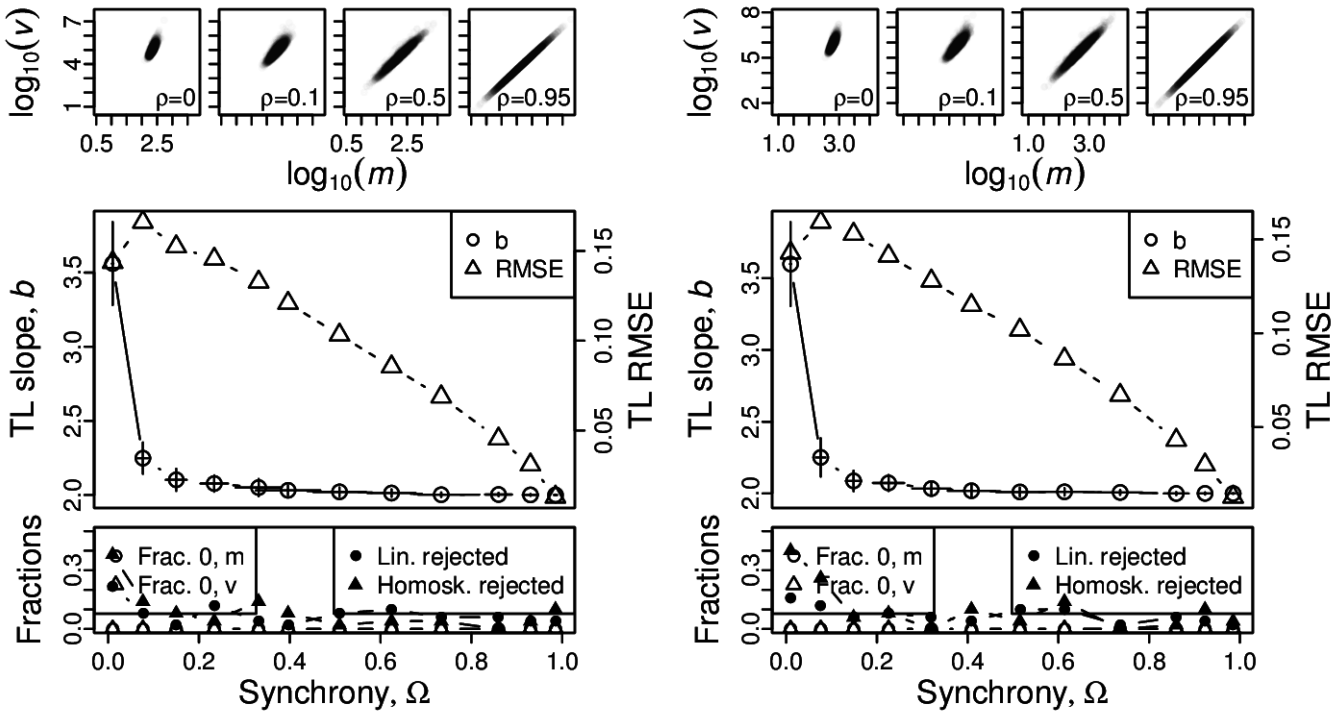

Figure S56: Omnibus plots (see section S6) for non-identically distributed log-normal marginals under the set up of section S4, for $n = 100$ and Y_1 with $\sigma = 1$ and $\mu = -1$ (A), $\mu = 0$ (B), $\mu = 1$ (C), and $\mu = 2$ (D).

A

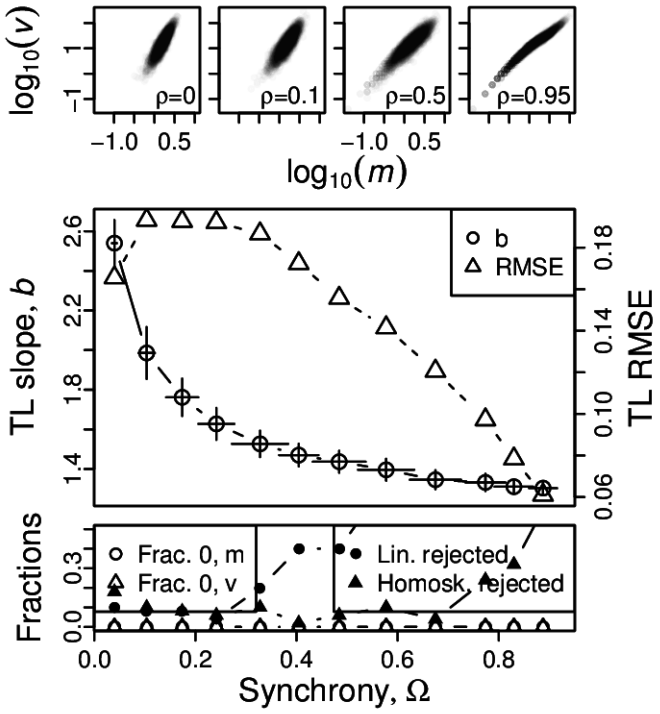

B, C

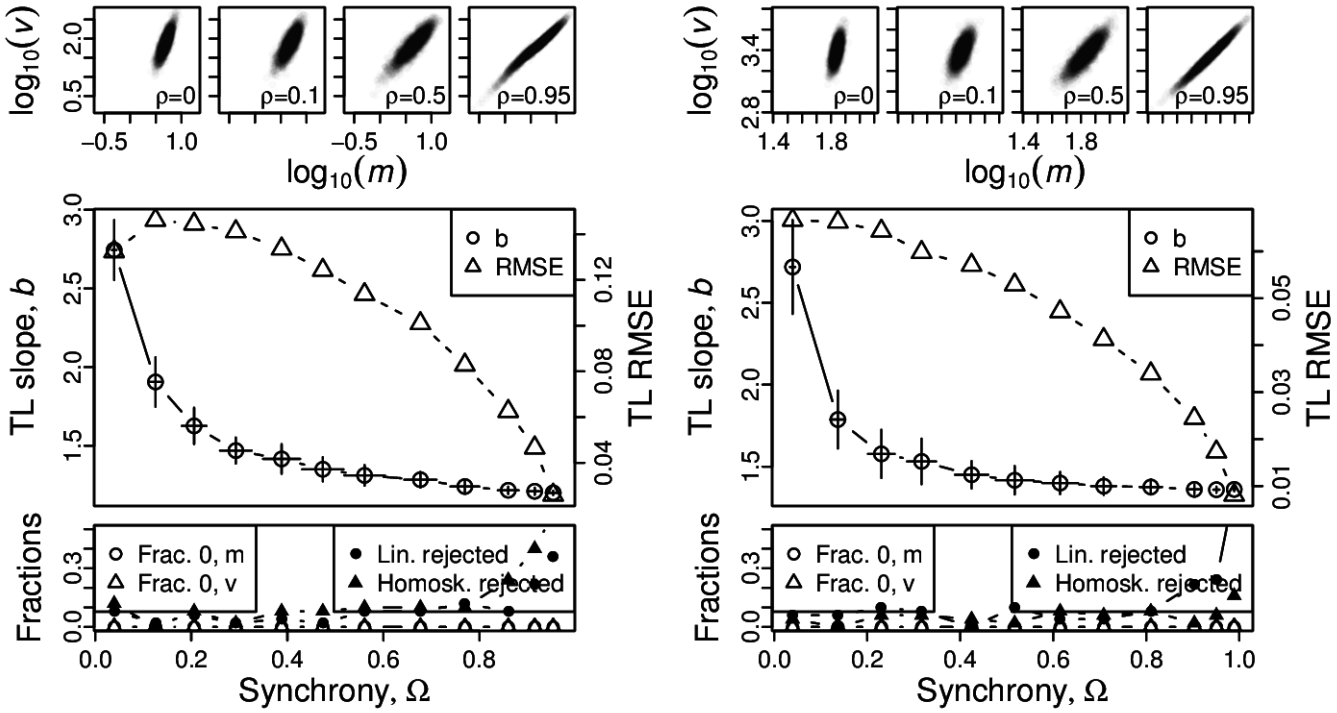

Figure S57: Omnibus plots (see section S6) for non-identically distributed negative binomial marginals under the set up of section S4, for $n = 25$ and Y_1 with $p = 0.2$ and $r = 5$ (A), $r = 10$ (B), $r = 50$ (C).

A

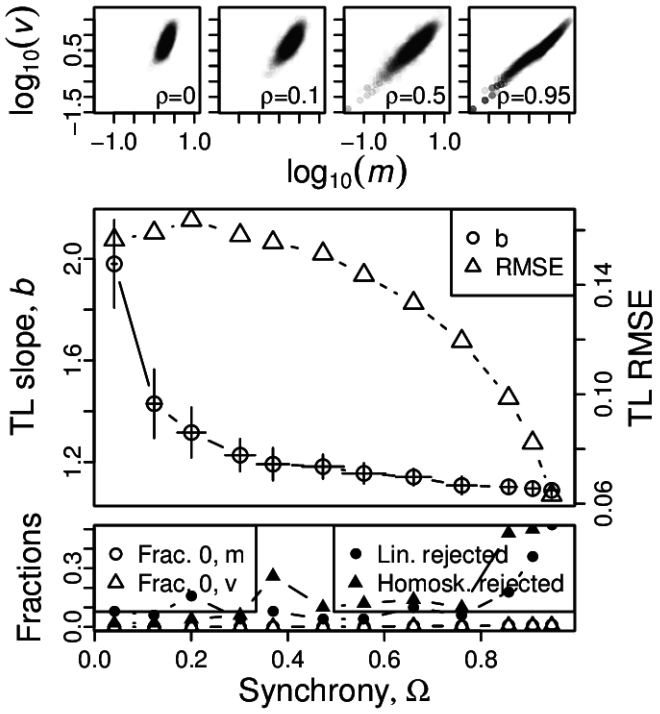

B, C

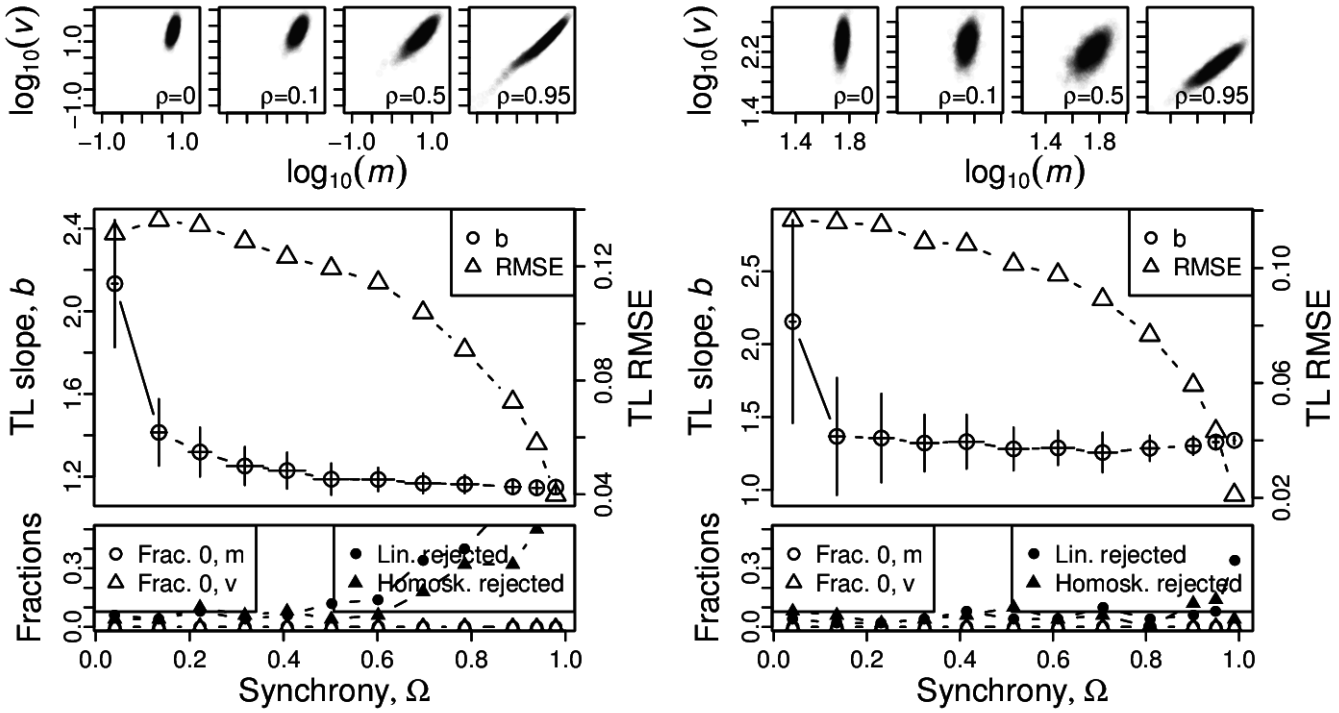

Figure S58: Omnibus plots (see section S6) for non-identically distributed negative binomial marginals under the set up of section S4, for $n = 25$ and Y_1 with $p = 0.4$ and $r = 5$ (A), $r = 10$ (B), $r = 50$ (C).

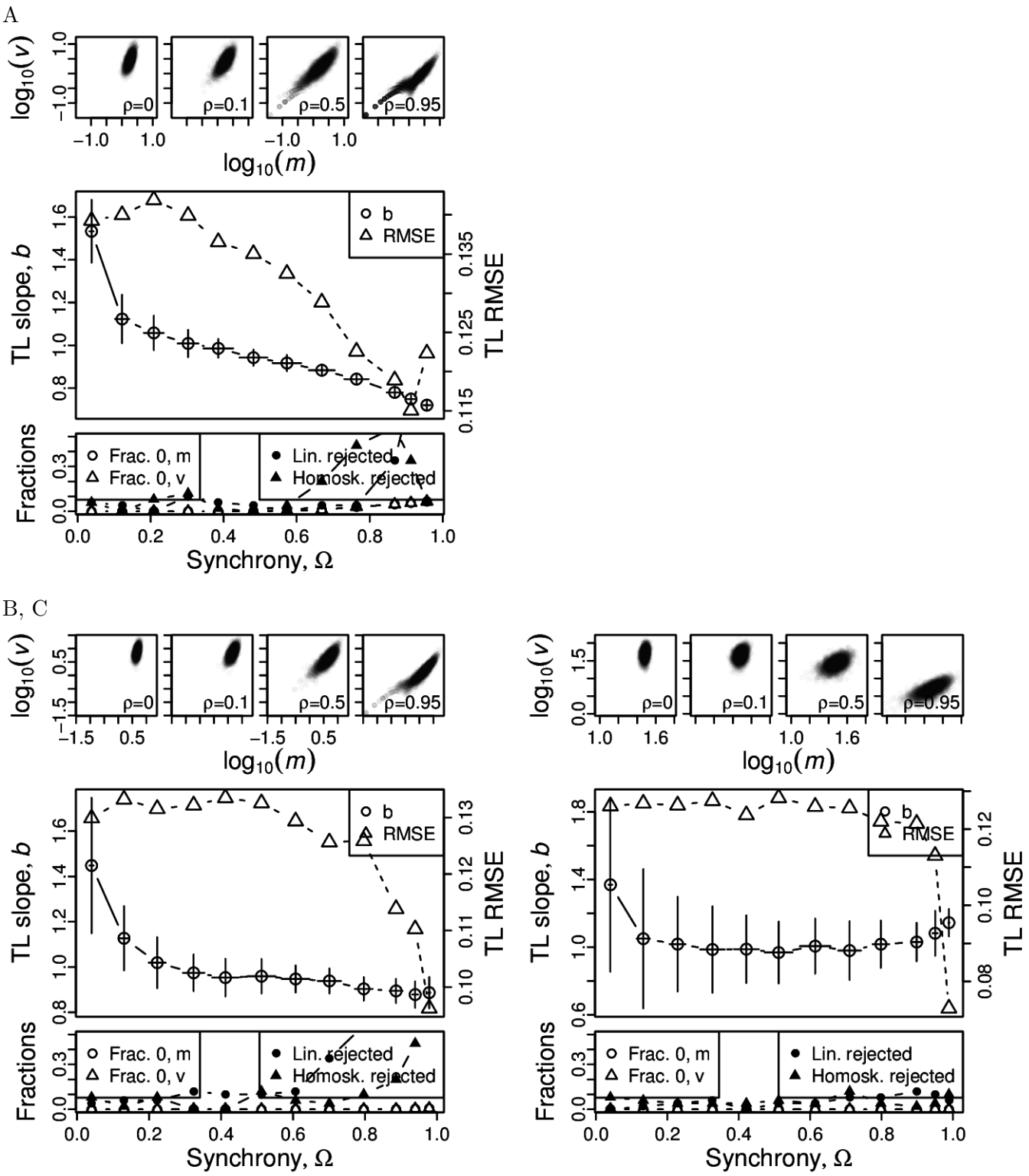

Figure S59: Omnibus plots (see section S6) for non-identically distributed negative binomial marginals under the set up of section S4, for $n = 25$ and Y_1 with $p = 0.6$ and $r = 5$ (A), $r = 10$ (B), $r = 50$ (C).

A

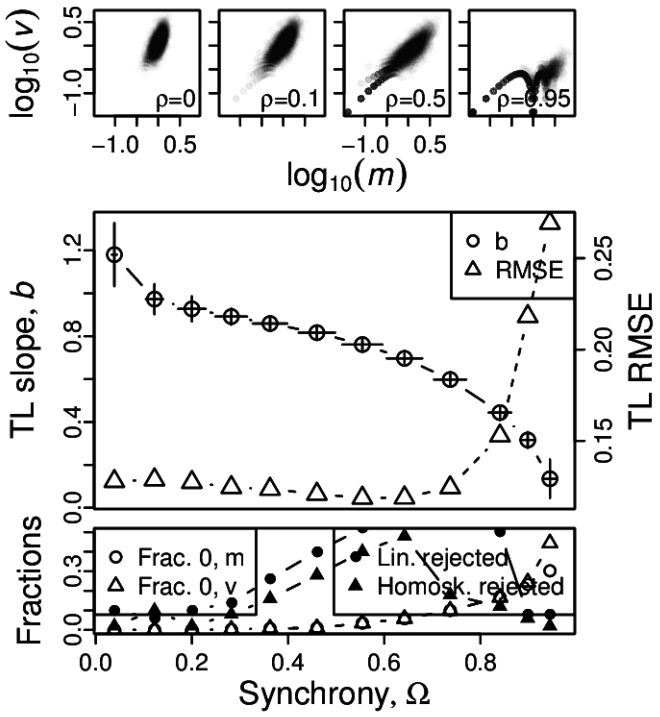

B, C

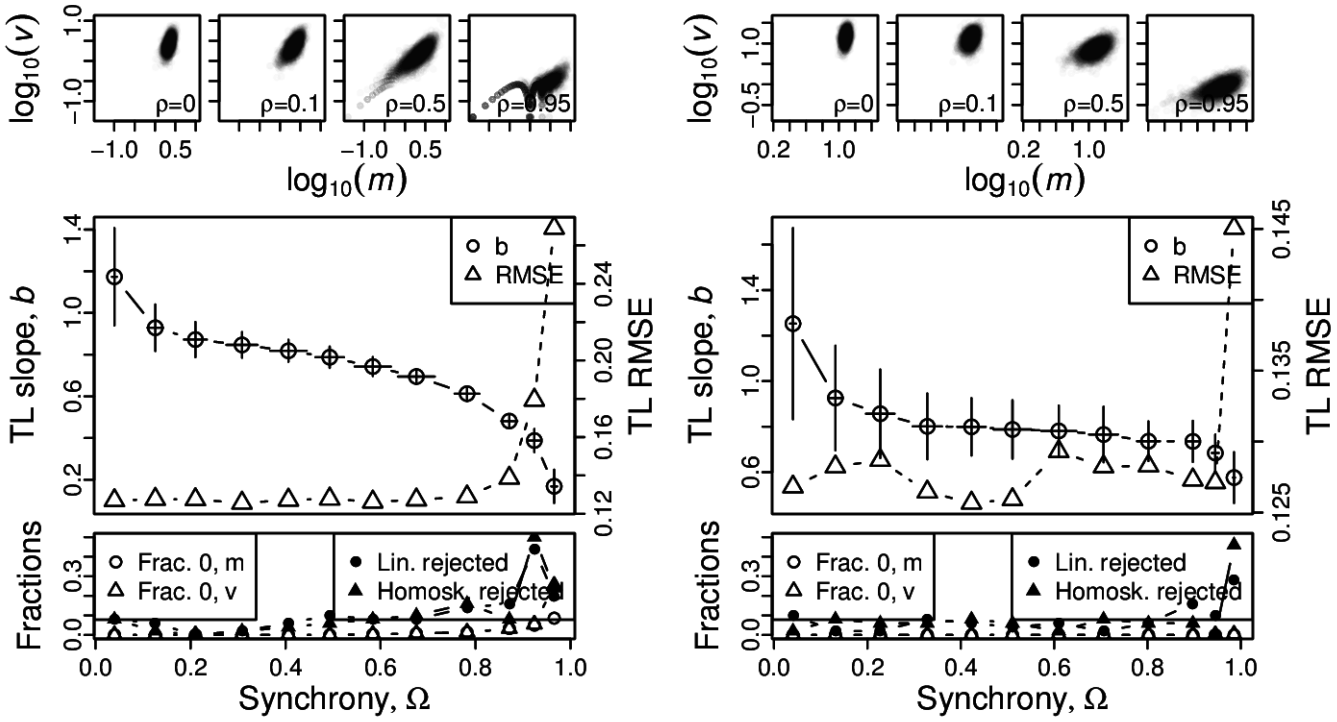

Figure S60: Omnibus plots (see section S6) for non-identically distributed negative binomial marginals under the set up of section S4, for $n = 25$ and Y_1 with $p = 0.8$ and $r = 5$ (A), $r = 10$ (B), $r = 50$ (C).

A

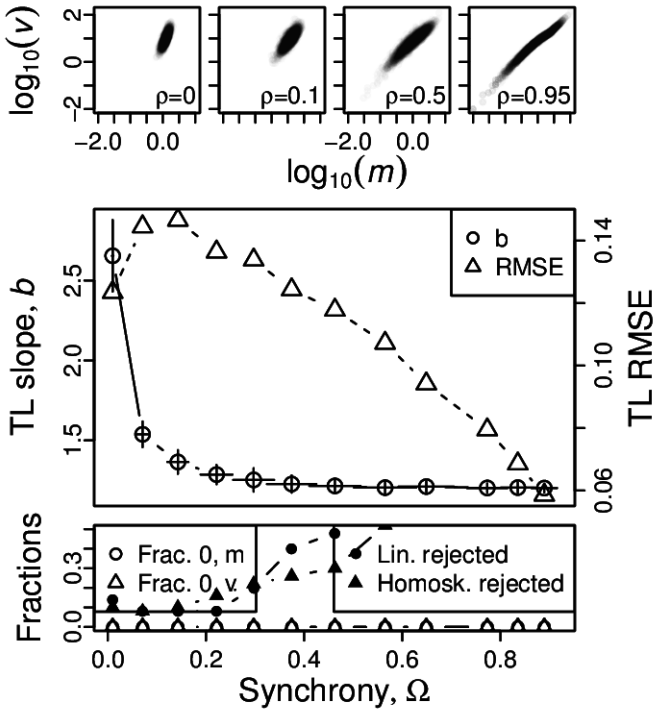

B, C

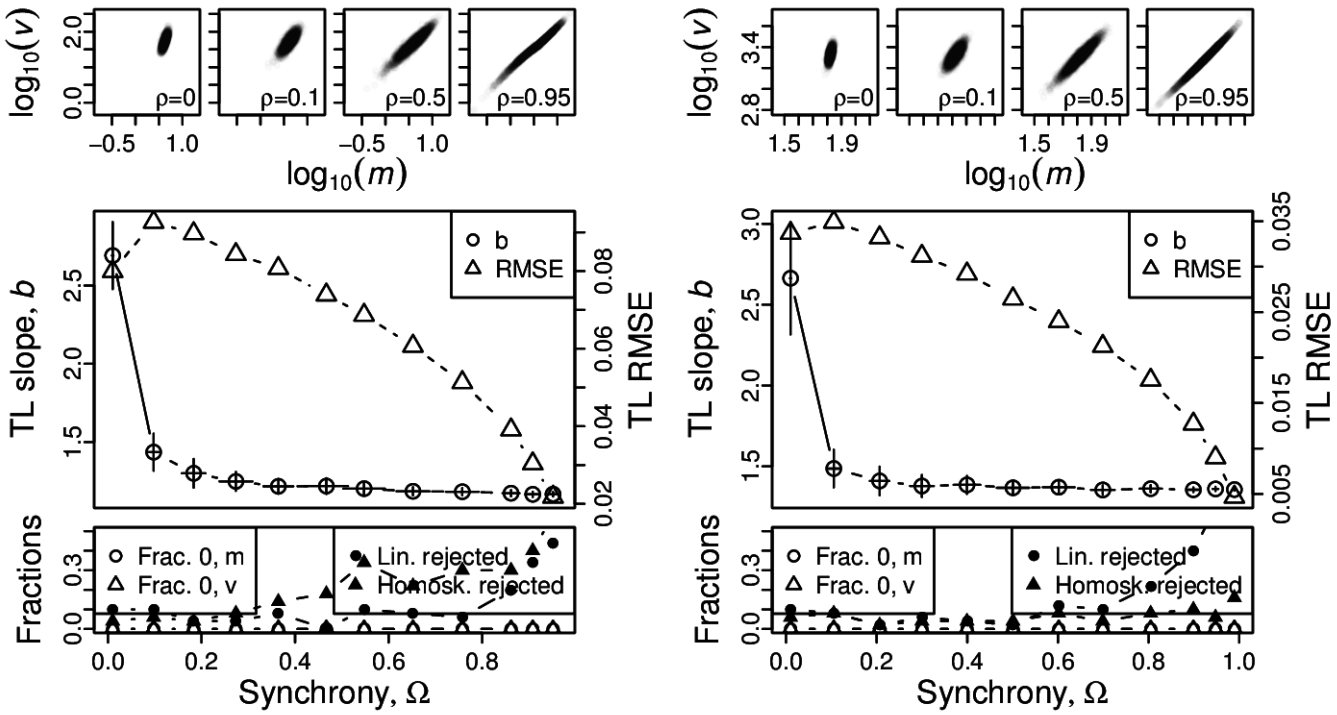

Figure S61: Omnibus plots (see section S6) for non-identically distributed negative binomial marginals under the set up of section S4, for $n = 100$ and Y_1 with $p = 0.2$ and $r = 5$ (A), $r = 10$ (B), $r = 50$ (C).

A

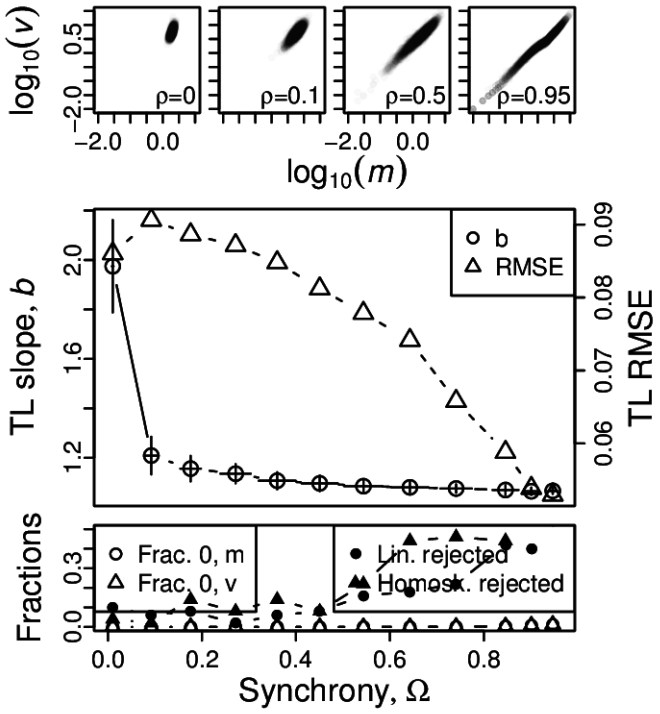

B, C

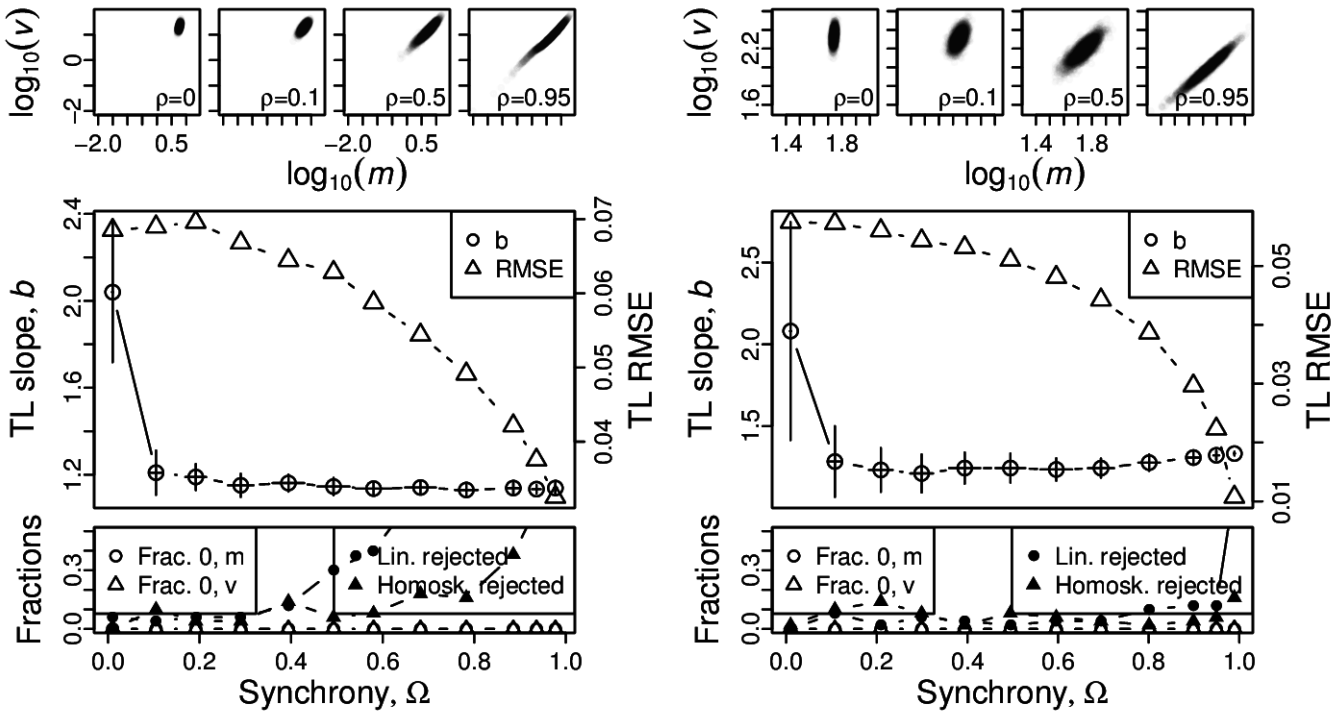

Figure S62: Omnibus plots (see section S6) for non-identically distributed negative binomial marginals under the set up of section S4, for $n = 100$ and Y_1 with $p = 0.4$ and $r = 5$ (A), $r = 10$ (B), $r = 50$ (C).

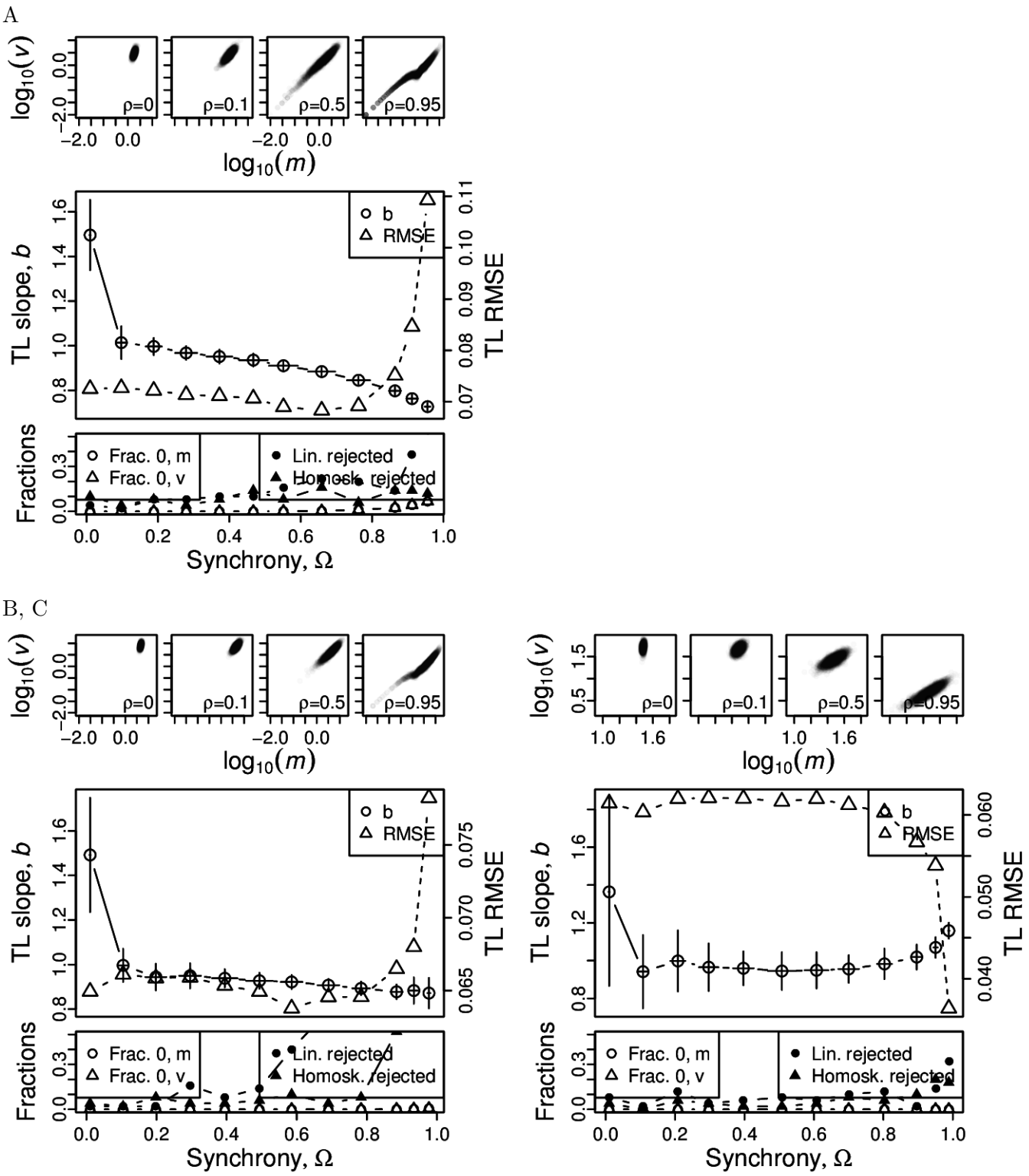

Figure S63: Omnibus plots (see section S6) for non-identically distributed negative binomial marginals under the set up of section S4, for $n = 100$ and Y_1 with $p = 0.6$ and $r = 5$ (A), $r = 10$ (B), $r = 50$ (C).

A

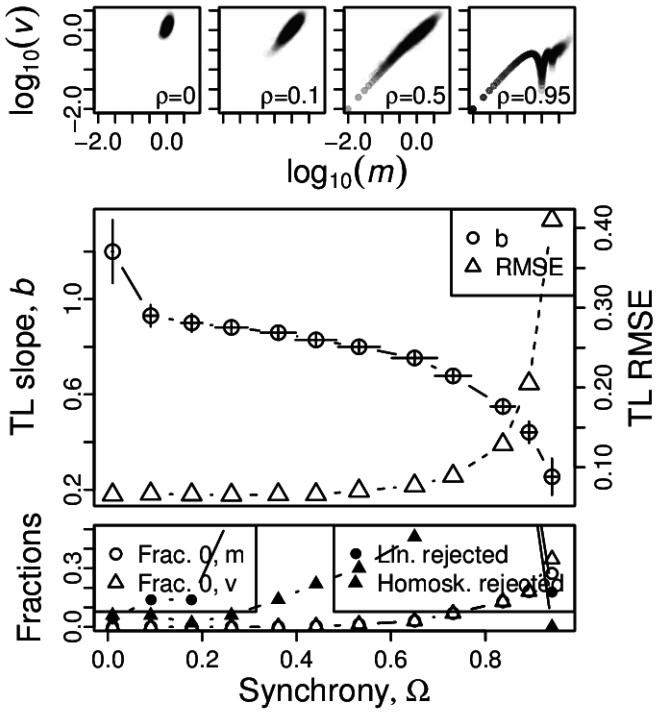

B, C

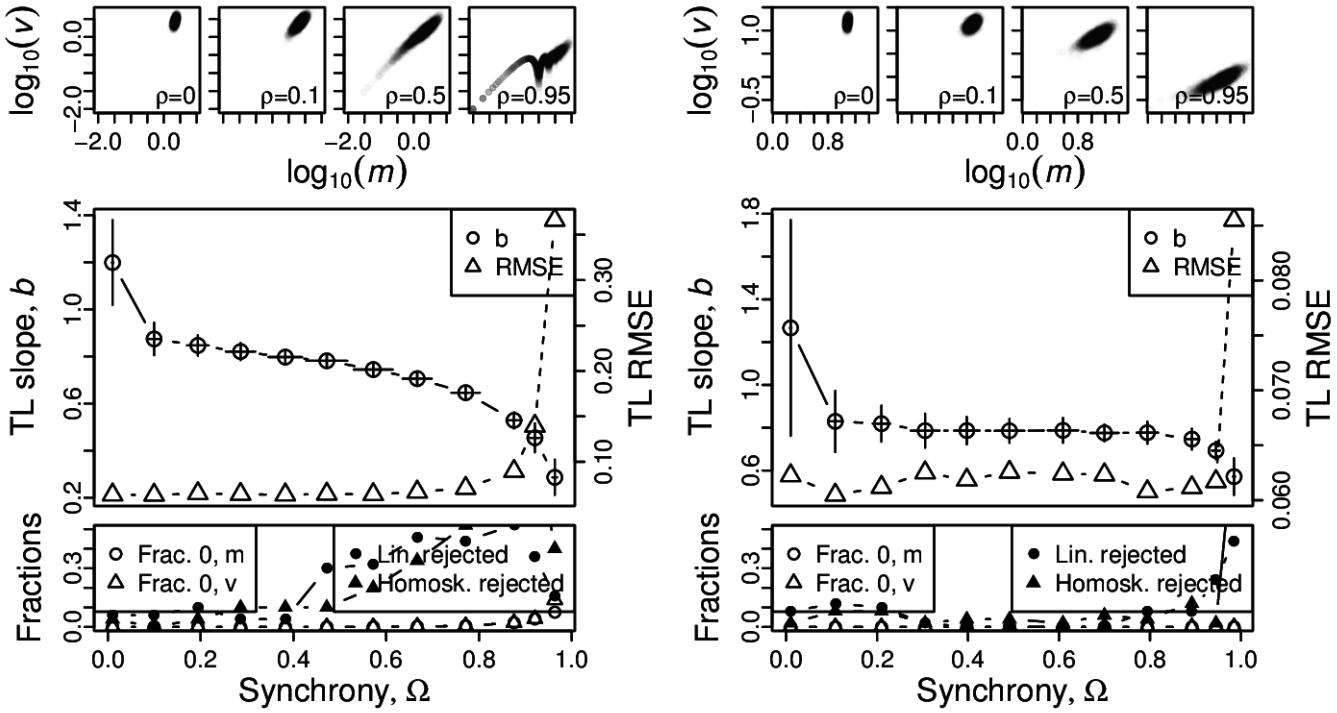

Figure S64: Omnibus plots (see section S6) for non-identically distributed negative binomial marginals under the set up of section S4, for $n = 100$ and Y_1 with $p = 0.8$ and $r = 5$ (A), $r = 10$ (B), $r = 50$ (C).

S10 Figures, distributions constructed using sums and identically distributed marginals

A, B

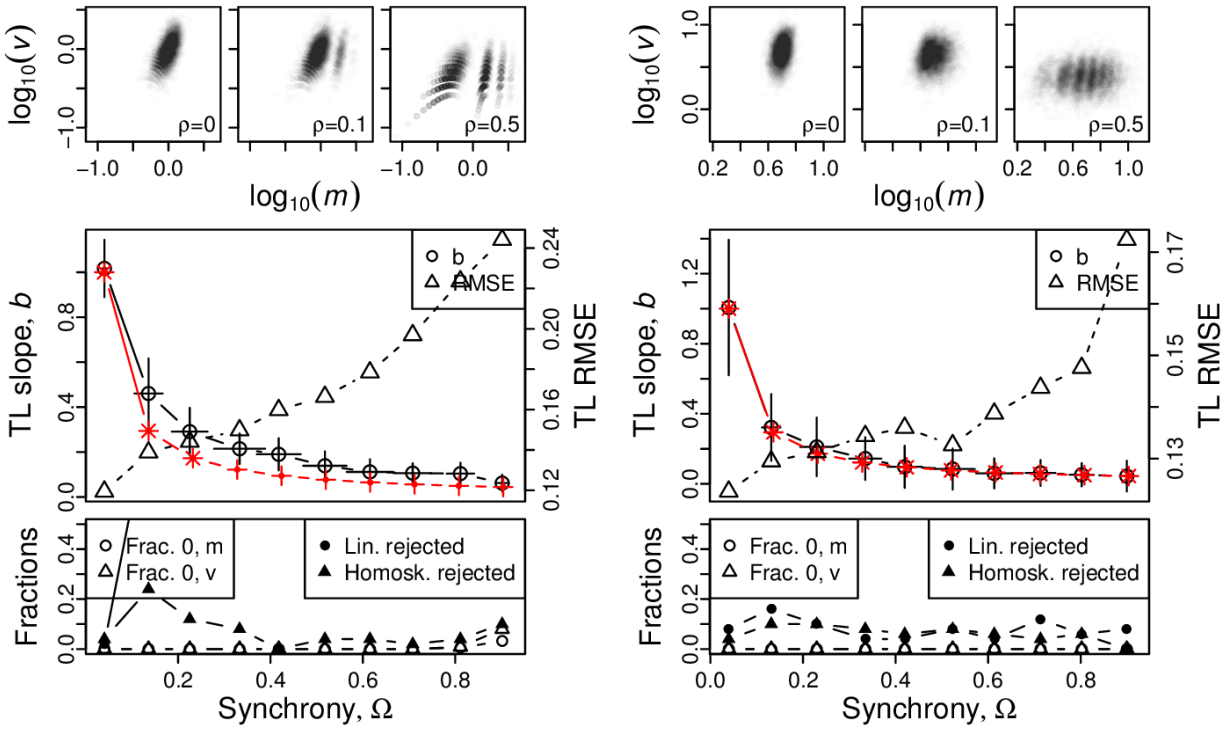

C, D

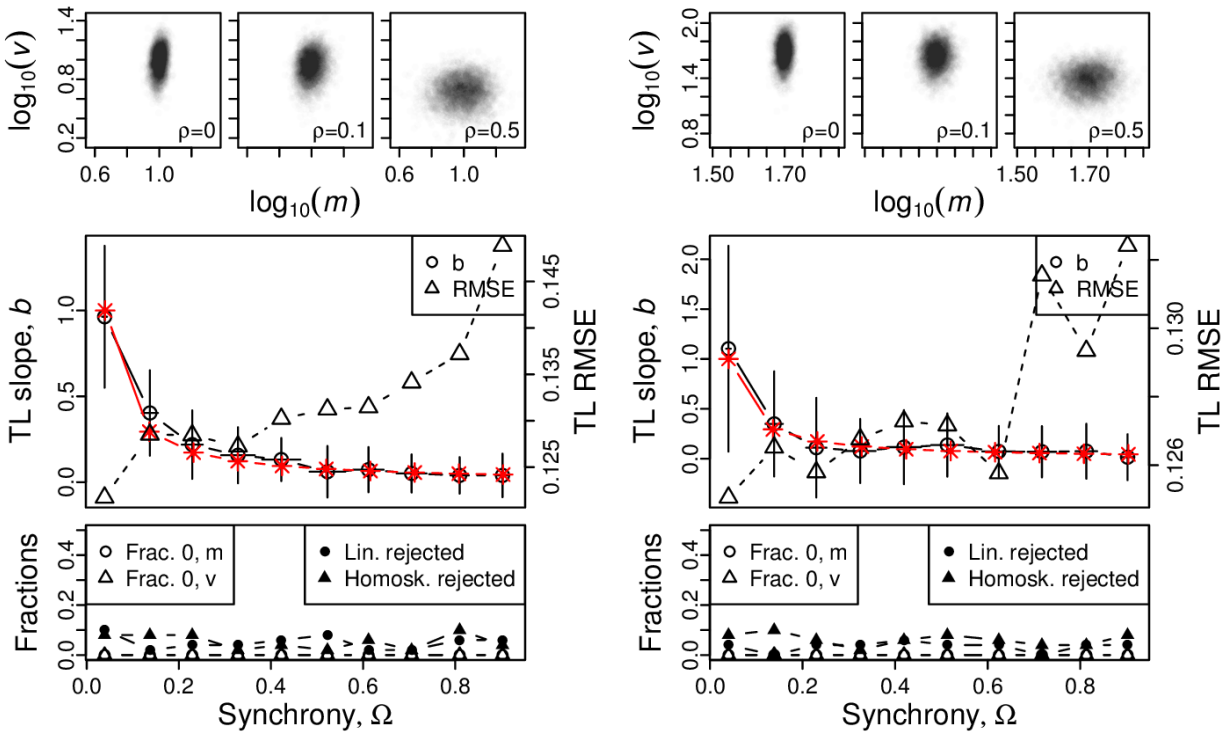

Figure S65: Omnibus plots (see section S6) for identically distributed Poisson marginals under the set up of section S5, for $n = 25$, for $\lambda = 1$ (A), $\lambda = 5$ (B), $\lambda = 10$ (C), and $\lambda = 50$ (D).

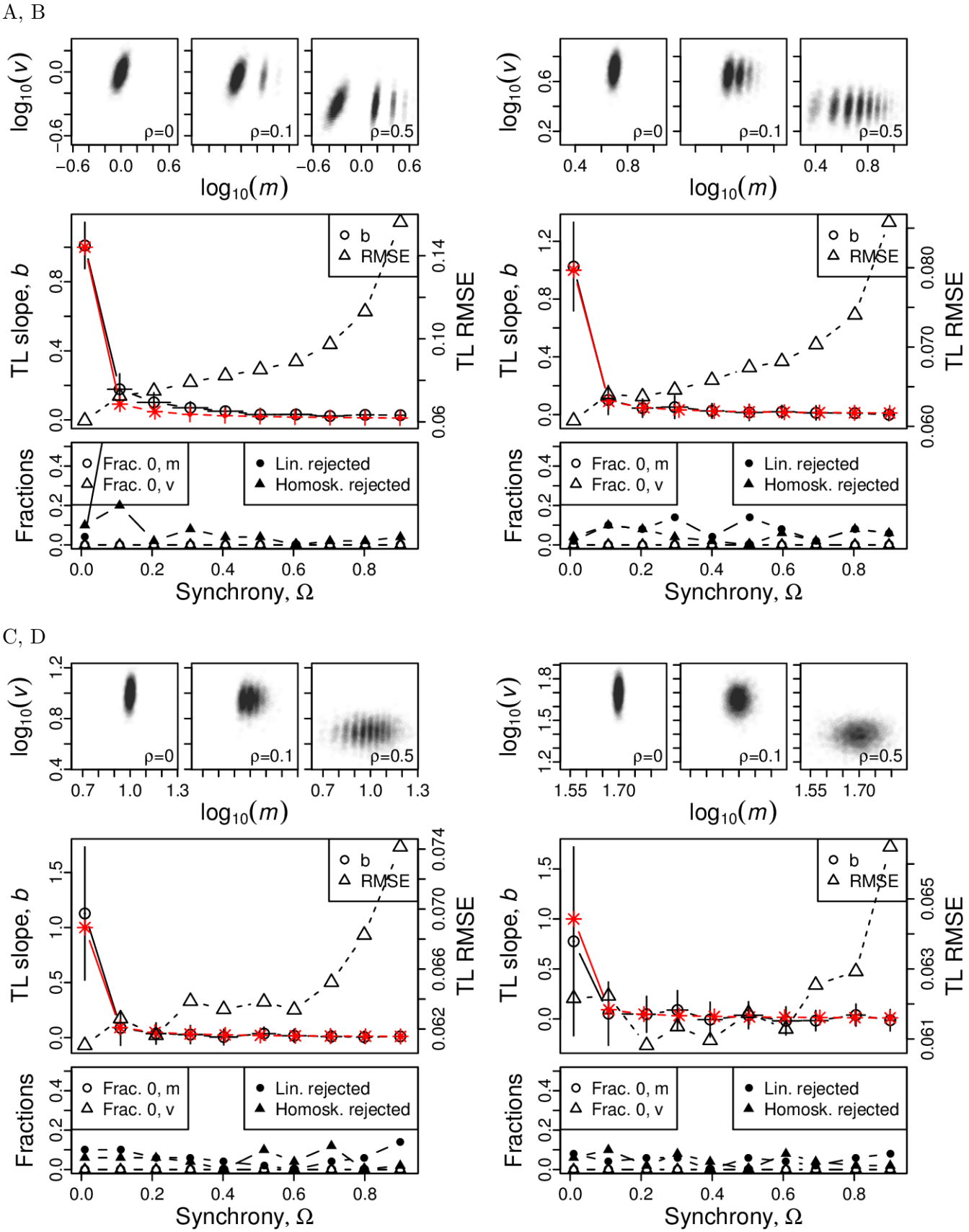

Figure S66: Omnibus plots (see section S6) for identically distributed Poisson marginals under the set up of section S5, for $n = 100$, for $\lambda = 1$ (A), $\lambda = 5$ (B), $\lambda = 10$ (C), and $\lambda = 50$ (D).

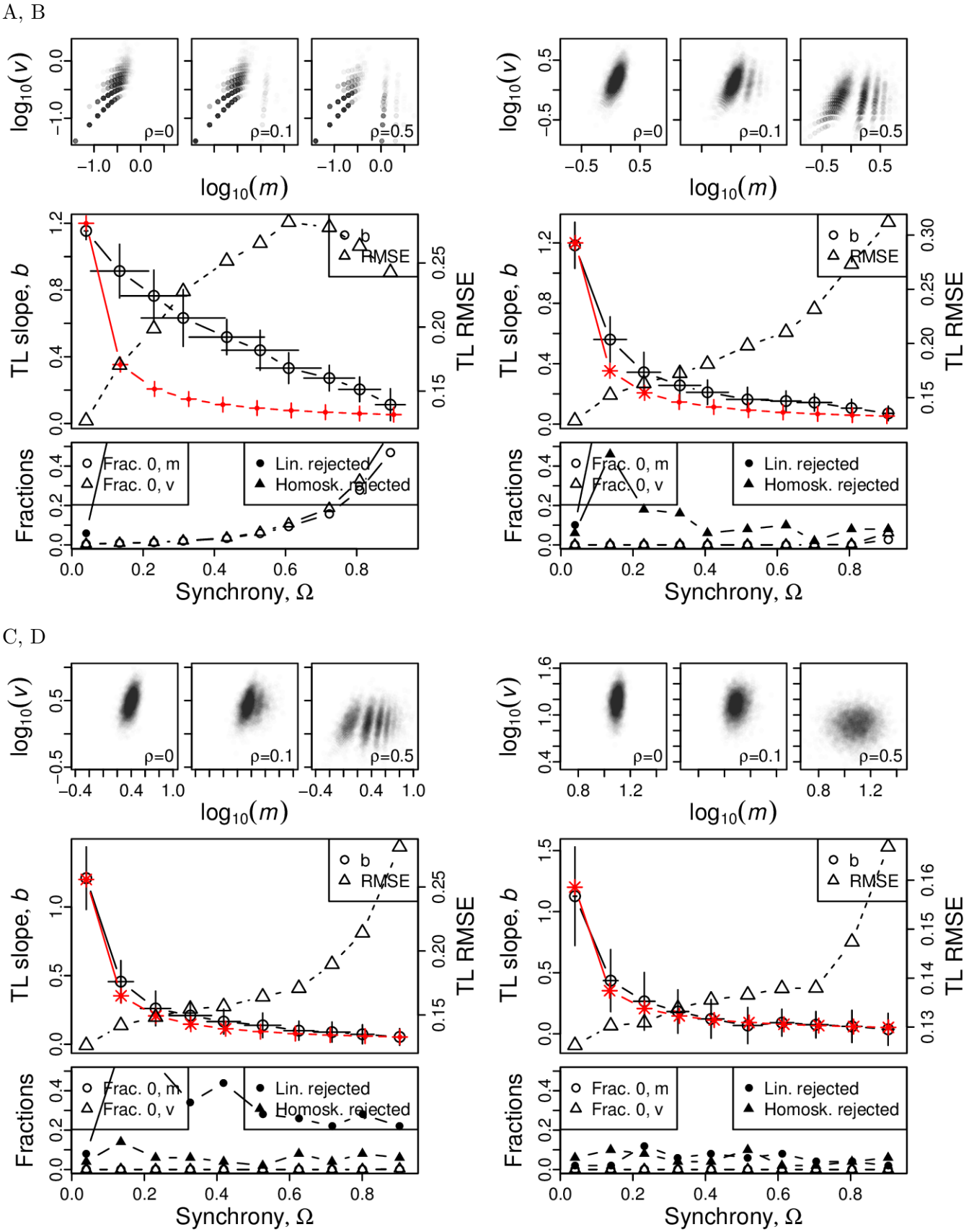

Figure S67: Omnibus plots (see section S6) for identically distributed negative binomial marginals under the set up of section S5, for $n = 25$ and $p = 0.2$, for $r = 1$ (A), $r = 5$ (B), $r = 10$ (C), and $r = 50$ (D).

A, B

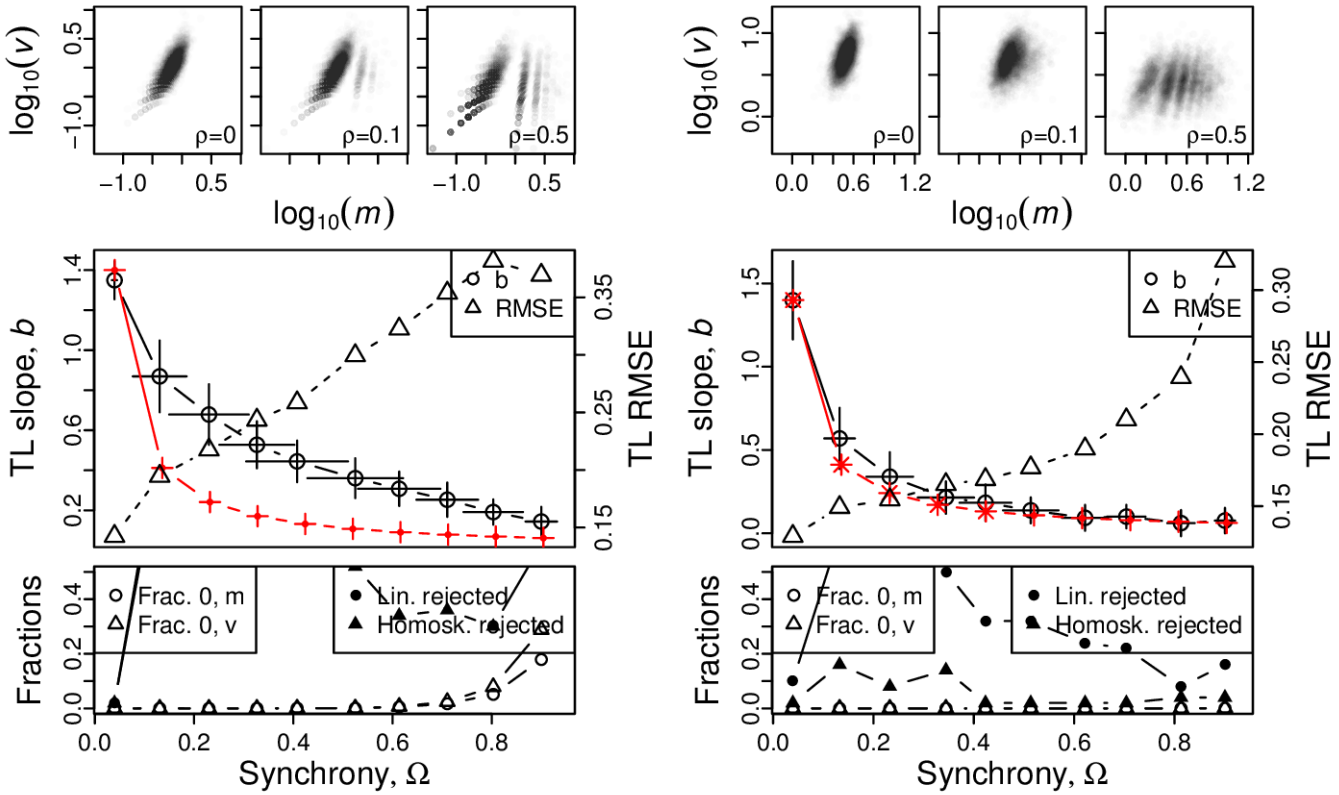

C, D

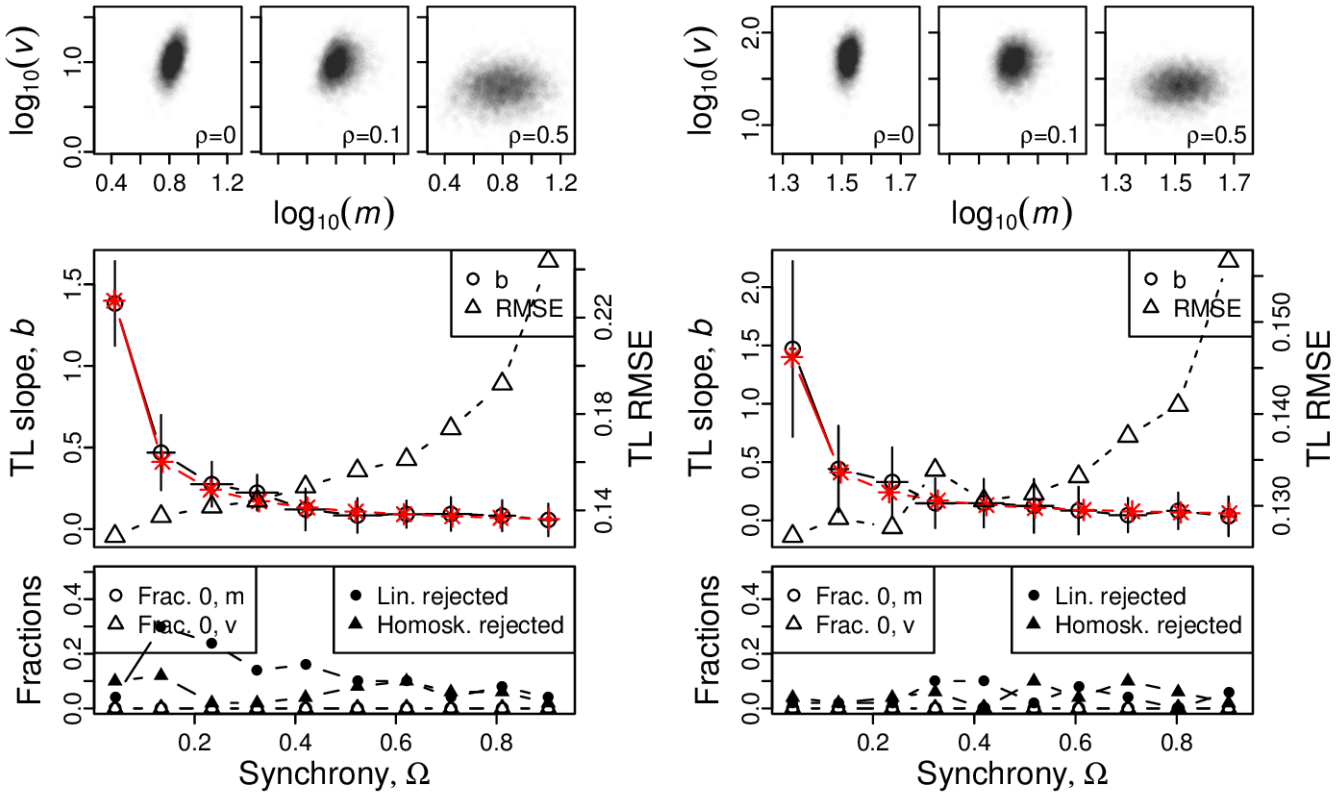

Figure S68: Omnibus plots (see section S6) for identically distributed negative binomial marginals under the set up of section S5, for $n = 25$ and $p = 0.4$, for $r = 1$ (A), $r = 5$ (B), $r = 10$ (C), and $r = 50$ (D).

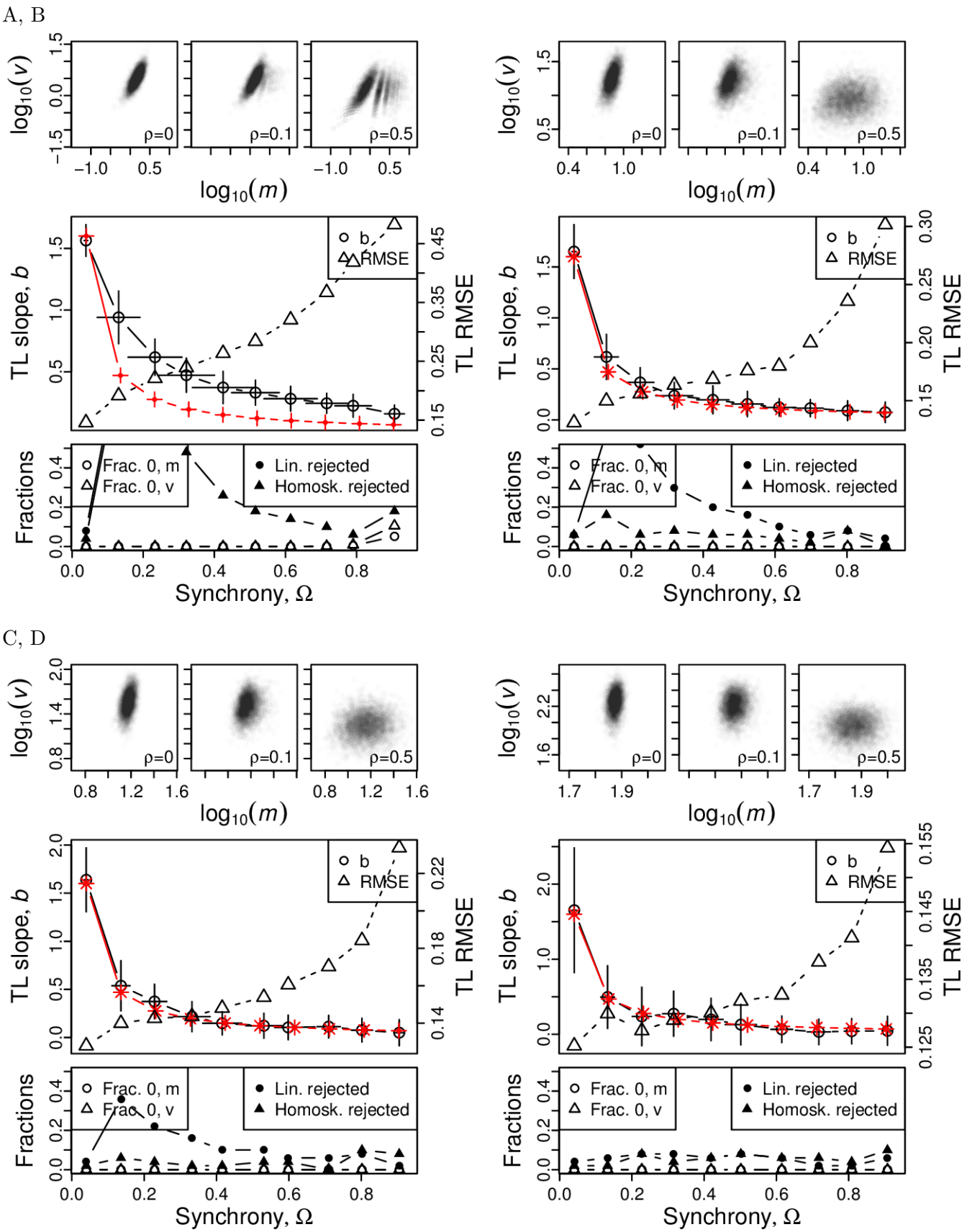

Figure S69: Omnibus plots (see section S6) for identically distributed negative binomial marginals under the set up of section S5, for $n = 25$ and $p = 0.6$, for $r = 1$ (A), $r = 5$ (B), $r = 10$ (C), and $r = 50$ (D).

A, B

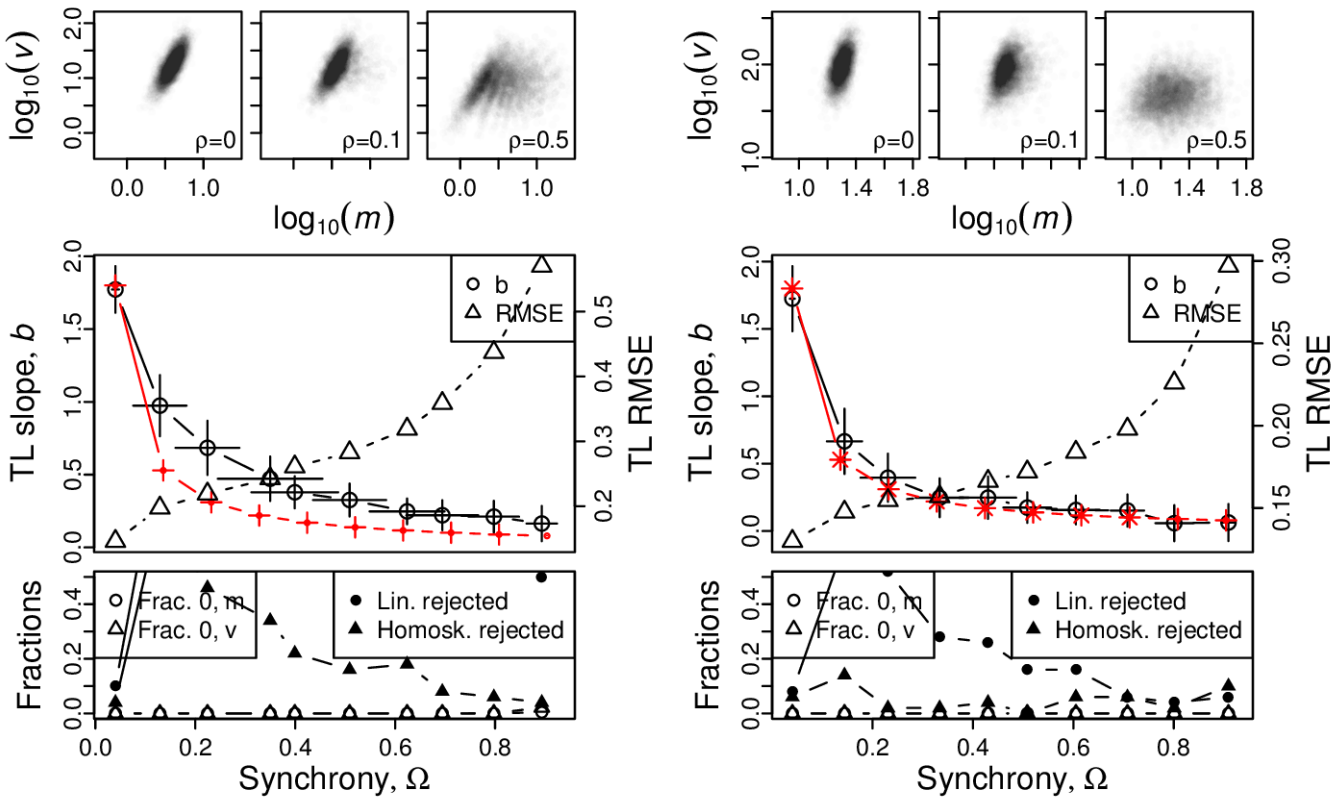

C, D

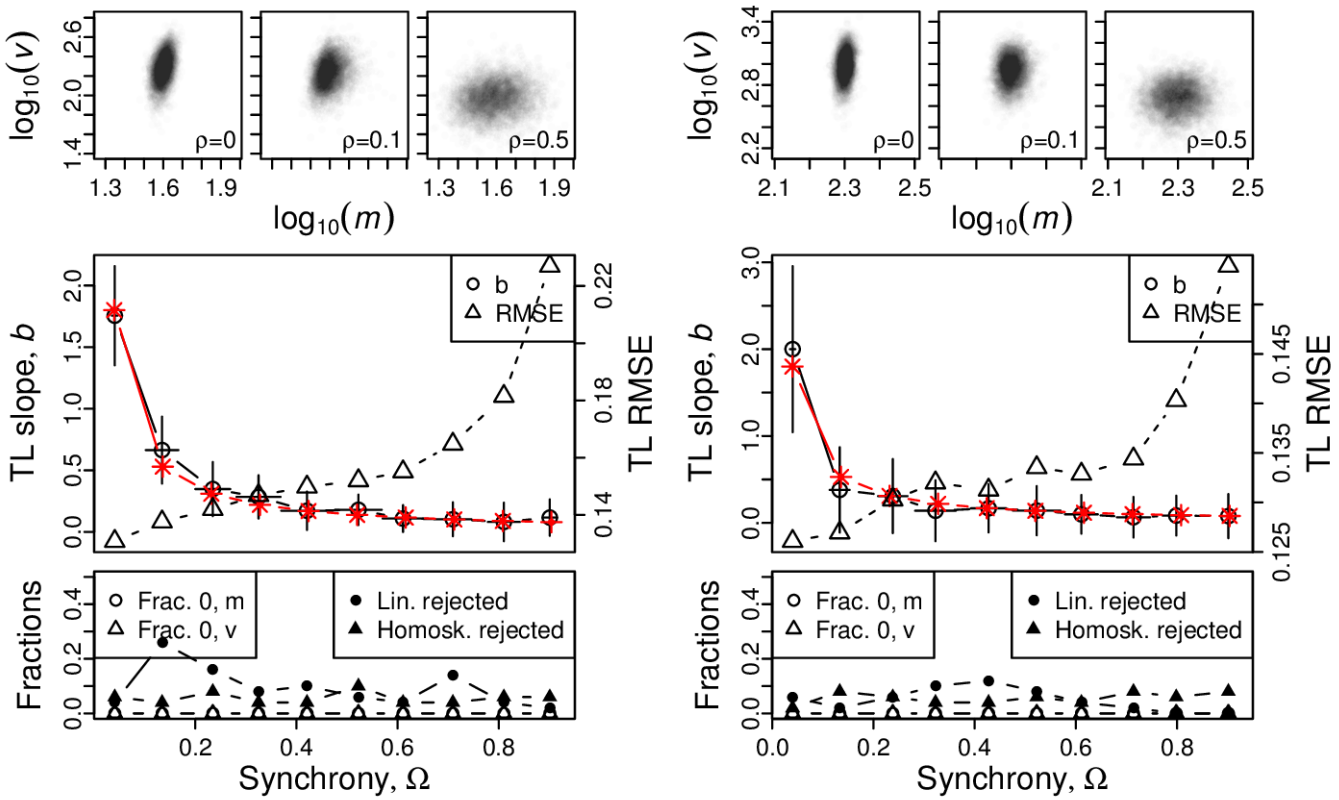

Figure S70: Omnibus plots (see section S6) for identically distributed negative binomial marginals under the set up of section S5, for $n = 25$ and $p = 0.8$, for $r = 1$ (A), $r = 5$ (B), $r = 10$ (C), and $r = 50$ (D).

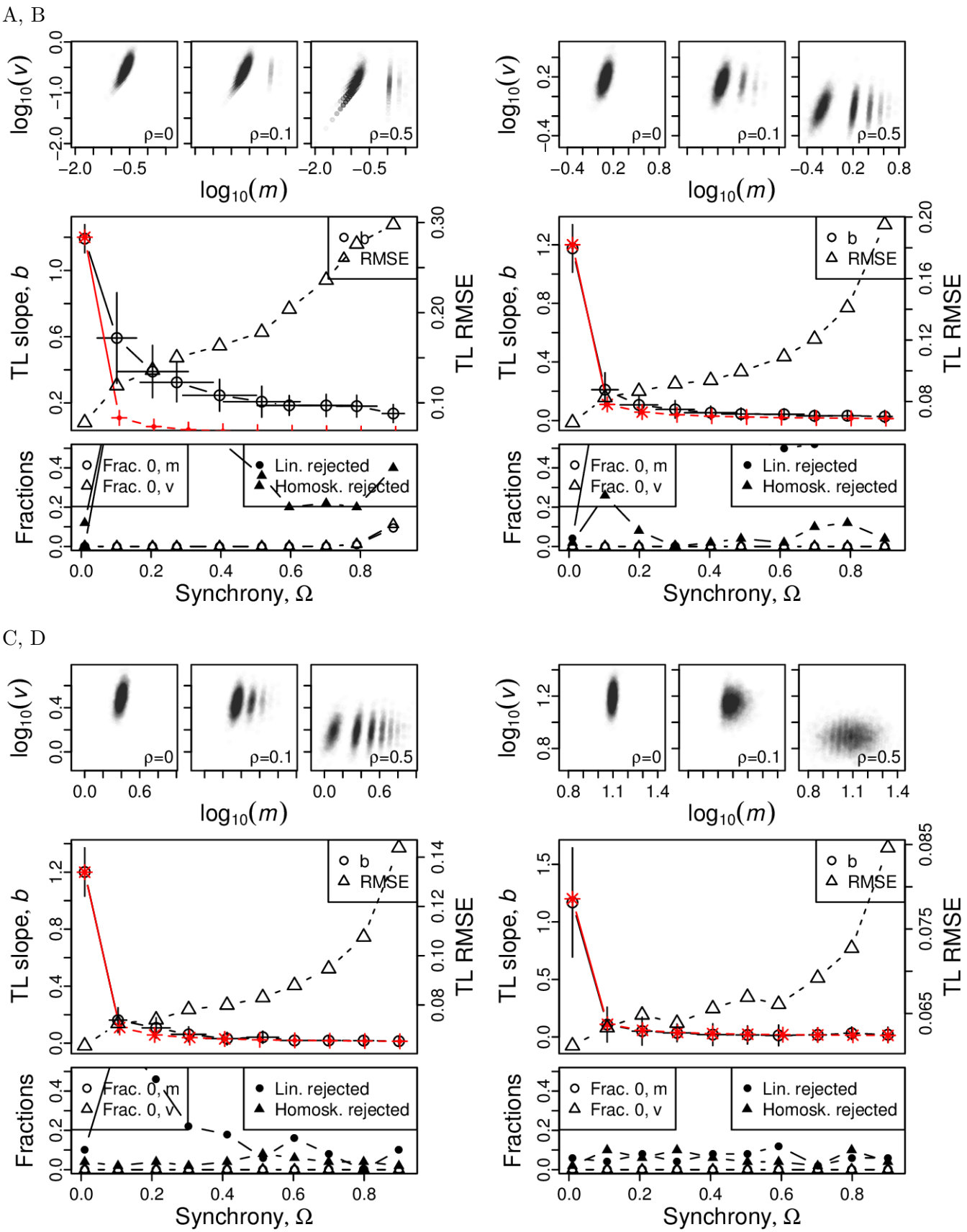

Figure S71: Omnibus plots (see section S6) for identically distributed negative binomial marginals under the set up of section S5, for $n = 100$ and $p = 0.2$, for $r = 1$ (A), $r = 5$ (B), $r = 10$ (C), and $r = 50$ (D).

A, B

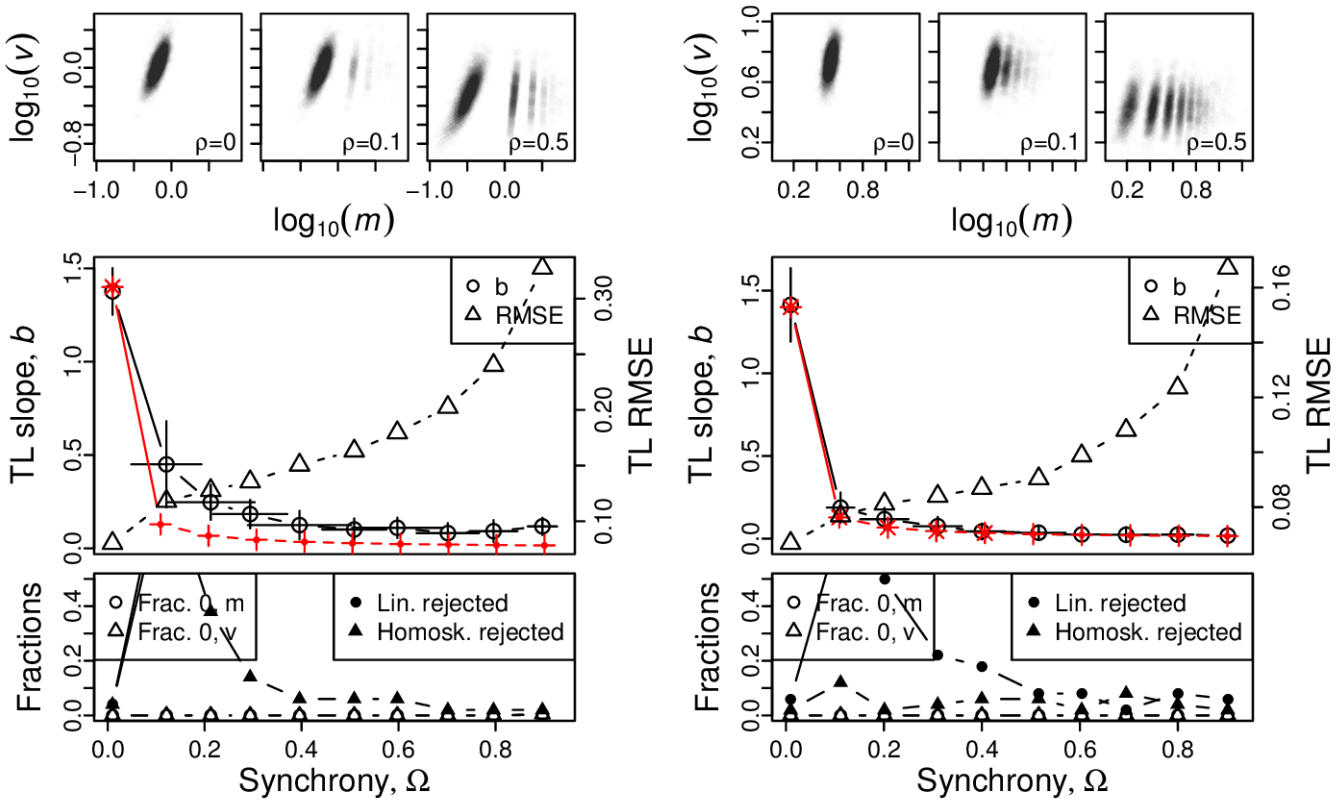

C, D

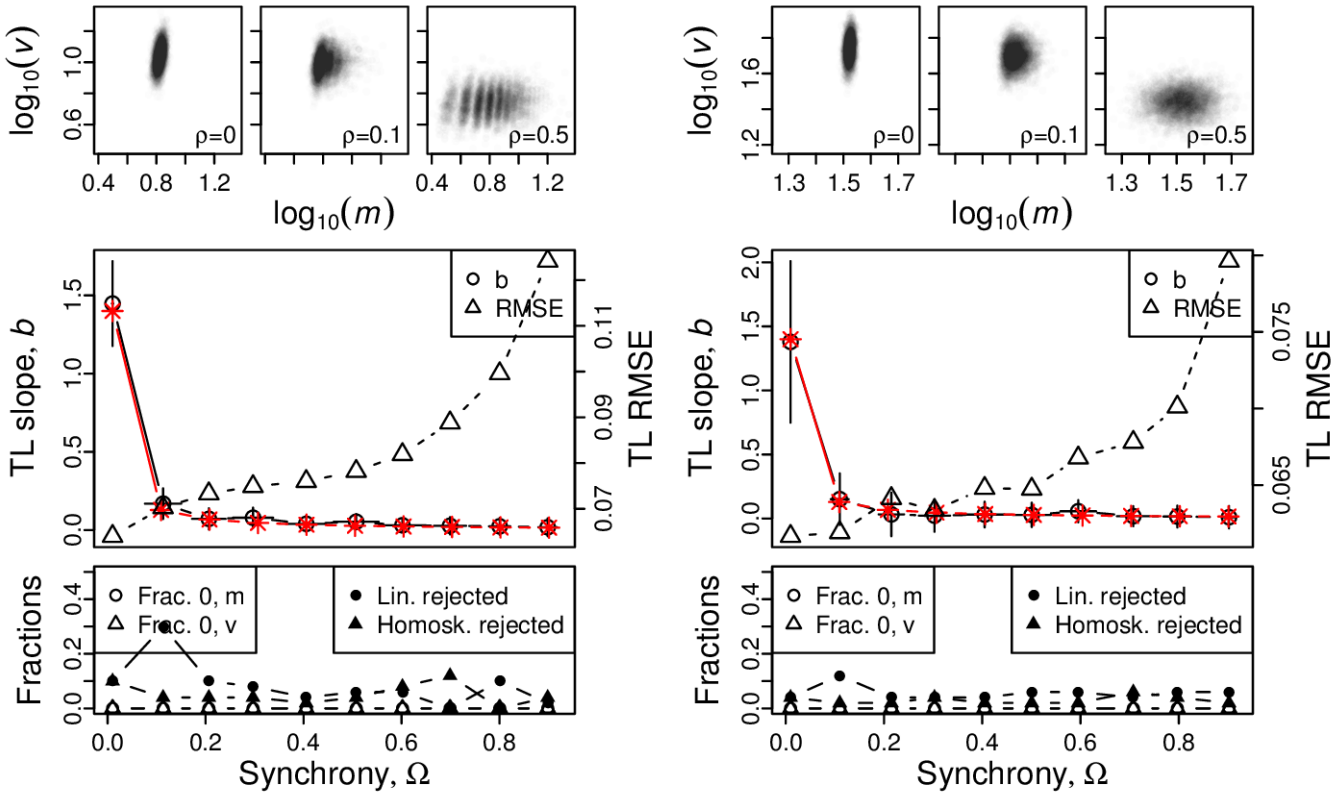

Figure S72: Omnibus plots (see section S6) for identically distributed negative binomial marginals under the set up of section S5, for $n = 100$ and $p = 0.4$, for $r = 1$ (A), $r = 5$ (B), $r = 10$ (C), and $r = 50$ (D).

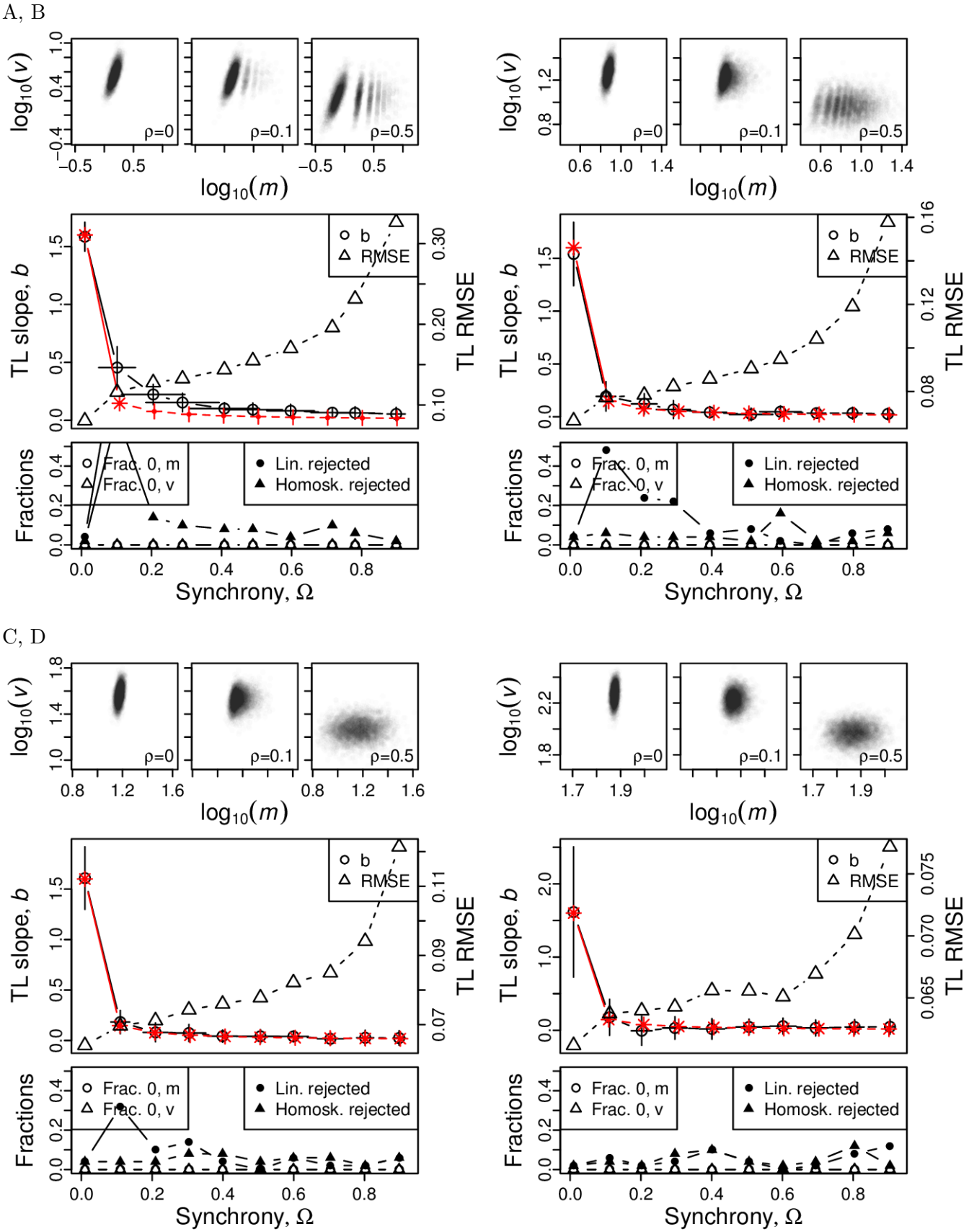

Figure S73: Omnibus plots (see section S6) for identically distributed negative binomial marginals under the set up of section S5, for $n = 100$ and $p = 0.6$, for $r = 1$ (A), $r = 5$ (B), $r = 10$ (C), and $r = 50$ (D).

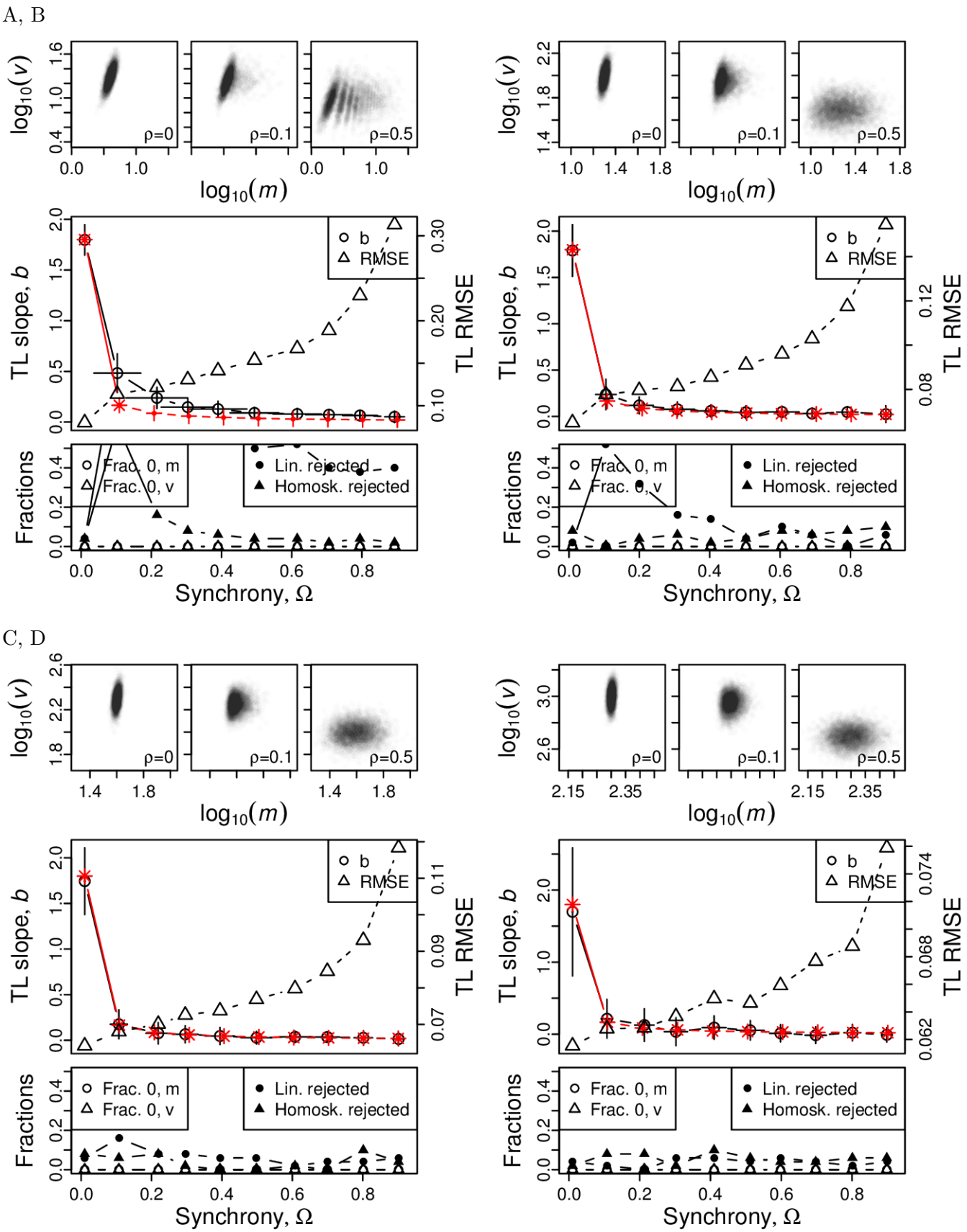

Figure S74: Omnibus plots (see section S6) for identically distributed negative binomial marginals under the set up of section S5, for $n = 100$ and $p = 0.8$, for $r = 1$ (A), $r = 5$ (B), $r = 10$ (C), and $r = 50$ (D).

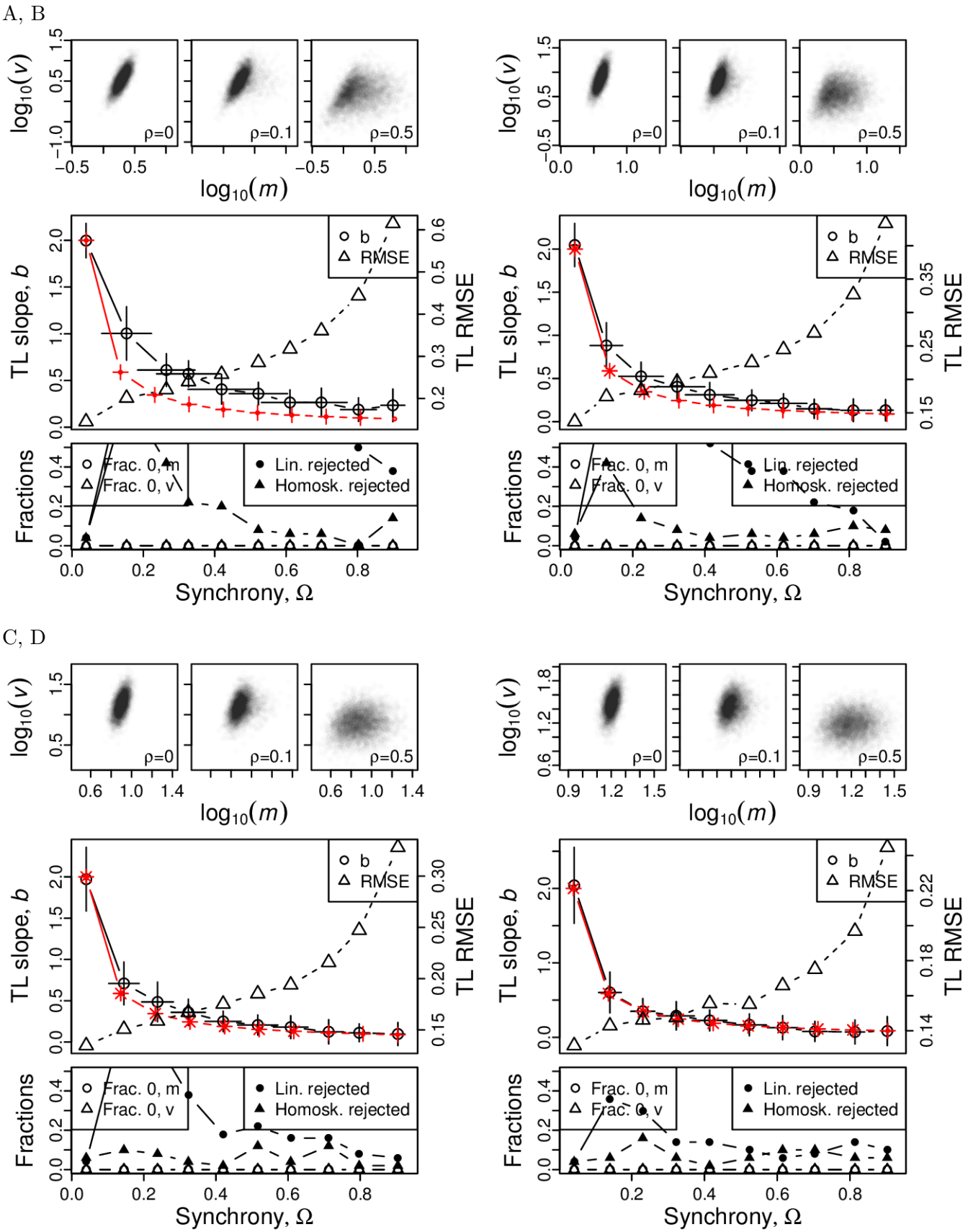

Figure S75: Omnibus plots (see section S6) for identically distributed gamma marginals under the set up of section S5, for $n = 25$ and $\beta = 0.5$, for $\alpha = 1$ (A), $\alpha = 2$ (B), $\alpha = 4$ (C), and $\alpha = 8$ (D).

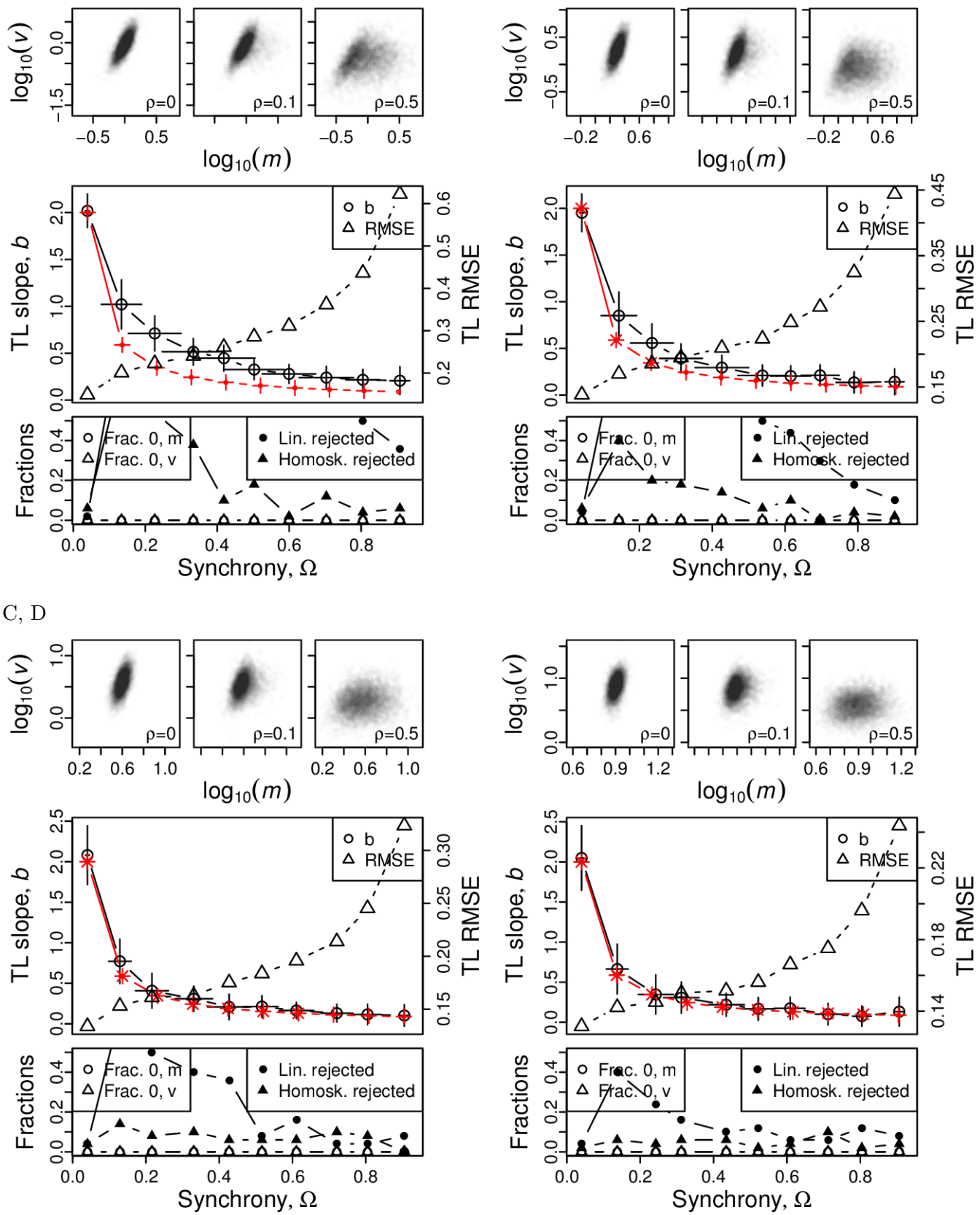

Figure S76: Omnibus plots (see section S6) for identically distributed gamma marginals under the set up of section S5, for $n = 25$ and $\beta = 1$, for $\alpha = 1$ (A), $\alpha = 2$ (B), $\alpha = 4$ (C), and $\alpha = 8$ (D).

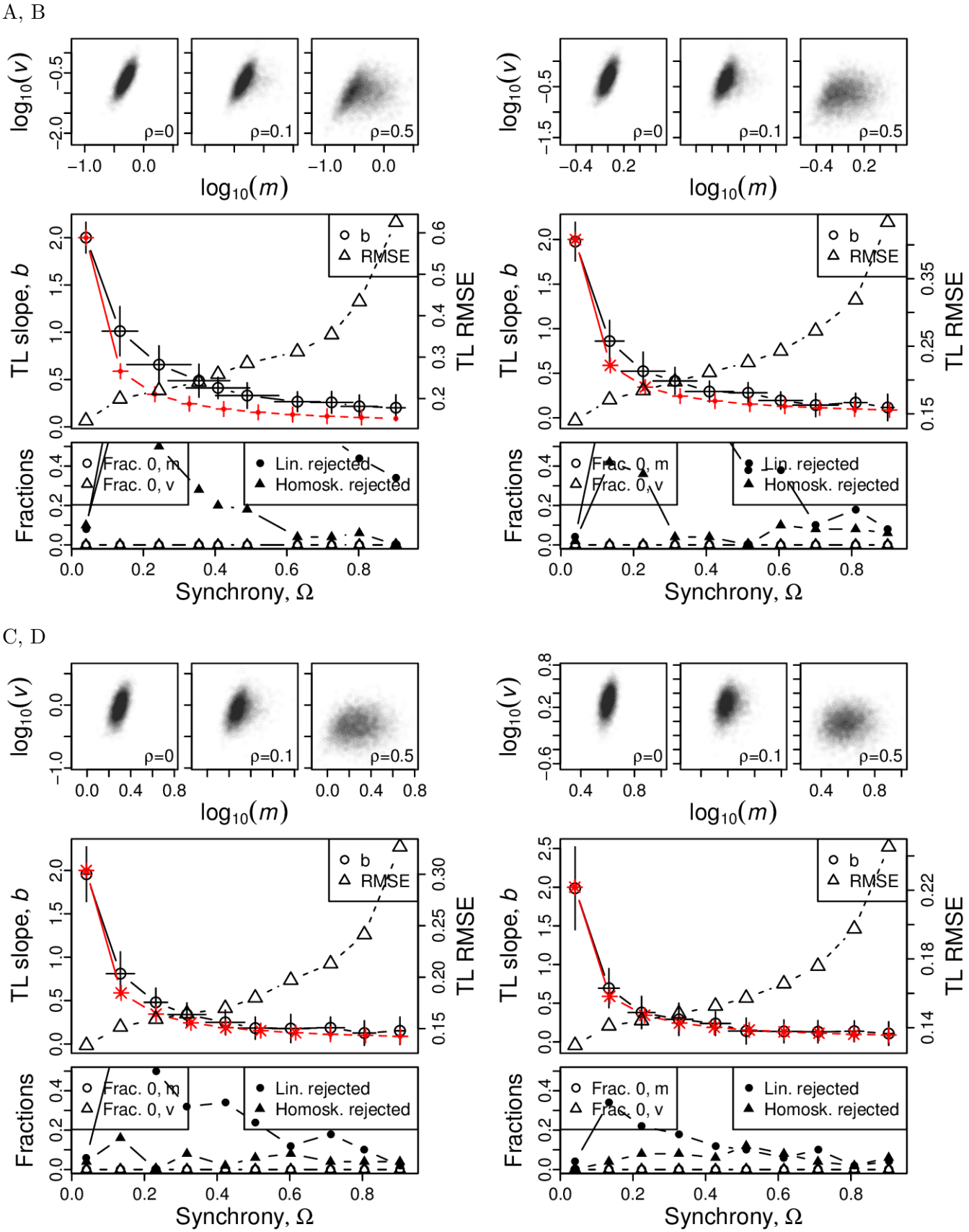

Figure S77: Omnibus plots (see section S6) for identically distributed gamma marginals under the set up of section S5, for $n = 25$ and $\beta = 2$, for $\alpha = 1$ (A), $\alpha = 2$ (B), $\alpha = 4$ (C), and $\alpha = 8$ (D).

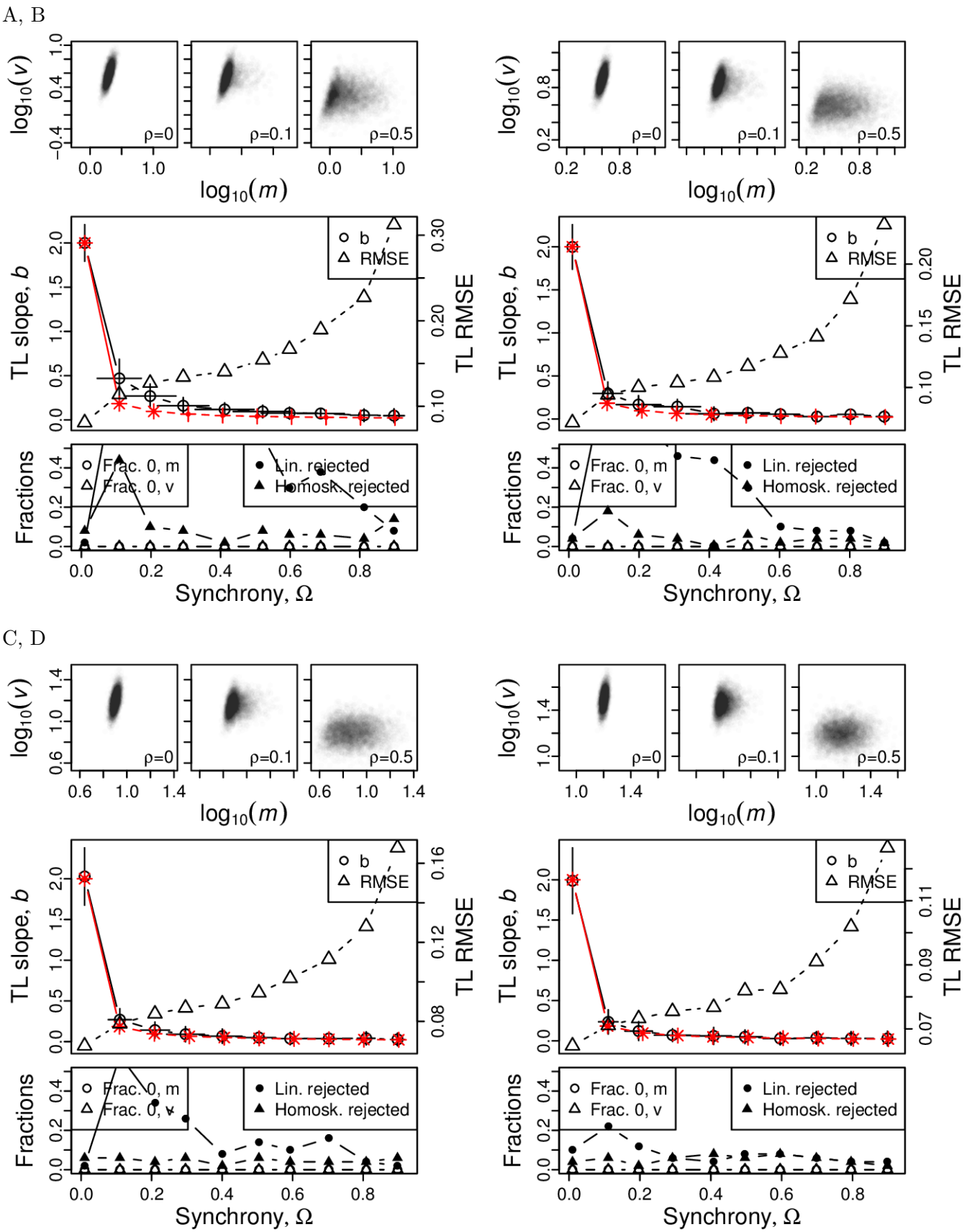

Figure S78: Omnibus plots (see section S6) for identically distributed gamma marginals under the set up of section S5, for $n = 100$ and $\beta = 0.5$, for $\alpha = 1$ (A), $\alpha = 2$ (B), $\alpha = 4$ (C), and $\alpha = 8$ (D).

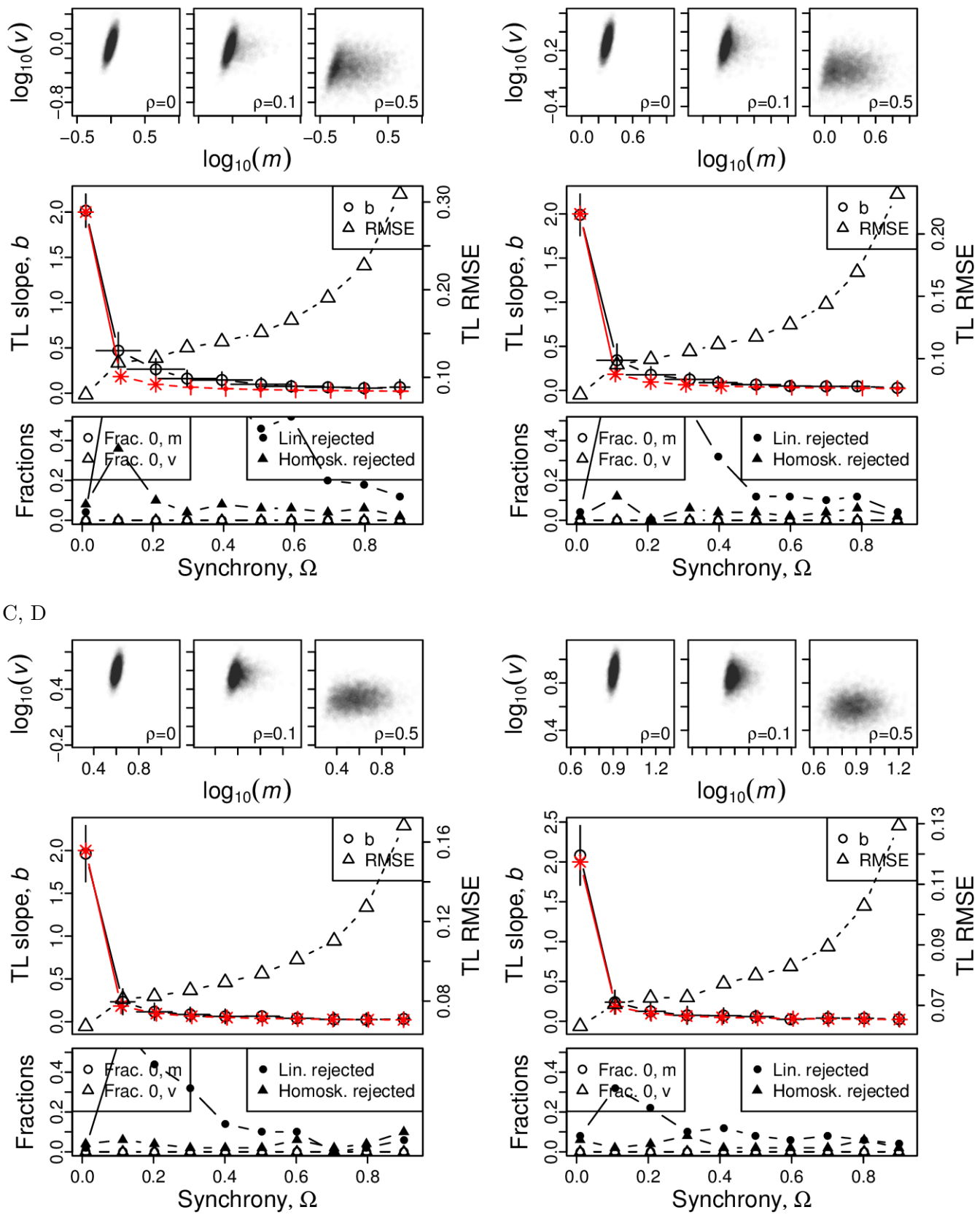

Figure S79: Omnibus plots (see section S6) for identically distributed gamma marginals under the set up of section S5, for $n = 100$ and $\beta = 1$, for $\alpha = 1$ (A), $\alpha = 2$ (B), $\alpha = 4$ (C), and $\alpha = 8$ (D).

A, B

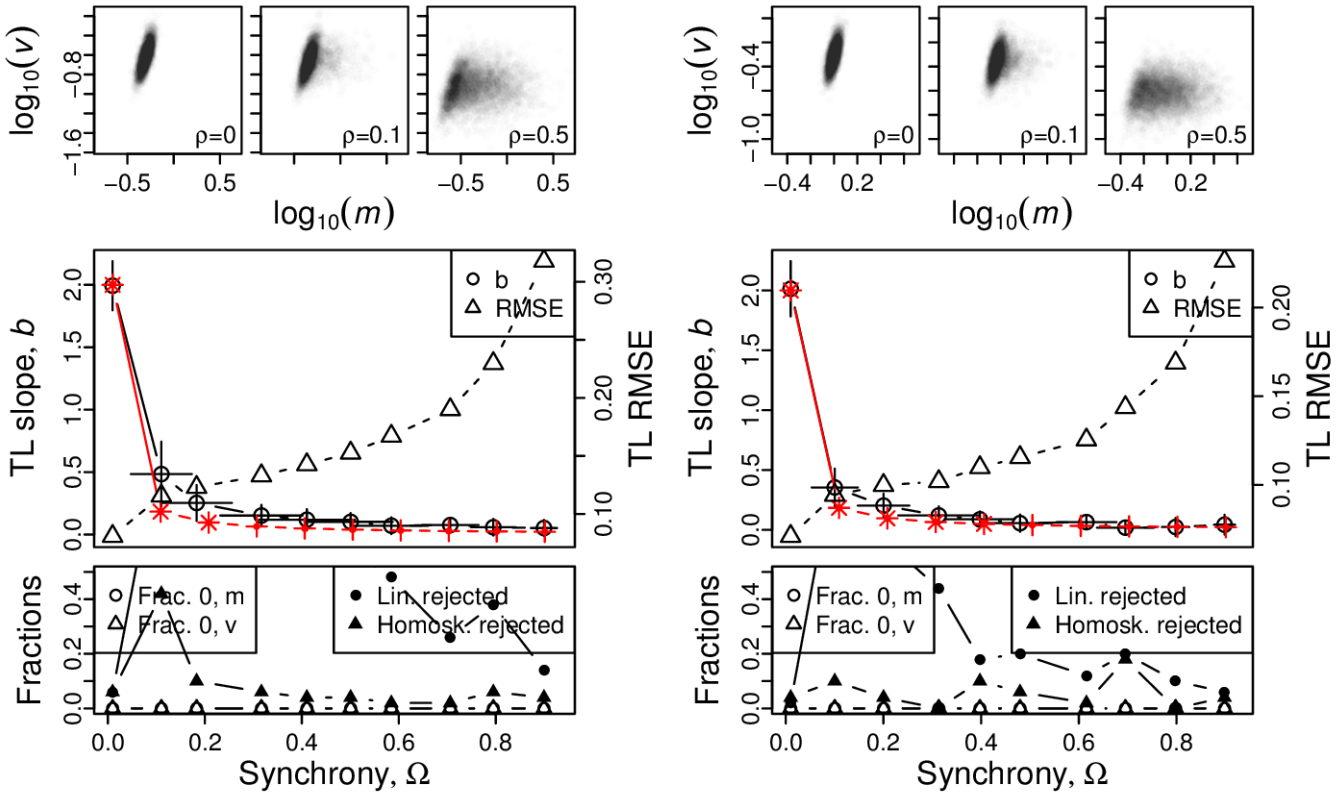

C, D

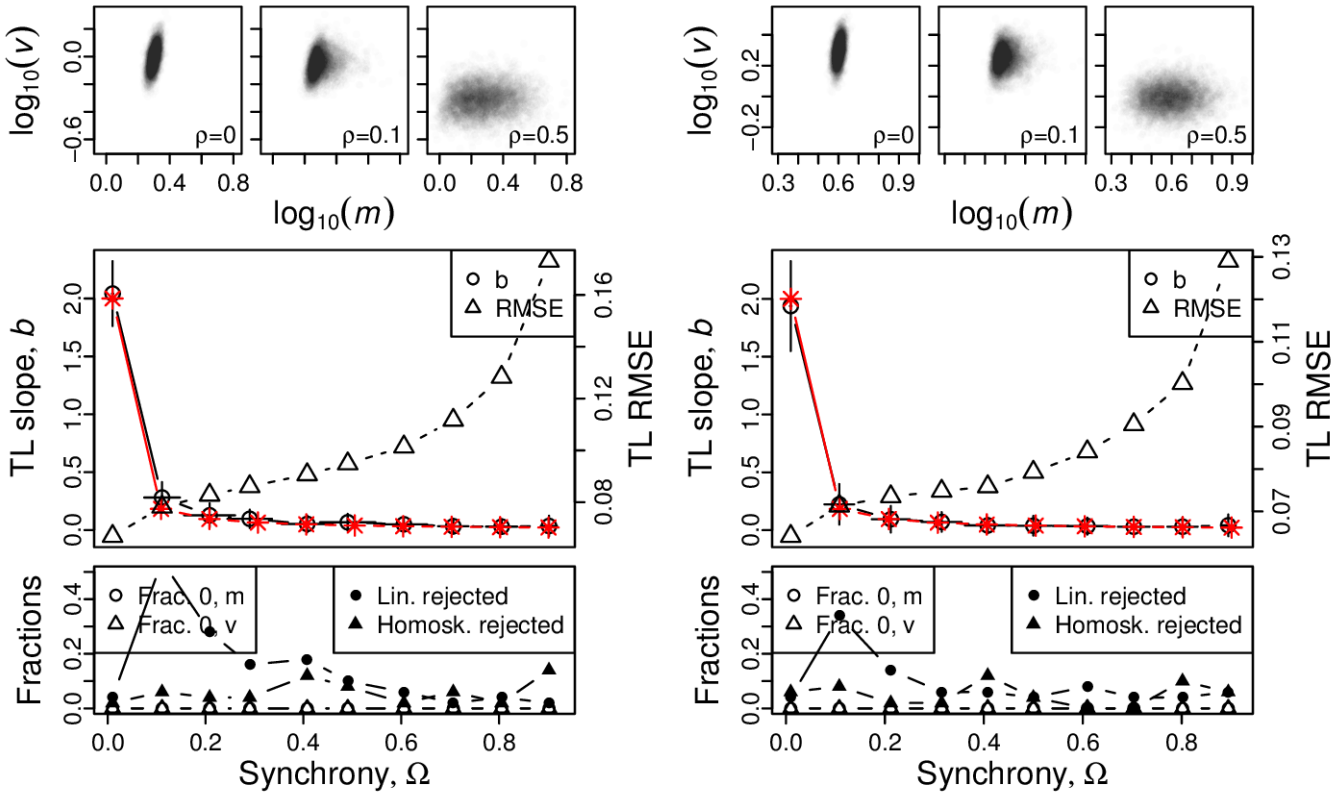

Figure S80: Omnibus plots (see section S6) for identically distributed gamma marginals under the set up of section S5, for $n = 100$ and $\beta = 2$, for $\alpha = 1$ (A), $\alpha = 2$ (B), $\alpha = 4$ (C), and $\alpha = 8$ (D).

A, B

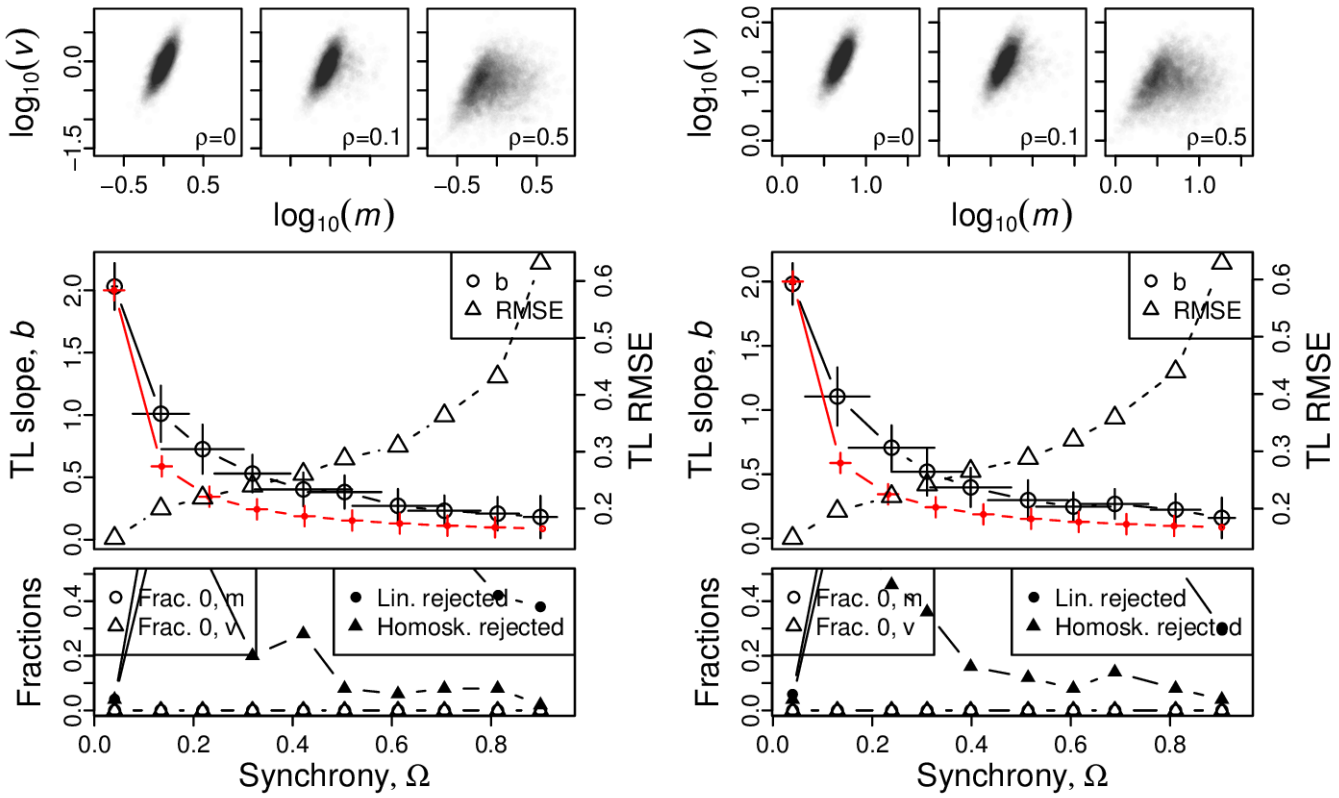

C, D

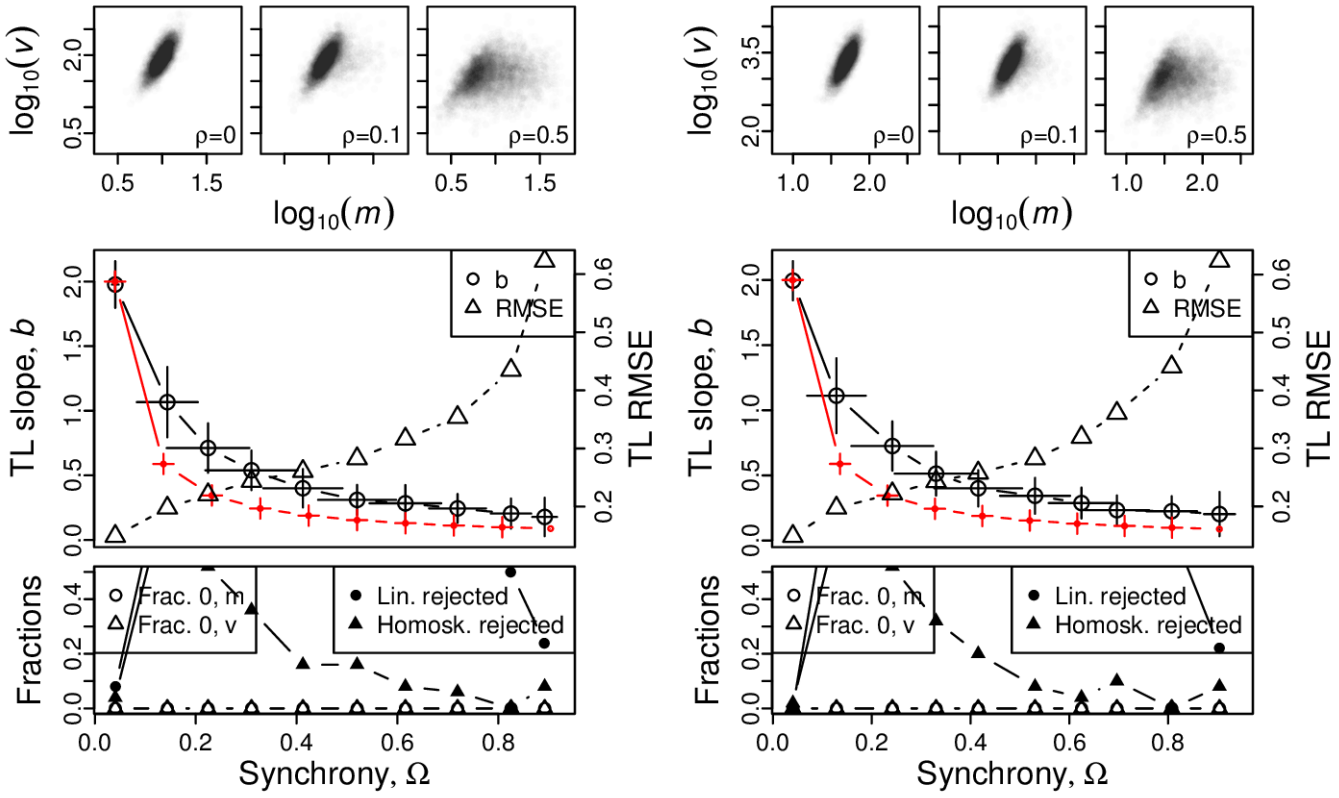

Figure S81: Omnibus plots (see section S6) for identically distributed exponentially distributed marginals under the set up of section S5, for $n = 25$, for $1/\lambda = 1$ (A), $1/\lambda = 5$ (B), $1/\lambda = 10$ (C), and $1/\lambda = 50$ (D).

A, B

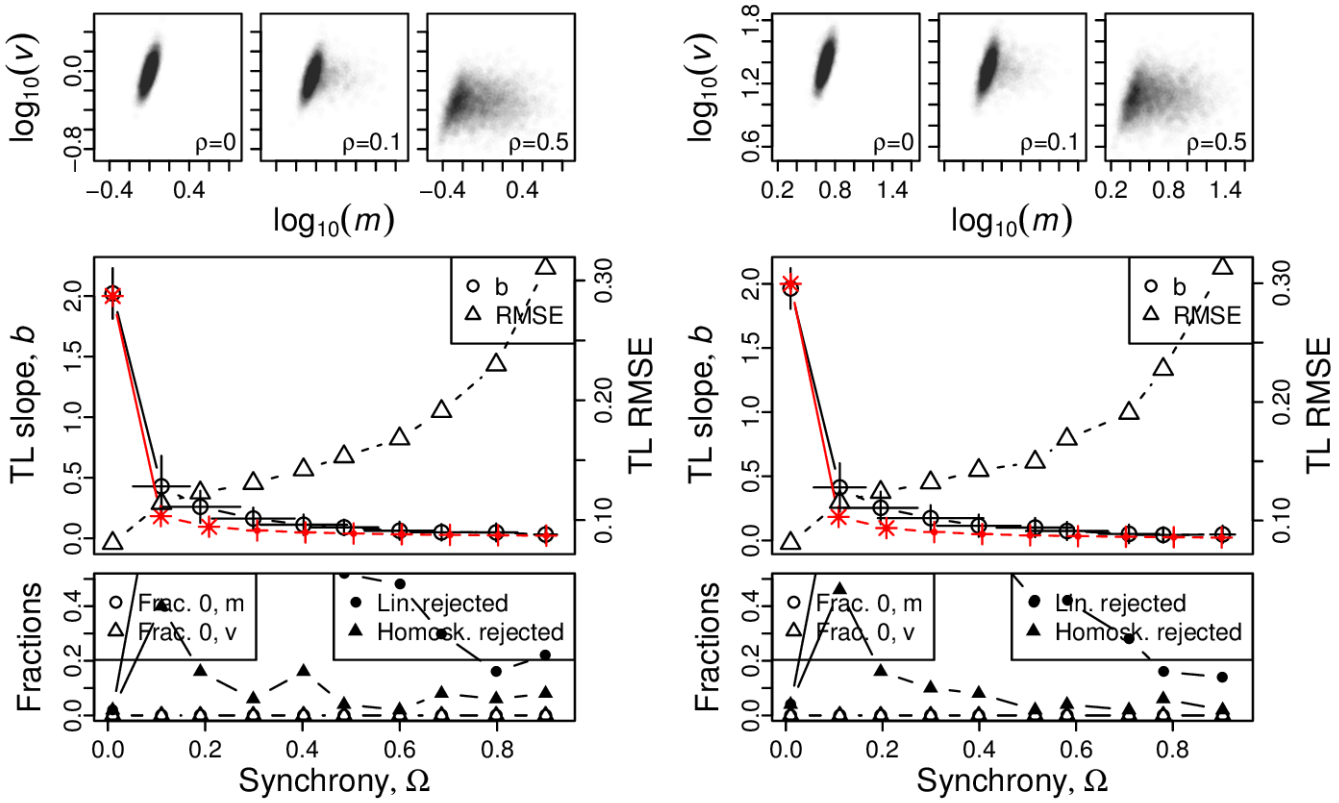

C, D

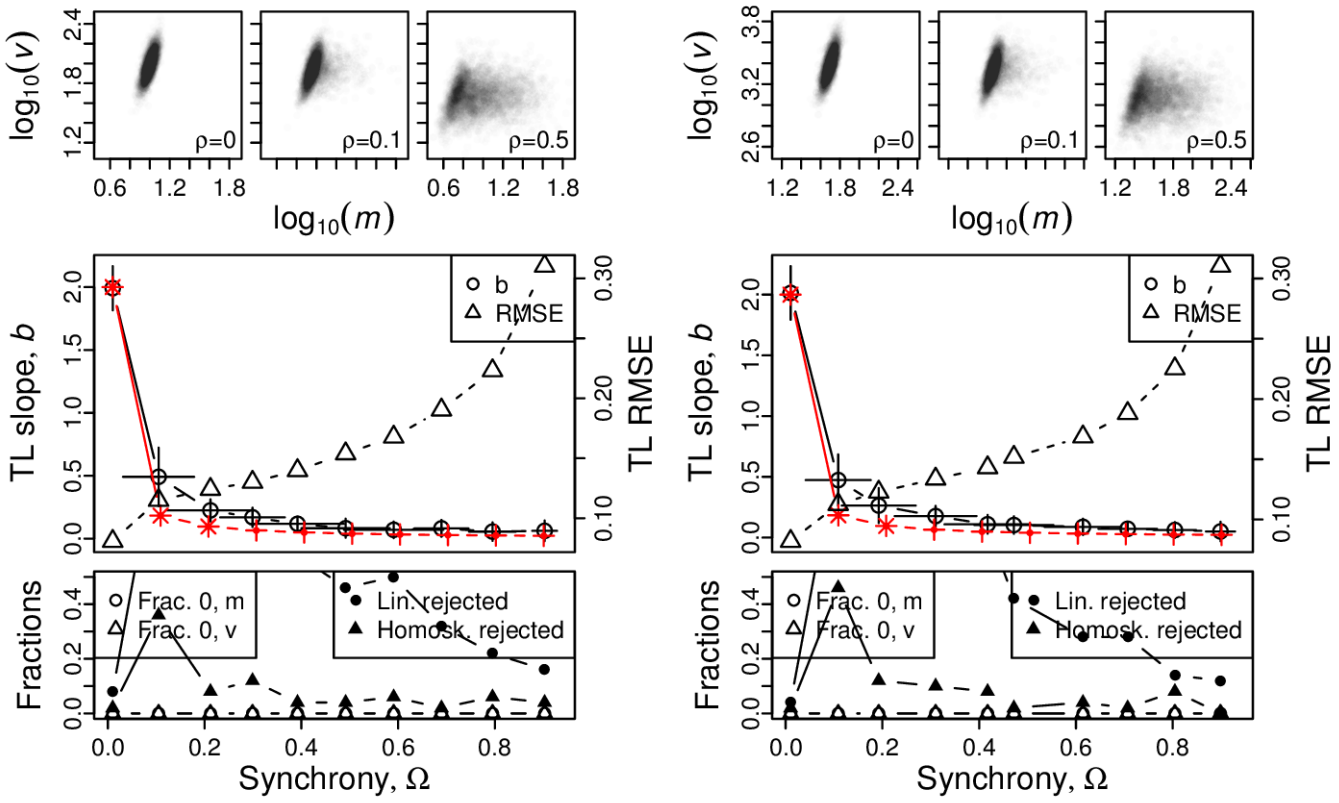

Figure S82: Omnibus plots (see section S6) for identically distributed exponentially distributed marginals under the set up of section S5, for $n = 100$, for $1/\lambda = 1$ (A), $1/\lambda = 5$ (B), $1/\lambda = 10$ (C), and $1/\lambda = 50$ (D).

A, B

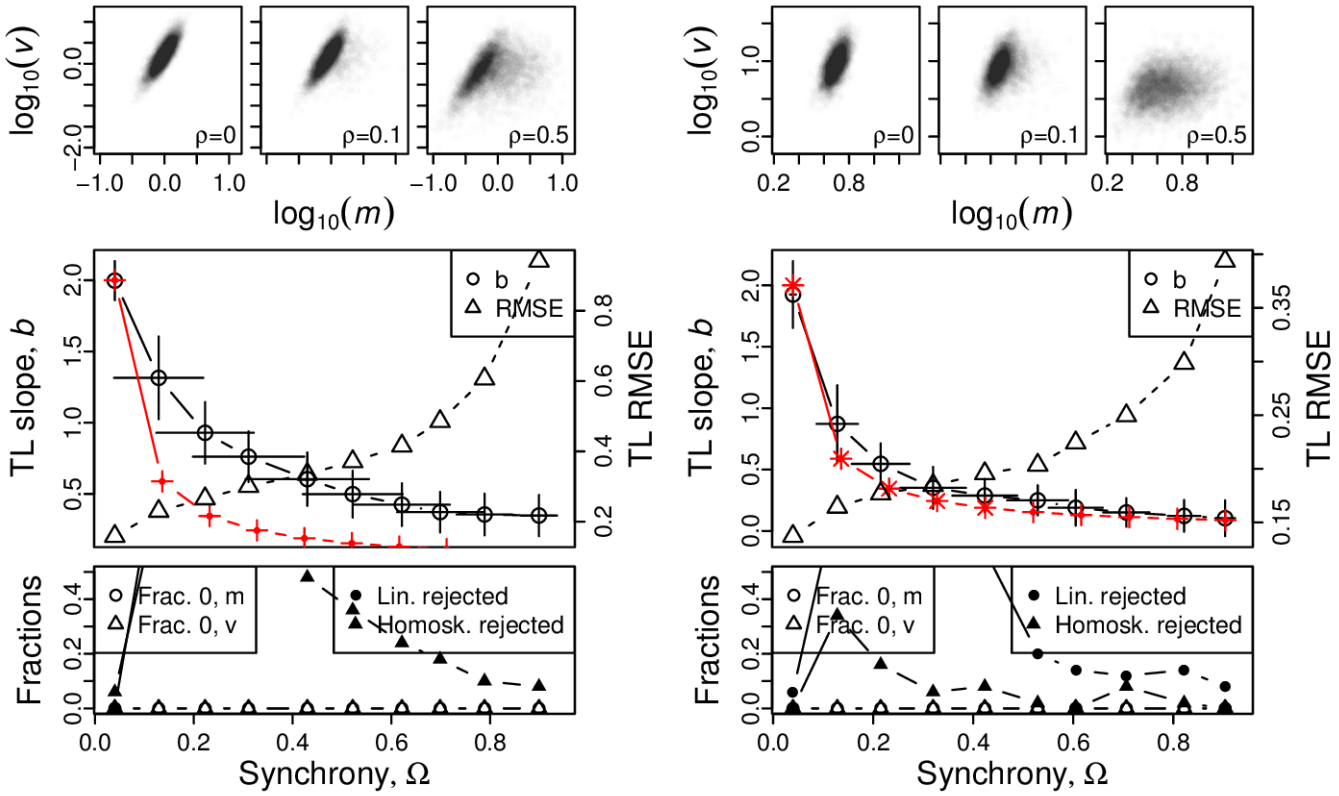

C, D

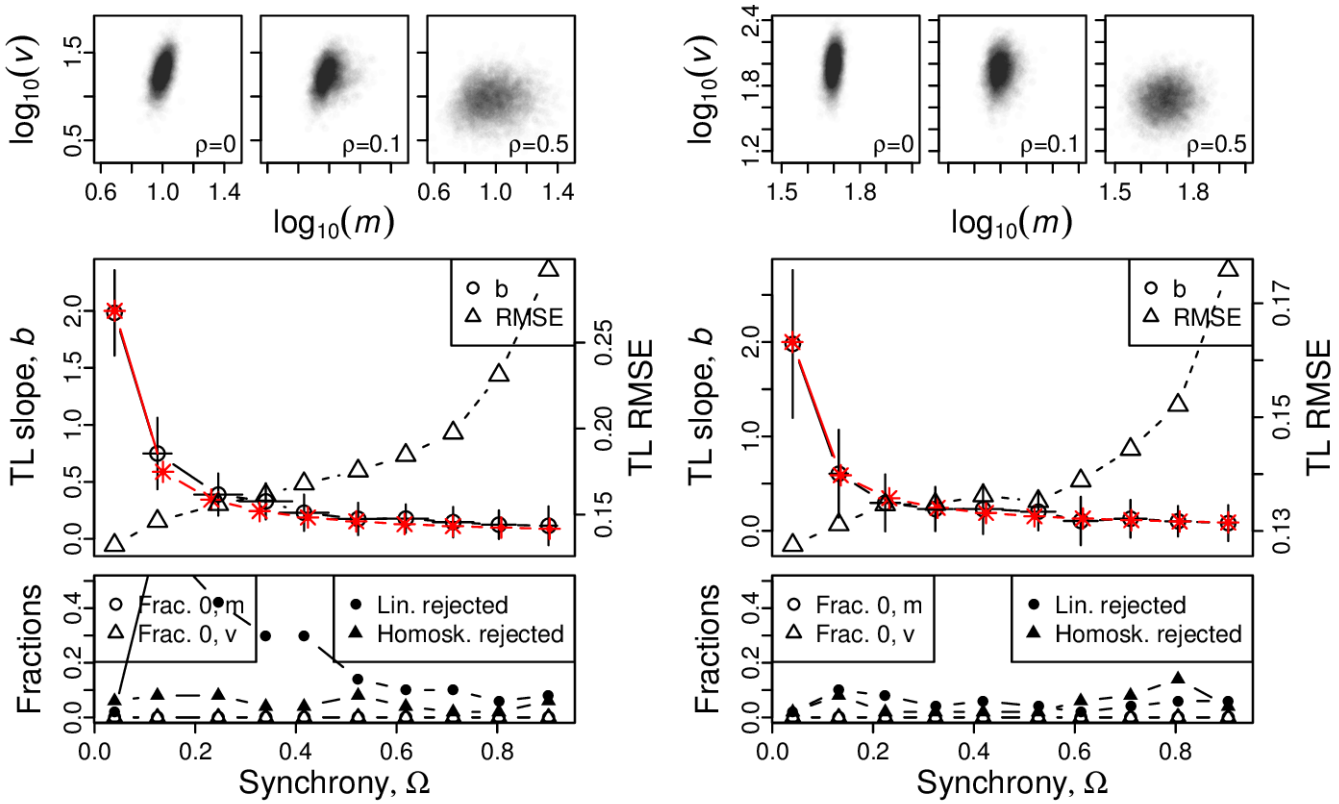

Figure S83: Omnibus plots (see section S6) for identically distributed chi-squared marginals under the set up of section S5, for $n = 25$, for $k = 1$ (A), $k = 5$ (B), $k = 10$ (C), and $k = 50$ (D).

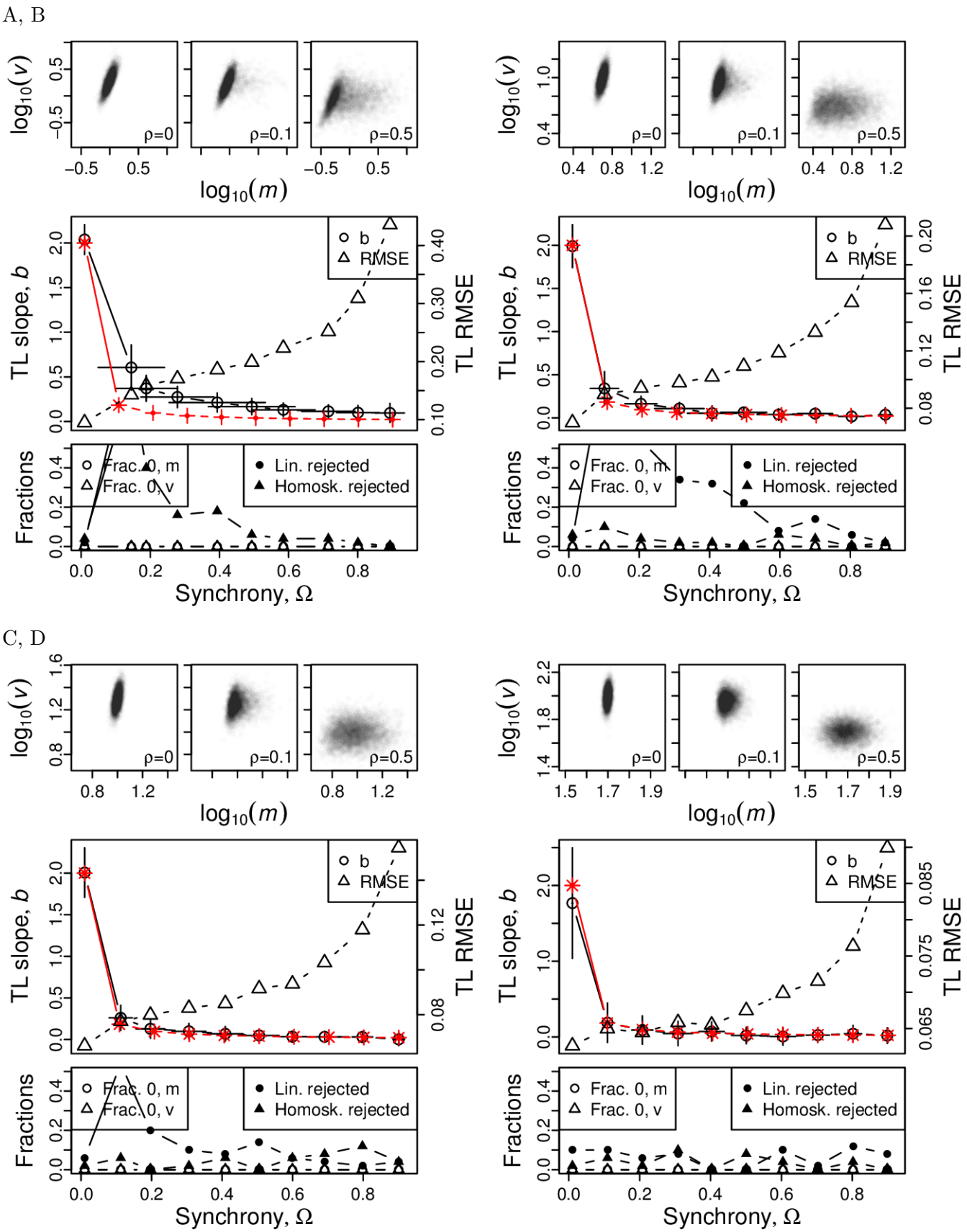

Figure S84: Omnibus plots (see section S6) for identically distributed chi-squared marginals under the set up of section S5, for $n = 100$, for $k = 1$ (A), $k = 5$ (B), $k = 10$ (C), and $k = 50$ (D).

A, B

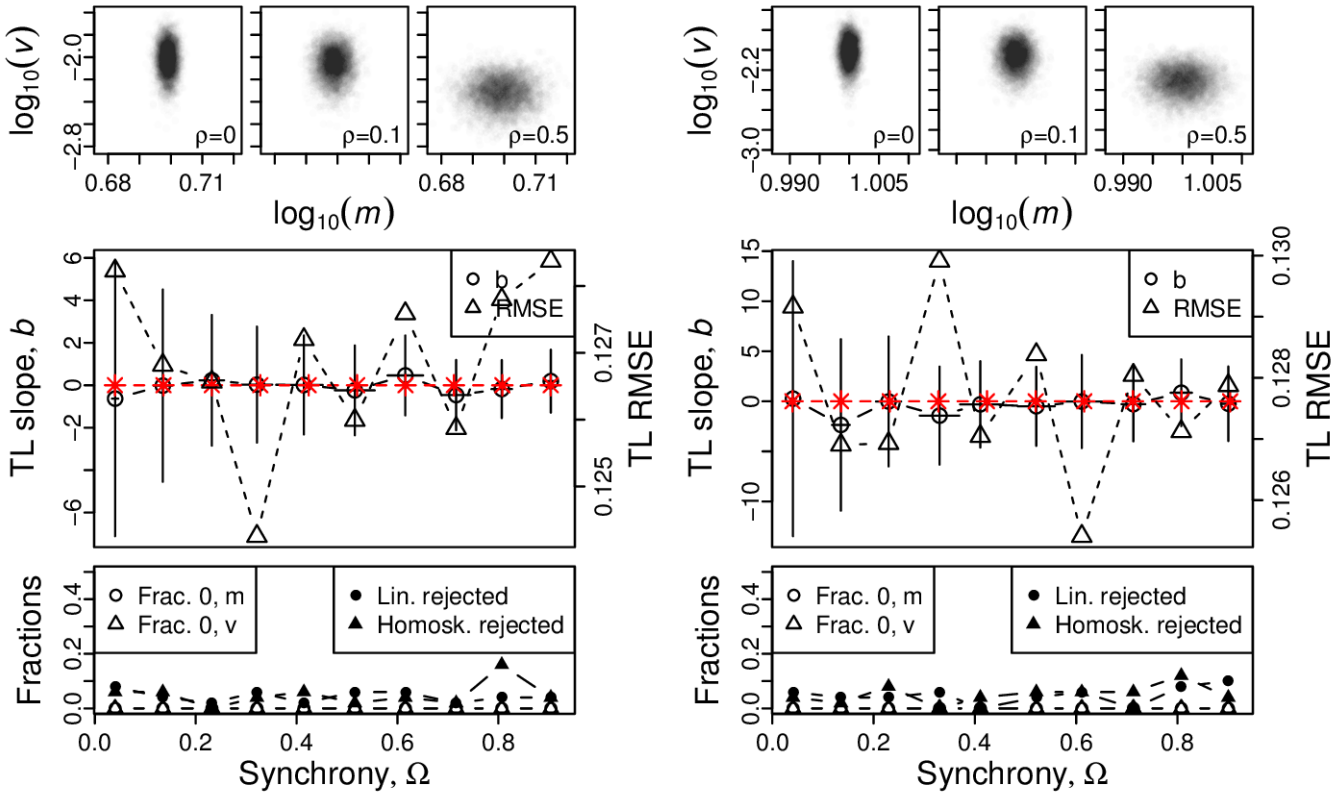

C, D

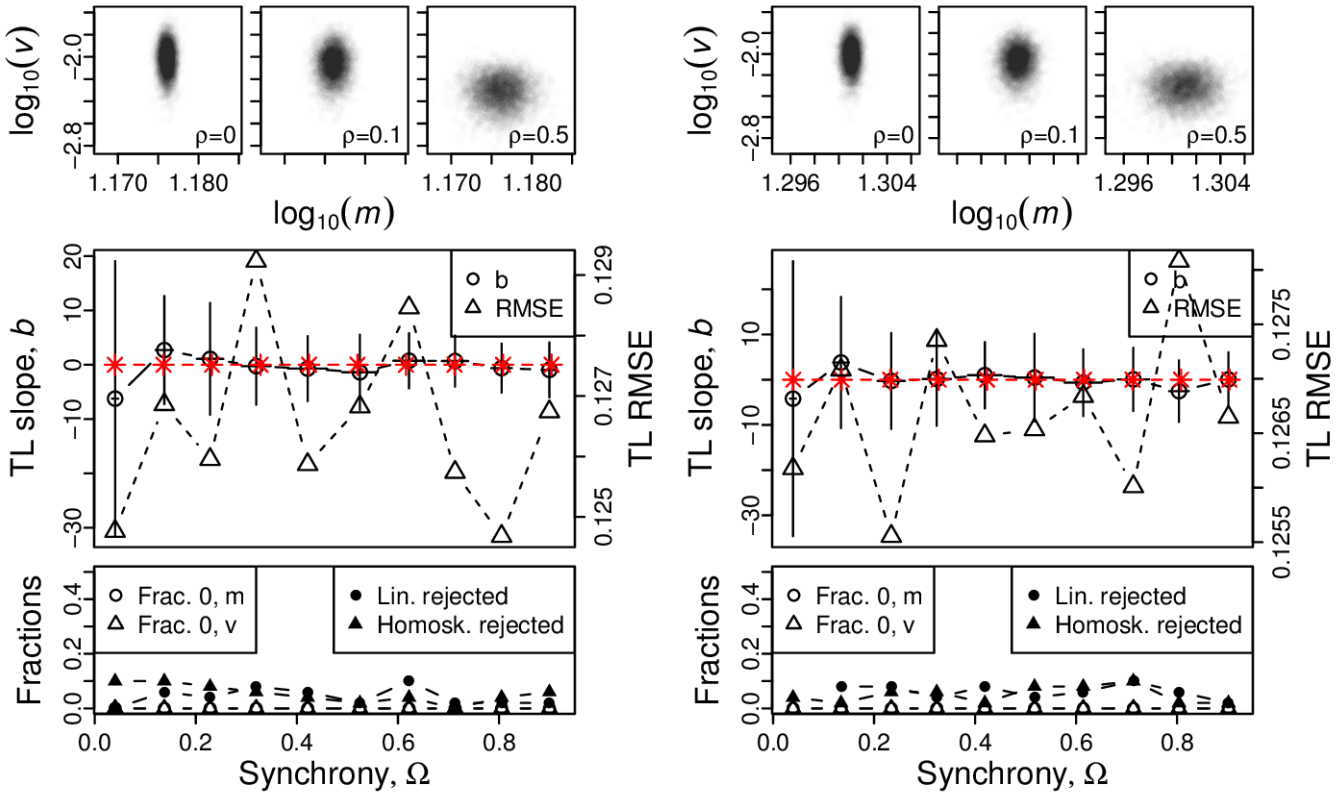

Figure S85: Omnibus plots (see section S6) for identically distributed normal marginals under the set up of section S5, for $n = 25$ and $\sigma = 0.1$, for $\mu = 5$ (A), $\mu = 10$ (B), $\mu = 15$ (C), and $\mu = 20$ (D).

A, B

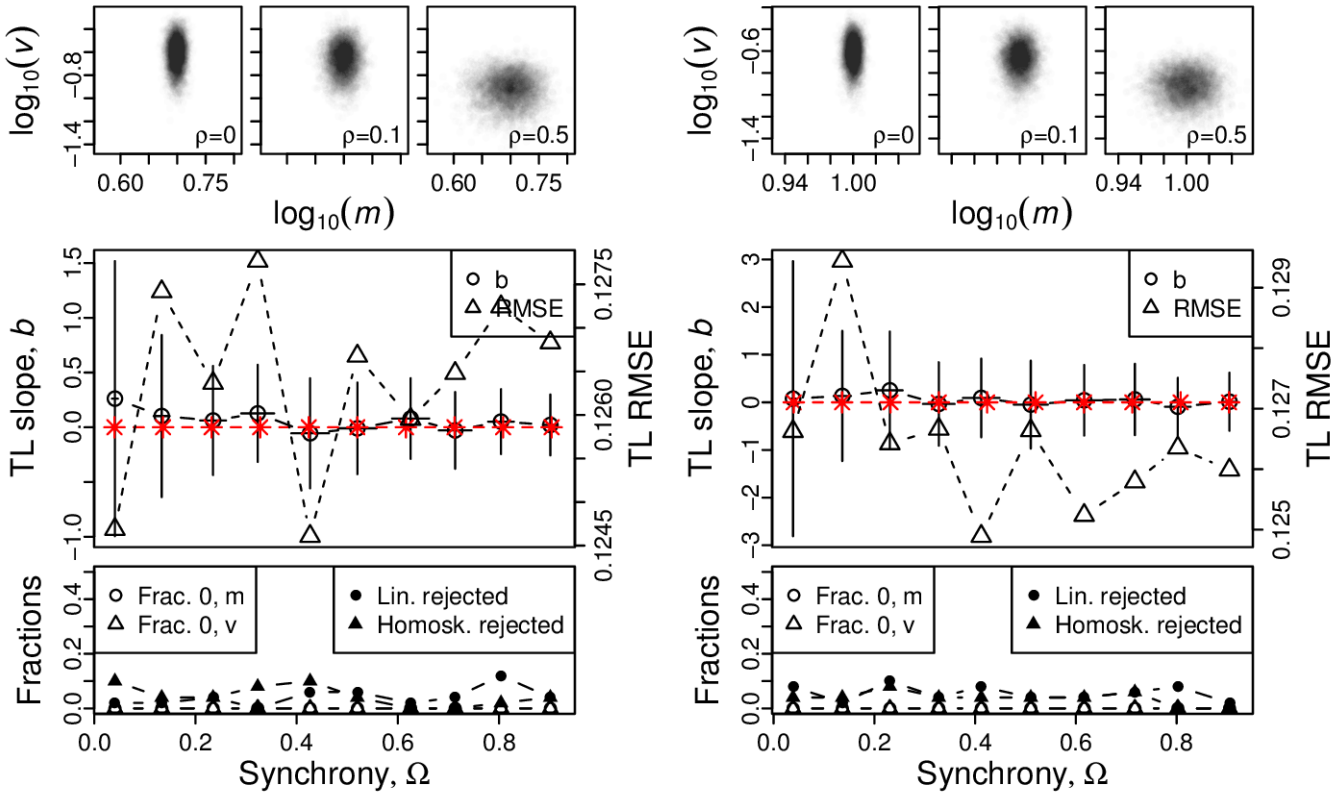

C, D

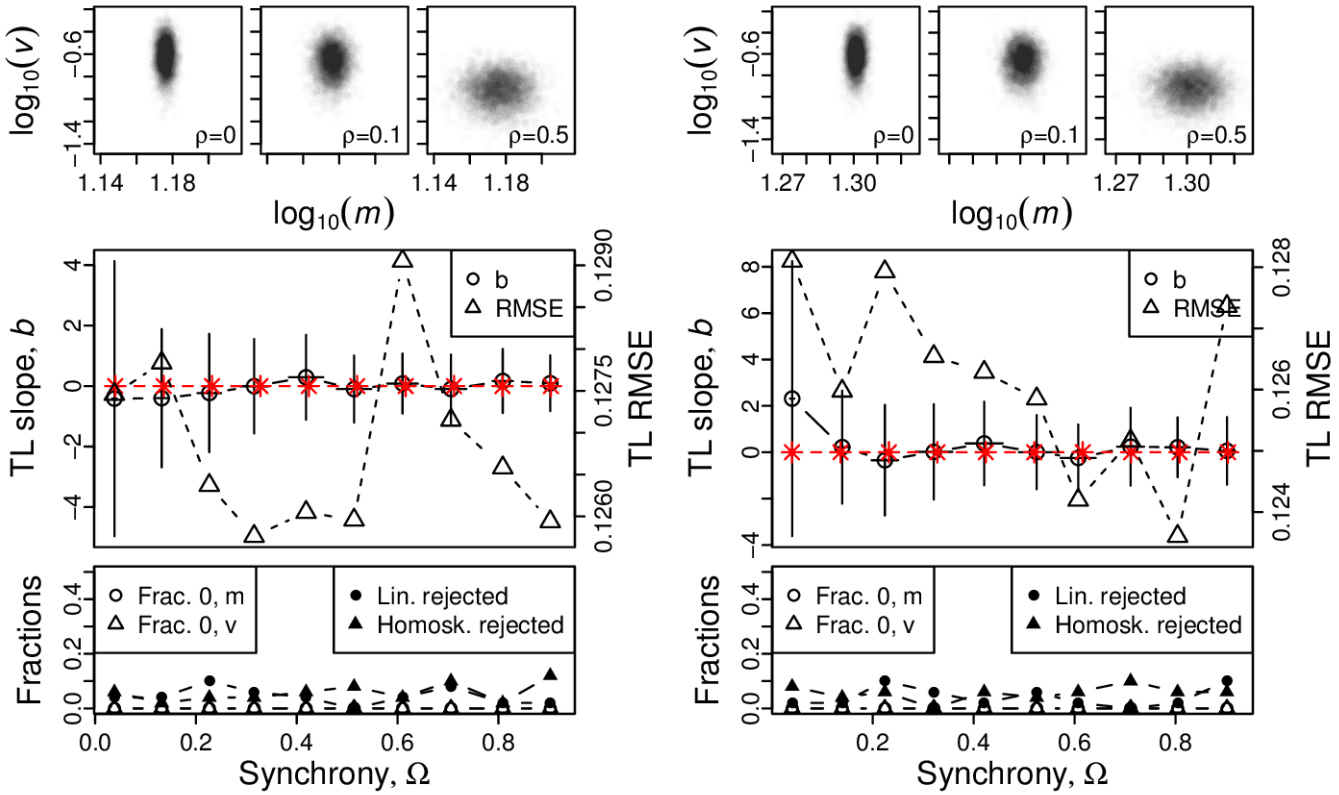

Figure S86: Omnibus plots (see section S6) for identically distributed normal marginals under the set up of section S5, for $n = 25$ and $\sigma = 0.5$, for $\mu = 5$ (A), $\mu = 10$ (B), $\mu = 15$ (C), and $\mu = 20$ (D).

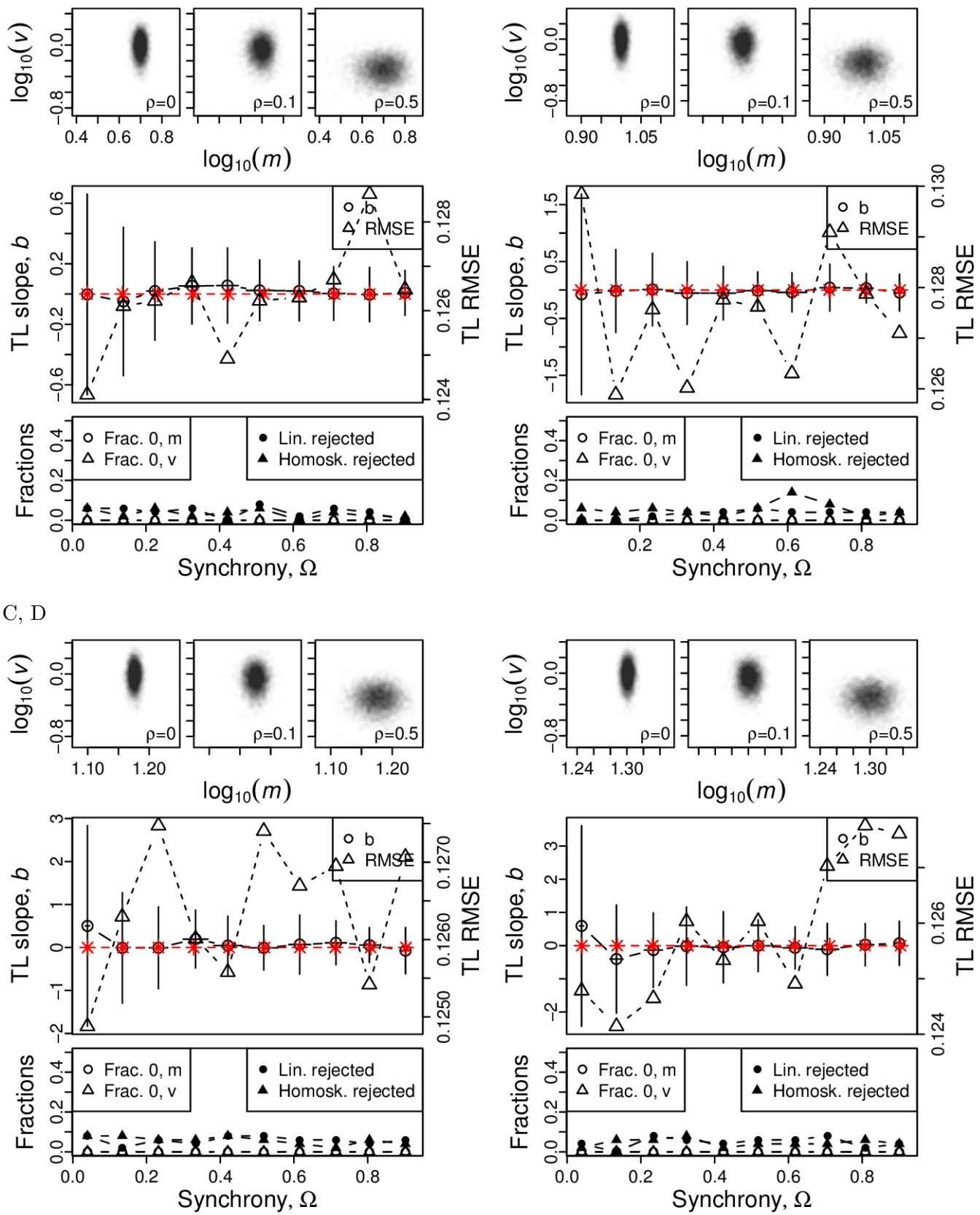

Figure S87: Omnibus plots (see section S6) for identically distributed normal marginals under the set up of section S5, for $n = 25$ and $\sigma = 1$, for $\mu = 5$ (A), $\mu = 10$ (B), $\mu = 15$ (C), and $\mu = 20$ (D).

A, B

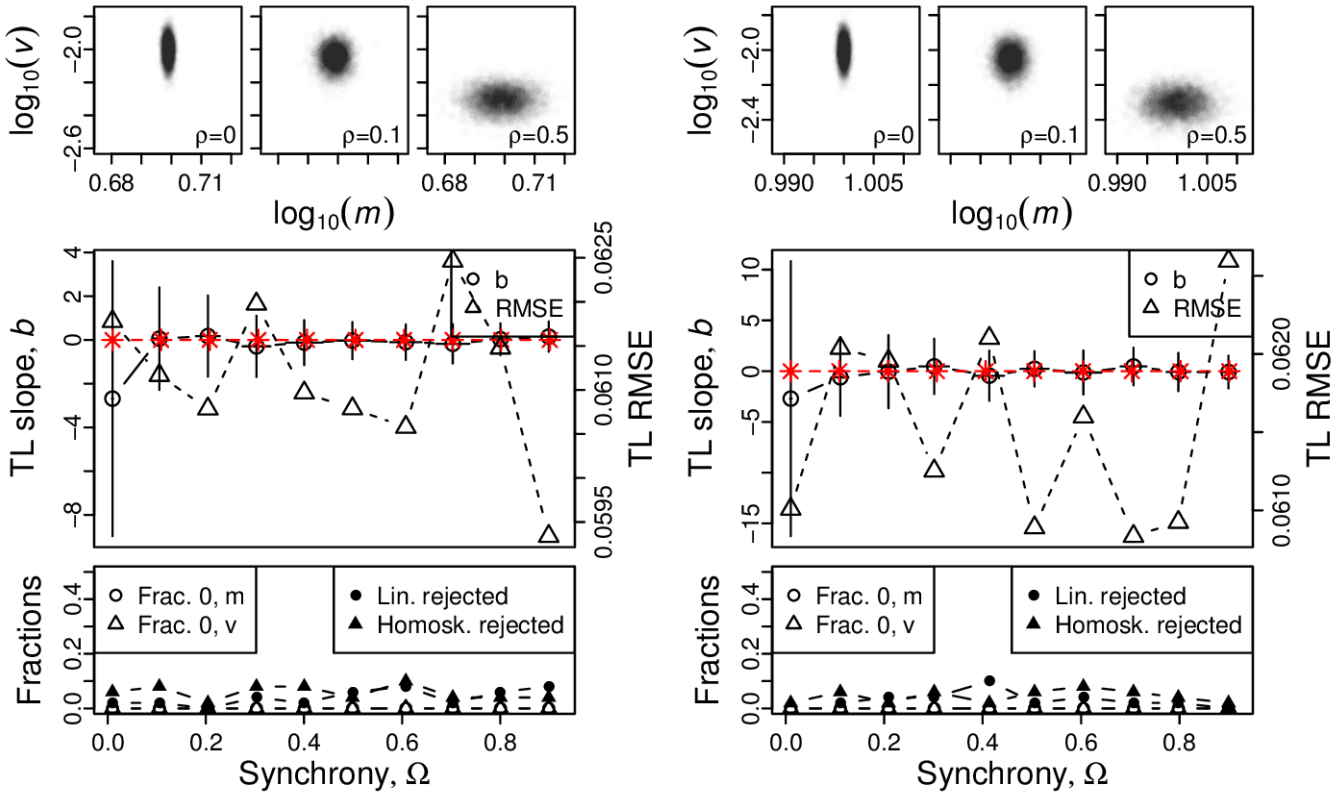

C, D

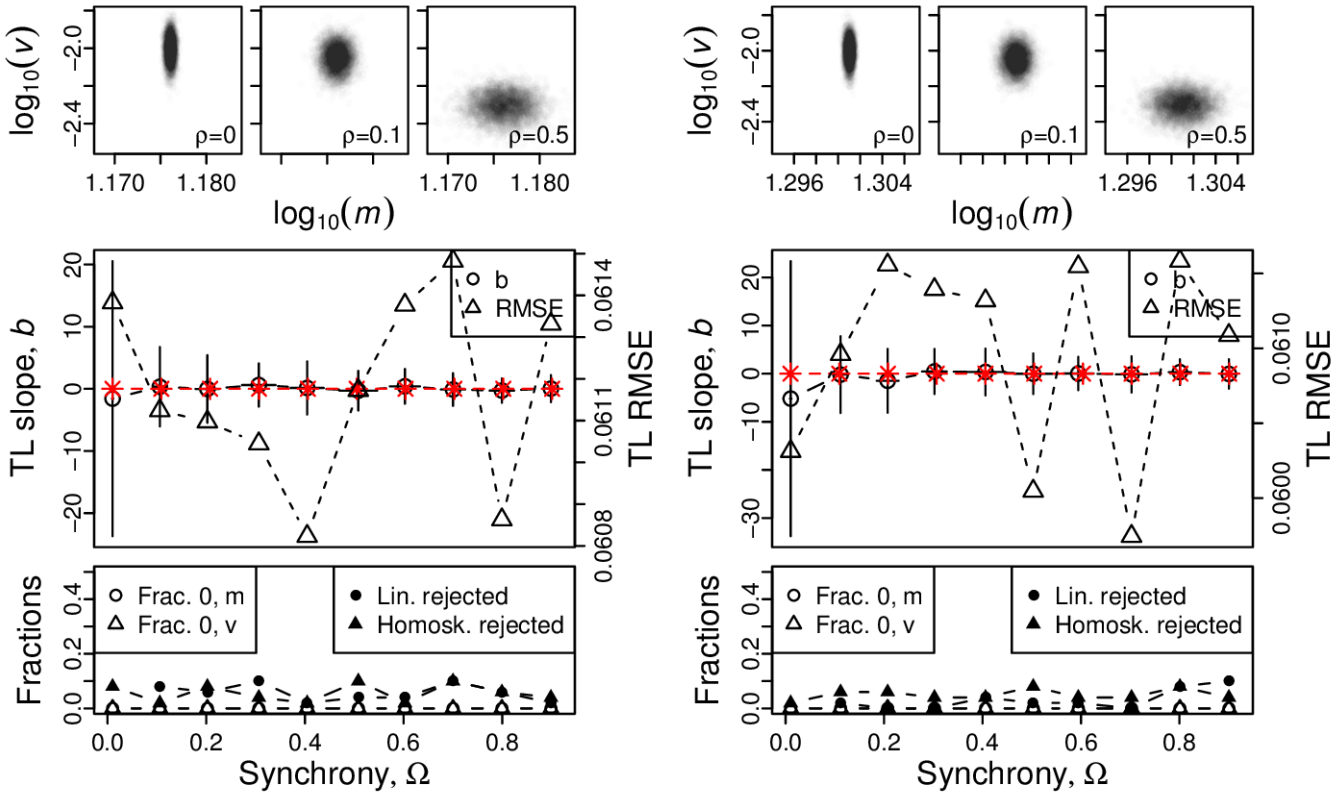

Figure S88: Omnibus plots (see section S6) for identically distributed normal marginals under the set up of section S5, for $n = 100$ and $\sigma = 0.1$, for $\mu = 5$ (A), $\mu = 10$ (B), $\mu = 15$ (C), and $\mu = 20$ (D).

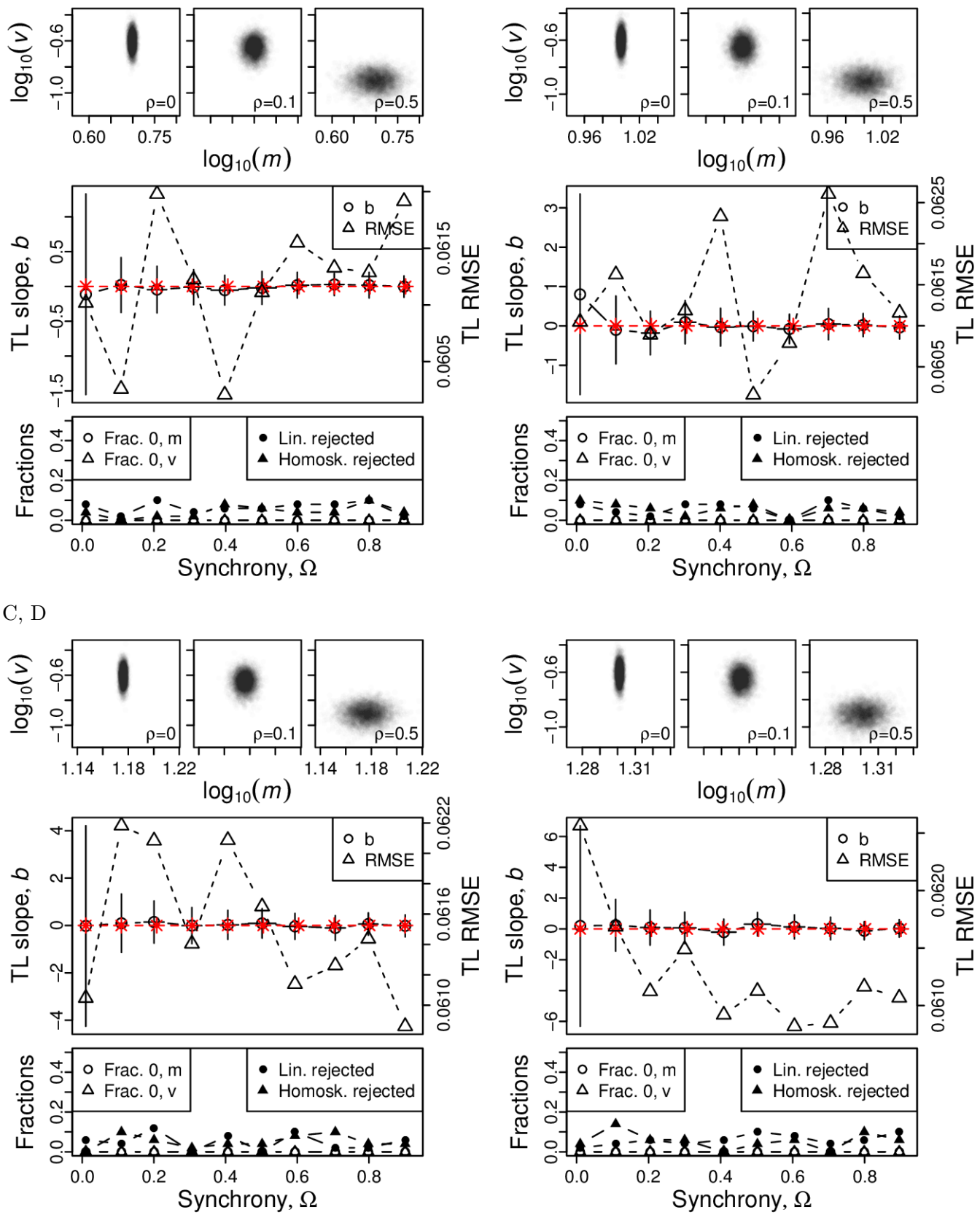

Figure S89: Omnibus plots (see section S6) for identically distributed normal marginals under the set up of section S5, for $n = 100$ and $\sigma = 0.5$, for $\mu = 5$ (A), $\mu = 10$ (B), $\mu = 15$ (C), and $\mu = 20$ (D).

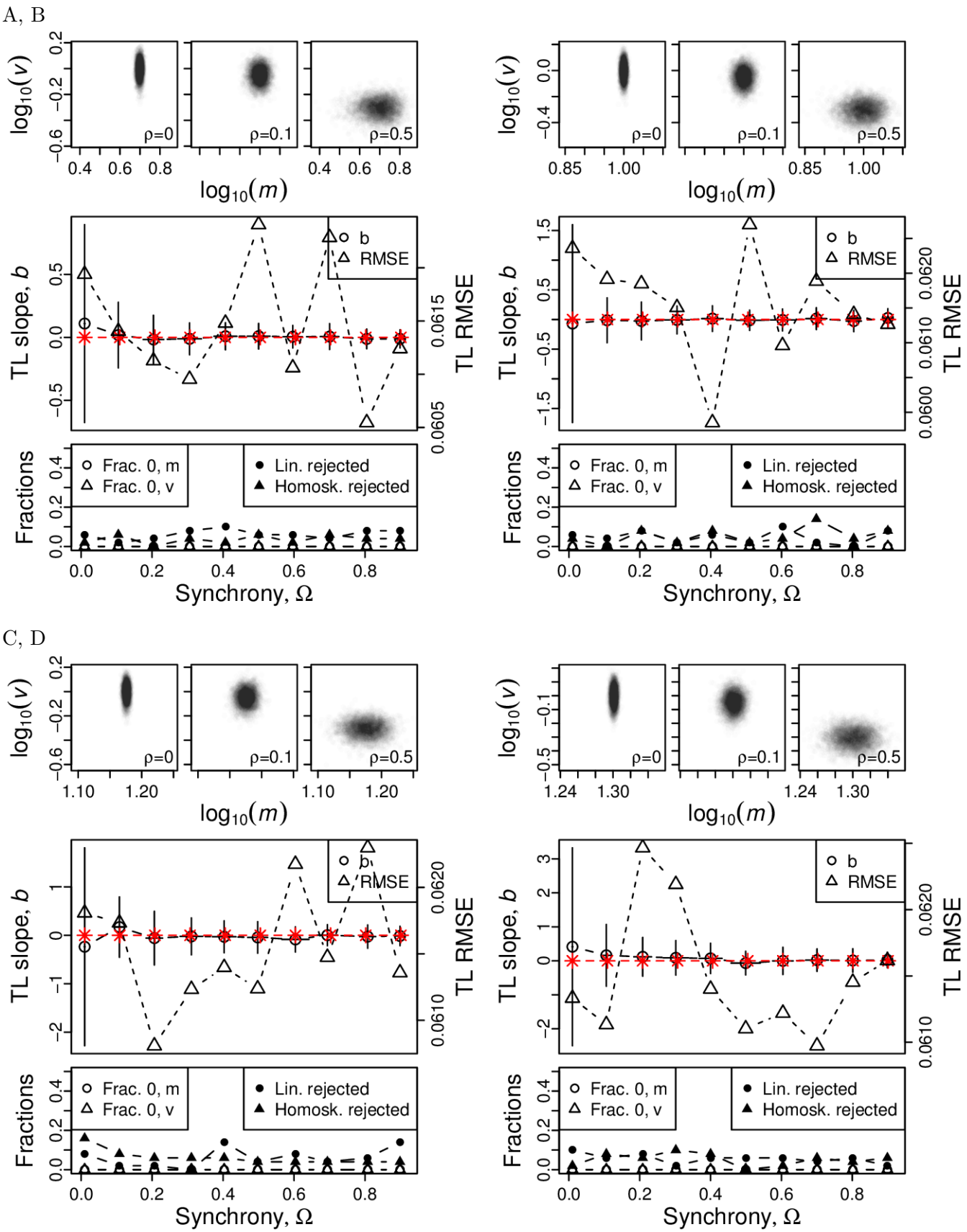

Figure S90: Omnibus plots (see section S6) for identically distributed normal marginals under the set up of section S5, for $n = 100$ and $\sigma = 1$, for $\mu = 5$ (A), $\mu = 10$ (B), $\mu = 15$ (C), and $\mu = 20$ (D).

S11 Figures testing spatial Taylor's law for empirical data

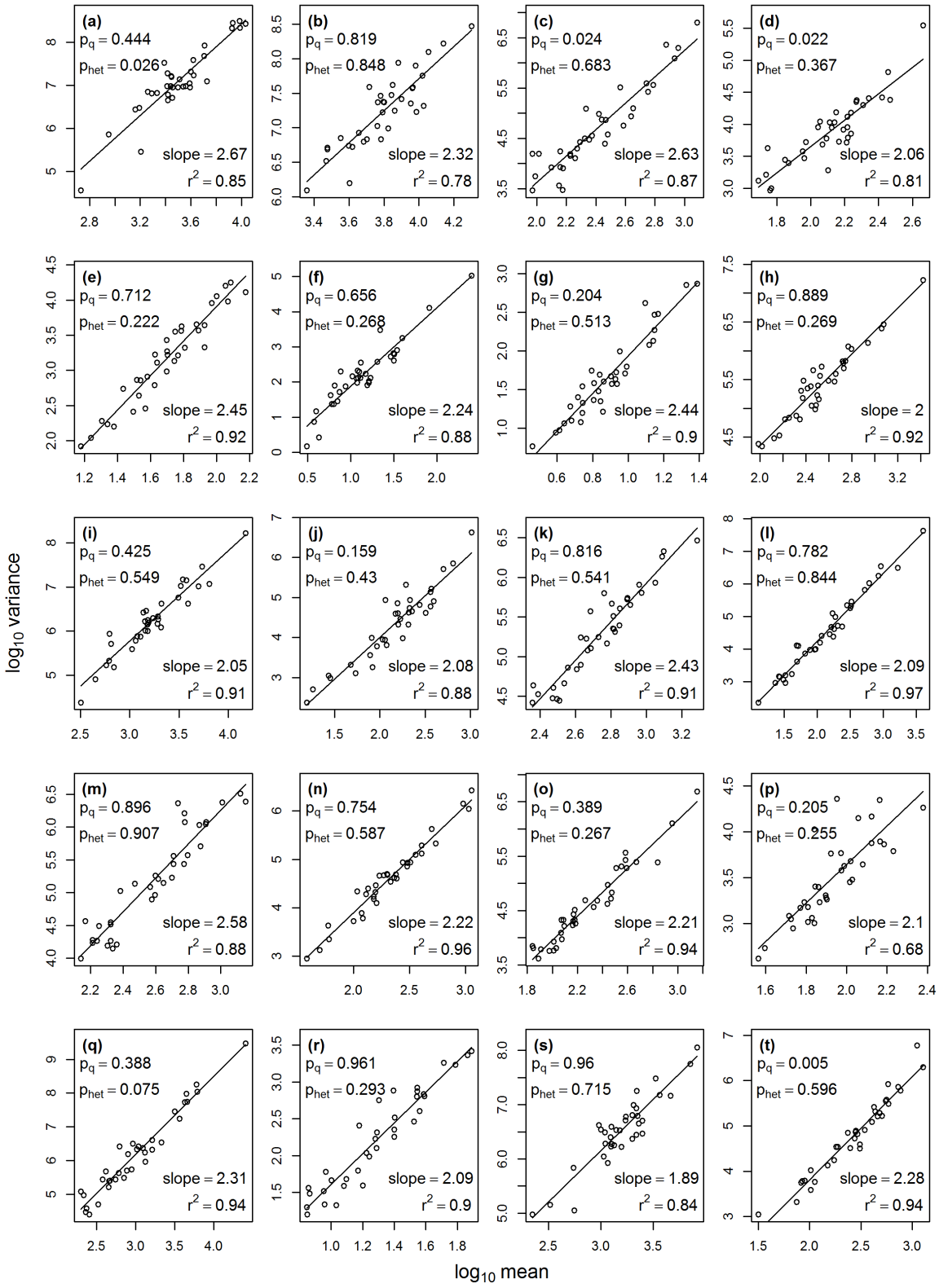

Figure S91: Plots of $\log_{10}$(variance) versus $\log_{10}$(mean) and results of statistical tests of whether data conformed to TL for 20 species of aphid from the UK (Methods). The value p_q tests linearity of the regression against a quadratic alternative; p_het tests for heteroskedasticity. Panels correspond to species listed in Table S1, in the same order.

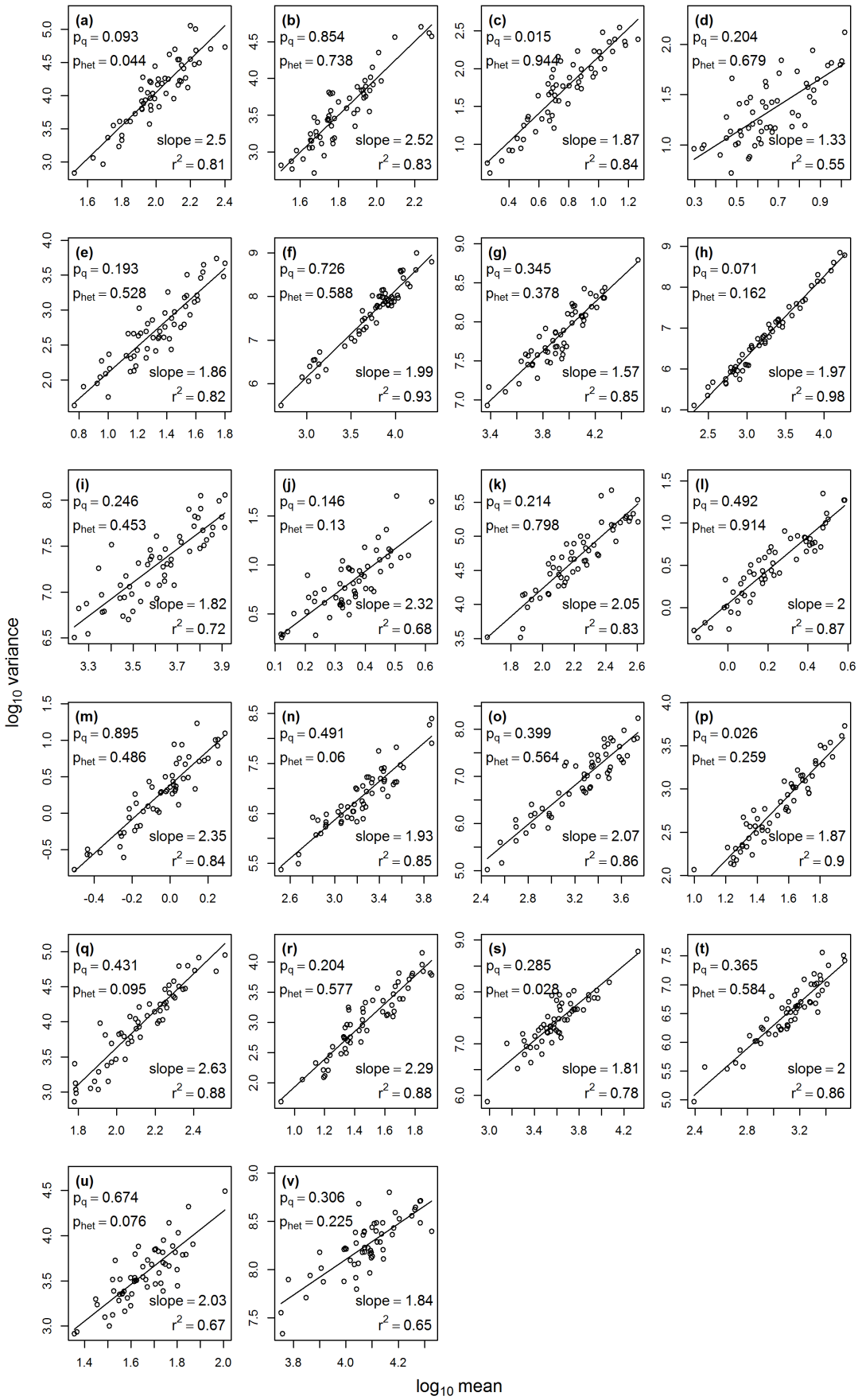

Figure S92: As for figure S91, but for plankton groups in the seas around the UK.

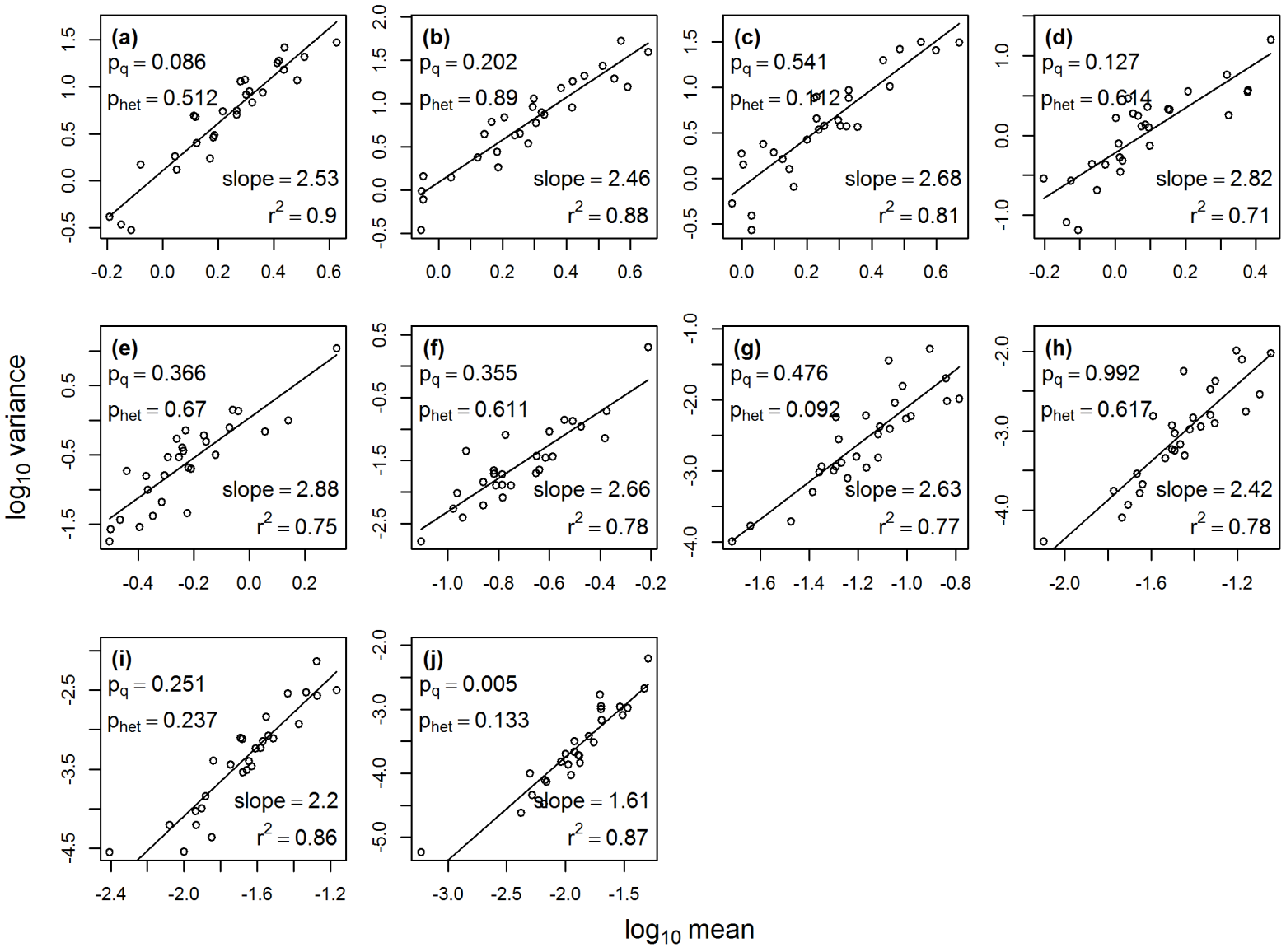

Figure S93: As for figure S91, but for chlorophyll-a abundances at different depths at sampling stations in the closest category to the shore (Methods).

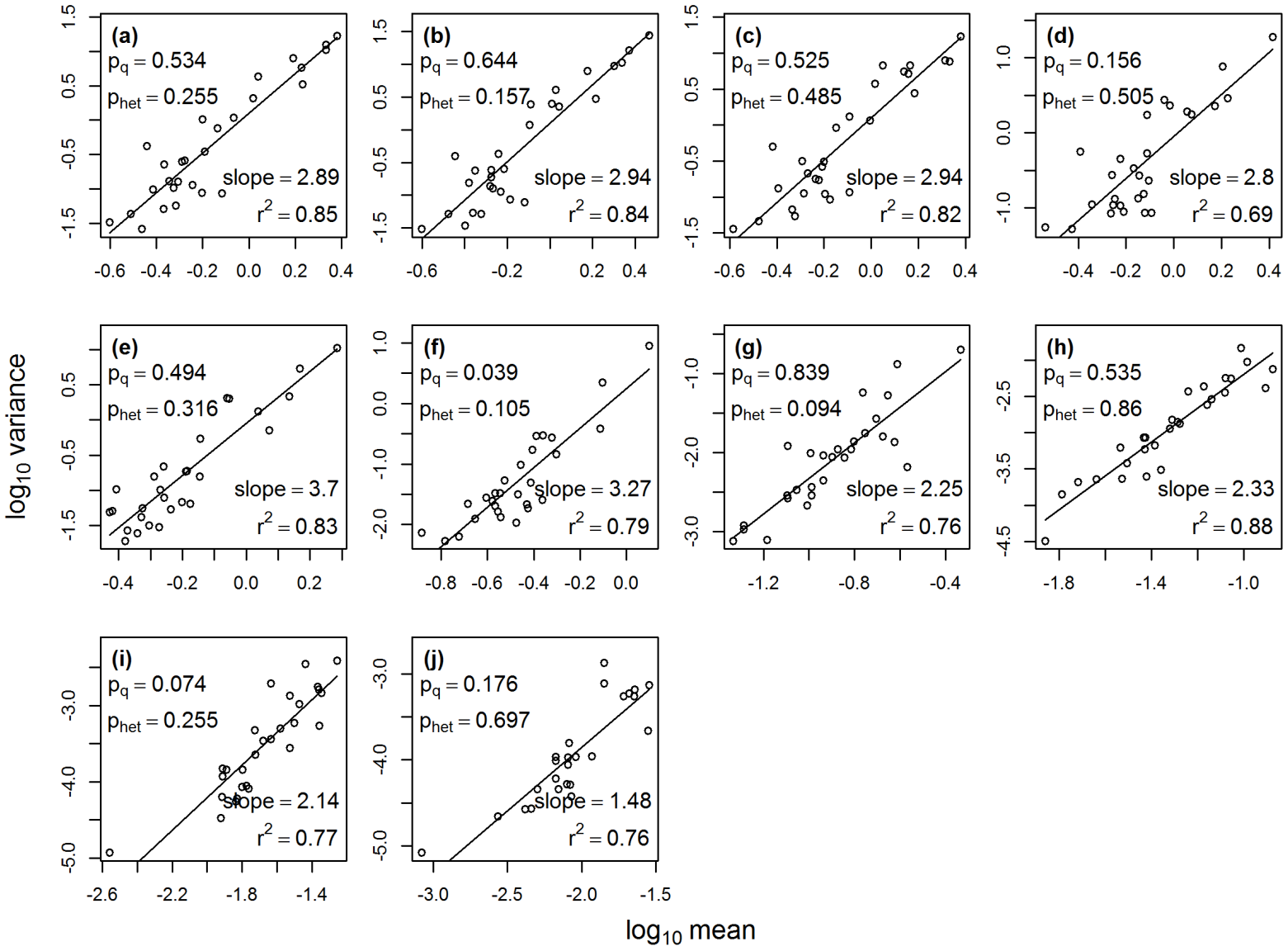

Figure S94: As for figure S91, but for chlorophyll-a abundances at different depths at sampling stations in the second closest category to the shore (Methods).

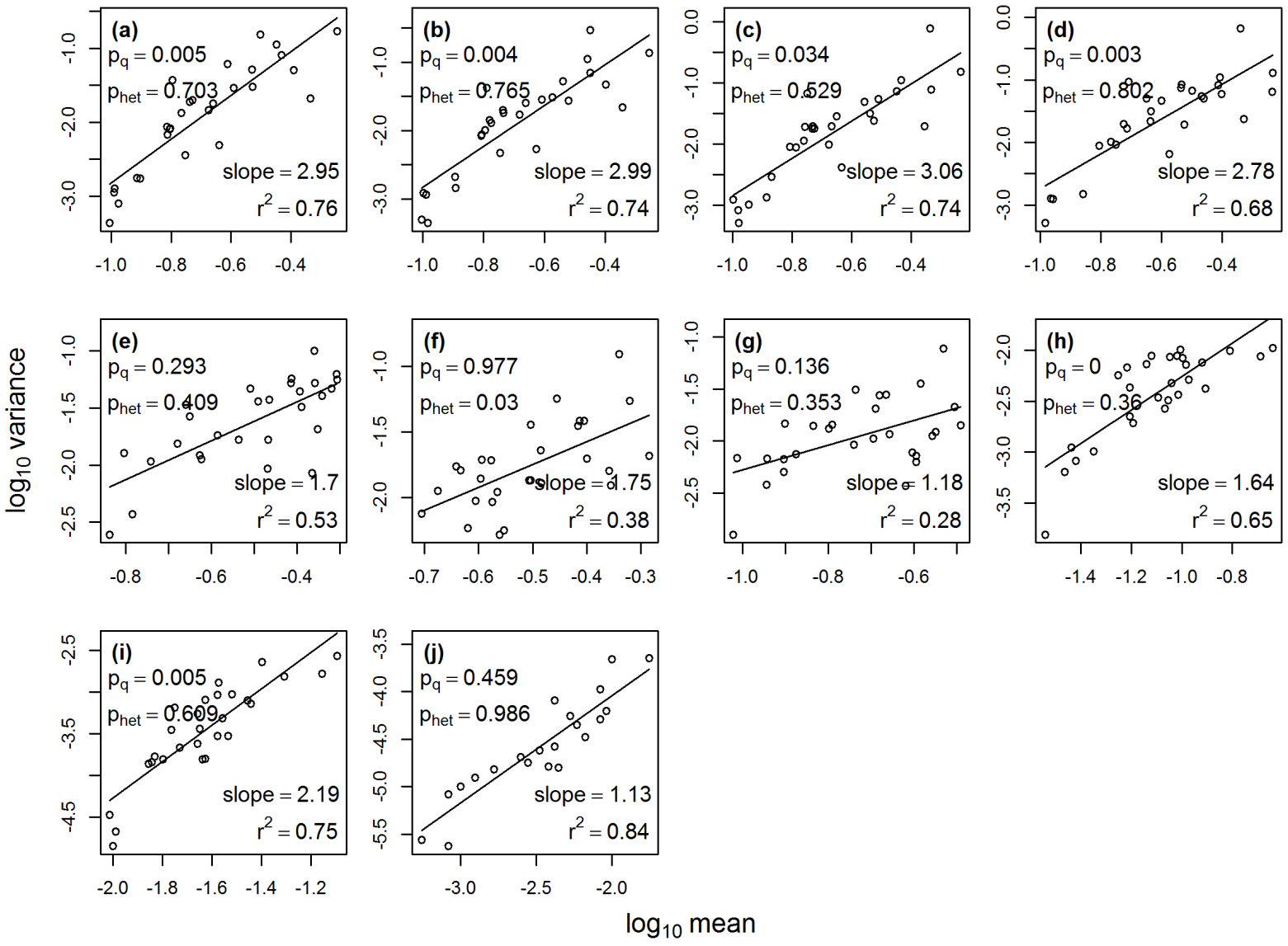

Figure S95: As for figure S91, but for chlorophyll-a abundances at different depths at sampling stations in the third closest category to the shore (Methods).

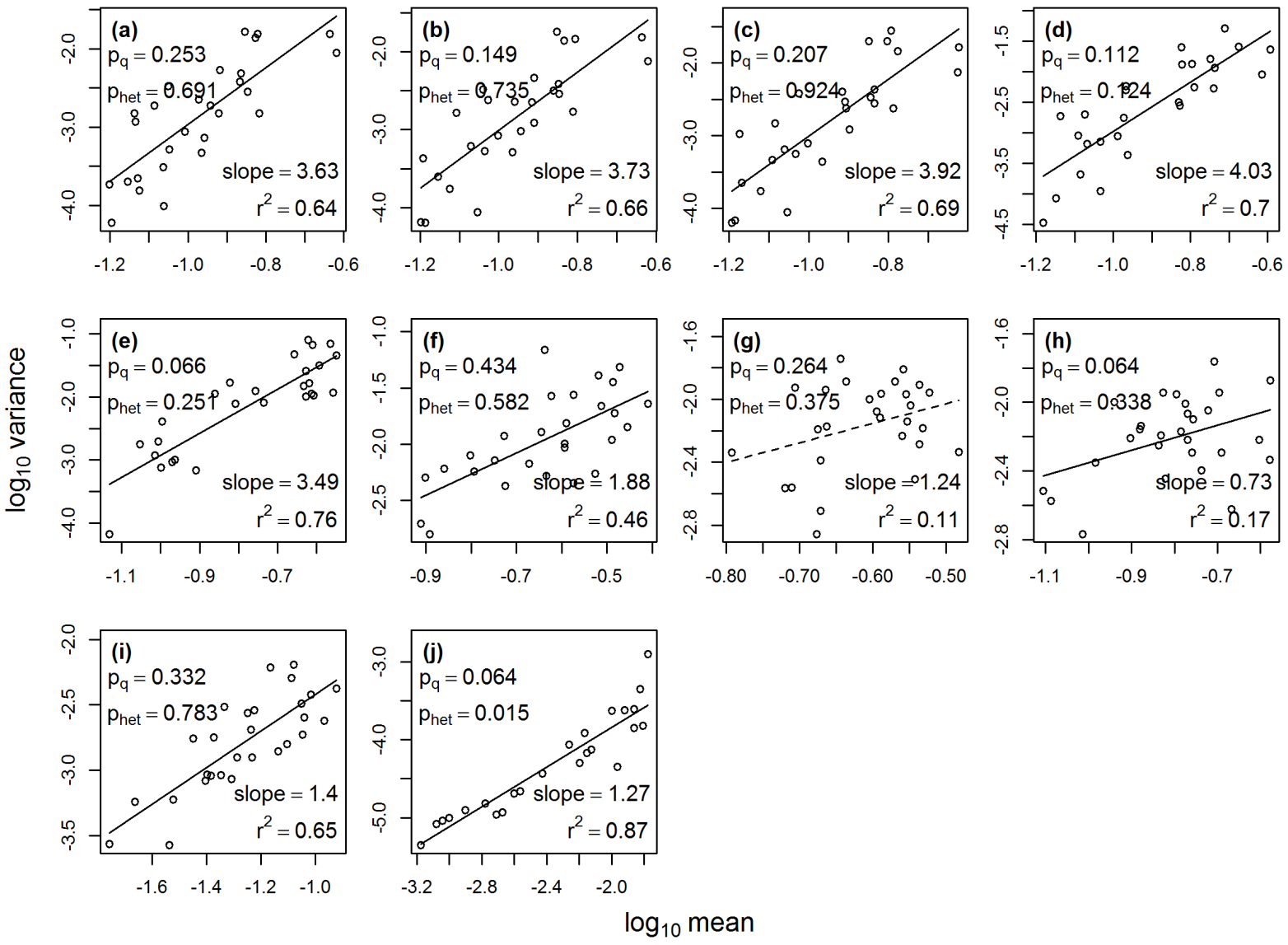

Figure S96: As for figure S91, but for chlorophyll-a abundances at different depths at sampling stations in the farthest category from the shore (Methods).

S12 Figures testing spatial Taylor's law for randomized or partially sorted data

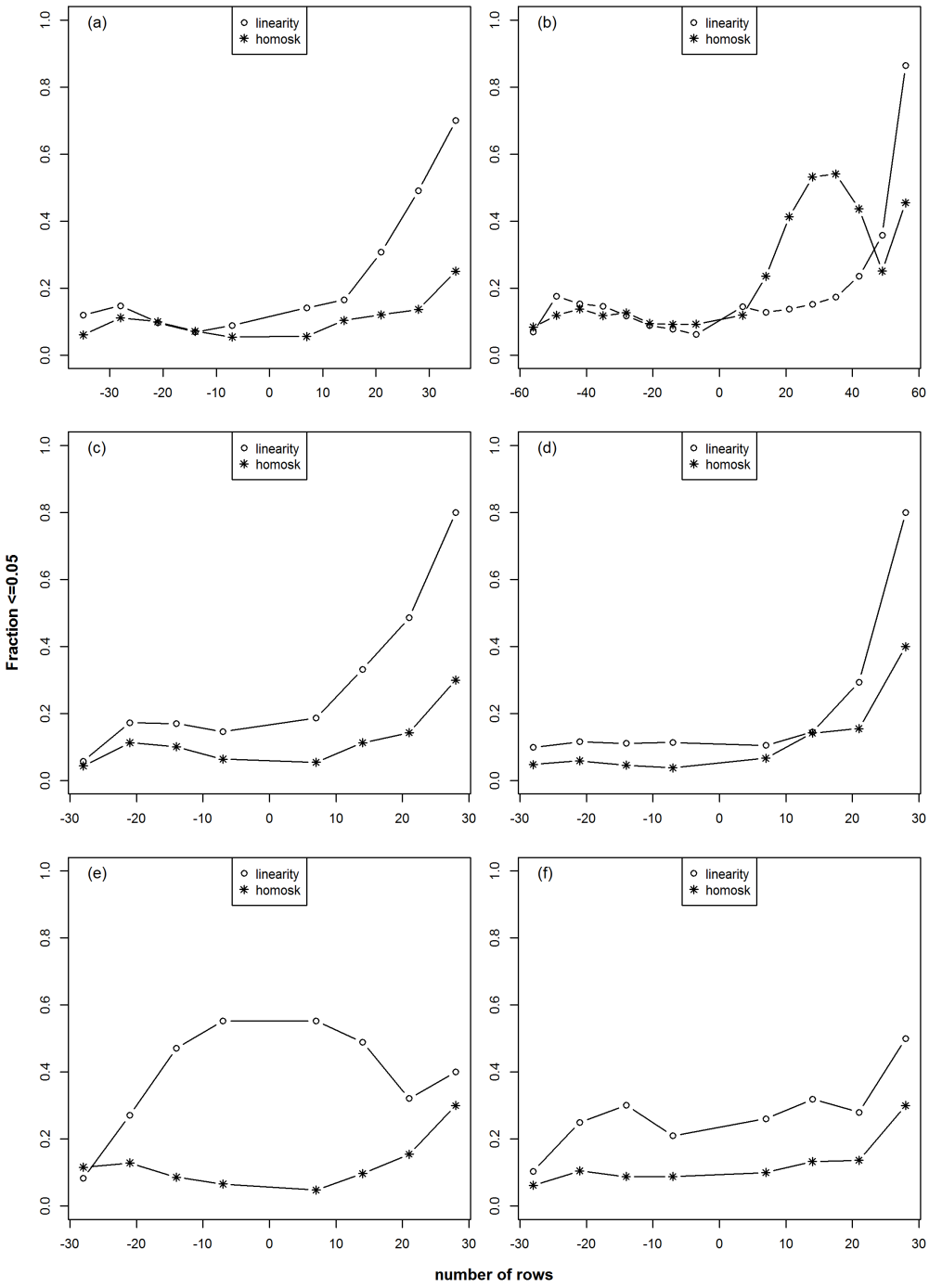

Figure S97: Statistical tests indicating whether the randomized or partially sorted data sets used in figure 3 in the main text conformed to TL. For each resampled/sorted dataset (Methods), conformity to TL was tested by testing linearity and homoskedasticity of the $\log_{10}$(variance)-versus-$\log_{10}$(mean) pattern for that randomization (as in figures S91 -S11). Shown are the fraction of tests rejecting the null hypothesis (of linearity or homoskedasticity) with 95% confidence; thus when values substantially exceed 0.05, linearity or homoskedasticity were less acceptable hypotheses. See, however, figure S98. Positive values on the x-axis show numbers of random rows within which time series were randomized. Negative values on the x-axis show numbers of random rows within which time series were randomized. Positive values show numbers of random rows within which time series were sorted. Thus the x-axis corresponds to strength of synchrony. Panels correspond to data sets in the same pattern as main text figure 3.

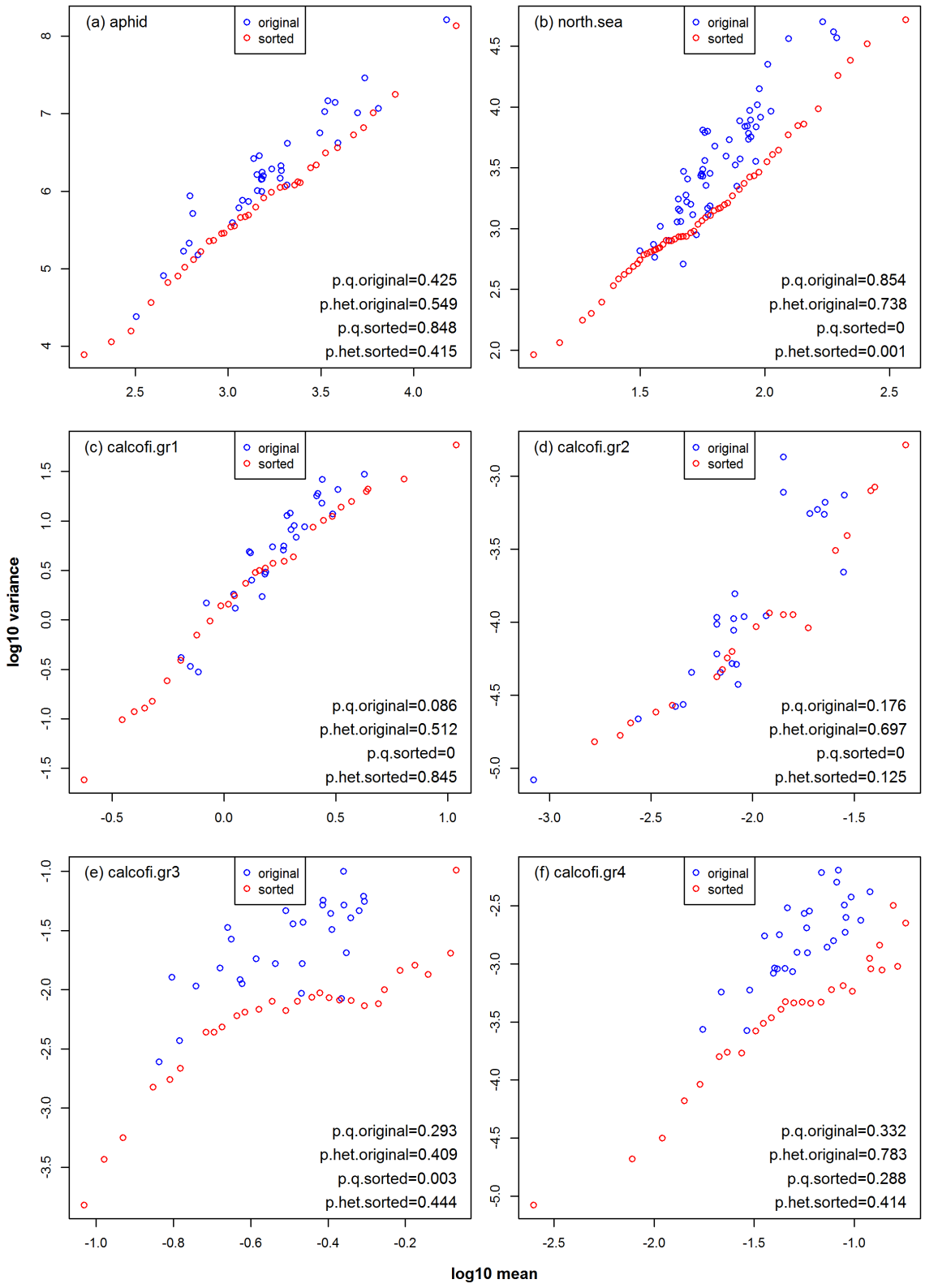

Figure S98: The $\log_{10}$(variance)-versus-$\log_{10}$(mean) pattern for sorted time series. Sorting time series (Methods) produced the most synchronous resampled data sets we considered, but these resampled data sets were among the worst we considered in conformity to TL (figure S97, right side of each panel). Nevertheless, these plots show TL may be a useful approximation for some purposes even for these cases.

S13 Other figures

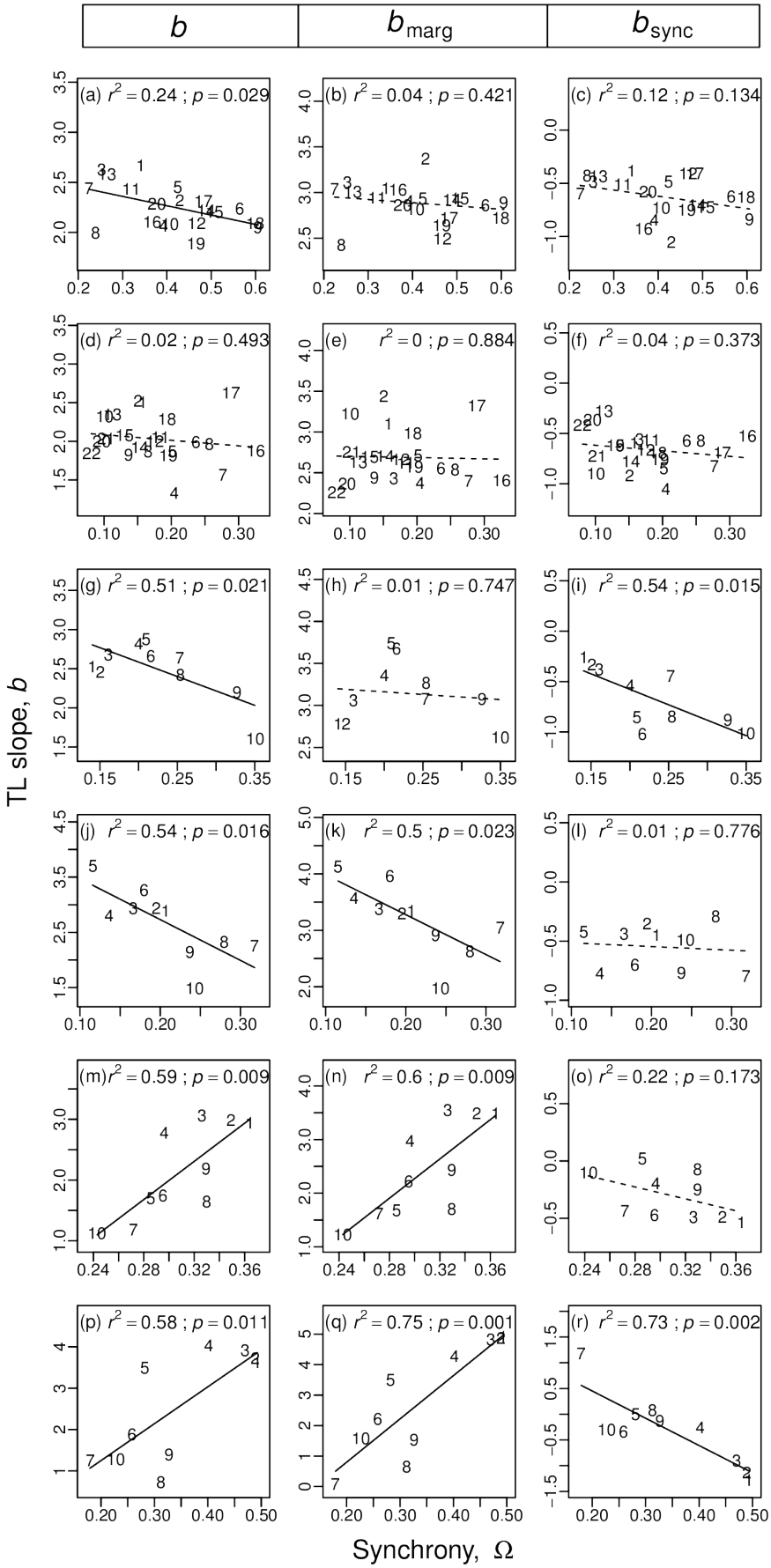

Figure S99: Same as main text figure 2, except points are numbered to identify aphid species, plankton groups, and depths, using the numbers of table S1.

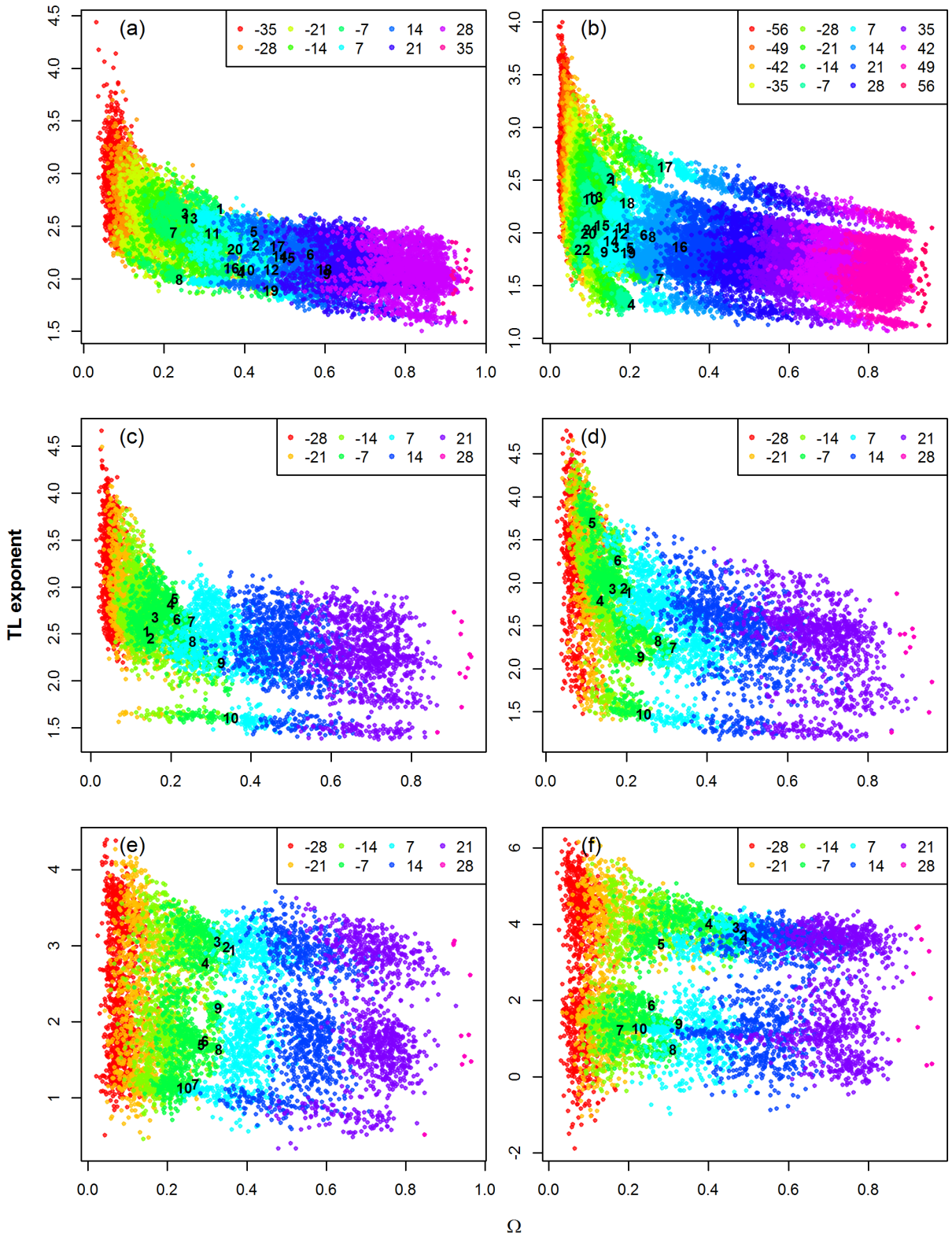

Figure S100: Points in figure 3 in the main text are averages over randomizations/sortings. This plot shows the individual randomizations/sortings. Colors correspond to numbers of rows within which time series were randomized or sorted, negative numbers of rows in figure legends corresponding to randomization and positive values to sorting. Panels correspond to data sets in the same pattern as main text figure 3.

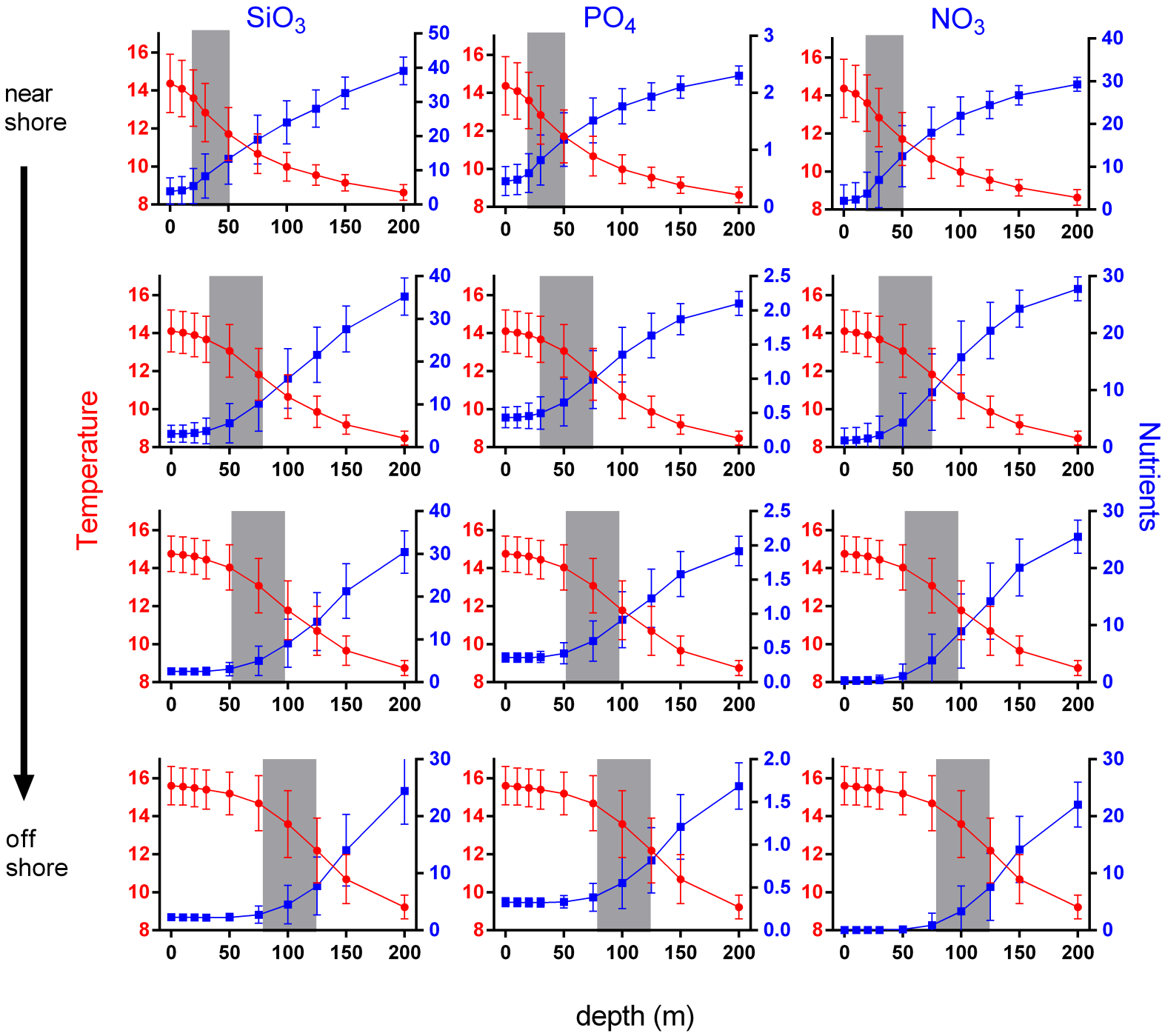

Figure S101: Temperature and nutrient depth gradients in near-shore, far-from-shore, and intermediate sampling stations for the CalCOFI data. Error bars give standard deviations across time and sampling location. Grey bars a put on by eye to approximately indicate the steepest part of the thermocline.

S14 Tables

Aphids		UK seas		CalCOFI	
Index	Species name	Index	Group name	Index	Depth (m)
1	Apple-grass aphid	1	*Acartia* spp (unidentified)	1	0
2	Bird cherry-oat aphid	2	*Calanus* I-IV	2	10
3	Black bean aphid	3	*Calanus finmarchicus*	3	20
4	Blackberry-cereal aphid	4	*Calanus helgolandicus*	4	30
5	Blackcurrant-sowthistle aphid	5	*Centropages typicus*	5	50
6	Corn leaf aphid	6	*Ceratium furca*	6	75
7	Currant-lettuce aphid	7	*Ceratium fusus*	7	100
8	Damson-hop aphid	8	*Ceratium macroceros*	8	125
9	Grain aphid	9	*Ceratium tripos*	9	150
10	Green spruce aphid	10	Decapoda larvae (Total)	10	200
11	Leaf-curling plum aphid	11	Echinoderm larvae		
12	Mealy cabbage aphid	12	Euphausiacea Total		
13	Mealy plum aphid	13	*Metridia lucens*		
14	Pea aphid	14	*Nitzschia delicatissima*		
15	Peach-potato aphid	15	*Nitzschia seriata*		
16	Potato aphid	16	*Oithona* spp		
17	Rose-grain aphid	17	Para-Pseudocalanus spp		
18	Shallot aphid	18	*Pseudocalanus elongates* Adult		
19	Sycamore aphid	19	*Rhizosolenia alata alata*		
20	Willow-carrot aphid	20	*Rhizosolenia styliformis*		
		21	*Temora longicornis*		
		22	*Thalassiosira* spp		

Table S1: Indices used in plots to refer to specific aphid species, plankton groups, or sampling depths.

Site	Latitude	Longitude	Operation dates through 2010
Ayr	55.477	-4.567	30/8/1974 - 9/12/2001; 23/3/2003 - 25/12/2005
Broom's Barn	52.26	0.57	22/3/1965 - end
Dundee	56.457	-3.069	12/5/1965 - 10/12/2006; 17/2/2008 - 30/12/2008; 25/4/2010 - end
Edinburgh	55.949	-3.312	3/4/1969 - 2/10/1971; 1/1/1972 - 30/12/2005; 18/5/2004 - 13/12/2009
Hereford	52.125	-2.637	12/7/1971 - end
Newcastle	55.213	-1.682	21/5/1965 - end, excluding 2009
Preston	53.854	-2.763	29/4/1971 - end
Rothamsted	51.807	-0.356	29/4/1964 - end
Starcross	50.628	-3.454	5/2/1970 - 21/12/2008
Writtle	51.733	0.427	22/5/1975 - 29/7/1991; 1/1/1992 - end
Wye	51.185	0.939	30/11/1966 - end, excluding 2009

Table S2: Sampling sites used. Operating dates given in day/month/year format. Edinburgh is the combination of two very nearby sites, East Craigs and Gogarbank. East Craigs operating dates were 3/4/1969 to 2/10/1971 and 1/1/1972 to 30/12/2005. Gogarbank operating dates were 18/5/2004 to 13/12/2009. Data for Edinburgh were taken from 1/1/2006 forward from Gogarbank. This table was taken from Sheppard et al. [2015].

Analytic results: Appendices S1 and S2					
Summary: Results apply when the Y_i are identically distributed. b depends on Ω approximately as equation (44). The approximation will be worse for larger Ω. b should decrease sharply as Ω increases from 0. Skewness of Y_i is necessary in the identically distributed case to get $b \neq 0$.					
Distribution	**TL holds?**	**b depends on Ω?**	**$b \downarrow$ as $\Omega \uparrow$ from 0**	**$b \uparrow$ as $\Omega \uparrow$ further**	**eq. (44) a good approximation?**
Numeric results for Y_i identically distributed, Gaussian copula: Appendix S3 and figs S1 through S32					
Poisson, figs S1-S2	large λ, yes; small λ, approx'ly	yes	yes	no	NA
neg. binom., figs S3-S10	yes, except for larger p and Ω	yes	yes	no	NA
gamma, figs S11-S16	yes, but approx'ly for small α and large Ω	yes	yes	sometimes no; sometimes slightly	qualitatively, yes; better for small Ω
exponential, figs S17-S18	small Ω, yes; large Ω, approx'ly	yes	yes	sometimes no; sometimes slightly	qualitatively, yes; better for small Ω
chi-squared, figs S19-S20	large k, yes; small k, approx'ly	yes	yes	sometimes no; sometimes slightly	qualitatively, yes; better for large k
normal, figs S21-S26	yes	no	no	no	yes
log-normal, figs S27-S32	yes, except when σ is large and Ω small	yes	yes	no	only for small σ
Numerical results for Y_i non-identically distributed, Gaussian copula: Appendix S4 and figs S33 through S64					
Poisson, figs S33-S34	yes	yes	yes	no	NA
neg. binom., figs S57-S64	small Ω yes; large Ω often no	yes	yes	usually no; sometimes yes	NA
gamma, figs S35-S40	small Ω yes; large Ω, approx'ly	yes	yes	yes	NA
exponential, figs S41-S42	small Ω yes; large Ω, approx'ly	yes	yes	yes	NA
chi-squared, figs S43-S44	small Ω yes; large Ω, approx'ly	yes	yes	no	NA
normal, figs S45-S50	yes, except for $\sigma = 1$, $\mu = 5$	yes	yes	no, except for $\sigma = 1$, $\mu = 5$	NA
log-normal, figs S51-S56	yes	yes	yes	no	NA
Numeric results for Y_i identically distributed, construction based on sums (common elements): Appendix S5 and figs S65 through S90					
Poisson, figs S65-S66	large λ yes ; small λ no	yes	yes	no	yes
neg. binom., figs S67-S74	large r approx'ly; small r no	yes	yes	no	better for large r
gamma, figs S75-S80	only for smallest and largest Ω	yes	yes	no	yes, but better for larger α
exponential, figs S81-S82	only for smallest Ω	yes	yes	no	qualitatively
chi-squared, figs S83-S84	only for small Ω or large k	yes	yes	no	qualitatively
normal, figs S85-S90	yes	no	no	no	yes

Table S3: Summary of analytic and numeric results. Color indicates hyperlinks that, when clicked inside a pdf viewer, will lead directly to the relevant material. A summary of randomization and empirical results is in table S14.

Empirical results: Main text, and main text fig. 2				
Data set	**TL holds?**	b **depends on** Ω**?**	$b_{\mathbf{marg}}$ **depends on** Ω**?**	$b_{\mathbf{sync}}$ **depends on** Ω**?**
Aphid data	yes, except 1 species	$b \downarrow$ as $\Omega \uparrow$, signif'ly	$b_{\text{marg}} \downarrow$ as $\Omega \uparrow$, non-signif'ly	$b_{\text{sync}} \downarrow$ as $\Omega \uparrow$, non-signif'ly
SAHFOS data	yes	$b \downarrow$ as $\Omega \uparrow$, non-signif'ly	$b_{\text{marg}} \downarrow$ as $\Omega \uparrow$, non-signif'ly	$b_{\text{sync}} \downarrow$ as $\Omega \uparrow$, non-signif'ly
CalCOFI gp. 1	yes, except 1 depth	$b \downarrow$ as $\Omega \uparrow$, signif'ly	$b_{\text{marg}} \downarrow$ as $\Omega \uparrow$, non-signif'ly	$b_{\text{sync}} \downarrow$ as $\Omega \uparrow$, signif'ly
CalCOFI gp. 2	yes	$b \downarrow$ as $\Omega \uparrow$, signif'ly	$b_{\text{marg}} \downarrow$ as $\Omega \uparrow$, signif'ly	$b_{\text{sync}} \downarrow$ as $\Omega \uparrow$, non-signif'ly
CalCOFI gp. 3	yes for 5 and no for 5 depths	$b \uparrow$ as $\Omega \uparrow$, signif'ly	$b_{\text{marg}} \uparrow$ as $\Omega \uparrow$, signif'ly	$b_{\text{sync}} \downarrow$ as $\Omega \uparrow$, non-signif'ly
CalCOFI gp. 4	yes	$b \uparrow$ as $\Omega \uparrow$, signif'ly	$b_{\text{marg}} \uparrow$ as $\Omega \uparrow$, signif'ly	$b_{\text{sync}} \downarrow$ as $\Omega \uparrow$, signif'ly

Randomization results: Main text, and main text fig. 3, figs S97 through S100				
Data set	**TL holds?**	b **depends on** Ω**?**	$b \downarrow$ **as** $\Omega \uparrow$ **from** 0	$b \uparrow$ **as** $\Omega \uparrow$ **further**
Aphid data	low sync., yes; high sync., approx'ly	yes	yes	no, except modestly for 1 case
SAHFOS data	low sync., yes; high sync., approx'ly	yes	yes	no, except modestly for 1 case
CalCOFI gp. 1	low sync., yes; high sync., approx'ly	yes	yes	no
CalCOFI gp. 2	low sync., yes; high sync., approx'ly	yes	yes	no, except modestly for 1 case
CalCOFI gp. 3	approx'ly	yes	yes	no, except modestly for a few cases
CalCOFI gp. 4	approx'ly	yes	yes, except 1 case	no, except a few cases

Table S4: Summary of randomization and empirical results. Color indicates hyperlinks that, when clicked inside a pdf viewer, will lead directly to the relevant material. For the empirical part of the table, TL was considered to hold except when linearity or homoskedasticity was rejected with 99% confidence. A summary of analytic and numeric results is in table S14.

S15 References

S.D. Batten, R. Clark, J. Flinkman, G.C. Hays, E. John, A.W.G. John, T. Jonas, J.A. Lindley, D.P. Stevens, and A. Walne. CPR sampling: the technical background, materials and methods, consistency and comparability. *Progress in Oceanography*, 58:193–215, 2003.

G. Beaugrand and P.C. Reid. Long-term changes in phytoplankton, zooplankton and salmon related to climate. *Global Change Biology*, 9:801–817, 2003.

J.R. Bell, L. Alderson, D. Izera, T. Kruger, S. Parker, J. Pickup, C.R. Shortall, M.S. Taylor, P. Verrier, and R. Harrington. Long-term phenological trends, species accumulation rates and climate: five decades of change in migrating aphids. *Journal of Animal Ecology*, 84:21–34, 2015.

D. Brillinger. *Time Series: Data Analysis and Theory*. SIAM, Philadelphia, 2001.

H. Caswell. *Matric population models: Construction, analysis, and interpretation*. Sinauer Associated, Inc., Sunderland, MA, 2001.

J.E. Cohen and M. Xu. Random sampling of skewed distributions implies Taylor's power law of fluctuation scaling. *Proceedings of the National Academy of Sciences*, 112:7749–7754, 2015. doi: 10.1073/pnas.1503824112.

C. H. Fischer. On correlation surfaces of sums with a certain number of random elements in common. *Annals of Mathematical Statistics*, 4:103–126, 1933.

R. Harrington. The Rothamsted Insect Survey strikes gold. *Antenna*, 38:158–166, 2014.

D.W. Hosmer, S. Lemeshow, and S. May. *Applied Survival Analysis: Regression Modeling of Time-to-Event Data*. Wiley, New York, 2 edition, 2008.

E. Macaulay, G. Tatchell, and L. Taylor. The Rothamsted Insect Survey 12-metre suction trap. *Bulletin of Entomological Research*, 78:121–129, 1988.

A.W. Mantayla, S.J. Bograd, and E.L. Venrick. Patterns and controls of chlorophyll-a and primary productivity cycles in the Southern California Bight. *Journal of Marine Systems*, 73:48–60, 2008.

R.M. Nisbet and S.C. Gurney. *Modelling fluctuating populations*. John Wiley and Sons, New York, 1982.

G.W. Oehlert. A note on the delta method. *American Statistician*, 46:27–29, 1992.

D.E. Raitsos, Y. Pradhan, S.J. Lavender, I. Hoteit, A. McQuatters-Gollop, P.C. Reid, and A.J. Richardson. From silk to satellite: half a century of ocean color anomalies in the Northeast Atlantic. *Global Change Biology*, 20:2117–2123, 2013.

L.W. Sheppard, J.R. Bell, R. Harrington, and D.C. Reuman. Changes in large-scale climate alter spatial synchrony of aphid pests. *Nature Climate Change*, 6:610, 2015.

P. Turchin. *Complex population dynamics: A theoretical/empirical synthesis*. Princeton University Press, Princeton, 2003.

L. Zhang. Sample mean and sample variance: their covariance and their (in)dependence. *American Statistician*, 61:159–160, 2007.